

***“Characterization of complex mixtures of the light
shredder waste fraction and caramelization processes
by mass spectrometry”***

by

Agnieszka Golon

A Thesis submitted in partial fulfillment
of the requirements for the degree of

Doctor of Philosophy in Chemistry

Approved Dissertation Committee

Prof. Dr. Nikolai Kuhnert (supervisor, Jacobs University Bremen)

Prof. Dr. Gerd-Volker Rösenthaller (Jacobs University Bremen)

Dr. Thorsten Dittmar (Max-Planck-Institut, Oldenburg)

Date of Defense: November 16, 2012

School of Engineering and Science

Dla rodziców Anny i Bogdana

“Ambition is the germ which all growth of nobleness proceeds“

Oscar Wilde

CONTENT

<u>ACKNOWLEDGMENTS</u>	<u>I</u>
-------------------------------------	-----------------

<u>LIST OF ABBREVIATIONS.....</u>	<u>III</u>
--	-------------------

<u>LIST OF FIGURES</u>	<u>VI</u>
-------------------------------------	------------------

<u>LIST OF TABLES</u>	<u>XIV</u>
------------------------------------	-------------------

<u>ABSTRACT</u>	<u>XV</u>
------------------------------	------------------

<u>1 CHARACTERIZATION OF THE LIGHT SHREDDER WASTE FRACTION.....</u>	<u>1</u>
--	-----------------

1.1 INTRODUCTION.....	1
------------------------------	----------

1.1.1 COMPLEX MIXTURES	1
------------------------------	---

1.1.2 CHEMOMETRIC TECHNIQUES USED IN COMPLEX MIXTURE ANALYSIS.....	2
--	---

1.1.3 CHARACTERIZATION OF THE UNRESOLVED COMPLEX MIXTURE (UCM)	4
--	---

1.1.4 CHARACTERIZATION OF THE LIGHT SHREDDER WASTE FRACTION.....	6
--	---

1.1.5 ANALYTICAL METHODS FOR HYDROCARBONS DETERMINATION	8
---	---

1.1.5.1 GC-FID	8
----------------------	---

1.1.5.2 GC×GC.....	10
--------------------	----

1.1.5.3 Mass spectrometry in hydrocarbons analysis	10
--	----

1.1.5.3.1 GC-EI-MS	12
--------------------------	----

1.1.5.3.2 GC-APCI-MS	12
----------------------------	----

1.2 EXPERIMENTAL SECTION.....	14
--------------------------------------	-----------

1.2.1 CHEMICALS	14
-----------------------	----

1.2.2 SAMPLE PREPARATION	14
--------------------------------	----

1.2.3 GC-FID.....	16
-------------------	----

1.2.4 GC-EI-MS	16
----------------------	----

1.2.5 GC-APCI-MS	17
------------------------	----

1.2.6 TGA.....	17
----------------	----

1.2.7	INFRARED (IR) SPECTROSCOPY	17
1.2.8	¹ H NMR	17
1.3	THE AIM OF THE STUDY (I).....	18
1.4	RESULTS AND DISCUSSION	19
1.4.1	THE LIGHT SHREDDER WASTE FRACTION SAMPLE PREPERATION AND EXTRACTION METHOD OPTIMAZATION	19
1.4.2	GC-FID METHOD DEVELOPMENT AND OPTIMIZATION.....	22
1.4.3	QUANTIFICATION OF THE LIGHT SHREDDER WASTE FRACTION	24
1.4.4	GC METHOD VALIDATION	27
1.4.4.1	Suitability.....	27
1.4.4.2	Specificity.....	28
1.4.4.3	Linearity.....	28
1.4.4.4	Limits of detection and quantification	28
1.4.4.5	Precision	29
1.4.4.6	Stability of samples.....	30
1.4.5	GC-EI-MS	31
1.4.5.1	GC-EI-MS of <i>n</i> -alkanes standard and the light shredder waste fraction.....	31
1.4.6	GC-APCI-MS	36
1.4.6.1	GC-APCI-MS of <i>n</i> -alkanes standard	36
1.4.6.2	GC-APCI-MS of the light shredder waste fraction.....	38
1.4.6.3	Chemometric study of the light shredder waste fraction	43
1.4.6.4	Tandem MS measurements.....	46
1.4.6.5	Identification of nonlinear hydrocarbons in the hump by GC-APCI-MS	47
1.4.7	¹ H NMR OF THE LIGHT SHREDDER WASTE FRACTION	50
1.4.8	INFRARED OF THE LIGHT SHREDDER WASTE FRACTION	50
1.4.9	THERMAL ANALYSES OF THE LIGHT SHREDDER WASTE FRACTION	51
1.4.10	BIOREACTOR ANALYSES	54
1.5	CONCLUSION	57
2	<u>CAMEL.....</u>	<u>59</u>

2.1	INTRODUCTION	60
2.1.1	THE IMPORTANCE OF HEATING OF CARBOHYDRATES	60
2.1.2	THE VOLATILE FRACTION OF CAMEL	61
2.1.3	THE NON-VOLATILE FRACTION OF CAMEL.....	63
2.1.4	MASS SPECTROMETRY AS A TECHNIQUE FOR CARBOHYDRATES STRUCTURE DETERMINATION	64
2.1.5	CAMEL COLOR AND OTHER FOOD COLORANTS	66
2.2	EXPERIMENTAL SECTION	69
2.2.1	SAMPLE PREPERATION.....	69
2.2.2	ESI-TOF-MS	69
2.2.3	MS DATA ANALYSIS.....	70
2.2.4	ESI-FT-ICR	70
2.2.5	LC-MS ⁿ	70
2.2.6	HPLC.....	71
2.2.7	MALDI-TOF-MS	71
2.2.8	THERMOGRAVIMETRIC ANALYSIS (TGA)	71
2.2.9	INFRARED (IR) ANALYSIS	72
2.2.10	¹ H NMR AND ¹³ C NMR	72
2.3	THE AIM OF THE STUDY (II)	73
2.4	RESULTS & DISCUSSION	74
2.4.1	CAMELIZATION OF MONOSACCHARIDES	74
2.4.1.1	ESI-TOF mass spectrometry.....	74
2.4.1.2	Oligomers of hexoses	81
2.4.1.3	Dehydration products.....	84
2.4.1.4	Hydration products	87
2.4.1.5	Redox disproportionation products.....	88
2.4.1.6	Comparison of caramelized monosaccharides	88
2.4.2	AROMATICS AND THE COLORED COMPOUNDS IN CAMEL	91
2.4.3	CAMELIZATION OF DISACCHARIDES.....	94
2.4.3.1	ESI-TOF mass spectrometry.....	94

2.4.3.2	Monomeric hexoses	100
2.4.3.3	Oligomers of hexoses	101
2.4.3.4	Dehydration products.....	104
2.4.3.5	Hydration products	107
2.4.3.6	Comparison of caramelized disaccharides.....	107
2.4.4	THERMAL TREATMENTS OF POLYSACCHARIDES AND BREAD.....	110
2.4.4.1	ESI-FT-ICR mass spectrometry.....	111
2.4.4.2	Oligomers of glucose.....	118
2.4.4.3	Dehydration products.....	120
2.4.4.4	Comparison of heated polysaccharides.....	121
2.4.4.5	MALDI-MS analysis of thermally treated glucose and polysaccharides.....	123
2.4.4.6	Analysis of polysaccharide thermal degradation products in bread.....	124
2.4.5	CAMELIC PRODUCTS AND CAMEL COLORS ANALYSIS.....	126
2.4.6	ROASTING PROCEDURE OF COFFEE CARBOHYDRATES.....	130
2.5	CONCLUSION	134
<u>3</u>	<u>REFERENCES</u>	<u>136</u>
<u>4</u>	<u>APPENDIX.....</u>	<u>149</u>

ACKNOWLEDGMENTS

I would like to thank Prof. Dr. Nikolai Kuhnert for giving me the opportunity to carry out my PhD study in his group, and for his constant scientific and personal support.

I would like to express my sincere appreciation to my dissertation committee members, Prof. Dr. Gerd-Volker Rösenthaller and Dr. Thorsten Dittmar for reviewing my thesis.

I am heartily thankful to Jacobs University Bremen and the Fond für Angewandte Umweltforschung des Landes Bremen and the Bremer Entsorgungsbetriebe for the financial support of research project.

I would like to acknowledge technical support and precious help of Anja Müller.

I am also grateful to current colleagues in Prof. Dr. Nikolai Kuhnert's group: Dr. Rakesh Jaiswal, Hande Karaköse M.Sc., Marius Febi Matei M.Sc., Sagar Desphande M.Sc., Ghada Yassin M.Sc., Mohamed Karar M.Sc., Maria Aleksandra Patras B.Sc., Borislav Milev B.Sc., Abinandan Shrestha M.Sc. as well as former members: Dr. Hany Fathy Nour, Dr. Nadim Hourani, Elias Arturo Halabi B.Sc.

I also would like to make a special reference to Prof. Dr. Ulrich Schwaneberg, Prof. Dr. Werner Nau, Prof. Dr. Ulrich Kortz for the opportunities to carry out the GC analyses and the members of their research groups for friendly cooperation.

All partners of the project including University of Bremen and Hochschule Bremerhaven and thank Bruker Daltonik GmbH, Bremen, and Instituto de Quimica Fisica Rocasolano CSIC in Madrid for collaboration.

I am heartily thankful to my parents Anna & Bogdan Golon for their love and work without whom I could not start that part of my live in Bremen.

I want to thank my brothers Mariusz and Artur for their constant care and support.

I wish to express my gratitude to Blazej for his stable encouragement with whom, I could share my weakness and success.

I want to thank my friends and all of those who supported me in any aspects.

LIST OF ABBREVIATIONS

°C	Degrees Celsius
Å	Angstrom
4-MEI	4-Methylimidazole
APCI	Atmospheric Pressure Chemical Ionization
APPI	Atmospheric Pressure Photoionization
ASR	Auto Shredder Residues
BEB	Bremer Entsorgungsbetriebe
CEN	European Committee for Standardization
CD	Circular Dichroism
CI	Chemical Ionization
CID	Collision-Induced Dissociation
cm	Centimeter
COC	Cold On-Column
DDF	Dihydroxydimethylfuranone
DFA	Difructosedianhydride
DHB	2,5-Dihydroxybenzoic acid
δ	Parts per million (ppm)
EC	Equivalent Carbon
ECD	Electron Capture Detector
EI	Electron Impact Ionization
EIC	Extracted Ion Chromatogram
ELV	End-of-Life-Vehicles
ESI	Electrospray Ionization
eV	Electronvolt
FAB	Fast Atom Bombardment
FDA	Food and Drug Administration
FI	Field Ionization
Fru	Fructose
FT-ICR	Fourier Transform Ion Cyclotron Resonance
G	Gram
Gal	Galactose
GC-FID	Gas Chromatography-Flame Ionization Detector

GC-MS	Gas Chromatography-Mass Spectrometry
Glu	Glucose
h	Hour
HC	Hydrocarbon
HAF	2-Hydroxyacetylfurane
HDF	Hydroxydimethylfuranone
Hex	Hexose
HMF	5-Hydroxymethylfurfural
HPLC	High Performance Liquid Chromatography
IR	Infrared
IRMPD	Infrared Multiple Photon Dissociation
IUPAC	International Union of Pure and Applied Chemistry
k'	Capacity Factor
KM	Kendrick Mass
KMD	Kendrick Mass Defect
i.d.	Inner Diameter
LC-MS	Liquid Chromatography-Mass Spectrometry
LIAD	Laser-Induced Acoustic Desorption
LOD	Limit of Detection
LOQ	Limit of Quantification
LSW	Light Shredder Waste
m	Meter
M	Monosaccharide
μm	Micrometer
Man	Mannose
MALDI	Matrix-Assisted Laser Desorption/Ionization
mg	Milligram
MHz	Megahertz
min	Minute
mL	Milliliter
mm	Millimeter
MS	Mass Spectrometry
Mt	Megaton
<i>m/z</i>	Mass-charge-ratio

N	Number of Theoretical Plates
NIST	National Institute of Standards and Technology
NKM	Nominal Kendrick Mass
nm	Nanometer
NMR	Nuclear Magnetic Resonance
PAH	Polycyclic Aromatic Hydrocarbon
PCB	Polychlorinated Biphenyl
PI	Penning Ionization
ppm	Parts per million
psi	Pound per square inch
PTV	Programmable Temperature Vaporizer
R	Correlation Coefficient
RSD	Relative Standard Deviation
RT	Room Temperature
Rt	Retention Time
SBA-15	Mesoporous Silica
SD	Standard Deviation
sec	Second
SPE	Solid Phase Extraction
TDS	Thermal Desorption Spectroscopy
TF	Peak Tailing Factor
TGA	Thermogravimetric Analysis
TIC	Total Ion Chromatogram
TOF	Time of Flight
TPD	Temperature Programmed Desorption
TPH	Total Petroleum Hydrocarbons
UCM	Unresolved Complex Mixture
UV/VIS	Ultraviolet-Visible Spectroscopy

LIST OF FIGURES

Figure 1. Two-dimensional Kendrick plot for mass increment CH_2 for a heavy crude oil ^[16] ..	3
Figure 2. Two-dimensional van Krevelen plot showing the O/C ratio <i>versus</i> the H/C ratio for black tea polyphenols (points) with compositional space for other classes of compounds ^[24]	4
Figure 3. Integrated gas chromatogram of petroleum hydrocarbons extracted from the waste	5
Figure 4. Schematic overview of the shredding process	6
Figure 5. EI-MS spectrum of <i>n</i> -triacontane (from Spectral Database for organic compounds SDBS)	11
Figure 6. Integrated GC-FID chromatogram of the light shredder waste fraction after the shaking extraction (175 rpm, 1 h, 35 °C, <i>n</i> -heptane:acetone (1:2, v:v) as the solvent, SPE with Florisil).....	20
Figure 7. Integrated GC-FID chromatogram of the light shredder waste fraction after the Soxhlet extraction (9 h, <i>n</i> -heptane:acetone (1:2, v:v), SPE with Florisil).....	20
Figure 8. GC-FID chromatogram of $\text{C}_{10}\text{H}_{22}$, $\text{C}_{20}\text{H}_{42}$ – $\text{C}_{40}\text{H}_{82}$ even <i>n</i> -alkanes standard mixture	23
Figure 9. a) Overlap of GC-FID chromatograms of the light shredder waste fraction (black) and $\text{C}_{7}\text{H}_{16}$ – $\text{C}_{40}\text{H}_{82}$ <i>n</i> -alkanes standard (blue), b) Fragment of two overlapping chromatograms of the light shredder waste fraction sample with $\text{C}_{20}\text{H}_{42}$ – $\text{C}_{28}\text{H}_{48}$ <i>n</i> -alkanes standard	24
Figure 10. The calibration curve for <i>n</i> -triacontane.....	25
Figure 11. GC-EI-MS chromatograms (TIC) of <i>n</i> -alkanes standard (green) and the light shredder waste fraction (red).....	31

Figure 12. Mass spectra (GC-EI-MS) of: a) $C_{20}H_{42}$ and b) $C_{40}H_{82}$ of the light shredder waste fraction in the positive ion mode	32
Figure 13. Analyzed PAHs (polyaromatic hydrocarbons)	33
Figure 14. Analyzed PCBs (polychlorinated biphenyls).....	34
Figure 15. Mass spectrum (GC-EI-MS) of phenanthrene (5) from the light shredder waste fraction in the positive ion mode.....	35
Figure 16. Mass spectrum (GC-EI-MS) of 2,2',3,4,4',5,5'-heptachlorobiphenyl (17) from the light shredder waste fraction in the positive ion mode.....	35
Figure 17. Mass spectra of: a) <i>n</i> -tetradecane ($C_{14}H_{30}$), b) <i>n</i> -eicosane ($C_{20}H_{42}$), and c) <i>n</i> -pentacosane ($C_{25}H_{52}$) from <i>n</i> -alkanes standard in the positive ion mode using GC-APCI-TOF-MS.....	36
Figure 18. GC chromatogram (TIC) of the light shredder waste fraction using GC-APCI-TOF-MS	39
Figure 19. MS spectrum (integrated) of the light shredder waste fraction in the positive ion mode using GC-APCI-TOF-MS	39
Figure 20. MS spectrum (enlarged) of the light shredder waste fraction in the positive ion mode using GC-APCI-TOF-MS	40
Figure 21. Extracted ion chromatograms (EICs) of pseudo-molecular ions at m/z : 281.0 ($C_{20}H_{41}$), 295.0 ($C_{21}H_{43}$), 309.0 ($C_{22}H_{45}$), 323.0 ($C_{23}H_{47}$), 337.0 ($C_{24}H_{49}$), 351.0 ($C_{25}H_{51}$) for saturated alkanes in the positive ion mode from GC-APCI-TOF-MS	42
Figure 22. EICs of pseudo-molecular ions at m/z : 281.0 ($C_{20}H_{41}$), 279.0 ($C_{20}H_{39}$), 277.0 ($C_{20}H_{37}$), 275.0 ($C_{20}H_{35}$), 337.0 ($C_{24}H_{49}$), 335.0 ($C_{24}H_{47}$), 333.0 ($C_{24}H_{45}$) for saturated alkanes and their unsaturated derivatives in the positive ion mode from GC-APCI-TOF-MS.....	43

Figure 23. Two dimensional van Krevelen plots showing the O/C <i>versus</i> H/C ratio for the UCM hump in the range: a) 8–12 min, b) 12–16 min, c) 16–20 min, d) of 20–24 min and e) 24–26.3 min for the light shredder waste fraction in the positive ion mode.....	44
Figure 24. Two dimensional Kendrick plots for mass increment CH ₂ showing the distribution of the KMD <i>versus</i> NKM of pseudo-molecular ions for the UCM hump in the range: a) 8–12 min, b) 12–16 min, c) 16–20 min, d) of 20–24 min and e) 24–26.30 min for the light shredder waste fraction in the positive ion mode.....	45
Figure 25. MS ² spectra of: a) <i>n</i> -hexane (C ₇ H ₁₆), b) <i>n</i> -octane (C ₈ H ₁₈), and c) <i>n</i> -tetradecane (C ₁₄ H ₃₀) (parent ions at <i>m/z</i> 115.1, 129.1, 213.2, corresponding to [(M-3)+H ₂ O] ⁺ from the light shredder waste fraction in the positive ion mode using GC-APCI-TOF-MS	47
Figure 26. GC chromatogram (enlarged) of the light shredder waste fraction (black) with extracted ion chromatogram (red) of pseudo-molecular ion at <i>m/z</i> 167.1 (C ₁₃ H ₁₂) for fluorene (4) in the positive ion mode using GC-APCI-TOF-MS.....	48
Figure 27. ¹ H NMR spectrum of the light shredder waste fraction.....	50
Figure 28. IR spectrum of the light shredder waste fraction	51
Figure 29. Thermogravimetric curves of: a) <i>n</i> -eicosane (C ₂₀ H ₄₂), b) <i>n</i> -tricosane (C ₂₃ H ₄₈), c) <i>n</i> -hexatriacontane (C ₃₆ H ₆₄), d) <i>n</i> -tetracontane (C ₄₀ H ₈₂)	52
Figure 30. Thermogravimetric curve of the light shredder waste fraction with derivatives curve obtained, when temperature raises from 25 to 800 °C at the rate 5 °C/min under a nitrogen atmosphere	53
Figure 31. Overlap of GC-FID chromatograms of the light shredder waste fraction from: R.1.2. (red), R.2.2. (black), R.3.2. (blue), Bremer Entsorgungsbetriebe (green) ..	55

Figure 32. Overlap of GC-FID chromatograms of the light shredder waste fraction from: R.1.2. (red), R.2.2. (blue), I3 (black)	56
Figure 33. Typical volatile caramel compounds	61
Figure 34. Schematic representation of reaction pathways for acids-catalyzed dehydration of fructose ^[147]	62
Figure 35. The formation of possible products of heated glucose	63
Figure 36. Difructose dianhydrides found in sucrose caramels ^[153]	64
Figure 37. The carbohydrates fragmentation ^[176]	65
Figure 38. Thermogravimetric curve of caramelized glucose (temperature was ramped from 25 to 180 °C and kept at final temperature for 2 h).....	74
Figure 39. Mass spectrum of caramelized glucose (32) in the negative ion mode using a direct infusion into an ESI-TOF-MS instrument.....	75
Figure 40. Mass spectrum of caramelized fructose (33) in the negative ion mode using a direct infusion into an ESI-TOF-MS instrument	76
Figure 41. Mass spectrum of caramelized galactose (34) in the negative ion mode using a direct infusion into an ESI-TOF-MS instrument	76
Figure 42. Mass spectrum of caramelized mannose (35) in the negative ion mode using a direct infusion into an ESI-TOF-MS instrument	77
Figure 43. Two dimensional van Krevelen plots showing the O/C <i>versus</i> H/C ratio for caramelized: a) glucose, b) fructose, c) galactose and d) mannose in the negative ion mode in <i>m/z</i> range between 50–1200.....	79
Figure 44. Two dimensional Kendrick plots for mass increment H ₂ O showing the distribution of the Kendrick mass defect plotted against the nominal Kendrick mass of pseudo- molecular ions for caramelized: a) 32 , b) 33 , c) 34 and d) 35 in the negative ion mode	80

Figure 45. Structures of carbohydrate monomers and potential caramelization products (please note that regiochemistry of glycosidic linkage in 36–42 , the regiochemistry of dehydration 37–38 and the regiochemistry of hydrate 40–42 is selected randomly)	82
Figure 46. Extracted ion chromatogram (top) and MS ² spectra (bottom) of pseudo-molecular ion at m/z 341.0 (C ₁₂ H ₂₂ O ₁₁) for three selected chromatographic peaks of caramelized glucose in the negative ion mode	83
Figure 47. Suggested fragmentation mechanism at m/z 485.1 for the dehydrated ions (regiochemistry of C=O chosen randomly)	86
Figure 48. Radar plots of classes of ions detected in a direct infusion negative mode mass spectra of heated monosaccharides 32–35 : a) oligomeric hexoses, b) dehydrated oligomeric hexoses, c) ratio of oligomeric to dehydrated hexoses	89
Figure 49. Formation of anhydro-galactose (47).....	90
Figure 50. UV chromatograms monitored at: a) 450, b) 500, c) 550 nm of caramelized glucose in the negative ion mode	91
Figure 51. Mass spectrum of a chromatographic peak at retention time 4.1 min from UV at 500 nm of caramelized glucose in the negative ion mode.....	92
Figure 52. UV chromatogram monitored at 550 nm (top) and mass spectrum of chromatographic peak at retention time 3.2 min (bottom) of caramelized fructose in the negative ion mode.....	92
Figure 53. Two dimensional van Krevelen plots showing the O/C <i>versus</i> H/C ratio for caramelized: a) glucose from MS spectrum of a chromatographic peak from UV chromatogram monitored at 500 nm with Rt = 4.1 min, b) fructose from MS spectrum of a chromatographic peak from UV chromatogram monitored at 550 nm with Rt = 3.2	93

Figure 54. Mass spectrum of caramelized sucrose (48) in the negative ion mode using a direct infusion into an ESI-TOF-MS instrument.....	95
Figure 55. Mass spectrum of caramelized maltose (49) in the negative ion mode using a direct infusion into an ESI-TOF-MS instrument	95
Figure 56. Mass spectrum of caramelized lactose (50) in the negative ion mode using a direct infusion into an ESI-TOF-MS instrument.....	96
Figure 57. Two dimensional van Krevelen plots showing the O/C ratio <i>versus</i> H/C ratio for caramelized: a) sucrose, b) maltose, c) lactose in the negative ion mode in m/z range between 50–1200.....	99
Figure 58. Two dimensional Kendrick plots for mass increment H_2O showing the distribution of the Kendrick mass defect plotted against the nominal Kendrick mass of pseudo-molecular ions for caramelized: a) 48 , b) 49 , c) 50 in the negative ion mode	100
Figure 59. The formation of monomeric hexoses from disaccharides 48–50' during heating	101
Figure 60. EIC (Extracted ion chromatogram) and MS^2 spectra of fragment at m/z 341.0 ($C_{12}H_{22}O_{11}$) for two chromatographic peaks of caramelized sucrose in the negative ion mode	102
Figure 61. The formation of oligomeric saccharides from 48–50' during heating (the regio- and stereochemistry of oligosaccharides remains open)	103
Figure 62. The formation of dehydrated hexoses from heated disaccharides 48–50' (the regiochemistry of water elimination was chosen randomly in 51)	105
Figure 63. Dehydration products of heated maltose (49') (the regiochemistry of water elimination was chosen randomly in 52, 53)	105

Figure 64. Radar plots of classes of ions detected in a direct infusion negative mode mass spectra of heated disaccharides 48–50 : a) oligomeric hexoses, b) dehydrated oligomeric hexoses, c) ratio of oligomeric to dehydrated hexoses	109
Figure 65. Thermogravimetric curve of starch.....	111
Figure 66. Mass spectrum of heated starch (54) in the negative ion mode using a direct infusion into an ESI-FT-ICR instrument.....	112
Figure 67. Mass spectrum of heated cellulose (55) in the negative ion mode using a direct infusion into an ESI-FT-ICR instrument	112
Figure 68. The chemical structures of starch, cellulose and fragmentation pattern observed for dehydrated tetramer of glucose (56) by IRMPD-FT-ICR-MS measurement.....	113
Figure 69. Structures of oligomeric and dehydrated oligomeric decomposition products 56–61 obtained from starch.....	115
Figure 70. Two dimensional van Krevelen plots showing the O/C ratio <i>versus</i> H/C ratio for heated: a) starch and b) cellulose in the negative ion mode in m/z range between 50–1200	116
Figure 71. Two dimensional Kendrick plots for mass increment H_2O showing the distribution of the Kendrick mass defect plotted against the nominal Kendrick mass of pseudo-molecular ions for: a) starch and b) cellulose in the negative ion mode	117
Figure 72. EICs from LC/MS experiments of pseudo-molecular ions at m/z : a) 665.0 ($C_{24}H_{42}O_{21}$) and b) 647.0 ($C_{24}H_{40}O_{20}$) of heated cellulose in negative ion mode	119
Figure 73. Reaction mechanism illustrating thermal decomposition of cellulose.....	120
Figure 74. Radar plots of classes of ions detected in a direct infusion negative mode mass spectra of heated polysaccharides 54, 55 and glucose 32 : a) oligomeric hexoses, b) dehydrated oligomeric hexoses, c) ratio of oligomeric to dehydrated hexoses...	122

Figure 75. Mass spectrum of heated starch in the positive ion mode using a MALDI-TOF-MS instrument	123
Figure 76. Mass spectrum of baked bread in the positive ion mode using a MALDI-TOF-MS instrument	124
Figure 77. Mass spectrum of a candy fudge (Krowka [®]) in the negative ion mode using a direct infusion into an ESI-TOF-MS instrument	126
Figure 78. Mass spectrum of a caramellic color E 150a in the negative ion mode using a direct infusion into an ESI-TOF-MS instrument	127
Figure 79. Mass spectrum of a caramellic color E 150b in the negative ion mode using a direct infusion into an ESI-TOF-MS instrument	127
Figure 80. Mass spectrum of a caramellic color E 150c in the negative ion mode using a direct infusion into an ESI-TOF-MS instrument	128
Figure 81. Mass spectrum of a caramellic color E 150d in the negative ion mode using a direct infusion into an ESI-TOF-MS instrument	128
Figure 82. Mass spectrum of Arabica coffee' carbohydrates in the negative ion mode using a direct infusion into an ESI-TOF-MS	131
Figure 83. Mass spectrum of Robusta coffee' carbohydrates in the negative ion mode using a direct infusion into an ESI-TOF-MS	132
Figure 84. Two dimensional van Krevelen plots showing the O/C ratio <i>versus</i> H/C ratio for: a) Arabica and b) Robusta coffee's carbohydrates in the negative ion mode in m/z range between 50–1200	133
Figure 85. Two dimensional Kendrick plots for mass increment H ₂ O showing the distribution of the Kendrick mass defect plotted against the nominal Kendrick mass of pseudo- molecular ions for: a) Arabica and b) Robusta coffee's carbohydrates in the negative ion mode	133

LIST OF TABLES

Table 1. Conditions for analyzed samples from bioreactors in Bremerhaven.....	15
Table 2. Comparing of shaking and Soxhlet extractions.....	21
Table 3. Calculated concentrations of <i>n</i> -alkanes in the range C ₂₀ H ₄₂ –C ₄₀ H ₈₂ of the light shredder waste fraction	26
Table 4. Suitability of the GC method.....	27
Table 5. Linearity, LODs, LOQs	29
Table 6. Reproducibility of peak areas of the light shredder waste fraction (interday)	30
Table 7. High-resolution mass (GC-APCI-TOF-MS) data for <i>n</i> -alkanes standard in the positive ion mode.....	38
Table 8. High-resolution mass (GC-APCI-TOF-MS) data for the light shredder waste fraction in the positive ion mode.....	41
Table 9. High-resolution mass (MS-TOF) data for caramelized glucose in the negative ion mode	78
Table 10. High-resolution mass (MS-TOF) data for caramelized sucrose in the negative ion mode	98
Table 11. High-resolution mass (ESI-FT-ICR) data for heated starch in the negative ion mode	114
Table 12. MALDI-MS/MS data for the bread sample in the positive ion mode (presented ions are sodiated adducts).....	125
Table 13. High-resolution mass (MS-TOF) data for a caramelic color E 150a in the negative ion mode	129
Table 14. High-resolution mass (MS-TOF) data for Arabica coffee' carbohydrates in the negative ion mode	132

ABSTRACT

The analysis of complex mixtures is one of the most challenging areas of analytical chemistry. Within this thesis the composition of two complex mixtures of environmental and food origin, such as the light shredder waste fraction and caramel was studied, respectively. This thesis is thus subdivided into two main parts.

In the last few decades, the light shredder waste fraction has attracted much interest due to the scarcity of space and the toxicological properties of some of its contaminants. Gas chromatograms of the light shredder waste fraction result in an unresolved complex mixture (UCM) containing thousands of compounds. In this work, gas chromatography with a flame ionization detector (FID) as well as coupled to mass spectrometry with electron impact (EI) and atmospheric pressure chemical ionization (APCI) has been applied to study the composition of the light shredder waste fraction focusing on non-volatile hydrocarbons. The new GC methods evaluated for the optimal separation and detection of *n*-alkanes that subsequently were applied for the analysis of the light shredder waste fraction after various optimized extraction procedures. Solid-phase extraction (SPE) was used as a clean up procedure, yielding less complex chromatograms. GC-FID has been successfully employed to monitor the bioremediation of such waste samples. GC-APCI with a time of flight mass analyzer was utilized for the first time in order to determine heavy hydrocarbons of *n*-alkanes standard and the light shredder waste fraction. Adducts, such as $[(M-3H)+H_2O]^+$ and $[M-H]^+$ were found to be the most abundant ions up to *n*-nonadecane ($C_{19}H_{40}$) and for higher hydrocarbons established by APCI, respectively. Notwithstanding the small level of fragmentations, the presence of the base peaks enabled the identification of *n*-alkanes. In addition, polyaromatic hydrocarbons and polychlorinated biphenyls have thus been found in the light shredder waste fraction.

In the second part of this thesis, the composition of caramel, one of the mankind's well-known dietary materials, obtained by the heating of carbohydrates, have been studied. While the volatile fraction of caramel has been investigated in details, the composition of the non-volatile fraction remains unresolved or if not, mysterious. Caramel formed by heating of glucose, fructose, galactose, mannose as well as disaccharides, such as sucrose, lactose and maltose using a conceptually novel combination of mass spectrometric techniques have yielded for the first time an unprecedented account of its chemical composition. The analytical strategy employed uses high-resolution mass spectrometry to identify the most

abundant molecular formulas followed by a van Krevelen and Kendrick analysis. A resulting structural hypothesis was further substantiated using targeted LC-tandem MS experiments. It has been shown that caramel is composed of several thousand of compounds formed by a small number of unselective and chemoselective reactions. The caramelization products include oligomers with up to six carbohydrate units produced through an unselective glycosidic bond formation, dehydration products of oligomers losing up to eight water molecules, hydration products of sugar oligomers, disproportionation and aromatic products. In addition, the molecular formulas of compounds responsible for a brown color of caramel were also proposed.

The investigation of thermal decomposition products of pure starch and cellulose as model systems followed by the investigation of bread obtained under comparable conditions has been performed. From both starch and cellulose, dehydrated oligomers of glucose were predominantly observed, with oligomers of more than four glucose moieties dominating. Commercial caramel products and caramel colors (E 150) were compared with studied carbohydrates. Furthermore, understanding of the composition of roasted coffee beans has been improved by the examination of their carbohydrates fraction.

**CHARACTERIZATION OF THE LIGHT SHREDDER
WASTE FRACTION**

1.1 INTRODUCTION

1.1.1 COMPLEX MIXTURES

A complex mixture is defined as a mixture that contains too many compounds to be resolved by chromatographic techniques (more than 1000 in gas chromatography and more than 300 in liquid chromatography). The analysis of complex mixtures is one of the most demanding tasks in modern analytical chemistry. Such complex mixtures can be found in many environmental samples.^[1] Many food materials, such as black tea thearubigins,^[2] coffee,^[3] oils,^[4] cocoa^[5] or caramel^[6] are considered as complex mixtures. Food processing for instance, roasting, cooking, frying, baking or fermentation dramatically increases the complexity of the new material. Moreover, organic matter in drinking water,^[7] cigarette smoke^[8] and many biologically occurring systems can also be classified as complex mixtures.^[9] They consist of tens, hundreds or thousands of compounds and their composition is not fully known, neither qualitatively nor quantitatively.^[10]

The constant development of new analytical methods and tools improves the capabilities of analytical chemistry. The analysis of complex mixtures has benefited greatly from the development of the instrumentation.^[11,12] In particular, modern mass spectrometry (MS) has become an important technique for the characterization of complex mixtures.^[13] MS combines ultimate resolving power with high sensitivity. Additionally, coupling MS to chromatography and UV/VIS provides multidimensional information on the sample, with tandem MS techniques allowing insight into structural information. Recently, the analytical strategy based upon mass spectrometry has been applied to the analysis of complex mixtures, such as black tea thearubigin,^[14] roasted coffee melanoidins^[3] and to the investigation of caramel formed from glucose, fructose and sucrose.^[6] High-resolution mass spectrometry (MS) provides the extensive lists of molecular formulas of compounds present in the sample. Novel graphical and chemometric tools, such as van Krevelen, Kendrick analysis or homologous series analysis are used to establish a structural and compositional hypothesis regarding all chemical processes in the sample. The LC-tandem MS can then verify these hypotheses and resolve isomeric compounds in the chromatographic dimension. Moreover, conventional

spectroscopic techniques such as NMR, IR, UV/VIS or CD offer a complete picture of compounds in the analyzed mixture.

1.1.2 CHEMOMETRIC TECHNIQUES USED IN COMPLEX MIXTURE ANALYSIS

Several mass spectrometry techniques are being applied to the analyses of complex mixtures. High-resolution MS spectra give very complex data that hinder the visual presentation and structural interpretation. Recently, several chemometric tools have been applied to visualize such complex high-resolution mass data.

The first graphical technique is Kendrick analysis, introduced by petroleum researchers.^[15-18] Homologous series of compounds can be easily identified in Kendrick plots because they possess the same Kendrick mass defect values and lie on the horizontal lines in the graph.

To generate Kendrick plots, the measured masses are converted from the IUPAC mass scale to the Kendrick mass scale. The following equations are used to define the Kendrick mass defect for CH₂, as an example.

$$\text{Kendrick mass (KM)} = \text{IUPAC mass} \times (14/14.01565)$$

$$\text{Kendrick mass defect (KMD)} = \text{Nominal Kendrick mass (NKM)} - \text{exact Kendrick mass (KM)}$$

The Kendrick mass is based on assigning the mass of CH₂ to be 14.0000 Da instead of the IUPAC value of 14.01565 Da.^[19] The same class and type of compounds, yet different in the number of CH₂ units will fall on a single horizontal line with peaks separated by 14 Da in the nominal mass but with no difference in the Kendrick mass defect.^[16] Molecules with a various number of rings plus double bonds, different heteroatom class will vary in the Kendrick mass defect and will appear below or above of the alkylation series. Figure 1 represents a two-dimensional display of the Kendrick mass defect *versus* the nominal Kendrick mass for the mass increment CH₂ for a crude oil sample. The same equations can be applied to other increment groups such as H₂O, O₂ or H₂ with inclusion of their masses^[20] depending on the purpose of the examination.

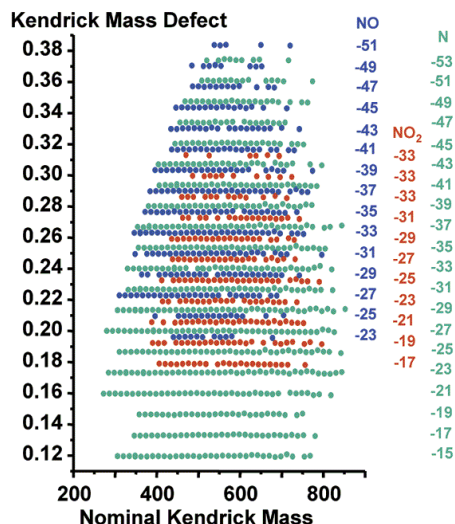


Figure 1. Two-dimensional Kendrick plot for mass increment CH_2 for a heavy crude oil^[16]

Another graphical composition image is the van Krevelen diagram or the elemental ratio analysis, generally constructed using the molar ratio of hydrogen to carbon (H/C) as the ordinate and the molar oxygen to carbon ratio (O/C) as the abscissa. The major biochemical classes of compounds (e.g., lipids, carbohydrates) have their own characteristic H/C or O/C ratio boundaries.^[21] As a result, each class of compounds projects in a specific location on the diagram. For instance, the O/C and H/C ratios, clustering between 0 and 0.4 and between 1.6 and 2.0, respectively plot in the range expected for lipid-type structures. The peaks in the plot located in the area where the O/C ratios are between 0.7–1.0 and the H/C ratios between 1.6 and 1.9 are characteristic for carbohydrates. The ratios of N/C or S/C have also been used to prepare graphs for nitrogen- or sulphur-containing compounds.^[22,23] The fact that typical reactions (e.g., oxidation, hydration, condensation) involve loss or gain of integral amounts of C, H, O atoms leads to unique layouts on the plot. In the van Krevelen diagrams, trends along the lines can indicate structural relationships among families of compounds. The van Krevelen diagram with the O/C ratio *versus* the H/C ratio for black tea polyphenols and other classes of compounds is illustrated in Figure 2.

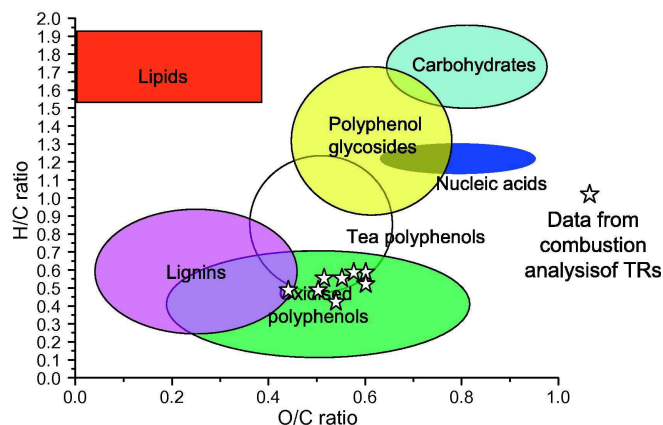


Figure 2. Two-dimensional van Krevelen plot showing the O/C ratio *versus* the H/C ratio for black tea polyphenols (points) with compositional space for other classes of compounds^[24]

1.1.3 CHARACTERIZATION OF THE UNRESOLVED COMPLEX MIXTURE (UCM)

The term “unresolved complex mixture” (UCM) describes hump-shaped chromatograms that are often observed in gas chromatograms of samples, including crude oil and petroleum environmental contaminations.^[25-27] The first reference to the UCM is uncertain, but in 1970 Blumer *et al.* examined petroleum hydrocarbons extracted from diesel fuel-contaminated shell-fish and described chromatograms containing a broad unresolved background.^[28] The term UCM was first introduced by Rowland while investigating crudes, lubricating oils and oil-spill samples.^[25] An example of a UCM contamination is shown in Figure 3 with a series of well resolved sharp peaks “floating” on the hump. The UCM may include thousands of compounds where usually only part of them can be successfully identified by target analysis.

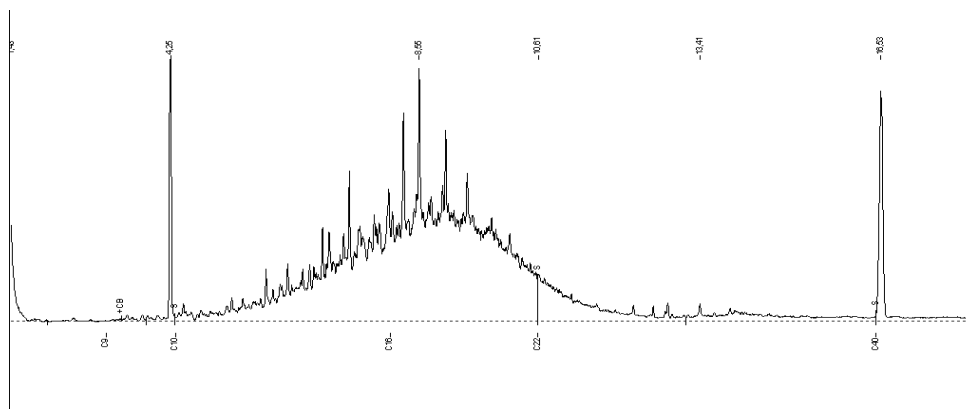


Figure 3. Integrated gas chromatogram of petroleum hydrocarbons extracted from the waste

A variety of analytical techniques have been applied to explore the chemical compositions of the UCMs,^[29] including thin-layer chromatography,^[30] silver-impregnated silica gel chromatography, open-column silica gel chromatography as well as spectroscopic methods, such as fluorescence,^[31] nuclear magnetic resonance (NMR),^[32] infrared (IR)^[30] and high-resolution mass spectroscopy.^[33] The most frequently used methods are gas chromatography (GC) and high-performance liquid chromatography (HPLC)^[34] or hyphenated methods such as gas chromatography-mass spectrometry (GC-MS)^[35,36] and more recently two dimensional chromatographic techniques.^[37] The UCM of petroleum based samples might contain alkanes, alkenes, alkynes, cycloalkanes, monoaromatics, polycyclic aromatic hydrocarbons (PAHs), steranes and also polychlorinated biphenyls (PCBs).^[26,27] The interest in environmental samples containing HCs is frequently motivated by the potentially toxic nature of some of its contaminants. The toxicology of UCM hydrocarbons has rarely been studied. Monitoring of the hydrocarbon contamination of sediments has routinely focused on polyaromatic hydrocarbons which are recognized as highly toxic with mutagenic and carcinogenic properties.^[38-41] The limited number of toxicological studies of aliphatic hydrocarbons showed that they are not a poison.^[41,42] It is well known that bioremediation is a cost-effective technique for the treatment of petroleum hydrocarbon-contaminated soils or sediments with microorganisms to reduce the UCM. Aerobic soil microbes can use petroleum hydrocarbons as a carbon source, degrading them with the aid of mono- and dioxygenase enzymes to CO₂, biomass or other metabolites.^[43] Various intermediates can be generated during this process, including alcohols, aldehydes, ketones and carboxylic acids. The degradation efficiency and kinetics are strongly affected by various parameters, for instance type of microorganism involved, hydrocarbons and soil type,

moisture content, oxygen, nutrient availability, pH and temperature.^[44,45] Bioremediation of petroleum hydrocarbons in soils and sediments has been mostly studied using conventional GC-FID and GC-MS.^[46,47] Experimental data showed that linear alkanes and aromatic hydrocarbons are more biodegradable than *i*-alkanes; whereas cycloalkanes are the least biodegradable. Aromatic hydrocarbons containing up to three rings showed better degradability if compared to *n*-alkanes.^[43]

1.1.4 CHARACTERIZATION OF THE LIGHT SHREDDER WASTE FRACTION

The light shredder waste fraction is a shredder residue derived from shredding of End-of-Life-Vehicles (ELV), white goods, electrical household and industrial items.^[48,49] It is produced by shredding of automobiles and major household appliances followed by separation and removal of metals. Figure 4 presents a schematic overview of the shredding process. The light shredder waste fraction is generally designed for landfill.^[50]

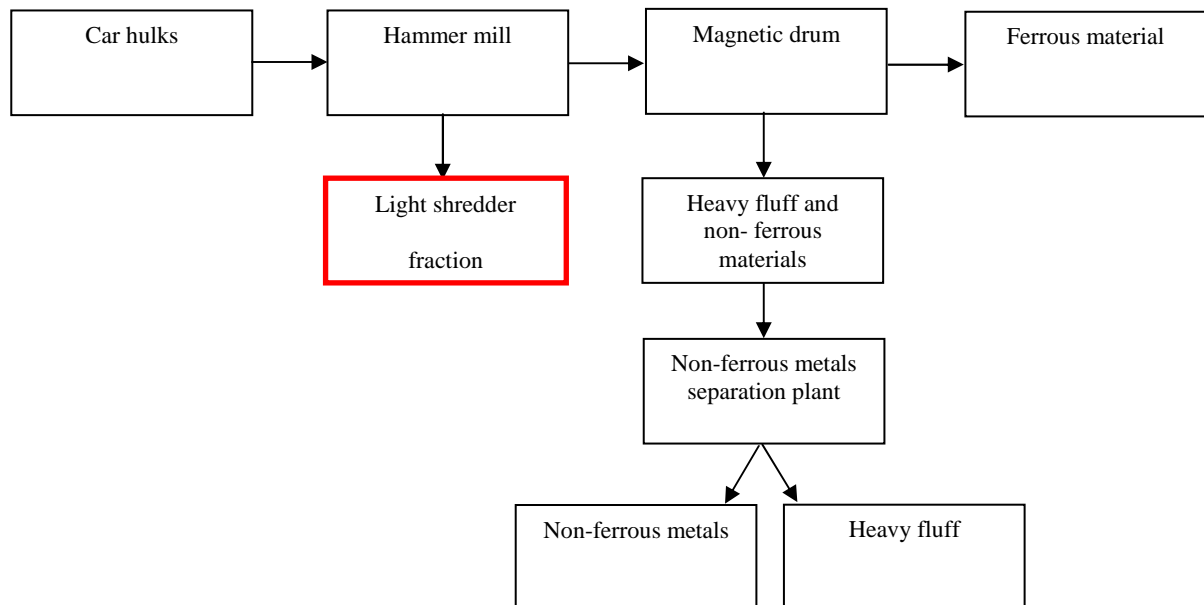


Figure 4. Schematic overview of the shredding process

It is estimated that 30 million ELVs arise worldwide annually, with Europe accounting for about 14 million ELVs and the USA numbering approximately 9–11 million ELVs. In the

European countries the number of ELVs will most likely rise up to 17 million by 2015 thus increasing the proportion of the waste derived from this source.^[51] The European legislation, through the ELV Directive and the Landfill Directive increases the pressure to reduce this waste. In particular, the light shredder waste fraction has become the subject of intense debates due to the increasing scarcity of the landfill space and potentially hazardous nature of some of their components. The enhanced chemical content of the waste is becoming a significant problem for the companies responsible for the waste management. The concentration of several components, such as aliphatic and aromatic hydrocarbons, polychlorinated biphenyls, volatile organic compounds and metals is very thoroughly monitored in the LSW fraction. Legal thresholds for these compounds are defined and the LSW must adhere to these legal limits prior to landfill. Different countries have their separate environmental legislation for those contaminants. In Germany the acceptable limit of hydrocarbons concentration in the light shredder waste fraction is 5 g/kg as determined by the KW/04 method.^[52] Recently, the Bremer Entsorgungsbetriebe (BEB) has optimized a novel technology to lower the volume and weight of the light shredder waste fraction. The method involves the treatment of the waste with microorganisms, using water irrigation at temperatures around 70–90 °C for 8 weeks. As a consequence of this treatment the volume is reduced by an average of 50%. Subsequent analytical investigations of the waste fraction are performed to check the concentration of contaminants of the material prior to disposal to the landfill.

In the past, the most critical parameter was the HC concentration, exceeding frequently the legal threshold of 5 g/kg. To perform the quantification, the UCM hump is typically uncritically integrated in order to determine the total hydrocarbon content. Whether the hump contains only hydrocarbons remains a matter of speculation rather than experimental proof and no detailed information currently exists on its actual composition. The challenge involves the determination of the nature of components present in the hump. If other non HC components are present, the KW/04 method must be modified and a new strategy for the analysis and quantification of other components must be optimized. The investigation of the HC containing fraction of the LSW forms part of this thesis with an aim to critically assess the connection of the KW/04 method.

1.1.5 ANALYTICAL METHODS FOR HYDROCARBONS DETERMINATION

1.1.5.1 GC-FID

Gas chromatography with a flame ionization detector (GC-FID) is nowadays the most common analytical technique for hydrocarbons determination.^[53,54] The analysis of hydrocarbons is certainly demanding and requires a good instrumentation system, mainly due to high-boiling components and numerous possible isomers with similar physico-chemical properties. There are a few aspects, which must be addressed before the analysis of a wide range of hydrocarbons.

The GC analysis of heavy hydrocarbons requires high oven, injector and detection port temperatures and a stable stationary phase. A stabilized non-polar polymer such as methylpolysiloxane is a suitable stationary phase for these type of components. The injection conditions should be carefully selected in order to prevent mass discrimination and thermal degradation of the analyte.^[55] A number of alternatives exist for inlet systems, including split/splitless, programmed temperature vaporizer (PTV) and cold-on-column (COC).^[56-58] Split/splitless injection in the splitless mode, is the most frequently used inlet, including environmental analysis. This technique is used for small injection volumes, typically 1–2 μL . The injector operates at high temperatures (200–280 $^{\circ}\text{C}$) and these can cause incomplete transfer of compounds to the column.

In cold-on-column (COC) injection sample aliquots can be directly introduced onto the analytical column or a retention gap at lower temperatures (60–80 $^{\circ}\text{C}$), in comparison with the hotter inlet of the split/splitless. Subsequently, cold-on-column produces less thermal stress on analytes.^[59] COC injectors have been successfully used for thermally unstable compounds or mixtures, such as toxophene,^[60] organophosphorous pesticides,^[61] organochlorines,^[62] chloroanilines,^[63] PAHs^[64] and alkanes.^[65] This injector can be applied with small (1–2 μL) and large volume injections (> 10–250 μL).^[61,66] The COC inlet has the lowest tolerance to co-injected matrix components followed by splitless and PTV injectors.^[61]

PTV has been successfully used to reduce the degradation of thermally labile pesticides^[67,68] and for compounds that exhibit discrimination with boiling point.^[69,70] It can be employed for small (< 5 μL) and large (> 10–400 μL) volume injections. Overall the PTV inlet is the most

powerful inlet currently available in the GC systems.

Due to demands for lower detection limits in environmental analysis and the wide range of analytes, large volume inlets and specifically the PTV inlet designs are expected to become more common in the future, replacing the classical 1 μL injections.

In some cases the selection of a proper liner type may affect the analysis. The investigation showed that the proper choice of a liner may minimize the mass discrimination, while an incorrect choice may even enhance discrimination problems. The most frequently used injection liners packed with glass wool are often more prone to thermal degradation or adsorption of analytes. Different splitless times are used for Total Petroleum Hydrocarbon (TPH) determination. Too short a splitless time results in mass discrimination, because the high-boiling point components do not have enough time to vaporize completely. Too long a splitless time can especially in the case of excessively large injection volumes lead to the loss of peak symmetry of early eluting compounds. An adjustment of the injection volume may also become important. Thus, a sufficiently high sample volume has to be injected in order to attain a high enough signal to noise ratio for trace analytcs. If the volume of injection is too large, it may cause liner overload related flashback-effects.^[59]

Flame Ionization Detector (FID) is the most popular detection employed by routine laboratories; nevertheless, there is a great variation in the FID temperature applied (250–360 °C) for hydrocarbons analysis. The FID temperature of around 250 °C can turn out to be exceptionally low due to a possible condensation of high-boiling point components taking place in the detector. Too high detector temperatures, on the other hand, strain the durability of the columns and cause the so called column-bleeding, which in turn reduces analytical precision.^[59]

The GC operating settings are freely modified by individual laboratories. In April 2004 great improvements were accomplished in the definition and analysis of TPHs by international organizations. The European Committee for Standardization (CEN) presented a draft European Standard defining determination of the total petroleum hydrocarbons in the waste in the boiling point range of C10–C40^[71] by gas chromatography with flame ionization detector (GC-FID). Such a method involves a simple shaking extraction at room temperature, clean up of extract with a halogen free solvent and determination of hydrocarbons by gas chromatography-flame ionization detector and integration of the peaks between *n*-decane and *n*-tetracontane.^[72,73] This is a potential method to be applied in the future for TPH determinations as it utilizes a simple shaking extraction, which is instrumentally not

demanding, hence easily accessible by laboratories. According to the recent draft standards proposed by CEN, the soil sample is extracted with an acetone/*n*-heptane mixture. Acetone is then removed from the extract with water. The resulting organic phase is solid phase extracted (Florisil) and the eluate analyzed by GC-FID. Additionally, each country establishes the acceptable limits for hydrocarbons concentration.

1.1.5.2 GC×GC

A relatively recent analytical tool that has been used for the separation of UCMs is a comprehensive two-dimensional gas chromatography (GC×GC).^[74,75] It has been already exploited to characterize the UCM in sediment,^[76] biota,^[26] crude oil^[77] and oil spills.^[78] This technique was pioneered by Liu and Philips in the early 1990s.^[79] The samples are injected into a first chromatographic column then a modulator periodically injects their contents into the second column. These fractions are quickly separated on the second column and elute into the detector, where they are measured. Most research into petrochemical hydrocarbons using GC×GC has utilized non-specific detectors (e.g., FID, ECD) and time of flight MS. Petroleum hydrocarbons in distillate range (i.e., C₈–C₄₀) can be quantitatively separated into groups: alkanes, alkenes, cycloalkanes, mono-aromatics, naphthenic mono-aromatics, di-aromatics, naphthenic di-aromatics, tri-aromatics, 3-ring polycyclic aromatics. Each group can be further divided by the boiling point or equivalent carbon (EC) number. Moreover, a system such as HPLC-GC×GC-FID has been also studied towards petroleum hydrocarbons in oil-contaminated soil.^[46,80] One of the main advantages of such a comprehensive system (GC×GC) is a very high separation power, making the technique useful for unraveling the composition of complex mixtures. Another important aspect of this technique is that it resolves and identifies the specific classes of compounds present in the UCM.

1.1.5.3 Mass spectrometry in hydrocarbons analysis

The past decade has been a time of rapid growth and change in instrumentation for mass spectrometry.^[81] The constant development of the analytical instrumentation improves the potential to characterize complex mixtures. Mass spectrometry, being one of the most informative techniques in complex mixtures analysis, is also an extremely challenging technique to be used especially, when the analyte contains saturated alkanes known to ionize reluctantly in mass spectrometry. Several ionization techniques, such as electron ionization

(EI),^[82] chemical ionization (CI),^[83] electrospray ionization (ESI),^[84-86] matrix-assisted laser desorption ionization (MALDI),^[87] laser-induced acoustic desorption (LIAD),^[88] atmospheric pressure photoionization (APPI)^[89] and atmospheric pressure chemical ionization (APCI)^[90,91] have been applied to analyze petroleum samples. Furthermore, the development of mass analyzers provides the introduction of different systems like an ion trap, time of flight or Fourier cyclotron mass analyzers utilizing improved resolution.

The next problem of HC analysis arises due to the ease of fragmentation of the HC ions, in particular if generated by EI or CI. The resulting radical cations fragment readily and mass spectra are dominated by target ions. Frequently, molecular ions are not observed resulting in difficulties of molecular formula assignment. The example spectrum of *n*-triacontane is present in Figure 5.

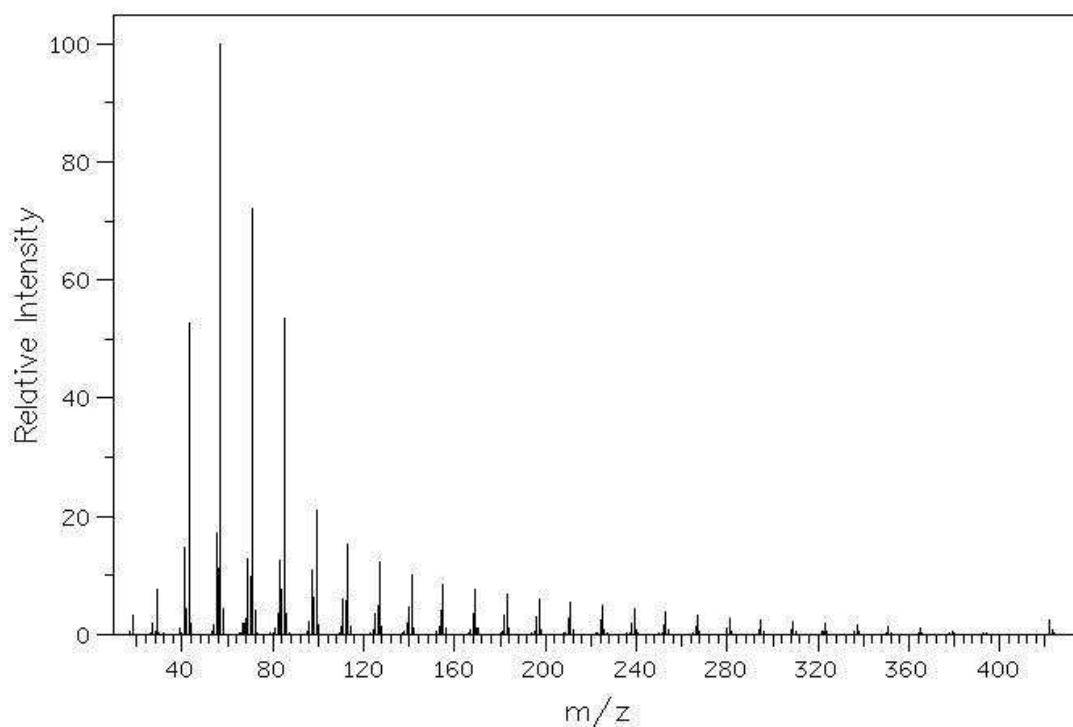


Figure 5. EI-MS spectrum of *n*-triacontane (from Spectral Database for organic compounds SDBS)

Coupling a separation technique with mass spectrometry greatly increases the efficiency of the analysis. A multi-dimensional technique, such as GC-MS provides an additional dimension and is useful in the complex mixtures analysis. The systems, such as GC-FI-MS,^[92] GC-PI-MS,^[93] GC-CI-MS,^[94,95] GC-EI-MS,^[96] GC-APCI-MS^[97] have been already used in

numerous applications. Two-dimensional techniques, GC-EI-MS and GC-APCI-MS, applied in this work will be described in the following part.

1.1.5.3.1 GC-EI-MS

GC with mass spectrometry was the first efficient tandem system developed and the first instrument assembled in the very early 1960s.^[98] Traditional GC/MS applies electron impact (EI) ionization, where molecules are ionized by electrons at energy usually of 70eV. This ionization technique works well for many gas phase molecules but induces extensive fragmentation so that the molecular ions are not always observed.^[81] The experiments with low energy were performed for petroleum analysis.^[95,99,100] The fragmentation pattern of *n*-alkanes is characterized by clusters of peaks and the corresponding peaks of each cluster are 14 mass units (CH₂) apart. The largest peak in every cluster represents the C_nH_{2n+1} fragment occurring at $m/z = 14n + 1$, which is accompanied by C_nH_{2n} and C_nH_{2n-1} fragments. The most abundant fragments are C₂ and C₄.^[81] Acyclic alkanes similarly to saturated hydrocarbons are characterized by clusters of peaks at intervals of 14 units. In these clusters the C_nH_{2n-1} and C_nH_{2n} peaks are more intense than the C_nH_{2n+1} peaks. In the case of aromatic molecules, the aromatic ring in a molecule stabilizes the molecular ion peak and M + 1 and M + 2 species of sufficiently large intensity in EI are generated.

Many reports on the characterization of environmental petroleum samples (UCM) are found in literature concerning hydrocarbons analyses with GC-EI-MS systems.^[101,102] Aliphatic hydrocarbons fragment heavily upon EI ionization, resulting in many smaller fragments, although indistinguishable. Consequently, high volatile alkanes do not yield significantly different mass spectra from branched isomers.

1.1.5.3.2 GC-APCI-MS

The atmospheric pressure chemical ionization (APCI) was introduced by Horning in the mid-1970s as an interference between high-performance liquid chromatography and MS.^[103] APCI is mainly applied to non-polar compounds and low molecular weights up to about 1500 Da. Such an ionization technique has been used in direct infusion experiments for petroleomic analyses^[104-106] and only limited experimental data are available for detection of

n-alkanes.^[90,107] The group of Karasek investigated *n*-alkyl halides^[108] and *n*-alkanes (C₅H₁₂–C₁₅H₃₂)^[109] using β -ionization. The obtained spectra of alkyl halides [RX]⁺ were attributed to formed alkyl backbones. The most abundant ions were assigned to [R-1]⁺ ions formed by hydrogen abstraction. Using APCI-MS with ⁶³Ni ionization, the most abundant ions turned out to be [M-3]⁺ and [(M-3)+H₂O]⁺.^[90] In the case of polyaromatic hydrocarbons, the protonated species were generated instead.^[110,111] Recently, APCI coupled to liquid chromatography have been applied to study aromatic hydrocarbons,^[103,112] linear and branched hydrocarbons.^[113] The spectra of the last showed the presence of [M-H]⁺ ions without fragmentations. Highly branched alkanes produced [M-H]⁺ as the most abundant ions, while highly unsaturated hydrocarbons yielded mostly [M+H]⁺. APCI coupled to GC was used only a few times in the analysis of environmental samples, including tetrachlorodibenzo-*p*-dioxin,^[114] tetrachlorodibenzofuran,^[115] nitro-polycyclic aromatic hydrocarbons (nitro-PAH),^[116] amino-PAH^[117] and pesticides.^[118] GC-APCI-TOF-MS has been employed only for metabolomic,^[119] pharmaceutical research^[120] and food material analysis.^[121]

Parallel to this work the investigation of the LSW fraction using APCI-methods was carried out by Kuhnert *et al.*^[122] Initially, different *n*-alkanes standards were injected into the MS instrument as a direct infusion. Next, the light shredder waste fraction was measured as a direct infusion using an optimized APCI-TOF-MS method. It was noticed that a monohydrated [(M-3)+H₂O]⁺ ion was the only intact ion corresponding to each individually injected *n*-alkanes (up to C₂₀). In contrast, high mass *n*-alkanes (C₂₀–C₄₀) formed additionally [M]⁺ and [M-1]⁺ ions; in the range of C₃₂–C₄₀ some low intensity species formed of a composition of [M-3]⁺ were observed. Almost 1000 molecular formulas could be obtained from the APCI-TOF-MS data of the LSW fraction. The quantification of selected hydrocarbons in the waste samples was achieved.

1.2 EXPERIMENTAL SECTION

1.2.1 CHEMICALS

All chemicals (Analytical grade) were purchased from Sigma-Aldrich (Germany), except *n*-octylbenzene, *n*-nonylbenzene, *n*-tetradecylbenzene, *n*-octadecylbenzene, *n*-octadecylcyclohexane, *n*-tetradecylcyclohexane, 2,6-dimethyldecane, 2,6,10,14-tetramethyl nonadecane and 2,6,10,14,18-pentamethylheneicosane, which were received from Chiron (Norway). The light shredder waste fraction was supplied by the Bremer Entsorgungsbetriebe (BEB) company in Bremen (Germany).

1.2.2 SAMPLE PREPARATION

The light shredder waste fraction was air-dried for 24 hours at ambient temperature to constant weight and fractionated by sieving after crashing of agglomerates using Laboratory Mortar Grinder (Fritsch “pulverisette 2”). Particle size fractions of < 2mm were used for all experiments. Soil samples were stored at 4 °C. The Soxhlet extraction and shaking extraction were applied for the light shredder waste fraction.

Shaking extraction. 20 g of the LSW fraction was weighed in 100 mL glass flask then a mixture of 20 mL of *n*-heptane and 40 mL of acetone added. The flask was shaken on platform shaker (Innovax 3000, Fisher Scientific) at 250 rpm for 1 h at 35 °C. Different shaking periods have been tested, ranging from 1 to 3.5 h along with the temperature and shaker speed. Different extraction solvents with varied proportions were tested. Extractions were carried out in *n*-heptane, *n*-pentane and mixture of acetone and *n*-heptane in ratios: 2:1, 1:1, 5:1, 3:1.

Soxhlet extraction (System B-811 Büchi). The mass of 20 g of the LSW fraction was extracted using a 140 mL mixture of *n*-heptane:acetone (1:2, v:v) for 9 hours.

The extracts after both extractions were transferred to a separatory funnel. The acetone was removed by washing three times with 15 mL water. The *n*-heptane layer was collected in the tube. The extract was clean up using SPE system to remove polar compounds, such as lipids (Visiprep SPE Vacuum Manifolds). The SPE analysis was carried out on columns,

prepared from 10 mL plastic syringe with cotton, 2 g of an absorbent and 2 g of an anhydrous sodium sulfate. As the absorbent: silica gel 60 (0.04 mm–0.063 mm), alumina (150 mesh; pore size 58 Å), Florisil® (60–100 mesh) were used and then compared. All fractions collected were evaporated to dryness with a rotary evaporator. The residue was thus dissolved in 5 mL of *n*-heptane, before the GC and GC-MS analyses were performed. The resulting elutes directly after extraction procedures without clean up step were analyzed by gas chromatography, too.

The same sample preparation protocol was applied for analytes from the project partner in Hochschule Bremerhaven, where the light shredder waste fraction was treated in small scale reactors. The conditions applied by a collaborator are shown in Table 1.

Table 1. Conditions for analyzed samples from bioreactors in Bremerhaven

Sample		Date	Conditions			Operating time
			Temp.	Air flow	Input water	
1.	I1	2010-12-14				
	R1.1	2010-12-14	60 °C	1.5 L/h	120 mL/d	22 days
	R2.1	2010-12-14	60 °C	1.5 L/h	120 mL/d	22 days
2.	I2	2010-12-22				
	R1.2	2010-12-22	60 °C	1.5 L/h	120 mL/d	20 days
	R2.2	2010-12-22	60 °C	3.0 L/h	120 mL/d	20 days
	R3.2	2010-12-22	60 °C	3.0 L/h	120 mL/d	20 days
3.	I3	2011-04-02				
	R1.3	2011-03-16	60 °C	3.0 L/h	120 mL/d	31 days
	R2.3	2011-03-16	60 °C	3.0 L/h	120 mL/d	22 days
	R3.3	2011-03-16	60 °C	3.0 L/h	120 mL/d	14 days
4.	R1.4	2011-04-21	60 °C	3.0 L/h	120 mL/d	2 days
	R2.4	2011-04-21	60 °C	3.0 L/h	120 mL/d	7 days
	R3.4	2011-04-21	60 °C	3.0 L/h	120 mL/d	10 days
	R4.4	2011-04-21	60 °C	3.0 L/h	120 mL/d	14 days
	R5.4	2011-04-21	60 °C	3.0 L/h	120 mL/d	16 days
5.	I5	2011-06-14				
	R1.5	2011-07-04	70 °C	3.0 L/h	120 mL/d	22 days
	R2.5	2011-07-04	70 °C	3.0 L/h	120 mL/d	22 days
	R3.5	2011-07-04	70 °C	3.0 L/h	120 mL/d	22 days

1.2.3 GC-FID

The GC analyses were performed on a GC-2010 (Shimadzu, Kyoto, Japan) instrument with a flame ionization detector and a split/splitless injector. Injector temperature was set at 290 °C and samples were injected using the autosampler (1 µL) with a split ratio of 1:10. Two different capillary columns were used, such as Rxi-5 ms (15 m × 0.25 mm, with film thickness of 0.25 µm) and Rxi-5 Sil MS (30 m × 0.25 mm, with film thickness of 0.1 µm) Restek. The temperature program was raised from 60 °C (1 min) to 300 °C at the rate 15 °C/min, and the final temperature was maintained for 23 min. A nitrogen gas was used as a carrier at a flow rate of 5 mL/min. The detector temperature was set at 310 °C. To form the flame, hydrogen gas flow, 40 mL/min, and air gas flow, 400 mL/min, were used. GC solution 2.10 software was used for data collection, and calculation of all parameters.

1.2.4 GC-EI-MS

The GC-EI-MS analyses were carried out with a Varian CP-3800 gas chromatograph (Palo Alto, CA, USA) equipped with a split/splitless injector and coupled to a Saturn 2000 ion trap Varian mass spectrometer (MS) and an Agilent gas chromatograph-mass spectrometer with PTV injector. The parameters for the latter are shown in brackets, when needed. Data acquisition in Varian GC was performed using a Star Toolbar system (Varian). In both cases, samples were injected manually with a split ratio of 1:10 at 290 (310) °C. The compounds were analyzed on a 30 m, 0.25 mm i.d. fused-silica capillary column coated with a 0.1µm layer of poly (5% phenyl/95% dimethylpolysiloxane) (Rxi-5Sil MS, Restek) and 0.5 µm (FS-Supreme-5), using helium as a carrier gas at a flow rate of 1.3 (1.2) mL/min, respectively. The oven was heated from 60 °C (1 min) to 300 °C (325 °C) at the rate 25 (18) °C/min and the final temperature was maintained for 20 (30) min. For MS, the electron multiplier was set to 1350 V to accomplish ionization by electron impact (EI). The transfer line temperature was set at 300 °C (325 °C), while temperatures 244 °C (230 °C) and 120 °C (150 °C) were used for the trap and manifold, respectively. Mass spectra were recorded from m/z 40–600. The compounds were identified by matching their GC retention times with those obtained from authentic standards analyzed under the same experimental conditions and from the comparison of their recorded mass spectra with those of the US National Institute of Standards and Technology (NIST) library.

1.2.5 GC-APCI-MS

The GC-APCI-MS analyses were carried out with an Agilent 450GC gas chromatograph equipped with a split/splitless injector and coupled to a microTOF-Q II Bruker mass spectrometer (MS). A data acquisition was performed using Bruker Daltonics software. An injector temperature was at 280 °C and 1 µL of the samples were injected using a CTC PAL autosampler with a split ratio of 1:10. Compounds were analyzed on a 30 m, 0.25 mm i.d., 0.25 µm fused-silica capillary column (HP-5, Agilent), using helium as a carrier gas at a flow rate of 1.3 mL/min. The oven temperature was raised from 40 °C (1 min) to 320 °C and the final temperature was maintained for 20 min. The ionization was accomplished by atmospheric pressure chemical ionization (APCI). The transfer line temperature was set at 300 °C. Mass spectra were recorded from m/z 50–750. The calibration was performed using an enhanced quadratic mode with a mixture of fatty acids. MS operating conditions were a nebulizer pressure of 2 bar, a corona discharge of 3000 nA, a dry gas of 3 L/min, a drying temperature of 250 °C and a vaporizer temperature of 300 °C. Molecular formulas were calculated by Bruker Data Analysis 4.0 software and subsequently exported to Excel to carry out mathematical operation, such as determination of H/C and O/C ratios or the Kendrick analysis. All graphs were created using Origin 7.5. The number of possible isomers was generated using MOLGEN (Molecular Structure Generation) program.

1.2.6 TGA

Thermogravimetric analyses were performed using a TA SDT Q600 instrument. The temperature was increased from 25 to 800 °C at the rate of 5 and 10 °C/min under a nitrogen atmosphere.

1.2.7 INFRARED (IR) SPECTROSCOPY

Infrared spectra were recorded using neat materials on a Bruker, Vector 33 spectrometer. IR absorptions are given in wavenumbers (cm^{-1}).

1.2.8 ^1H NMR

^1H NMR spectra were recorded on a JEOL ECX-400 spectrometer operating at 400 MHz, at room temperature in D_2O , using a 5 mm probe. The chemical shifts (δ) are reported in parts per million (ppm).

1.3 THE AIM OF THE STUDY (I)

The main aim of this study is to unravel the chemical composition of two complex mixtures, including the unresolved complex mixture (UCM) of the light shredder waste fraction and dietary material, namely caramel. Both materials belong to the most challenging tasks in modern analytical chemistry due to their extreme complexities.

The first part considers the characterization of environmental samples of the light shredder waste fraction possessing the UCM in gas chromatography. More importantly, the UCM is analyzed in order to find out if such a mixture is consisted of only hydrocarbons or more classes of compounds. Therefore, the new analytical GC (GC/MS) methods along with sample preparation and extraction procedure need to be developed. The study also involves the quantitative analysis of hydrocarbons to gain information on the concentration of contaminants, which are legally regulated. For the GC/MS method, both ionization techniques, namely electron impact (EI) and atmospheric pressure chemical ionization (APCI) are investigated. The efforts to develop more accurate method for hydrocarbons determination are taken to estimate the suitability of the KW/04 method.

1.4 RESULTS AND DISCUSSION

1.4.1 THE LIGHT SHREDDER WASTE FRACTION SAMPLE PREPERATION AND EXTRACTION METHOD OPTIMAZATION

The analysis of the light shredder waste fraction by gas chromatography requires firstly the preparation of the sample. The effect of drying and grinding of the light shredder waste fraction has been investigated. They showed an important impact on GC chromatographic profile and hydrocarbons concentrations. Subsampling variability is lower in dry than in wet soil, due to the greater homogeneity. The preparation of a homogenized material significantly influences on the recovery of hydrocarbons. Storage of the LSW fraction samples at proper temperatures has affected their stability.

Secondly, the extraction procedures, such as shaking and Soxhlet have been investigated. Gas chromatography with a flame ionization detector (GC-FID) was used to analyze all extracts after both extraction procedures. The investigations of shaking extraction parameters started with the evaluation of shaking parameters for the LSW fraction samples, such as different speed and time. The GC analyses of the waste extracts showed that shaker parameters did not influence the GC results. The choice of solvent (*n*-pentane, *n*-heptane, acetone/*n*-heptane in different proportions) was essential in order to develop a proper extraction protocol. Shaking with *n*-heptane/acetone (1:2, v/v) turned out to be the most effective method; whereas the use of *n*-pentane met with failure. The subsequent clean up of the extracts was performed by a solid phase extraction (SPE) to minimize the amount of polar compounds. In fact, the reduced amount of interferences was observed. Dark extracts, obtained after both Soxhlet and shaking extractions became colorless after the clean up procedure. Subsequently, well-known sorbents, such as silica, alumina and Florisil were tested. The type of an adsorbent was found to be a key factor. It must be noted here that Florisil and alumina tubes with Na₂SO₄ gave an acceptable reduction of the amount of interferences; whereas silica was insufficient. The shaking extraction of dried and grounded soil samples in a mixture of *n*-heptane:acetone (1:2, v:v) after shaking at 175 rpm for 1 h at 35 °C and solid phase extraction with Florisil provided the best separation of the peaks. This method was further applied for all experiments,

including the quantitative analysis in GC. Figure 6 illustrates the GC chromatogram of the light shredder waste fraction under the optimized shaking extraction conditions.

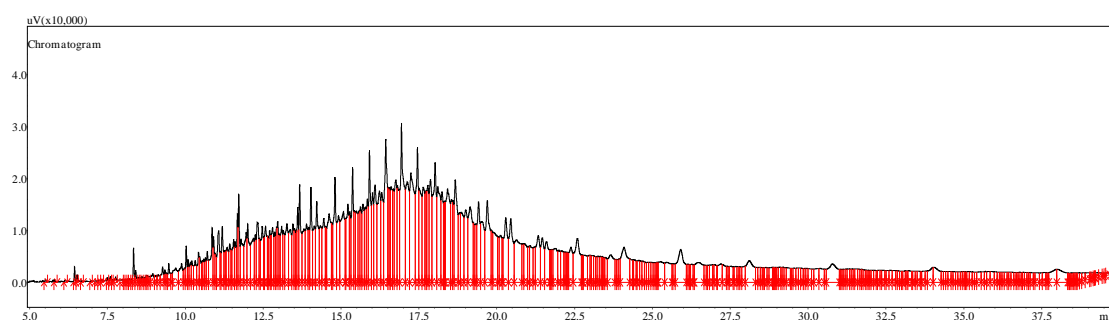


Figure 6. Integrated GC-FID chromatogram of the light shredder waste fraction after the shaking extraction (175 rpm, 1 h, 35 °C, *n*-heptane:acetone (1:2, v:v) as the solvent, SPE with Florisil)

In the case of Soxhlet extraction, *n*-heptane and *n*-hexane were tested as a solvent with different number of cycles: 5 and 10, respectively. Finally, the mixture of *n*-heptane:acetone (1:2, v:v) was used. The required volume of the corresponding solvent was calculated according to the shaking extraction. The heating parameters based on boiling points of exploited solvents were thus chosen. After nine hours of extraction, the extracts have been treated in the same way like after the shaking extraction*. The UCM profiles after shaking and Soxhlet extractions were the same. The most visible differences in the GC chromatograms were observed in the intensity of the hump and the height of well-resolved peaks. The chromatograms indicated that the peak heights achieved from the Soxhlet extraction were higher than those for shaking extraction (Figure 7).

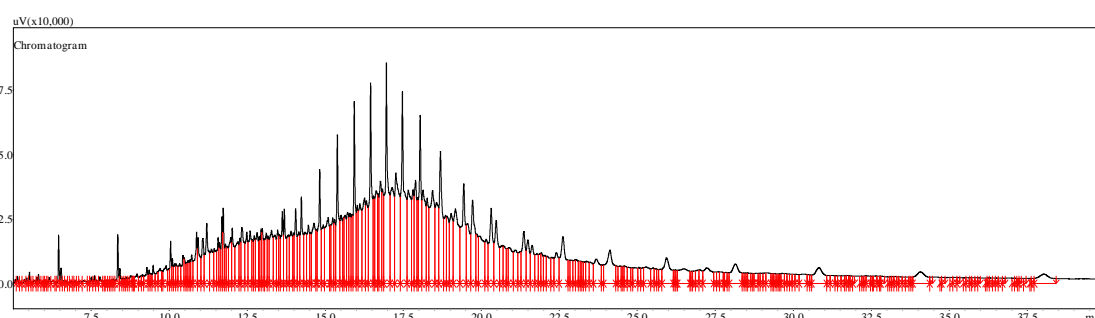


Figure 7. Integrated GC-FID chromatogram of the light shredder waste fraction after the Soxhlet extraction (9 h, *n*-heptane:acetone (1:2, v:v), SPE with Florisil)

* Washed three times with water and cleaned using solid phase extraction (SPE)

The Soxhlet and shaking extraction procedures have been compared, as shown in Table 2. The comparison is performed in terms of costs, time, recovery and efficiency. The peak areas after Soxhlet extraction procedure are two times larger than after shaking. Particularly, higher amount of solvent, and a specialized instrument is needed for the Soxhlet extraction. In term of time, around 6–9 h was used for the Soxhlet extraction, while for shaking 1 h. In the case of Soxhlet extraction, 4 samples can be extracted simultaneously. The recovery of the shaking extraction was calculated to be 60%, while for the Soxhlet extraction is 75%. As a result, the Soxhlet extraction proved to be the best choice. The calculation of the recovery of extraction procedures will be discussed later*.

Table 2. Comparing of shaking and Soxhlet extractions

Parameters	Shaking extraction	Soxhlet extraction
Costs	+	-
Time	+	-
Recovery	60%	75%
Efficiency	-	+

* See on page 24

1.4.2 GC-FID METHOD DEVELOPMENT AND OPTIMIZATION

Gas chromatography with the flame ionization detection (GC-FID) is a routine analytical technique for hydrocarbons determination. The method development for the assay of hydrocarbons was based on their physico-chemical properties. As, hydrocarbons being non-polar molecules, the capillary columns coated with a 5% diphenyl/95% dimethylpolysiloxane and a silarylene phase were therefore chosen for the separation. Due to the better efficiency and improved peak separations, capillary columns instead of packed columns were used. The fact that some aromatic components were expected in analyzed samples low polarity columns with phenyl groups in a stationary phase were employed instead of non-polar. Columns with 0.25 μm and 0.1 μm film thicknesses were chosen. The 0.25 μm worked well for most samples and thin film 0.1 μm is available for components eluted at higher temperatures. The 0.25 mm of inner diameter of the column is suitable for the analysis of hydrocarbons. The injection port and detector temperatures were set to 290 and 310 $^{\circ}\text{C}$, respectively. For high-boiling compounds is recommended to use an injector temperature of 275–300 $^{\circ}\text{C}$. It was important to check if a septum can tolerate the high injector temperature. The split mode was chosen with a split ratio of 1:10. Linear velocity was set to 25 cm/sec to ensure a nitrogen flow of 11.6 mL/min. Hydrogen and helium could provide better resolution in the shorter period of time. Nevertheless, nitrogen gave good resolution of the peaks in longer, yet still acceptable analysis time. Different temperature programs were investigated for a GC oven. At the end of this examination, the isothermal temperature program with a run time of 40 min was as follows: initial temperature 60 $^{\circ}\text{C}$ held for 1.0 min, then increased to 300 $^{\circ}\text{C}$ at a rate of 15 $^{\circ}\text{C}/\text{min}$ and kept for 23 min. The initial temperature was found to be ideal to start the separation of the compound of interest. Different temperature ramp rates were considered from 15, 25 to 35 $^{\circ}\text{C}/\text{min}$. As an optimum, 15 $^{\circ}\text{C}/\text{min}$ was chosen as a compromise between the time of analysis and the shape of peaks. It has been noticed that faster temperature rate caused shorter time of the analysis, although the bordering of the last eluting peaks was observed, which is undesirable. Final 23 min hold time was required to elute all compounds until *n*-tetracontane. An optimization of GC parameters was performed applying *n*-alkanes as a standard mixture. The objective of the method development has achieved the satisfactory separation, peaks width and fulfils the required value of the peak area ratio of *n*-tetracontane to *n*-eicosane. As defined in KW/04, the peak area ratio of *n*-tetracontane to *n*-eicosane should be higher than 0.8. The peak area ratio of C40/C20 was estimated to be about 0.86–1.1, which

is above the required value of 0.8. The retention time of *n*-tetracontane was approximately 38 min with a good peak shape and subsequently no further optimization of such a method was required. The typical chromatogram obtained with *n*-alkanes standard mixture is shown in Figure 8.

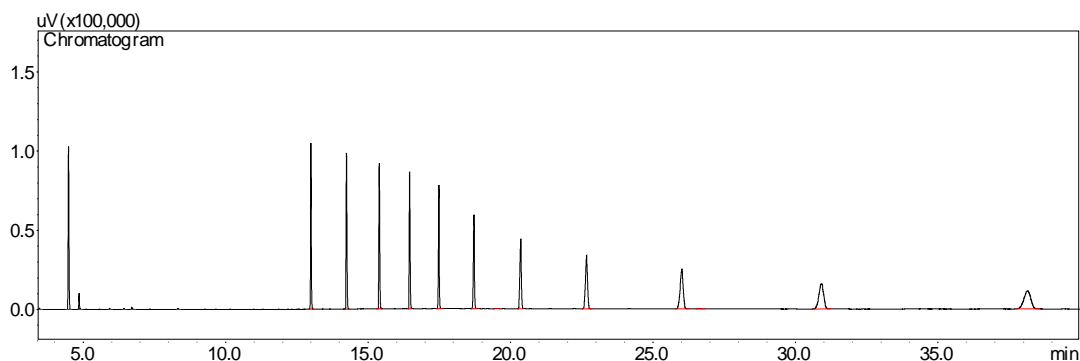


Figure 8. GC-FID chromatogram of $C_{10}H_{22}$, $C_{20}H_{42}$ – $C_{40}H_{82}$ even *n*-alkanes standard mixture

For most GC measurements, a comparison of retention times of an unknown sample with the standard usually performs the peak identification. After the optimization of the parameters for the standard mixture, the same method has been applied for the analysis of the light shredder waste fraction. The resulting chromatograms were integrated using a straight line, between retention times of $C_{10}H_{22}$ and $C_{40}H_{82}$, as defined in KW/04. Figure 9 illustrates the overlap of two chromatograms of the light shredder waste fraction sample with C_7H_{16} – $C_{40}H_{82}$ *n*-alkanes standard mixture. Peaks of the waste samples with the highest intensity correspond to *n*-alkanes from interest range, which was also confirmed by GC-MS.

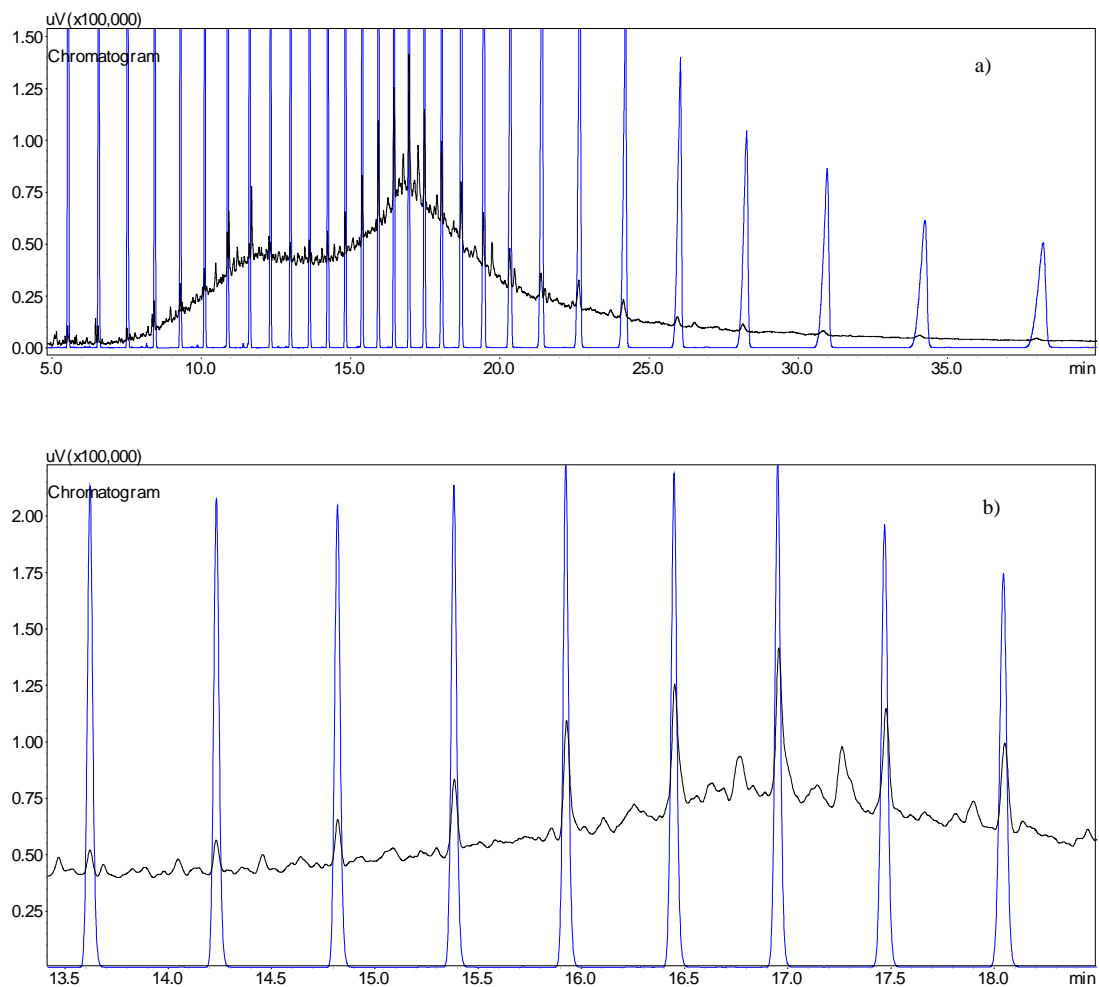


Figure 9. a) Overlap of GC-FID chromatograms of the light shredder waste fraction (black) and C_7H_{16} – $C_{40}H_{82}$ *n*-alkanes standard (blue), b) Fragment of two overlapping chromatograms of the light shredder waste fraction sample with $C_{20}H_{42}$ – $C_{28}H_{48}$ *n*-alkanes standard

1.4.3 QUANTIFICATION OF THE LIGHT SHREDDER WASTE FRACTION

The quantitative analyses have been initiated by generation of the calibration curves for *n*-alkanes from the range of $C_{20}H_{42}$ – $C_{40}H_{82}$. The calibration curves were generated by plotting peaks areas of C_7 – C_{40} *n*-alkanes standard mixture as a function of concentration. In doing so, *n*-alkanes C_7 – C_{40} standard solution (1000 mg/L) was diluted with *n*-heptane to a series of standards with concentrations of 5, 50, 100, 333, 250, 750 and 500 mg/L. The calculated concentrations for *n*-alkanes from the range of $C_{20}H_{42}$ – $C_{40}H_{82}$ are shown in Table 3. The total

concentration of these *n*-alkanes in the light shredder waste fraction resulted in 568 mg/kg assuming 100% recovery of the extraction procedure. The accomplished results for the waste samples are still below the HCs guideline value, due to the presence of only unbranched alkanes excluding the rest of compounds in the hump. The analytical recovery experiments were performed by adding the known amount of pure hydrocarbons to pre-analyzed samples before extraction procedures. The mass of 20 g of the light shredder waste fraction samples were mixed with 5 and 7.5 mg of *n*-eicosane, *n*-tricosane and *n*-hexatriacontane, then shaken and extracted according to the aforementioned procedure. The experiment was repeated three times for two concentration levels. The percentage of the recovery values was calculated by comparing the obtained concentrations from the waste samples with and without added hydrocarbons. The calculated recovery was above 60% for shaking and 75% for Soxhlet extraction.

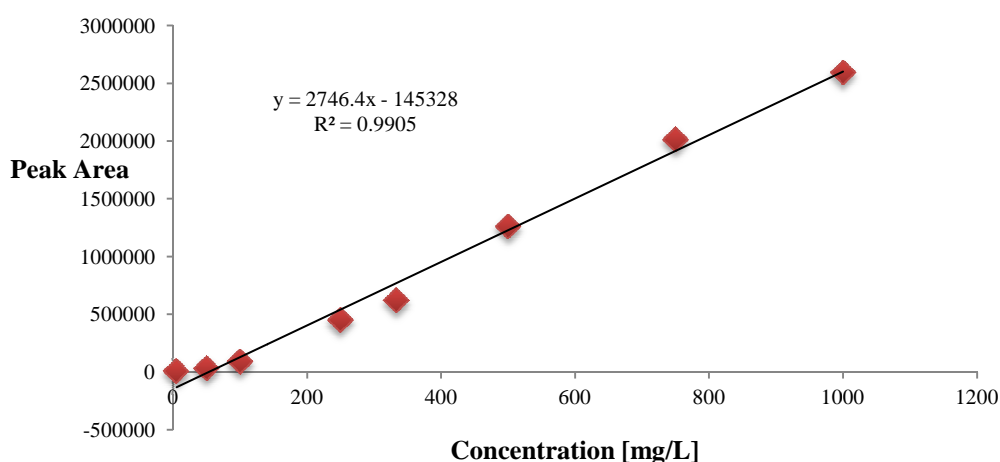


Figure 10. The calibration curve for *n*-triacontane

An isotope dilution experiment with selected polydeuterated *n*-alkane $C_{32}D_{66}$ was performed by Kuhnert *et al.* using APCI method, and a linear response was found. It allows the adequate quantification of single *n*-alkanes or groups of *n*-alkanes in the mixture.

Table 3. Calculated concentrations of *n*-alkanes in the range C₂₀H₄₂–C₄₀H₈₂ of the light shredder waste fraction

Compound	Area 1 ^a	Conc 1 [mg/L] ^a	Area 2 ^b	Conc 2 [mg/L] ^b
C ₂₀ H ₄₂	110423.7	105.2202	112920.8	106.1434
C ₂₁ H ₄₄	129131.6	111.5375	73325.6	90.1016
C ₂₂ H ₄₆	122798.3	108.9402	124891.5	109.7520
C ₂₃ H ₄₈	135572.8	112.1602	90017.3	94.6772
C ₂₄ H ₅₀	182722.0	124.7595	173366.6	121.1885
C ₂₅ H ₅₂	156396.4	114.9369	255479.0	152.0243
C ₂₆ H ₅₄	267218.8	153.3557	245654.7	145.4942
C ₂₇ H ₅₆	250582.6	146.6271	297761.2	164.1130
C ₂₈ H ₅₈	185830.7	121.9665	280354.9	156.7769
C ₂₉ H ₆₀	187587.0	123.2538	179545.1	120.2175
C ₃₀ H ₆₂	193954.4	123.5371	211239.5	129.8309
C ₃₁ H ₆₄	126289.0	99.54783	161058.4	112.5089
C ₃₂ H ₆₆	144691.3	106.5795	148152.1	107.8574
C ₃₃ H ₆₈	86791.4	85.60983	89668.9	86.6766
C ₃₄ H ₇₀	145483.4	108.9484	145946.9	109.1230
C ₃₅ H ₇₂	128377.1	101.3943	164833.1	115.3429
C ₃₆ H ₇₄	93973.6	89.83625	96829.0	90.9053
C ₃₇ H ₇₆	78221.8	85.86892	66707.0	81.1931
C ₃₈ H ₇₈	80020.8	86.31431	66198.5	80.7558
C ₃₉ H ₈₀	58511.1	80.35061	47897.7	75.6997
C ₄₀ H ₈₂	53106.6	79.67197	51903.0	79.1430
Total		2270.417		2329.525

^a Peak area and calculated concentration after one extraction; ^b Peak area and calculated concentration after second extraction

1.4.4 GC METHOD VALIDATION

The GC method has been validated in terms of suitability, specificity, linearity, intra and interday precision, limits of detection and quantification.^[123]

1.4.4.1 Suitability

Factors, such as the peak resolution, number of theoretical plates, peak tailing and capacity have been measured to determine the suitability of the used method. Generally, an acceptable limit for the peak resolution is ≥ 2.0 . A peak resolution was detected ranging from 9.4–13 according to the optimized method. The number of theoretical plates (N) should be ≥ 2000 . The peak tailing factor (TF) can be in the range of 0.5–2.0. Commonly, the value of a capacity factor (k') is > 2 . The aforementioned parameters in the appropriate ranges are shown in Table 4.

Table 4. Suitability of the GC method

Compound	Resolution	N	Tailing F.	k'
$C_{20}H_{42}$	13.685	1101499.396	1.112	9.666
$C_{21}H_{44}$	13.006	1233718.865	1.101	10.191
$C_{22}H_{46}$	12.495	1348459.288	1.111	10.693
$C_{23}H_{48}$	11.992	1453608.840	1.084	11.176
$C_{24}H_{50}$	11.419	1532402.949	1.106	11.638
$C_{25}H_{52}$	11.077	1727944.321	1.102	12.084
$C_{26}H_{54}$	10.527	1656163.462	1.104	12.513
$C_{27}H_{56}$	9.918	1790724.632	1.099	12.927
$C_{28}H_{58}$	9.832	1623718.036	1.068	13.352
$C_{29}H_{60}$	9.750	1311110.599	1.053	13.822
$C_{30}H_{62}$	9.865	1170125.115	1.031	14.356
$C_{31}H_{64}$	9.896	884337.087	1.010	14.972
$C_{32}H_{66}$	9.958	733655.766	0.964	15.696
$C_{33}H_{68}$	10.098	570948.713	0.907	16.557
$C_{34}H_{70}$	10.268	476191.607	0.930	17.585
$C_{35}H_{72}$	9.980	316212.032	0.925	18.818
$C_{36}H_{74}$	9.914	271890.102	0.849	20.324
$C_{37}H_{76}$	9.733	194213.476	0.837	22.137
$C_{38}H_{78}$	9.448	154729.164	0.817	24.341
$C_{39}H_{80}$	9.664	142890.988	0.795	27.011
$C_{40}H_{82}$	9.560	106437.344	0.802	30.251

1.4.4.2 Specificity

The specificity of the method has been evaluated by recording chromatograms of the analytical standard of *n*-alkanes C7–C40 in *n*-heptane on two different columns (Rxi-5 MS and Rxi-5Sil MS) at the same chromatographic conditions. The analysis on Rxi-5Sil MS column gave a minutely better resolution of the peaks. Different retention times of particular hydrocarbons on two tested columns confirmed the identity of such peaks.

1.4.4.3 Linearity

The linearity has been studied by plotting the standard peak area *versus* concentrations of *n*-alkanes C7–C40 standard mixture. Eight standard concentration levels that cover the expected working range were prepared between concentrations 5–1000 mg/L. The constructed calibration curves were then evaluated by their correlation coefficients. The calibration equations for compounds C₂₀H₄₂–C₄₀H₈₂ demonstrate the linearity of the method. The correlation coefficients for *n*-alkanes (from *n*-eicosane to *n*-tetracontane) possessed the R² value higher than 0.98 or 0.99 for all compounds. The calibration equations and correlation coefficients are shown in Table 5.

1.4.4.4 Limits of detection and quantification

The limits of detection (LOD) and limits of quantitation (LOQ) have been evaluated by serial dilutions of *n*-alkanes standard mixtures in order to obtain signal to noise ratios of 3:1 for LOD and 10:1 for LOQ. LOD values for analytes were found to be 1 mg/L for C20–C35 and 2.5 mg/L for C35–C40; whereas the LOQ values 3 mg/L for C20–C35 and 7.5 mg/L for C35–C40 (Table 5). As a result, LOQ and LOD values proved that the method is well suited.

Table 5. Linearity, LODs, LOQs

Compound	Calibration equation	R ² ^a	LOD [mg/L]	LOQ [mg/L]
C ₂₀ H ₄₂	y=2705x-174197	0.9841	1	3
C ₂₁ H ₄₄	y=2603.4x-161245	0.9844	1	3
C ₂₂ H ₄₆	y=2578.6x-158115	0.9857	1	3
C ₂₃ H ₄₈	y=2605.7x-156683	0.9872	1	3
C ₂₄ H ₅₀	y=2619.8x-144123	0.9869	1	3
C ₂₅ H ₅₂	y=2671.6x-150669	0.9880	1	3
C ₂₆ H ₅₄	y=2743x-153436	0.9893	1	3
C ₂₇ H ₅₆	y=2698.1x-145032	0.9899	1	3
C ₂₈ H ₅₈	y=2715.4x-145357	0.9899	1	3
C ₂₉ H ₆₀	y=2648.6x-138863	0.9906	1	3
C ₃₀ H ₆₂	y=2746.4x-145328	0.9905	1	3
C ₃₁ H ₆₄	y=2682.6x-140758	0.9908	1	3
C ₃₂ H ₆₆	y=2708.3x-143958	0.9912	1	3
C ₃₃ H ₆₈	y=2697.3x-144124	0.9913	1	3
C ₃₄ H ₇₀	y=2654.6x-143731	0.9915	1	3
C ₃₅ H ₇₂	y=2613.6x-136627	0.9927	2.5	7.5
C ₃₆ H ₇₄	y=2671.1x-145988	0.9919	2.5	7.5
C ₃₇ H ₇₆	y=2462.6x-133239	0.9922	2.5	7.5
C ₃₈ H ₇₈	y=2486.7x-134617	0.9922	2.5	7.5
C ₃₉ H ₈₀	y=2282x-124849	0.9916	2.5	7.5
C ₄₀ H ₈₂	y=2275.4x-128179	0.9908	2.5	7.5

^a Correlation coefficient

1.4.4.5 Precision

The precision, expressed as a relative standard deviation (RSD) has been estimated by performing intraday and interday precision studies for the standard and the waste samples. *n*-Alkanes standard mixtures were analyzed daily for four days. The reproducibility of retention times were excellent, with standard deviation of < 0.18 %RSD, where peak areas were observed between 2.2–5.7%. Next, the extracted light shredder waste fraction sample was regularly analyzed for five days and five times a day. The reproducibilities of Rt and peak areas were certainly good with acceptable values, shown in Tables A1, A2 (Appendix)*. Moreover, the light shredder waste fraction after different extraction procedures, performed within five days were investigated and the data for the peak area reproducibility are listed in Table 6. The RSDs were calculated to be in the range of 5.7–28.7% for straight-chain alkanes (C₂₀H₄₂–C₄₀H₈₂), which are good for complex mixture samples.

* See on page 149

Table 6. Reproducibility of peak areas of the light shredder waste fraction (interday)

Compound	P. area 1	P. area 2	P. area 3	P. area 4	P. area 5	Mean	SD ^a	RSD[%] ^b
C ₂₀ H ₄₂	52039.9	29036.5	23613.5	45981.7	33693.9	36873.1	10586.17	28.7
C ₂₁ H ₄₄	60458.0	59419.3	28715.0	45821.8	43096.9	47502.2	11705.21	24.6
C ₂₂ H ₄₆	81340.6	77830.2	50485.9	68726.4	79705.2	71617.66	11431.97	16.0
C ₂₃ H ₄₈	93397.1	86971.5	66893.7	77196.4	99266.3	84745.0	11544.13	13.6
C ₂₄ H ₅₀	119404.2	100412.0	60010.2	80086.6	108540.7	93690.7	21195.90	22.6
C ₂₅ H ₅₂	122198.6	104439.3	75152.0	89002.9	103808.0	98920.2	15871.45	16.1
C ₂₆ H ₅₄	159792.9	158416.0	100126.8	161766.9	157410.5	147502.6	23732.92	16.1
C ₂₇ H ₅₆	253493.8	195431.6	173812.7	179808.0	252036.3	210916.5	34893.77	16.5
C ₂₈ H ₅₈	136880.5	123548.8	100767.9	99514.7	129703.5	118083.1	15250.26	12.9
C ₂₉ H ₆₀	127723.7	152884.9	89127.5	104446.9	119107.6	118658.1	21577.19	18.2
C ₃₀ H ₆₂	150406.8	130491.5	107074.7	117456.8	125778.2	126241.6	14469.11	11.5
C ₃₁ H ₆₄	86430.9	88059.6	65016.3	69480.9	75944.6	76986.5	9083.12	11.8
C ₃₂ H ₆₆	90706.6	84008.4	82316.9	89895.3	104188.4	90223.1	7700.67	8.5
C ₃₃ H ₆₈	68251.2	73317.9	63503.8	64343.4	63437.8	66570.8	3808.69	5.7
C ₃₄ H ₇₀	96322.6	100700.7	76569.9	99119.5	99129.3	94368.4	9010.47	9.6
C ₃₅ H ₇₂	100159.2	102303.3	105496.0	171512.4	132386.7	122371.5	27188.36	22.2
C ₃₆ H ₇₄	91359.7	82955.5	68462.2	78485.6	104228.7	85098.34	12085.17	14.2
C ₃₇ H ₇₆	90886.1	77973.9	77080.6	89227.9	84730.5	83979.8	5647.53	6.7
C ₃₈ H ₇₈	76034.1	59960.8	70777.1	73146.4	68825.7	69748.8	5454.60	7.8
C ₃₉ H ₈₀	84636.5	68774.6	54527.9	70949.1	66715.9	69120.8	9622.22	13.9
C ₄₀ H ₈₂	73776.6	56939.2	71192.1	76784.9	84801.6	72698.9	9110.11	12.5
Total	2215700.0	2013876.0	1610723.0	1952755.0	2136536.0			

^a Standard deviation; ^b Relative standard deviation

1.4.4.6 Stability of samples

The stability of prepared samples has been evaluated during five days, which is actually enough for testing environmental samples in the routine analyses. A sample was injected at 5 different days and the obtained results gave an acceptable criterion for RSD% for constituents. As a consequence, prepared samples, kept at 4 °C are stable at least for five days after a completion of the sample extraction.

1.4.5 GC-EI-MS

1.4.5.1 GC-EI-MS of *n*-alkanes standard and the light shredder waste fraction

After the GC-FID study, gas chromatographs coupled to mass spectrometers were applied to investigate the composition of the UCM of the light shredder waste fraction. Firstly, the *n*-alkanes standard was analyzed by GC-EI-MS, and when achieving a good separation, the same method was used for the light shredder waste fraction analysis. A 30 m column instead of 15 m was applied, which is preferable for a gas chromatograph coupled to a mass spectrometer. The injector temperature and column temperature program were applied from the GC instrument. Helium was used as a carrier gas with the flow rate of 1.3 mL/min, which is recommended for high-boiling hydrocarbons. Parameters for mass spectrometer, including temperature of a transfer line, manifold and trap were set at high values due to the nature of high-boiling compounds. The complete separation of all compounds from *n*-alkanes standard mixture ranging from C_7H_{16} – $C_{40}H_{82}$ was achieved within 21 min. Profiles of the analyzed waste samples were in similarity to the obtained by the GC-FID instrument. GC-EI-MS chromatograms of overlapped *n*-alkanes standard and the light shredder waste fraction are shown in Figure 11.

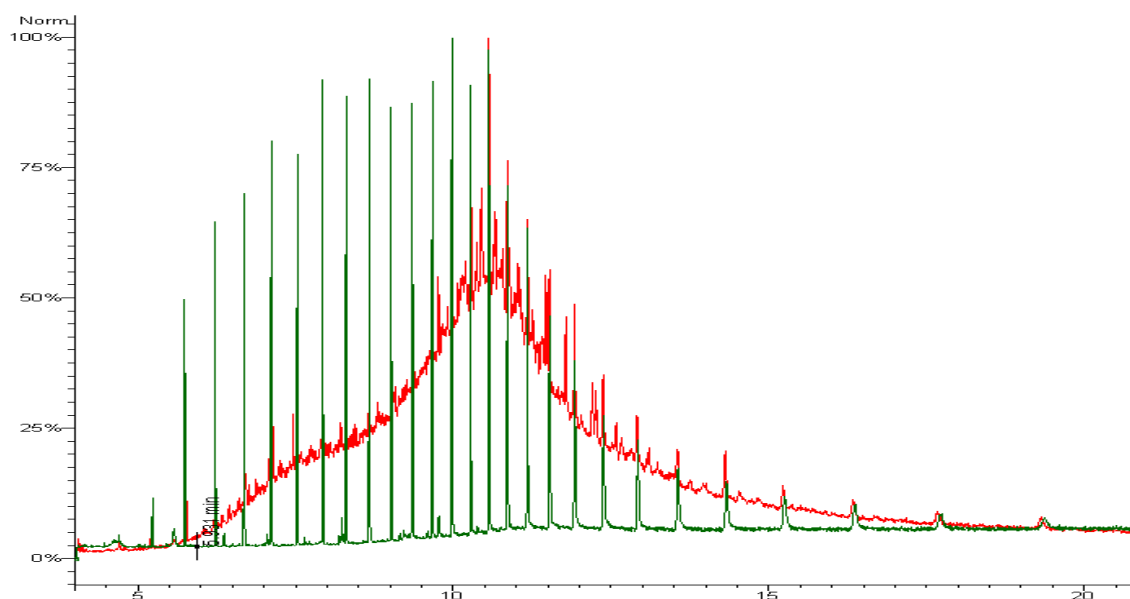
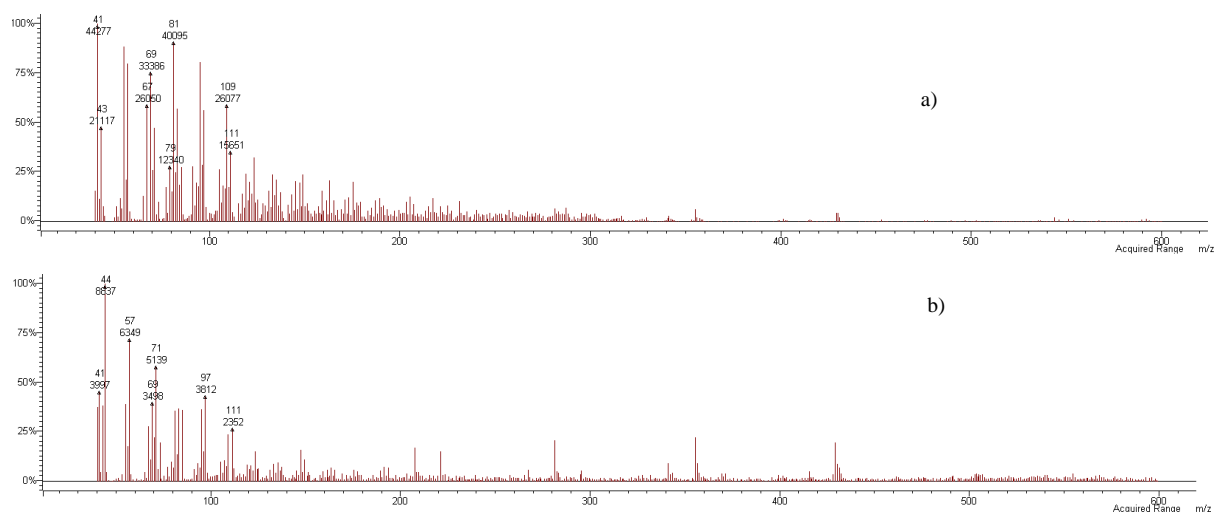


Figure 11. GC-EI-MS chromatograms (TIC) of *n*-alkanes standard (green) and the light shredder waste fraction (red)

The mass spectra were recorded in the positive ion mode in the mass range of m/z 50–600. The most of the ionization methods of neutral saturated hydrocarbons, including electron impact (EI) ionization produce an extensive fragmentation, thereby making it hard to identify individual compounds. The MS spectra of *n*-eicosane and *n*-tetracontane from GC-EI-MS experiments as examples are shown in Figure 12.



fact, some of PCBs and PAHs were successfully found. The mixture of 16 PAHs: naphthalene (**1**), acenaphthylene (**2**), acenaphthene (**3**), fluorene (**4**), phenanthrene (**5**), anthracene (**6**), fluoranthene (**7**), pyrene (**8**), benzo[a]anthracene (**9**), chrysene (**10**), benzo[b]fluoroanthene (**11**), benzo[k]fluoroanthene (**12**), benzo[a]pyrene (**13**), indeno[1.2.3-cd]pyrene (**14**), dibenzo[a,h]anthracene (**15**) and benzo[ghi]perylene (**16**) has been analyzed and first eight of them were detected (Figure 13).

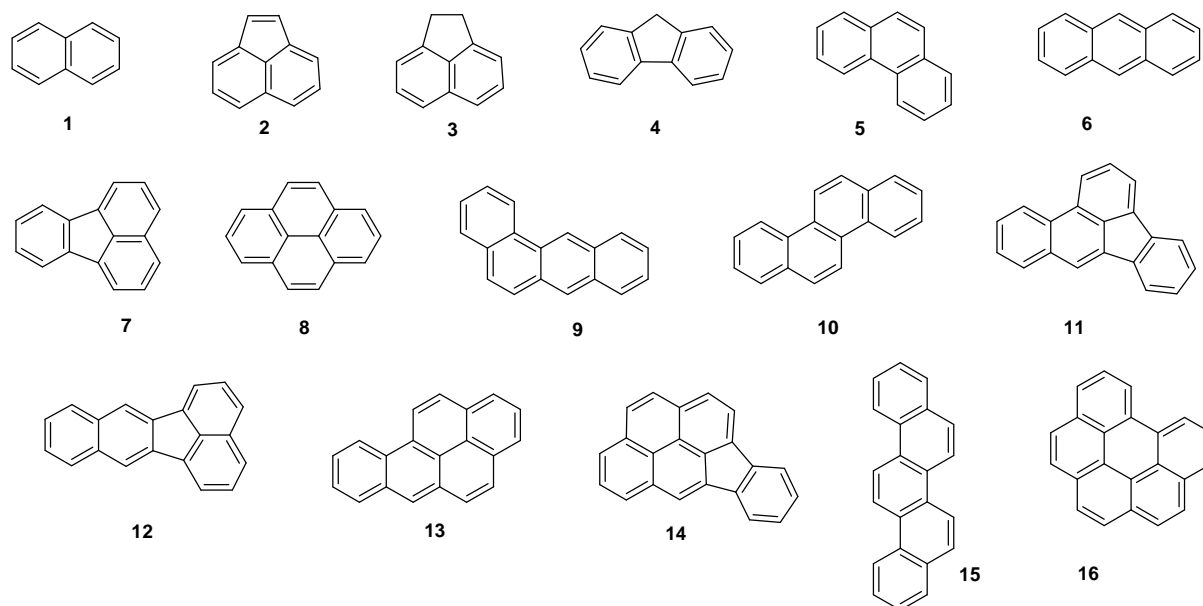


Figure 13. Analyzed PAHs (polyaromatic hydrocarbons)

PCBs standard containing tri-, tetra-, penta-, hexa-, hepta- and octa-biphenyls have been measured by GC-EI-MS and eleven out of twelve components were found in the waste samples. In particular, the standard mixture includes: 2,2',3,4,4',5,5'-heptachlorobiphenyl (**17**), 2,2',3,4,4',5'-hexachlorobiphenyl (**18**), 2,2',3,4',5',6-hexachlorobiphenyl (**19**), 2,2',4,4',5,5'-hexachlorobiphenyl (**20**), 2,2',3,3',4,4',5,5'-octachlorobiphenyl (**21**), 2,2',4,5,5'-pentachlorobiphenyl (**22**), 2,3',4,4',5-pentachlorobiphenyl (**23**), 2,2',3,5'-tetrachlorobiphenyl (**24**), 2,2',5,5'-tetrachlorobiphenyl (**25**), 2,2',5-trichlorobiphenyl (**26**), 2,4,4'-trichlorobiphenyl (**27**) and 2,4,5-trichlorobiphenyl (**28**). Analyzing three particular PCBs, namely 3,5-dichlorobiphenyl (**29**), 4,4'-dichlorobiphenyl (**30**), 2,2',3,3',4,4',5,5',6,6'-decachlorobiphenyl (**31**), where the last two were found in the LSW fraction (Figure 14).

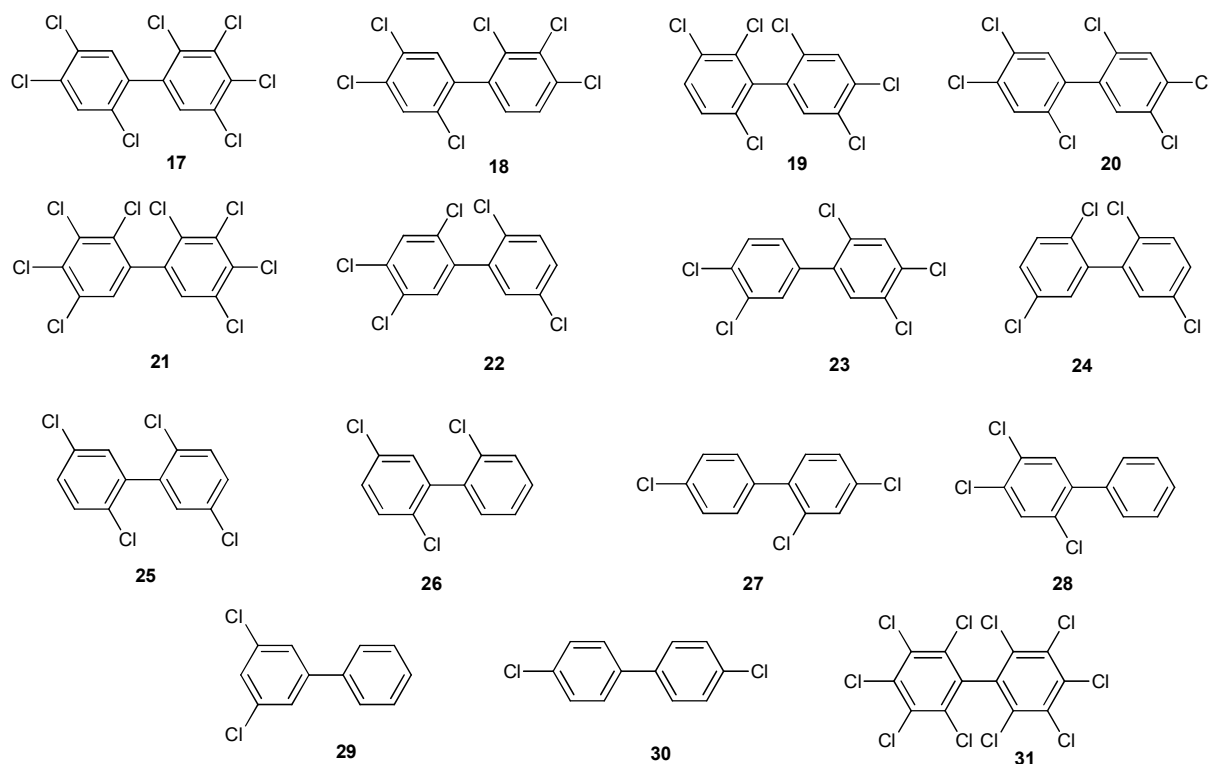


Figure 14. Analyzed PCBs (polychlorinated biphenyls)

Moreover, based on studies of mass spectra of corresponding peaks in the waste samples monochlorobiphenyl also exists with m/z of 189. All analyzed chlorobiphenyls except nona-derivatives, that should appear at m/z 464, were present in the light shredder waste fraction. Furthermore, the mass spectra of the light shredder waste fraction were studied in order to detect the presence of organochlorine pesticides, often analyzed in environmental samples, such as endrin, aldrin or dieldrin, but none of them were found.

Some reference materials, including branched alkanes, alkenes, monosubstituted benzene and cyclohexane derivatives were analyzed. A comparison of the retention times and mass spectra of the reference materials with the LSW fraction samples, was thus provided. Analyzed monoalkylated benzene derivatives, namely *n*-octylbenzene, *n*-nonylbenzene, *n*-tetradecylbenzene and *n*-octadecylbenzene were not detected in the waste samples. In the case of the branched alkanes, 2,6-dimethyldecane, 2,6,10,14-tetramethylnonadecane, 2,6,10,14,18-pentamethylheneicosane and 2,6,10,14-tetramethylhexadecane (known as phytane) were analyzed and the last-mentioned was found in the light shredder waste fraction. Subsequently, alkenes, for instance 1-ctadecene, 1-nonadecene, squalene (2,6,10,15,19,23-hexamethyltetracosane-2,6,10,14,18,22-hexene) were analyzed. The analyses of *n*-alkanes

standard mixture, PAHs, PCBs and the extracted light shredder waste fraction were performed on a second gas chromatograph with an EI ionization equipped with an enlarged library. It was possible to eventually identify 14 out of 20 *n*-alkanes in the range of $C_{20}H_{42}$ – $C_{40}H_{82}$ of the standard using the mass spectra library. The rest six compounds turned out to be straight-chain *n*-alkanes but the lack of molecular ions make it undistinguishable. These studies support the fact how difficult is to observe molecular ions of the analyzed compounds in an EI and discern even between particular *n*-alkanes. In the case of PAHs and PCBs, the identities of compounds have been confirmed with more than 98% spectra quality matches (Figure 15 - Figure 16).

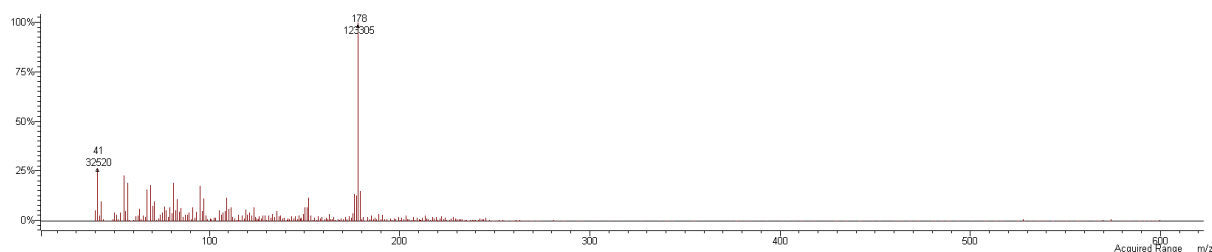


Figure 15. Mass spectrum (GC-EI-MS) of phenanthrene (**5**) from the light shredder waste fraction in the positive ion mode

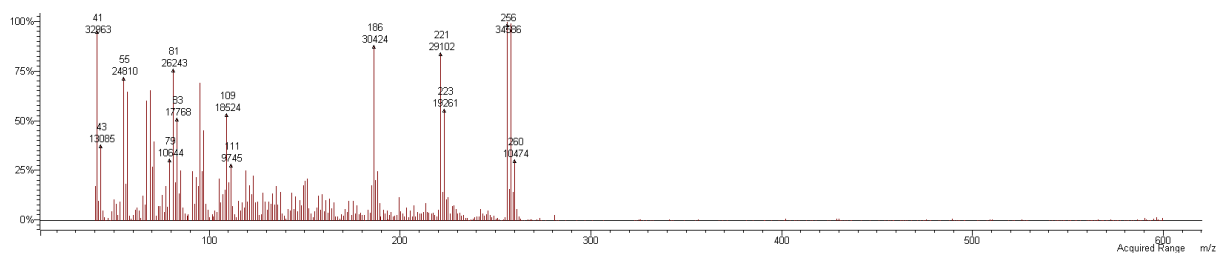


Figure 16. Mass spectrum (GC-EI-MS) of 2,2',3,4,4',5,5'-heptachlorobiphenyl (**17**) from the light shredder waste fraction in the positive ion mode

1.4.6 GC-APCI-MS

1.4.6.1 GC-APCI-MS of *n*-alkanes standard

Gas chromatography with atmospheric pressure chemical ionization coupled to time of flight mass spectrometry has been utilized to *n*-alkanes standard containing all even and odd straight-chain alkanes ranging from *n*-heptane to *n*-tetracontane. The mass spectra were recorded in the positive ion mode. *n*-Alkanes up to *n*-pentatriacontane were detected. The MS spectra of *n*-tetradecane ($C_{14}H_{30}$), *n*-eicosane ($C_{20}H_{42}$), and *n*-pentacosane ($C_{25}H_{52}$) are shown in Figure 17.

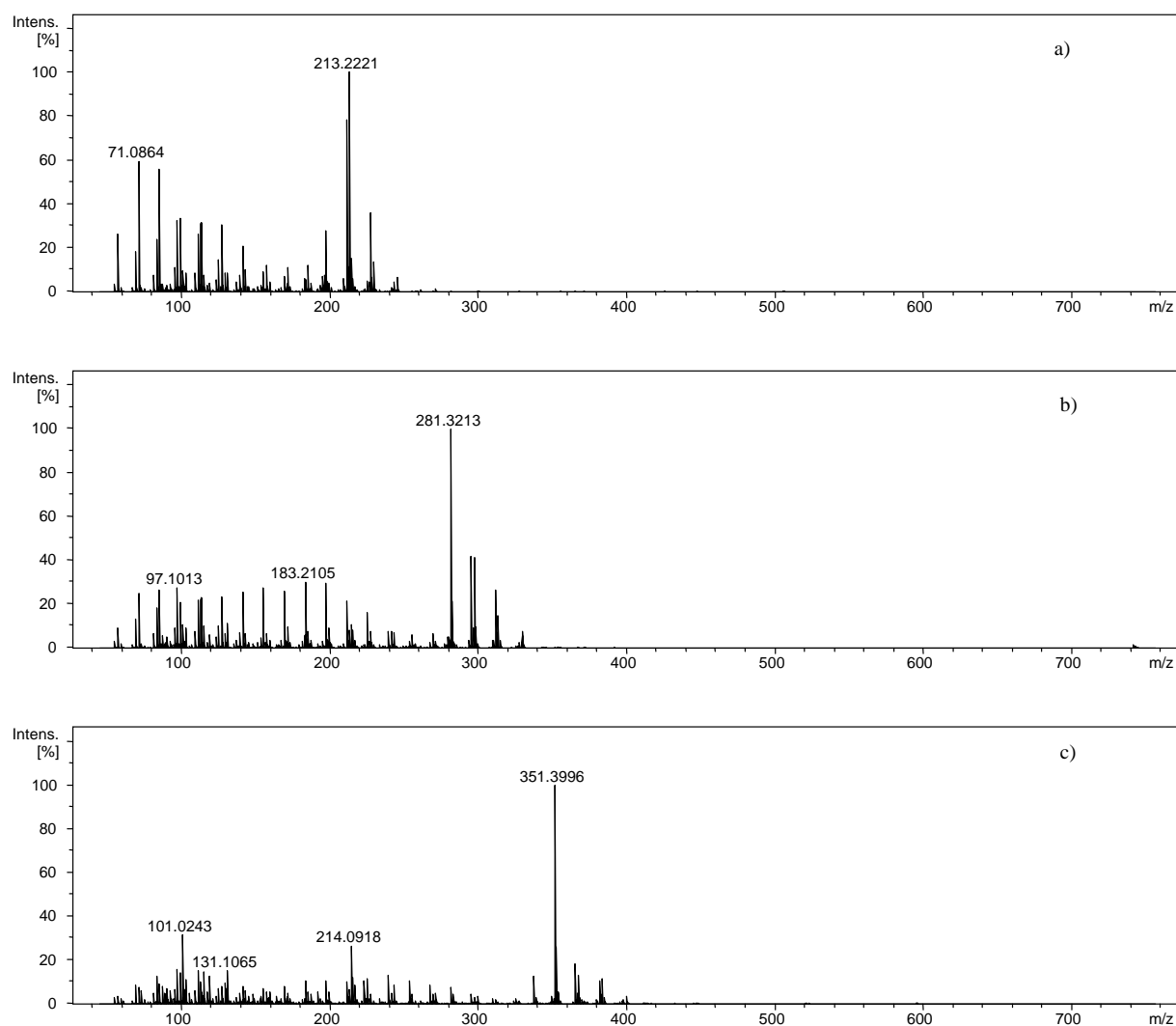


Figure 17. Mass spectra of: a) *n*-tetradecane ($C_{14}H_{30}$), b) *n*-eicosane ($C_{20}H_{42}$), and c) *n*-pentacosane ($C_{25}H_{52}$) from *n*-alkanes standard in the positive ion mode using GC-APCI-TOF-MS

The MS spectra showed the presence of monohydrated ions $[(M-3)+H_2O]^+$ as base peaks for *n*-alkanes up to *n*-nonadecane ($C_{19}H_{40}$). In contrast, mass spectra of higher *n*-alkanes exhibited $[M-1]^+$ ions as base peaks. This observation is in agreement with the results reported previously by Kuhnert *et al.*^[122] and Bell *et al.*^[90] Some low intensity species, such as $[(M-3)+H_2O]^+$ and $[M-1]^+$ were observed for earlier and further eluted *n*-alkanes, respectively. Fragment ions characteristic for *n*-alkanes as at m/z 71.1, 85.1, 127.2 were also present in low intensities in the spectra of these particular compounds. The enormous improvement has been achieved in the identification of particular *n*-alkanes. The pseudo-molecular ion peaks of hydrocarbons, including high-volatile components were observed, which was not possible using GC-EI-MS and these enabled the identification of single *n*-alkanes. Table 7 illustrates the high-resolution mass data for *n*-alkanes standard with the mass/charge ratio (m/z) of the product ions, elemental composition, mass error and retention time.

An enhanced quadratic calibration using a mixture of fatty acids as the calibrant showed to be suitable for *n*-alkanes determination. Moreover, the reference material of branched alkane, namely 2,6,10,14-tetramethylhexadecane (phytane) was analyzed. The base peak at m/z 297.3158 (-2.0 ppm) corresponding to $C_{20}H_{41}O$ $[(M-3)+H_2O]^+$ was observed in the MS spectrum, however, accompanied with ions at m/z 57.1, 71.1, 85.1, 97.1, 111.1, 125.1, 141.2, 155.2, 171.2, 185.2, 197.2, 213.2, 227.2, 241.3, 255.3, 267.3 and 281.3. Furthermore, these ions appeared as a cluster with protonated $[M+H]^+$ and deprotonated $[M-H]^+$ species. The base peak that belongs to studied analyte is present in the MS spectrum, although accompanied with fragment ions.

Table 7. High-resolution mass (GC-APCI-TOF-MS) data for *n*-alkanes standard in the positive ion mode

Peak numbering	Rt [min]	Ion formula	Experimental m/z	Theoretical m/z	Error [ppm]
1	5.94	C ₁₀ H ₂₁ O	157.1590	157.1587	-1.7
2	6.95	C ₁₁ H ₂₃ O	171.1745	171.1743	-0.7
3	7.94	C ₁₂ H ₂₅ O	185.1906	185.1900	-3.1
4	8.88	C ₁₃ H ₂₇ O	199.2060	199.2056	-2.0
5	9.77	C ₁₄ H ₂₉ O	213.2217	213.2213	-1.9
6	10.61	C ₁₅ H ₃₁ O	227.2377	227.2369	-3.4
7	11.40	C ₁₆ H ₃₃ O	241.2536	241.2526	-4.3
8	12.16	C ₁₇ H ₃₅ O	255.2692	255.2682	-3.8
9	12.88	C ₁₈ H ₃₇ O	269.2851	269.2839	-4.6
10	13.60	C ₁₉ H ₃₉ O	283.3007	283.2995	-4.1
11	14.22	C ₂₀ H ₄₁	281.3216	281.3203	-1.3
12	14.84	C ₂₁ H ₄₃	295.3371	295.3359	-3.8
13	15.50	C ₂₂ H ₄₅	309.3527	309.3516	-3.8
14	16.01	C ₂₃ H ₄₇	323.3685	323.3672	-3.9
15	16.68	C ₂₄ H ₄₉	337.3844	337.3829	-4.6
16	17.23	C ₂₅ H ₅₁	351.3998	351.3985	-3.5
17	17.70	C ₂₆ H ₅₃	365.4148	365.4142	-1.8
18	18.40	C ₂₇ H ₅₅	379.4311	379.4298	-3.3
19	18.90	C ₂₈ H ₅₇	393.4464	393.4455	-2.4
20	19.50	C ₂₉ H ₅₉	407.4619	407.4611	-1.9
21	20.40	C ₃₀ H ₆₁	421.4778	421.4768	-2.5
22	21.31	C ₃₁ H ₆₃	435.4923	435.4924	0.2
23	22.70	C ₃₂ H ₆₅	449.5080	449.5081	0.2
24	23.19	C ₃₃ H ₆₇	463.5231	463.5237	1.3
25	24.86	C ₃₄ H ₆₉	477.5397	477.5394	-0.7
26	28.23	C ₃₅ H ₇₁	491.5566	491.5550	-3.1

1.4.6.2 GC-APCI-MS of the light shredder waste fraction

After the extraction, the light shredder waste fraction was analyzed by GC-APCI-MS using the same method as for the reference standard. Indeed, the GC chromatogram gave the expected hump, shown in Figure 18. The MS spectrum of the LSW fraction and its enlarged fragment are illustrated in Figure 19 and Figure 20, respectively.

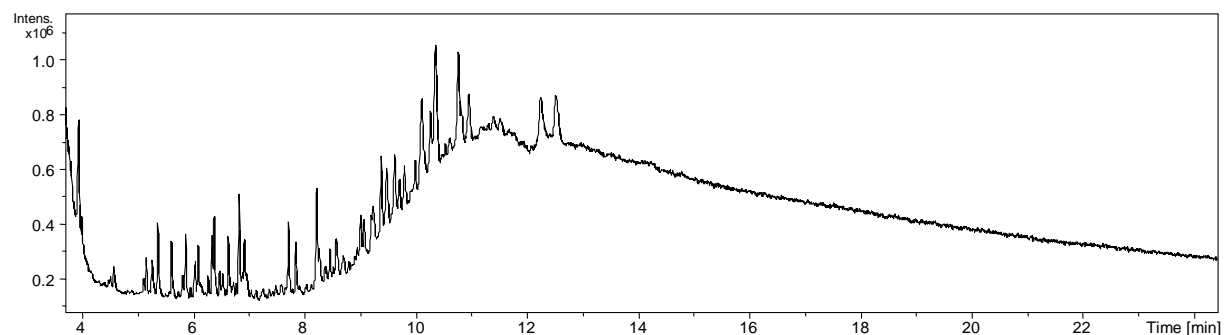


Figure 18. GC chromatogram (TIC) of the light shredder waste fraction using GC-APCI-TOF-MS

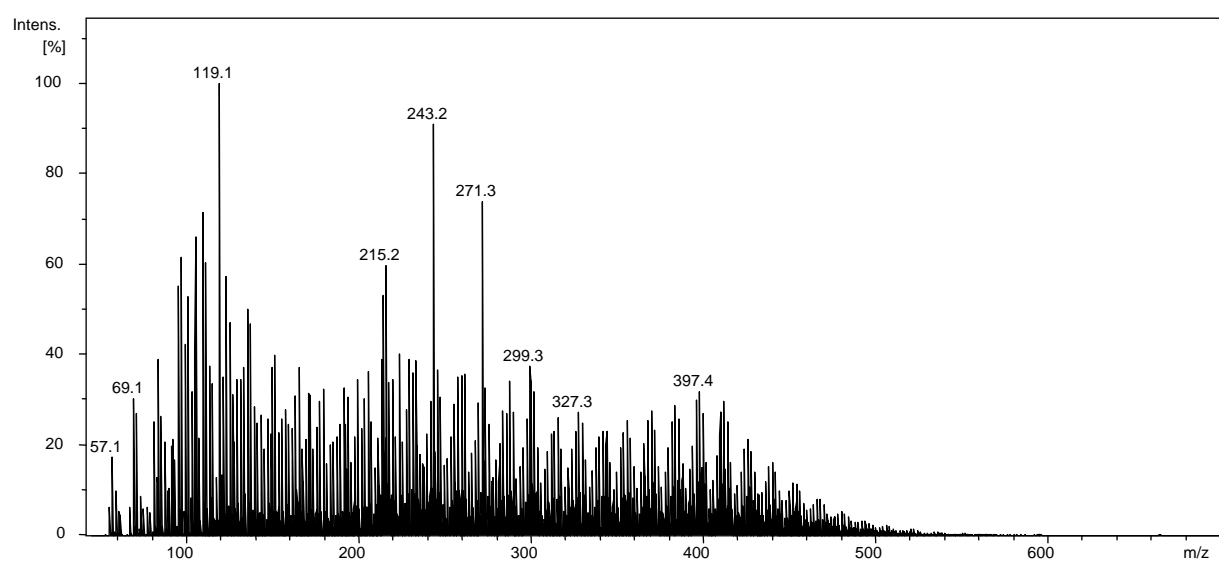


Figure 19. MS spectrum (integrated) of the light shredder waste fraction in the positive ion mode using GC-APCI-TOF-MS

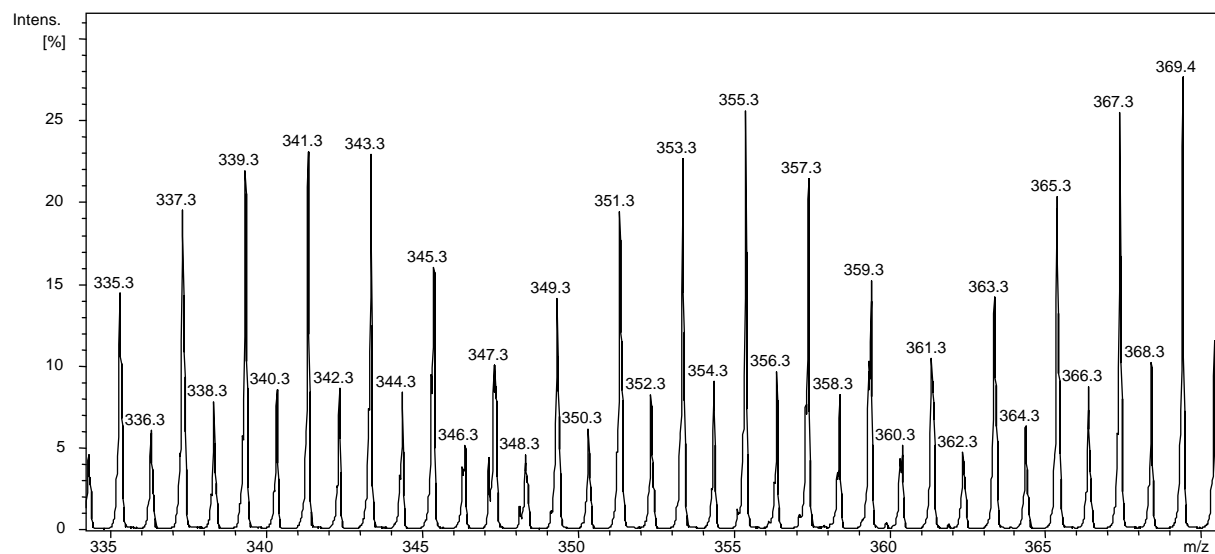


Figure 20. MS spectrum (enlarged) of the light shredder waste fraction in the positive ion mode using GC-APCI-TOF-MS

The analyses of the high-resolution mass data of components from the hump provided the identification of all saturated *n*-alkanes ranging from C_7H_{16} – $C_{35}H_{72}$. A list of all saturated *n*-alkanes identified in the light shredder waste fraction with their high-resolution mass data is present in Table 8. As observed for *n*-alkanes standard, water adducts $[(M-3)+H_2O]^+$ are being characteristic ions for earlier eluted compounds up to *n*-nonadecane, while $[M-1]^+$ species for later *n*-alkanes. Except saturated hydrocarbons, unsaturated have been found in the waste samples.

Table 8. High-resolution mass (GC-APCI-TOF-MS) data for the light shredder waste fraction in the positive ion mode

Peak numbering	Rt [min]	Ion Formula	Experimental m/z	Theoretical m/z	Error [ppm]
1	3.29	C ₇ H ₁₅ O	115.1120	115.1117	-2.0
2	3.97	C ₈ H ₁₇ O	129.1264	129.1279	7.9
3	4.60	C ₉ H ₁₉ O	143.1437	143.1430	-4.4
4	5.39	C ₁₀ H ₂₁ O	157.1587	157.1587	-0.0
5	6.0	C ₁₁ H ₂₃ O	171.1745	171.1743	-0.9
6	6.67	C ₁₂ H ₂₅ O	185.1899	185.1900	0.3
7	7.27	C ₁₃ H ₂₇ O	199.2028	199.2056	14.3
8	7.73	C ₁₄ H ₂₉ O	213.2208	213.2213	2.1
9	8.52	C ₁₅ H ₃₁ O	227.2340	227.2369	12.7
10	9.32	C ₁₆ H ₃₃ O	241.2518	241.2526	3.4
11	10.10	C ₁₇ H ₃₅ O	255.2662	255.2682	8.1
12	10.66	C ₁₈ H ₃₇ O	269.2805	269.2839	12.5
13	11.16	C ₁₉ H ₃₉ O	283.2947	283.2995	17.2
14	11.39	C ₂₀ H ₄₁	281.3185	281.3203	6.3
15	12.08	C ₂₁ H ₄₃	295.3325	295.3359	11.6
16	12.73	C ₂₂ H ₄₅	309.3503	309.3516	4.3
17	13.35	C ₂₃ H ₄₇	323.3660	323.3672	3.7
18	13.97	C ₂₄ H ₄₉	337.3816	337.3829	3.8
19	14.67	C ₂₅ H ₅₁	351.3984	351.3985	0.4
20	15.43	C ₂₆ H ₅₃	365.4130	365.4142	3.3
21	16.48	C ₂₇ H ₅₅	379.4283	379.4298	4.1
22	17.80	C ₂₈ H ₅₇	393.4439	393.4455	4.3
23	19.25	C ₂₉ H ₅₉	407.4598	407.4611	3.4
24	20.20	C ₃₀ H ₆₁	421.4736	421.4768	7.6
25	21.18	C ₃₁ H ₆₃	435.4962	435.4924	-8.7
26	22.27	C ₃₂ H ₆₅	449.5111	449.5081	-6.7
27	23.24	C ₃₃ H ₆₇	463.5287	463.5237	-10.7
28	24.37	C ₃₄ H ₆₉	477.5389	477.5394	1.0
29	25.66	C ₃₅ H ₇₁	491.5537	491.5550	2.8

Interfering of chromatographic techniques to mass spectrometer provides an advantage of the extracted ion chromatograms (EICs) generation. Thus, the EICs of *n*-alkanes were created and the sequence of *n*-eicosane (C₂₀H₄₂) to *n*-pentacosane (C₂₅H₅₂) is shown in Figure 21. They exhibited broad peaks instead of single sharp peaks.

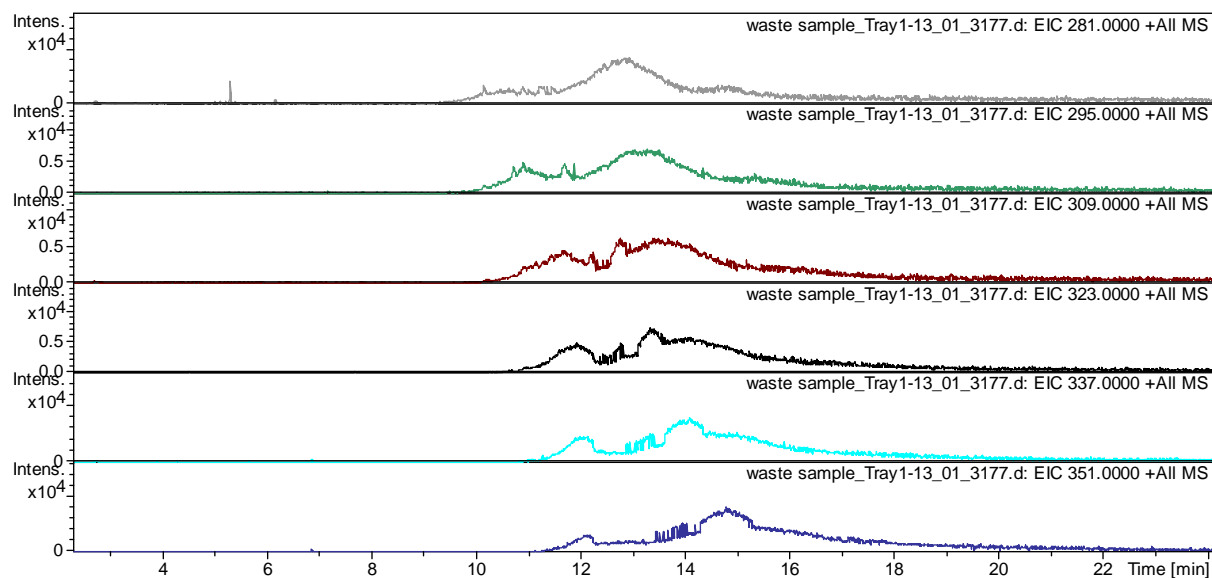


Figure 21. Extracted ion chromatograms (EICs) of pseudo-molecular ions at m/z : 281.0 ($C_{20}H_{41}$), 295.0 ($C_{21}H_{43}$), 309.0 ($C_{22}H_{45}$), 323.0 ($C_{23}H_{47}$), 337.0 ($C_{24}H_{49}$), 351.0 ($C_{25}H_{51}$) for saturated alkanes in the positive ion mode from GC-APCI-TOF-MS

The EICs of the particular n -alkanes incorporate small humps with three maxima. The first maxima correspond to branched derivatives, the second to the studied n -alkanes by comparing their retention times, whereas the latter maxima (with the latest retention time) to fragment ions. This suggestion is based on the fact that retention times of branched derivatives are lower than for their linear analogues. Additionally, the number of possible isomers of few n -alkanes, for instance $C_{20}H_{42}$, $C_{21}H_{44}$ and $C_{22}H_{46}$ was calculated to be 366319, 910726, 2278658, respectively. Subsequently, the EICs of saturated n -alkanes with their unsaturated homologous were created (Figure 22). The retention times of unsaturated to saturated hydrocarbons in EICs are shifted to the latest retention times.

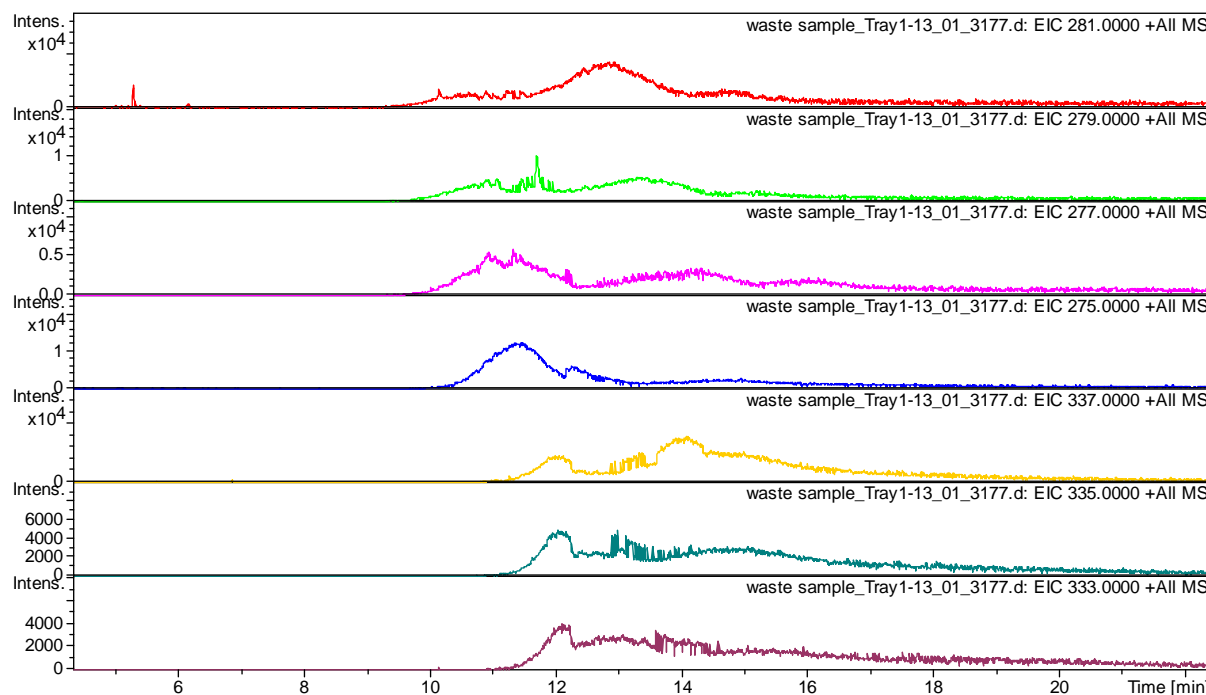


Figure 22. EICs of pseudo-molecular ions at m/z : 281.0 ($C_{20}H_{41}$), 279.0 ($C_{20}H_{39}$), 277.0 ($C_{20}H_{37}$), 275.0 ($C_{20}H_{35}$), 337.0 ($C_{24}H_{49}$), 335.0 ($C_{24}H_{47}$), 333.0 ($C_{24}H_{45}$) for saturated alkanes and their unsaturated derivatives in the positive ion mode from GC-APCI-TOF-MS

1.4.6.3 Chemometric study of the light shredder waste fraction

The Kendrick and van Krevelen plots were prepared for the waste sample from the high-resolution GC-APCI-MS data. Such chemometric techniques, used for the first time for petroleum researches, lead to informative visualization of complex data. The graphs were constructed from each of four minutes time range starting from 8 minutes, when the hump started to appear in the chromatogram, resulting in six Kendrick and six van Krevelen plots.

The first graph so called the van Krevelen graph is formed from the high-resolution mass data by calculating H/C and O/C atomic ratios from a molecular list of the compounds.^[124] Different classes of compounds have typical ratios, for instance carbohydrates H/C is ~ 2 and O/C is ~ 1 , allowing fast interpretation of the complex data. Figure 23 represents the van Krevelen diagrams (consisting of a plot of H/C vs O/C atomic ratios) for six ranges of the hump. A significant number of points was found in the range of 0–0.3 for O/C ratio and 0–1.75 for H/C, which refers to the good oil. Some points out of this range are present in the graphs and can correspond to the ions that exist as water adducts.

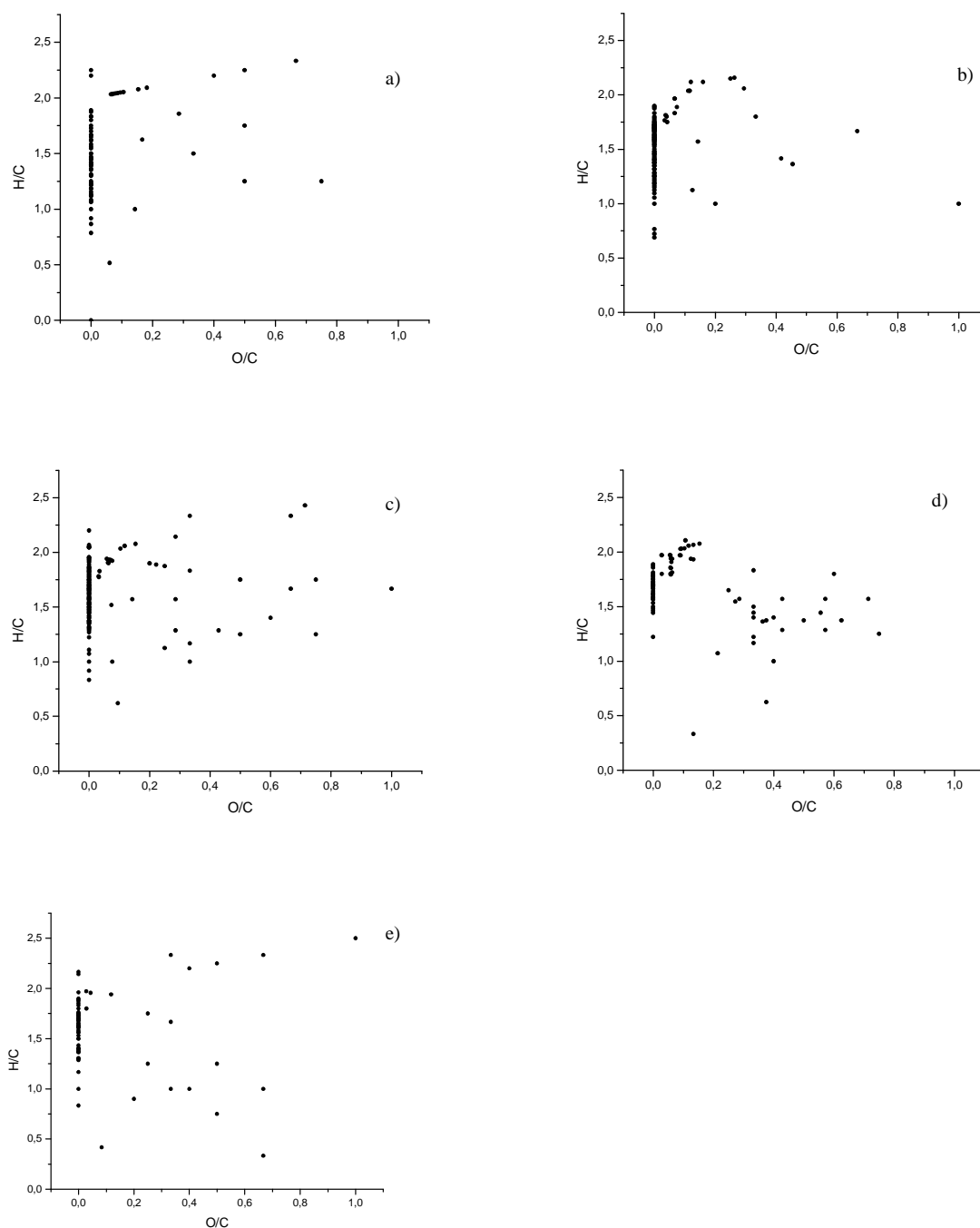


Figure 23. Two dimensional van Krevelen plots showing the O/C *versus* H/C ratio for the UCM hump in the range: a) 8–12 min, b) 12–16 min, c) 16–20 min, d) of 20–24 min and e) 24–26.3 min for the light shredder waste fraction in the positive ion mode

The Kendrick plots with the CH_2 increment were produced from the high-resolution mass data derived from GC-APCI-TOF-MS experiments for the different regions of the hump. Figure 24

presents a two-dimensional display of Kendrick mass defect *versus* nominal Kendrick mass for the mentioned regions of the hump.

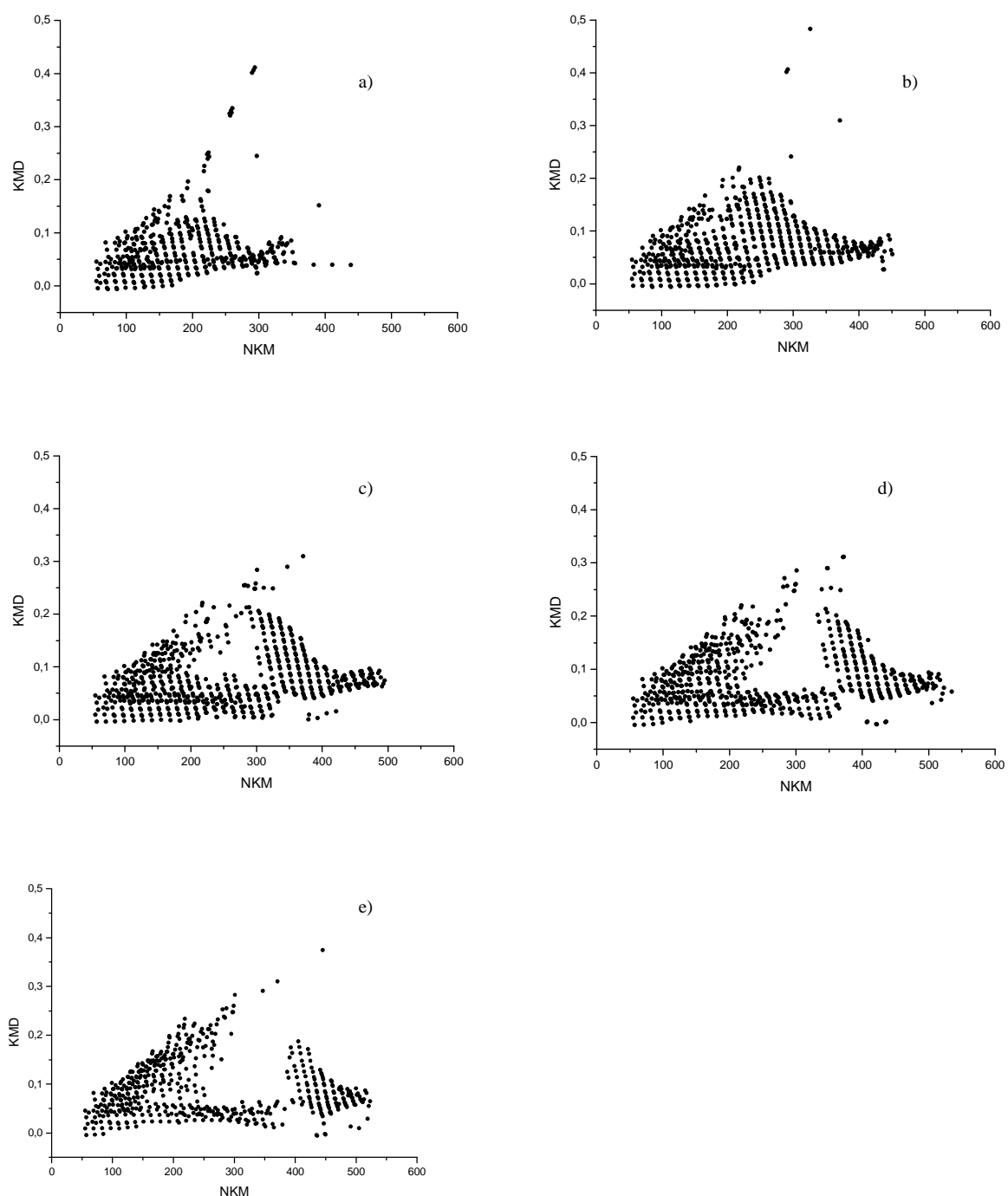


Figure 24. Two dimensional Kendrick plots for mass increment CH_2 showing the distribution of the KMD *versus* NKM of pseudo-molecular ions for the UCM hump in the range: a) 8–12 min, b) 12–16 min, c) 16–20 min, d) of 20–24 min and e) 24–26.30 min for the light shredder waste fraction in the positive ion mode

The compounds, which belong to the same homologous series have the same Kendrick mass defect values (KMD) and lay on the horizontal line in the graph.^[125] The diagrams confirmed the presence of several homologous series of hydrocarbons.

The points with higher KMD values indicate the compounds with increasing degree of unsaturation or number of heteroatoms. The diagrams from different time regions exhibit slight differences. The first graph exhibits points up to 400 in NKM (Nominal Kendrick Mass). In the rest plots the rise of the masses up to 600 in comparison with the first one is observed. The number of points with the value of KMD higher than 0.2 is bigger for all except the first one. It particularly shows higher degree of unsaturation. The points in all graphs form the shape of the triangle, which is typical for the natural organic matter.

1.4.6.4 Tandem MS measurements

Tandem MS data for the components from the hump have been recorded in the positive ion mode using a microTOF-Q II Bruker mass spectrometer with APCI ionization in Auto MSⁿ. Tandem MS spectra for *n*-hexane (C₇H₁₆), *n*-octane (C₈H₁₈) and *n*-tetradecane (C₁₄H₃₀) as examples are present in Figure 25. Typical for *n*-alkanes fragments at *m/z* 43, 57, 71, 85 *etc* were observed in the MS² spectra, although with varied intensities of components. These fragments are often accompanied with species, such as [M-H]⁺ or [M-2H]⁺, suggesting that they originated from different coeluting isomers. In some of the spectra of *n*-alkanes, characteristic fragment ions for both saturated and unsaturated derivatives were detected, where some of unsaturated compounds can be distinguished from the saturated.

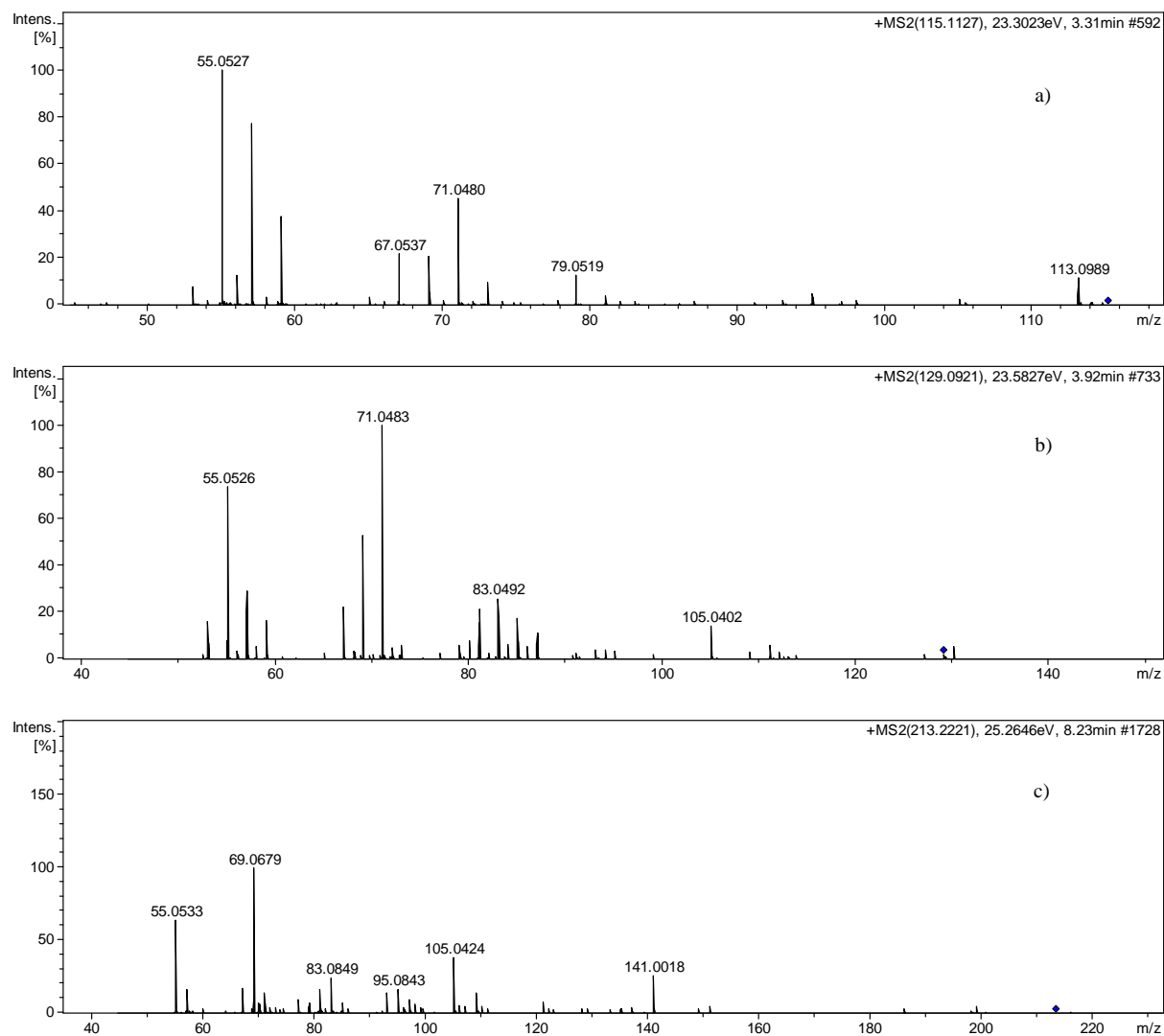


Figure 25. MS² spectra of: a) *n*-hexane (C₇H₁₆), b) *n*-octane (C₈H₁₈), and c) *n*-tetradecane (C₁₄H₃₀) (parent ions at *m/z* 115.1, 129.1, 213.2, corresponding to [(M-3)+H₂O]⁺ from the light shredder waste fraction in the positive ion mode using GC-APCI-TOF-MS

Tandem MS data confirmed the presence of several aromatic components. The spectra with *m/z* 91, that correspond to tropylium ion [C₇H₇]⁺, suggest the existence of some linear alkylbenzene derivatives in the light shredder waste fraction.

1.4.6.5 Identification of nonlinear hydrocarbons in the hump by GC-APCI-MS

As reported in previous sections, the unresolved complex mixture of the light shredder waste fraction can contain several classes of components. An application of GC-APCI-TOF provided the high-resolution mass data of the analyte. The EICs of PAHs have been generated

and 13 out of 16 (previously studied) polyaromatic hydrocarbons of the standard were identified, excluding indeno[1.2.3-cd]pyrene (**14**), dibenzo[a,h]anthracene (**15**) and benzo[ghi]perylene (**16**)^{*}. The EIC of fluorene (**4**) as an example is shown in Figure 26. The accurate mass values for these compounds were obtained (high-resolution data are present in Table A3 Appendix)[†]. The EICs of PAHs appeared as sharp peaks in contrast to broad peaks of *n*-alkanes. It can be explained by the fact that PAHs appear as single components, whereas in the case of *n*-alkanes more than single isomer. From the GC-APCI-MS data of the light shredder waste fraction, the EICs of PCBs have been generated, although with only the high-resolution mass data of dichlorobiphenyl. Possibly, the rest of PCBs appeared in lower quantity or was not efficiently ionized in the positive ion mode.

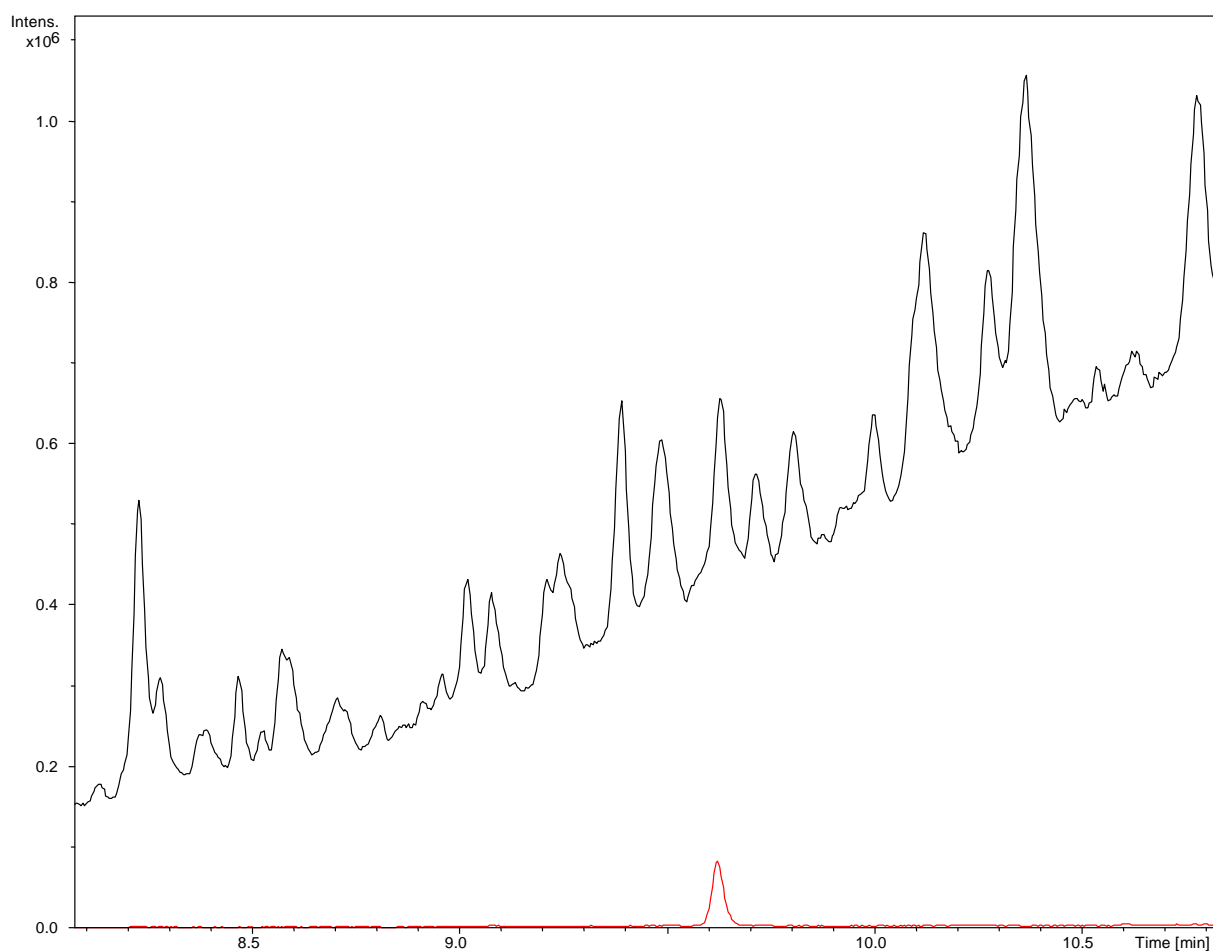


Figure 26. GC chromatogram (enlarged) of the light shredder waste fraction (black) with extracted ion chromatogram (red) of pseudo-molecular ion at m/z 167.1 ($C_{13}H_{12}$) for fluorene (**4**) in the positive ion mode using GC-APCI-TOF-MS

* The list of compounds on page 33

† See on page 150

The waste sample was screened in term to find additional components. The EICs of steranes used as oft-monitored biomarkers in crude oil, such as 5- α -stigmastane, 5- α -androstandane, 5- α -pregnane, 5- α -cholestane, 5- α -ergostane and 5- α -stigmastane were generated. All EICs at m/z 259.2410, 287.2725, 371.3659, 385.3809 and 399.3963 were obtained along with molecular formulas and error values. More likely, all of them are present in the light shredder waste fraction, although the lack of tandem MS data for these compounds, does not exclude the identity of olefins. Afterwards, the EICs of diamondoids hydrocarbons have been generated. Adamantine at m/z 135.1169 with the formula $C_{10}H_{16}$ was found in the waste sample with additional diamondoids and their EICs were created along with high-resolution data. In fact, adamantane, diamantane, triamantane and isotetramantane can be present in the light shredder waste fraction, but these ions rather correspond to unsaturated hydrocarbons.

The UCM has been analyzed mainly by gas chromatography and mass spectrometry. Although, alternative techniques, such as nuclear magnetic resonance (NMR) or infrared spectroscopy (IR) can also be beneficial in the characterization of the complex analyte. Information obtained here can be complementary and supports finding for the MS analysis. These data are discussed in the following sections.

1.4.7 ^1H NMR OF THE LIGHT SHREDDER WASTE FRACTION

Nuclear magnetic resonance (NMR) spectroscopy has been applied to help establishing the identity of a compounds' existence in the light shredder waste fraction. The ^1H NMR spectrum exhibited signals corresponding to hydrocarbons (Figure 27). The multiple signals were observed at $\delta = 0.3\text{--}2.0$ and $\delta = 6.8\text{--}7.8$ that can be assigned to alkyl groups and aromatic protons, respectively.

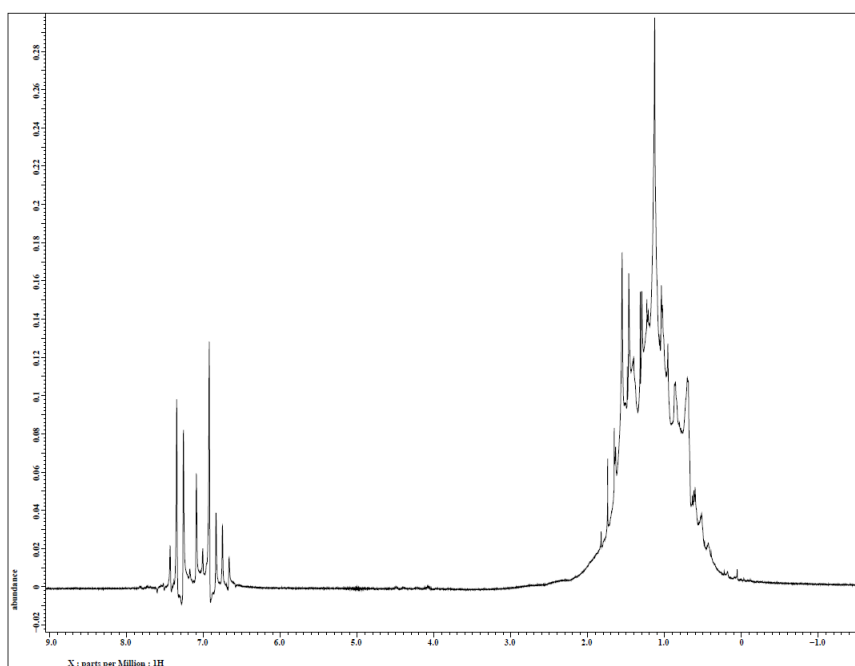


Figure 27. ^1H NMR spectrum of the light shredder waste fraction

1.4.8 INFRARED OF THE LIGHT SHREDDER WASTE FRACTION

An infrared (IR) spectrum of the light shredder waste fraction reveals a few weak absorption bands (Figure 28). Signals typical for alkanes near 3000 cm^{-1} were detected along with the absorption near $1650\text{--}1450\text{ cm}^{-1}$. The latter absorption region most likely corresponds to double bonds.

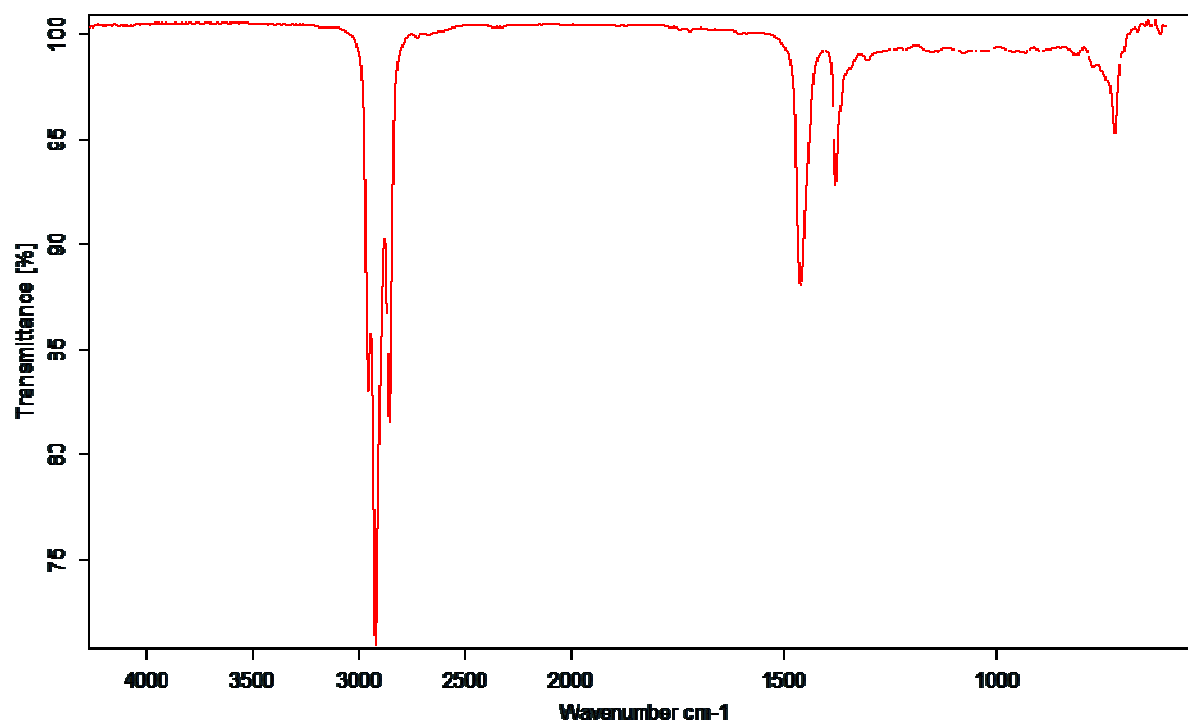


Figure 28. IR spectrum of the light shredder waste fraction

1.4.9 THERMAL ANALYSES OF THE LIGHT SHREDDER WASTE FRACTION

Two types of thermal analyses, namely thermogravimetric analyses (TGA) and temperature programmed desorption (TPD) have been applied to study the light shredder waste fraction. Thermogravimetric analysis determines the weight changes in a relation to different temperatures.^[126] The TGA curves of the reference materials, including *n*-eicosane, *n*-tricosane, *n*-hexatriacontane, *n*-tetracontane and the waste sample were recorded with the isothermal temperature program. The temperature raised from 25 to 800 °C at the rate 5 °C/min under a nitrogen atmosphere (Figure 29). Curves of the light shredder waste fraction were obtained at the rate 5 and 10 °C/min, although both exhibited the same profiles. Three main steps can be observed on the curve of the waste sample (Figure 30). The first step of a decomposition ends at 200 °C, the second mass loss step occurs from 200 to 600 °C and the third ends at 800 °C. The reduction of the weight of the samples was around 3, 17 and 2.5% in

the first, second and third step, respectively. The TGA experiments have been applied to help in the optimization of the parameters of TPD.

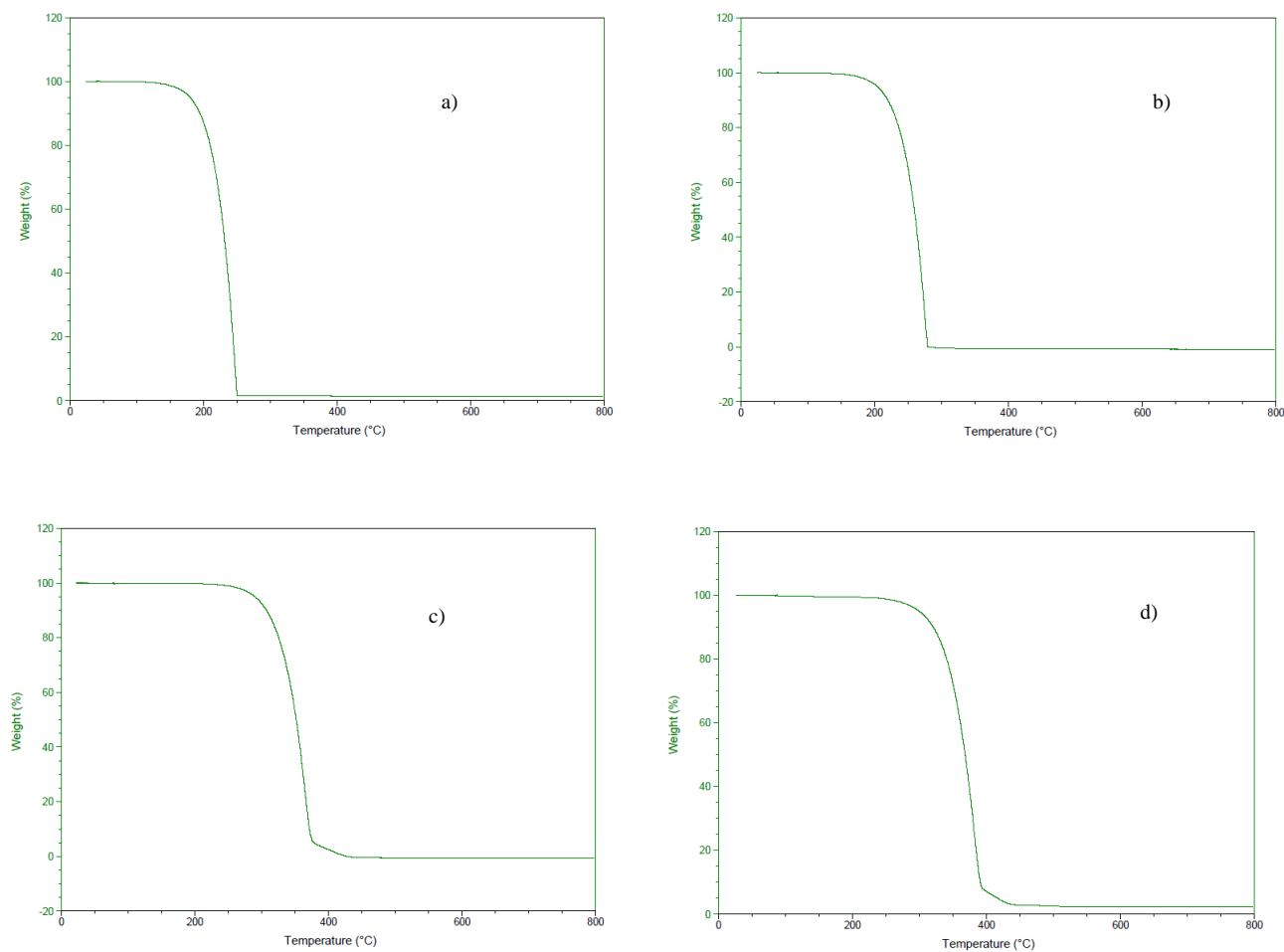


Figure 29. Thermogravimetric curves of: a) *n*-eicosane ($C_{20}H_{42}$), b) *n*-tricosane ($C_{23}H_{48}$), c) *n*-hexatriacontane ($C_{36}H_{74}$), d) *n*-tetracontane ($C_{40}H_{82}$)

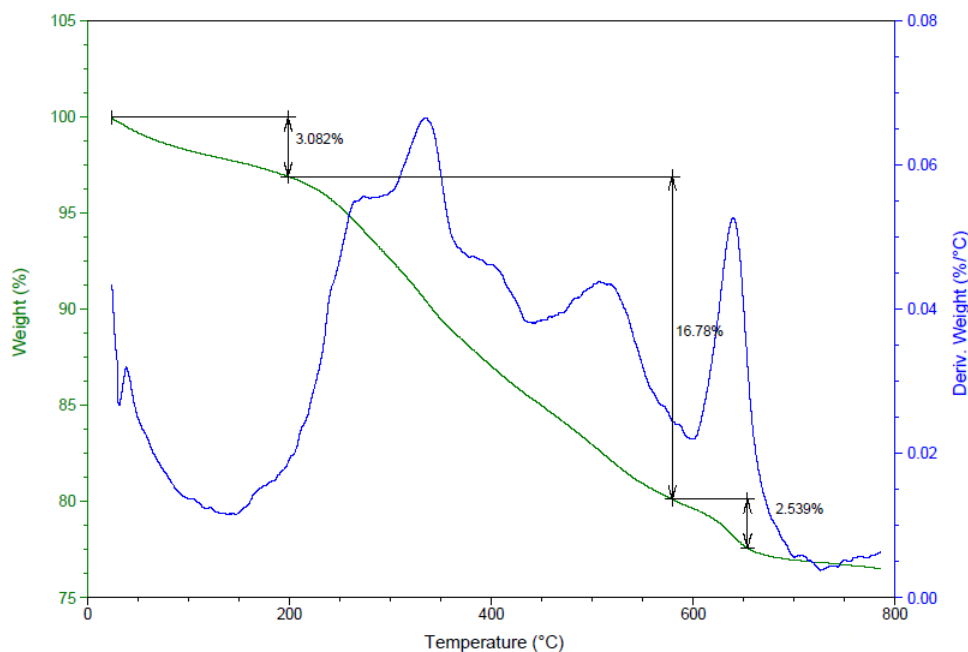


Figure 30. Thermogravimetric curve of the light shredder waste fraction with derivatives curve obtained, when temperature raises from 25 to 800 °C at the rate 5 °C/min under a nitrogen atmosphere

Temperature programmed desorption (TPD) is a method, where desorbed molecules from the surface are observed, when the surface temperature is rising. The waste sample and *n*-alkanes reference materials were adsorbed on charcoal and mesoporous silica (SBA-15) and analyzed, accordingly. Unfortunately, high-boiling hydrocarbons are too heavy and were not able to stripe from TDS tubes into the MS part of the instrument. The previously completed TGA analyses assumed that the majority of compounds of the light shredder waste fraction degraded between 400–500 °C and consequently do not appear in the MS spectra.

1.4.10 BIOREACTOR ANALYSES

As mentioned in the previous sections, the Bremer Entsorgungsbetriebe (BEB) optimized biological methods to decrease the weight and volume of the light shredder waste fraction. The project partner in Hochschule Bremerhaven performed biological processes of the light shredder waste fraction in small scale reactors to find the optimum condition. To reach better understanding on the processes influencing HC production and degradation such samples were subsequently monitored using GC-FID*. The samples were extracted using the same method applied previously for the analytes from the Bremer Entsorgungsbetriebe (BEB) and then subsequently analyzed by GC-FID. Figure 31 compares GC chromatograms of three samples from bioreactors with one from the Bremer Entsorgungsbetriebe. The resolved peaks floating on the similarly profiled humps, belonged to *n*-alkanes in the range of C20–C40. The visible difference between the samples from bioreactors and the Bremer Entsorgungsbetriebe is the intensity of the humps, which is higher in the case of samples from Bremerhaven originating from different time period. The sample from Bremerhaven have been delivered and placed in the reactors just after shredding, while BEB samples were analyzed longer time after this process. The time of bioremediation seemed to be very important, where microorganisms consisted in the light shredder waste fraction significantly decrease the concentration of hydrocarbons.

* See Table 1 on page 15

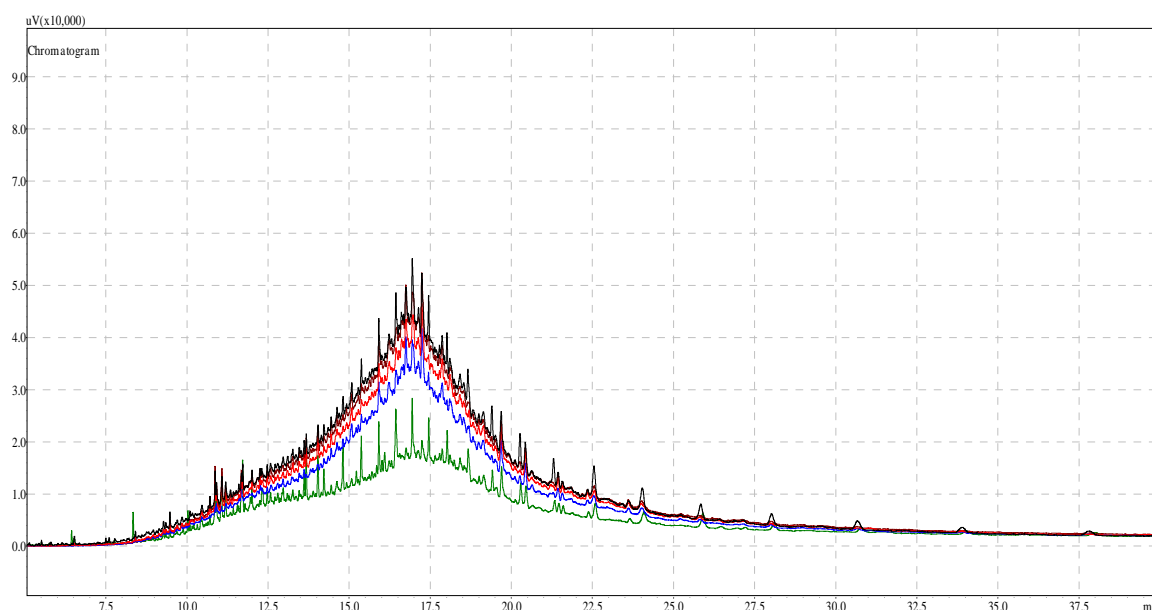


Figure 31. Overlap of GC-FID chromatograms of the light shredder waste fraction from: R.1.2. (red), R.2.2. (black), R.3.2. (blue), Bremer Entsorgungsbetriebe (green)

In particular, the chromatograms of the samples from the collaborator are really similar one to another. Changing the parameters of bioprocess, including temperature, airflow and operating time did not affect significantly the profiles of such GC chromatograms. The greatest difference can be found in the chromatograms of R1.2 or R2.2 and I3^{*}, after reactions in bioreactors and sample before treatment with microorganisms, just after shredding (Figure 32). In the case of I3, the high intensity of the hump suggested the higher concentration of compounds. The bioremediation process caused a dramatic reduction of intensities of the hump as well as the peaks of straight-chain alkanes, when keeping under biological conditions.

* See Table 1 on page 15

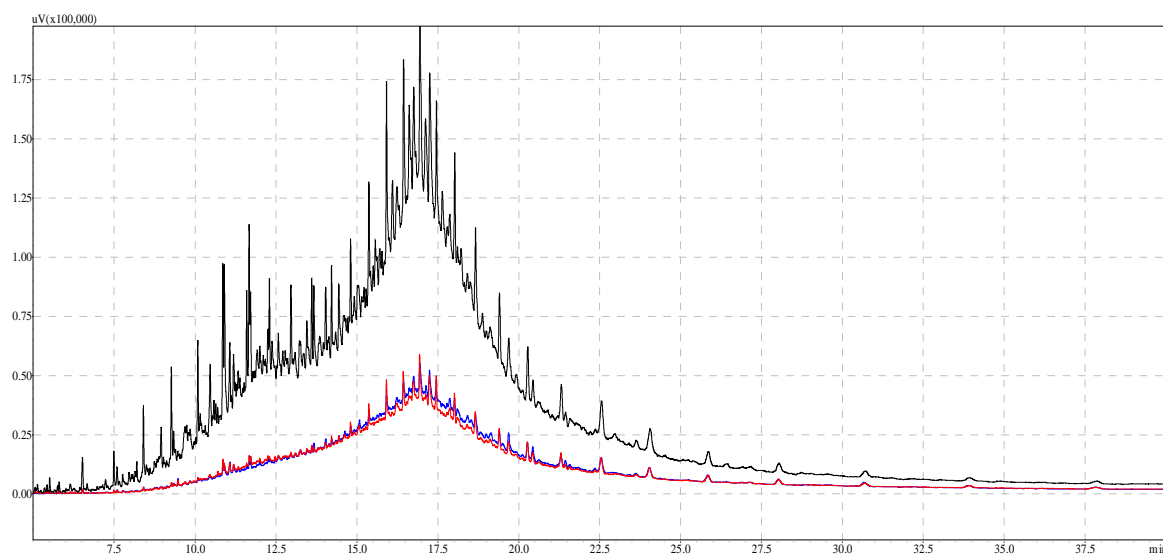


Figure 32. Overlap of GC-FID chromatograms of the light shredder waste fraction from: R.1.2. (red), R.2.2. (blue), I3 (black)

1.5 CONCLUSION

The chemical composition of the unresolved complex mixture (UCM) of hydrocarbons of the light shredder waste fraction has been thoroughly studied using gas chromatography and gas chromatography-mass spectrometry. The gas chromatography (GC) method was optimized for a wide range of boiling points *n*-alkanes and successfully applied for the analysis of the light shredder waste fraction. Shaking and Soxhlet extraction procedures of such analyte were explored. A clean up process of extracts involved the solid phase extraction with Florisil cartridges providing suitable extracts for the GC analysis. This procedure gave good recovery and reproducibility. It has been shown that gas chromatography with a flame ionization detector (GC-FID) could thus be used for the quantification of linear *n*-alkanes. The work allows for a significant improvement of the KW/04 method.

Gas chromatography-mass-spectrometry (GC/MS) with two ionization techniques, namely electron impact (EI) and atmospheric pressure chemical ionization (APCI) was explored in order to find the composition of the light shredder waste fraction. GC-APCI was applied for the first time to high non-volatile *n*-alkanes and environmental samples, such as the light shredder waste fraction. The APCI ionization resulted in ions $[(M-3)+H_2O]^+$ and $[M-H]^+$ as base peaks in *n*-alkanes standard as well as in the environmental samples, up to $C_{19}H_{40}$ and for higher hydrocarbons, respectively. The improvement of *n*-alkanes identification has been achieved based on their molecular ion peaks. All *n*-alkanes in the range C_7H_{16} – $C_{35}H_{72}$ and some unsaturated derivatives were found in analyzed samples. Tandem MS studies have been used to confirm the identity some of heavy hydrocarbons. The van Krevelen and the Kendrick plot analyses have been successfully applied for the representation of the complex mass data. Due to the lack of molecular ions in an EI the identification of all heavy *n*-alkanes was not possible. Nevertheless, the presence of polynuclear aromatic hydrocarbons and some branched derivatives of *n*-alkanes has been confirmed. All analyzed chlorinated biphenyls except nonabiphenyls were found in the light shredder waste fraction. In the light of GC-MS studies supported by spectroscopic techniques, hydrocarbons are present, exclusively. It has been shown that GC-APCI-TOF-MS is efficient for the characterization of the wide boiling points range of compounds including heavy hydrocarbons and complex environmental matrix. Temperature program desorption for high-boiling hydrocarbons failed, most probably because of the pyrolysis process, which can be defined by the thermogravimetric analysis. GC-FID is

a sufficient technique to demonstrate the efficiency of bioremediation procedure of the light shredder waste fraction.

CARMEL

2.1 INTRODUCTION

2.1.1 THE IMPORTANCE OF HEATING OF CARBOHYDRATES

Caramel constitutes one of the mankind's oldest and most important dietary materials produced by thermal treatment of sugars. Thermally treated sugars are consumed at a level of an estimated 50 Mt per annum.^[127] It is a complex mixture of volatile and non-volatile fractions of low- and high-molecular-weight compounds.^[128] Caramel is widely used for coloring and flavoring foods and beverages, for instance beer, soft drinks, soups and candies.^[129]

Most foods are consumed by humans after thermal treatments, which involve cooking, baking, frying or roasting to generate the brown color and the pleasurable aroma of caramel.^[130,131] In the process of such thermal treatments all carbohydrates in food undergo significant chemical changes frequently described as non-enzymatic browning reactions. Well-known examples in the carbohydrate chemistry are the thermal conversion of glucose and sucrose to caramel and the Maillard reaction between saccharides and amino acids at elevated temperatures towards materials referred to as melanoidins. Such molecules are present in all thermally treated carbohydrate-enriched foods with a human intake from all dietary sources estimated by Fogliano and Morales to be 10 g per day.^[132] Melanoidins are composed from reaction products arising from the thermal treatment of carbohydrates alone and from reaction products of carbohydrates with nitrogen-containing species, including amino acids and proteins. Despite the progress in the field the molecular composition of melanoidins and the mechanism of formation of thermally treated carbohydrates must be considered as sketchy.^[133] This is obviously related to the limitations of analytical chemistry, which has to date struggled to propose capable methods of analyzing extremely complex materials containing thousands of individual analytes. Despite its high profile, the chemical composition of the reaction products of heated sugar remains hitherto largely elusive if not mysterious. Several studies have been carried out on the thermodynamic properties of sugars^[134,135] and have demonstrated an enhanced interest in the chemistry of heated carbohydrates. Beyond the area of food chemistry, the thermal treatment of carbohydrates is used in many other industries. It is worth mentioning that such carbohydrates have also found their significance in the production of materials as paper, adhesives, cosmetics, bioplastics

and most importantly, biofuel.^[136] For instance, cellulose is the main cell wall polysaccharide and the most abundant biological material on Earth with a production of approximately 1.5×10^{12} tons annually.^[137] In particular, the production of biofuel from cellulose-enriched agricultural plants takes frequently advantage of thermal processing steps to achieve carbonization.

2.1.2 THE VOLATILE FRACTION OF CARMEL

The volatile fraction of caramel has been thoroughly studied^[131,138] and is represented by a broad spectrum of compounds. One of the best characterized aroma compounds is caramel diacetyl,^[139] associated with a butterscotch type flavor and accompanied by hundreds of other flavor compounds identified (Figure 33).

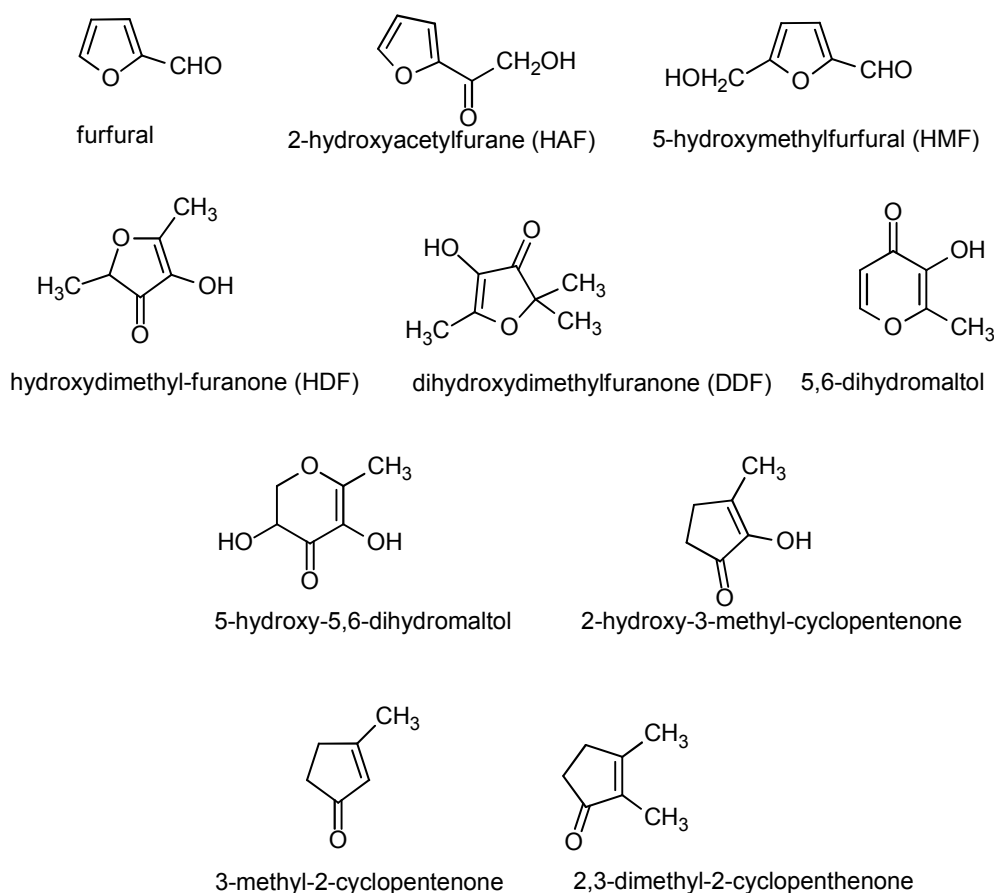


Figure 33. Typical volatile caramel compounds

The most frequently studied compounds are classified as oxygen-containing five- and six-membered heterocyclic molecules. In particular, hydroxymethylfurfural (HMF), hydroxyacetylfuran (HAF), hydroxydimethylfuranone (HDF), dihydroxydimethylfuranone (DDF) and maltol from disaccharides and hydroxymaltol from monosaccharides are formed after dehydration of carbohydrates.^[140]

Among them, the well-characterized volatile components of caramel, for example methylglyoxal,^[141] 2-hydroxypropanedial and other carbonyl compounds can be found.^[142] They have been analyzed particularly by gas chromatography with or without mass spectrometry. It should be mentioned however that compound HMF has received significant attention since it can possess possible carcinogenic properties. Moreover, it has been found in a wide variety of heat processed foods such as milk, spirits, honey,^[143] coffee,^[144] bakery products,^[145] *etc.* with the estimation that around 5–10 mg of HMF are consumed daily.^[146] The formation of HMF^[147] by an acid-catalyzed dehydration of fructose is shown in Figure 34.

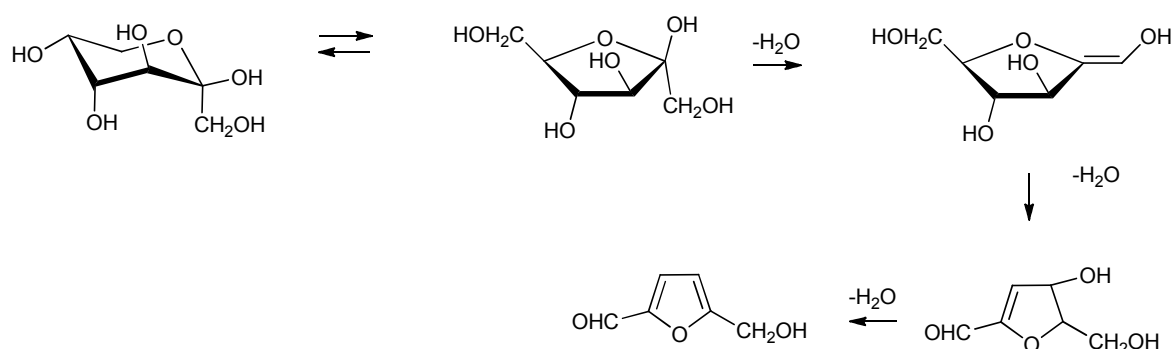


Figure 34. Schematic representation of reaction pathways for acids-catalyzed dehydration of fructose^[147]

α -Dicarbonyl compounds play important roles in carbohydrate degradation. The formation of reaction products with an α -dicarbonyl moiety has been extensively researched for common carbohydrates.^[148,149] The formation pathway of α -dicarbonyl compounds with some Maillard reaction products from glucose is shown in Figure 35.

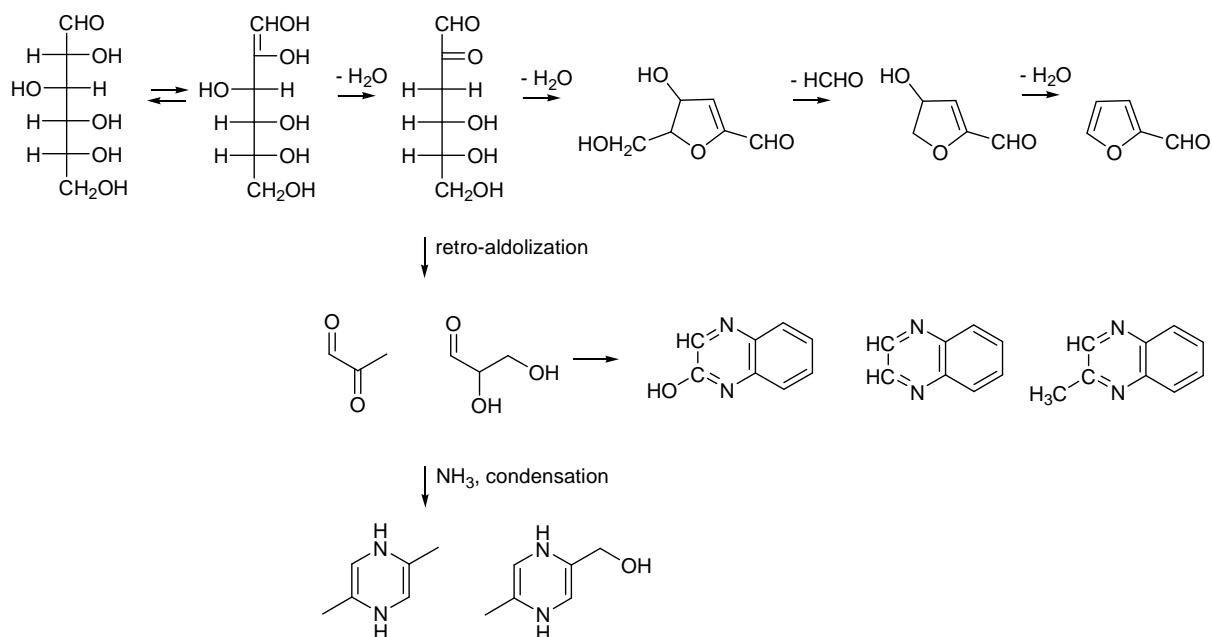


Figure 35. The formation of possible products of heated glucose

2.1.3 THE NON-VOLATILE FRACTION OF CARAMEL

Since the volatile low-molecular weight fraction of caramel is well known, the non-volatile components represent more than 95%. It must be pointed out that the non-volatile fractions remain poorly characterized.^[150] The high molecular weight non-volatile products have been divided by Kitaoka in the 1960s into three classes: Caramelans tetramers of hexoses (C₂₄H₃₆O₁₈), Caramelens hexamers of glucose (C₃₆H₅₀O₂₅) and Caramelins polymers of glucose (C₁₂₅H₁₈₈O₈₀).^[151,152] Although this classification is reported frequently, these products have never been further studied, due to the complexity of created compounds during caramelization. Difructose dianhydrides (DFAs) are among the few well described reaction products of the non-volatile fraction of caramel. They are cyclic products derived from the condensation of two D-fructose molecules with the loss of two water molecules furnishing a 1,4-dioxane intersaccharide ring as the main structural feature (Figure 36).^[150]

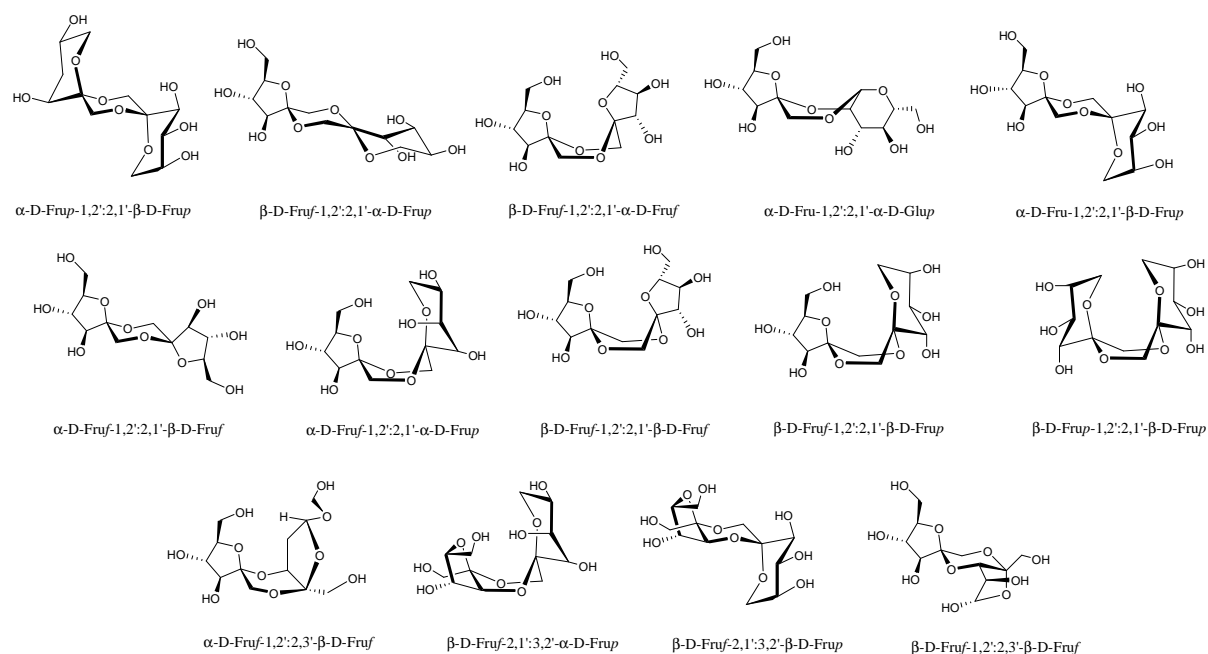


Figure 36. Difructose dianhydrides found in sucrose caramels^[153]

The formation of DFAs under the acidic treatment of carbohydrates has been widely reported in literature.^[154-157] The presence of DFAs in caramel was first suggested by Tschiersky and Baltes in 1989.^[158] Furthermore, such anhydrides have been isolated from commercial caramels^[159] and from the products of the thermal treatment of acidified carbohydrates and insulin.^[160-163] The amounts of DFAs depend on the nature of sugar used for caramelization; the study of the three most common carbohydrates showed that fructose caramel contains the greatest amount of DFAs, glucose caramel contains mainly glucobioses, while in sucrose caramel both types of compounds were formed in similar quantities.^[150] The studies of DFAs in caramel have been mostly performed using gas chromatography-mass spectrometry on TMS-derivatized carbohydrates.

2.1.4 MASS SPECTROMETRY AS A TECHNIQUE FOR CARBOHYDRATES STRUCTURE DETERMINATION

The determination of the complete structure of oligosaccharides is more complicated than for proteins or nucleotides due to the isomeric nature of monosaccharides and their

ability to form branched and linear oligosaccharides. Monosaccharides in their cyclic forms can have pyran/furan isomers.^[164] The oligosaccharides structures can be solved by determining their monosaccharides sequence, their branching pattern and also the isomer position and the anomeric configuration of each of the glycosidic bonds.

The use of GC/MS towards the identification of monosaccharides or very small oligosaccharides, has been hitherto described in literature.^[165] The analysis of saccharides by gas chromatography requires a derivatization process, such as methylation, acetylation or trimethylsilylation to take place heretofore.^[166] This technique is still widely used for the characterization of the monosaccharide composition of oligosaccharides after the hydrolysis and derivatization steps. The analysis of oligosaccharides without hydrolysis has been initiated with the fast atom bombardment ionization (FAB).^[167] Nowadays, a number of powerful mass spectrometry techniques have been employed to investigate the structure of saccharide molecules, including electrospray ionization (ESI) mass spectrometry^[168-170] and matrix-assisted laser desorption/ionization (MALDI).^[171-173] Furthermore, tandem mass spectrometry (MS/MS) proved to be a valuable tool in the structural characterization of carbohydrates to achieve a comprehensive view of their structures.^[174,175] Oligosaccharides are often analyzed by ESI after derivatization, either by acetylation or methylation since this ionization technique is not as efficient for native oligosaccharides as MALDI. The ionizations of saccharides by ESI, MALDI or FAB mainly result in deprotonated species $[M-H]^-$ in the negative ion mode and protonated species $[M+H]^+$ and also species cationized by alkali metals $[M+\text{alkali metal}]^+$ in the positive ion mode. In ESI multiple charged ions can be generated. The nomenclature suggested by Domon and Costello is commonly used to describe the various fragments obtained by mass spectrometry (Figure 37).^[176]

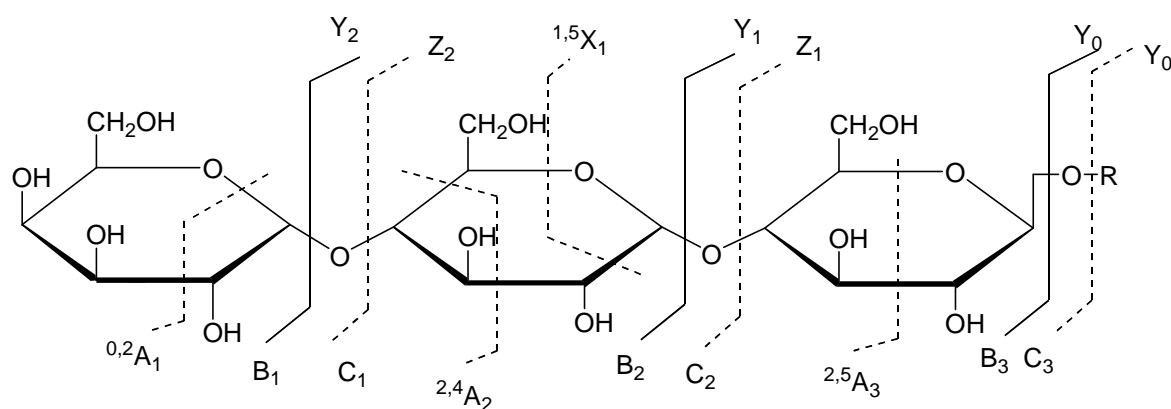


Figure 37. The carbohydrates fragmentation^[176]

The charge-retained fragments on the non-reducing side are referred to as A_i , B_i or C_i , where i represents the number of the glycosidic bond cleaved, counted from the non-reducing end of the carbohydrate. When the charge is retained on the reducing side, fragments are referred to as X_j , Y_j and Z_j , where j is the number of the interglycosidic bond counted from the reducing end. The determination of the sequence and the branching pattern of oligosaccharides and the isomer position of each of their glycosidic bonds can be accomplished by tandem MS. The anomeric configuration of the glycosidic bonds and the distinction of diastereoisomeric monosaccharides are seldom accessible by this technique.^[164] There are several procedures for chemical and enzymatic degradations of oligosaccharides that have been applied in combination with mass spectrometry in order to determine their structures, for example enzymatic degradation of oligosaccharides by endoglucosidases.^[177]

2.1.5 CARMEL COLOR AND OTHER FOOD COLORANTS

Colorants enhance the properties of food, cosmetics and clothing. Until the 19th century, the colorants used were of natural origin like saffron providing color and flavor to food.^[178] The rapid growth of the chemical synthesis has led to the industrial production of a large amount of organic synthetic colorants. They were the first food additives subjected to governmental regulation in the United States of America. After several toxicological evaluations the Food and Drug Administration (FDA) has established a list of permitted colorants. Notwithstanding the new orientation towards the utilization of natural compounds, synthetic colorants are easier to obtain, stable, less expensive and possess better coloring properties than the natural ones.

Synthetic colorants used as food additives can be classified as follows:

Azo dyes: Allura Red AC, Amaranth, Azorubine, Brilliant Black BN, Brown FK, Brown HT, Lithol Rubine BK, Ponceau 4R, Red 2G, Sunset Yellow, Tartrazine

Triarylmethane (triphenylmethane) dyes: Brilliant Blue FCF, Fast green FCF, Green S, Patent Blue V

Quinophthalon dyes: Quinoline yellow

Xanthene dyes: Erythrosine

Indigo deys: Indigotine

The natural sources of some natural food colorants are as follows:

Anthocyanins (E 163), found in mature fruits (blueberries, grapes, cherries) and vegetables (onions, cabbages), seeds (purple sunflower) and flowers

Betanin (E 162), found in red beets

Caramel color (E 150), obtained by heating of carbohydrates

Carotenoids (E 160), distributed in nature as β -carotene, lycopene, lutein

Chlorophyll and **chlorophyllin** (E 140 and E 141)

Curcumin (E 110), the major pigment of turmeric^[179]

The European Union introduced E numbers for all additives, both synthetic and natural.

In particular, caramel colors numbered as E 150 are the most widely used food coloring agents found in foods and beverages. They represent a significant segment of the color market at about 11% of the total food color production.^[178] Commercial caramel colors are classified into four classes, which differ in their chemical and functional properties as well as their application.^[180] Caramel color E 150a (synonym: plain caramel) is prepared by the controlled heat treatment of carbohydrates and is commonly used in spirits, desserts and spice blends. Caramel color E 150b (synonym: caustic sulphite) is prepared by the controlled heat treatment of carbohydrates with sulphite-containing compounds and is frequently used in liqueurs. Caramel color E 150c (synonym: ammonia caramel) is prepared by the controlled heat treatment of carbohydrates with ammonia compounds and is found in many products for human consumption, including various bakery products, soya-bean souses, vinegars and beer. Caramel color E 150d (synonym: ammonia-sulphite caramel) is prepared by the controlled heat treatment of carbohydrates with ammonia-containing and sulphite-containing compounds and is usually found in soft drinks, pet foods or soups.^[181] The use of the third class accounts for 20–25% of the total use caramel colors in the USA and for 60% in Europe.^[182] Caramel colors were first commercially manufactured in the Unites States of America in 1863, whereas in the United Kingdom food colors were first evaluated in 1923 by the Minister of Health.^[180] The color properties are characterized by the hue index and tinctorial power, calculated *via* the followings formulas:

$$\text{Hue index} = 10 \log (A_{510}/A_{610})$$

$$\text{Tintorial power} = K = K_{560} = A_{560}/cb$$

Where A = absorbance at 510, 610 and 560 nm; c = concentration (g/L); b = cell thickness

According to the EU purity criteria, the color intensity is defined as the absorbance of 0.1% (w/v) solution of caramel color solids in water in a 1 cm cell at 610 nm.^[178]

Numerous studies have been conducted on the safety of caramel colors. In this paragraph the nomenclature of caramel colors has been changed to classes I, II, III and IV. Class I, II, IV caramel colors did not show any toxicologically significant effects in mammals. However, toxicity studies of caramel colors III revealed the possible reduction of white blood cells in rats.^[182] This effect of caramel color III in rats only occurred when animals were fed a low vitamin B6 diet.

The flavor of caramel produces the changes from mild, caramel-like and sweet to burning bitter. Users of caramel colors employ these materials primarily as colorants; however, they have other valuable functional properties. In particular, caramel colors slowly absorb oxygen and stabilize a colloidal system thus facilitating flavor retentions as well as preventing hazes in products such as beer. Some of the caramel colors are manufactured to have increasing foaming properties, which are desirable for a root beer production.^[180]

2.2 EXPERIMENTAL SECTION

2.2.1 SAMPLE PREPERATION

All chemicals (Analytical grade) were purchased from Sigma-Aldrich (Germany). All sugar samples (1 g) were heated in an oven for 2 h at 140 °C (fructose), at 180 °C (glucose, galactose, mannose, sucrose, maltose), at 200 °C (lactose) and at 220 °C (starch and cellulose). The heated samples were stored at room temperature. Heated mono- and disaccharides (1 mg) were dissolved in methanol/water (1:1, v/v, 1 mL) and directly used for mass spectrometry analyses. Heated polysaccharides (1 mg) were dissolved in water, filtered and used for mass spectrometry measurements. Caramelic products were purchased from supermarket in Bremen, Germany. Toast was prepared from bread purchased from supermarket in Bremen, Germany. The slices of bread were heated in the toaster for 3 min. Afterwards the crust was removed and dissolved in water for analyses. Caramelic colors were obtained from FELIX KOCH OFFENBACH Couleur und Karamel GmbH. For the model roasting experiment coffee's carbohydrates were stirred and heated for 1 h at 180 °C. All heating procedures were performed in the oven with the power of 1.2 kW.

2.2.2 ESI-TOF-MS

High-resolution mass spectra were recorded using a Bruker Daltonics micrOTOF instrument employing both negative and positive electrospray ionization modes. MicrOTOF Focus mass spectrometer (Bruker Daltonics) was fitted with an ESI source and internal calibration was achieved with 10 mL of 0.1 M sodium formate solution. Calibration was carried out using the enhanced quadratic calibration mode. All MS measurements were performed in both negative and positive ion modes. It should be noted that the intensities of the measured peaks in a TOF calibration, influenced the magnitude of the mass error with high-intensity peaks resulting in detector saturation displaying larger mass errors. Usually this problem can be overcome by using spectra averaging on the side flanks of a chromatographic peak or by taking more diluted samples.

2.2.3 MS DATA ANALYSIS

Molecular formulas were calculated using Bruker Data Analysis 4.0 software. The data were subsequently exported to Excel to carry out a simple mathematical operation such as determination of H/C and O/C ratios or the Kendrick analysis. All graphs were created using Origin 7.5.

2.2.4 ESI-FT-ICR

ESI-FT-ICR experiments were performed on a high-resolution mass spectrometer FT-ICR (Fourier Transform Ion Cyclotron Resonance) Varian-920, provided with a 7.0 T actively shielded superconducting magnet and equipped with an ESI source in line with a Triple-quadrupole Varian-320 MS. The solution was directly infused into the ESI source at 20 $\mu\text{L}/\text{min}$ of the flow rate. Quadrupole and hexapole ion guides, accumulation ion hexapole and the other key components were optimized in order to maximize the detection in the 200–1500 m/z range. Commercial beer maltooligosaccharides were used as mass calibrants and tuning standards in both positive and negative ion modes. Tandem MS experiments were performed pulsing a 10.6 μm -CO₂ laser (Synrad Model 48-2, Mukilteo-WA, USA) for Infrared multiphoton dissociation (IRMPD). Product ion formation was optimized by varying IRMPD laser pulse around of 400 ms at $\sim 45\%$ of total power (25 W).

2.2.5 LC-MSⁿ

The LC equipment (Agilent 1100 series, Bremen, Germany) comprised a binary pump, an auto sampler with a 100 μL loop, and a DAD detector with a light-pipe flow cell (recording at 320 and 254 nm and scanning from 200 to 600 nm). This was interfaced with an ion trap mass spectrometer fitted with an ESI source (Bruker Daltonics HCT Ultra, Bremen, Germany) operating in an Auto MSⁿ mode to obtain fragment ion m/z . As necessary, MS², MS³, and MS⁴ fragment-targeted experiments were performed to focus only on compounds producing a parent ion at m/z 143, 161, 179, 197, 287, 305, 323, 341, 359, 449, 431, 467, 485, 503, 521, 611, 629, 647, 665, 683, 773, 791, 809, 827 and 845. Tandem mass spectra were acquired in an Auto-MSⁿ mode (smart fragmentation) using a ramping of the collision energy. Maximum fragmentation amplitude was set to 1 V, starting at 30% and ending at 200%. MS operating

conditions (negative mode) have been optimized using glucose with a capillary temperature of 365 °C, a dry gas flow rate of 10 L/min and a nebulizer pressure of 12 psi.

2.2.6 HPLC

Separation was achieved on a 250 × 4.6 mm i.d. column containing diphenyl 5 μ m and 5 × 4.6 mm i.d. guard column of the same material (Varian, Darmstadt, Germany). Solvent (water:formic acid 1000:0.05 v/v) was delivered at a total flow rate of 850 μ L/min by 25 min isocratic.

2.2.7 MALDI-TOF-MS

All experiments were performed in the positive ion mode using an Ultraflex II MALDI TOF/TOF mass spectrometer (Bruker Daltonics) equipped with a pulsed 50 Hz N₂ laser (wavelength 337 nm) and controlled by FlexControl 3.0. software (Bruker Daltonics). The laser intensity was varied in the range from 30 to 45%. Samples (0.5 μ L) were deposited on top of a layer of crystals of 2,5-dihydroxybenzoic acid (DHB) formed by decomposition of 0.5 μ L of DHB solution on the MALDI plate and allowing it dry at ambient temperature. A MALDI matrix was prepared by dissolving 5 mg of DHB in 1 mL mixture of acetonitrile/methanol/aqueous trifluoroacetic acid (1%, v/v) (1:1:1, v/v/v). The MS/MS experiments were carried out using the LIFT method.

2.2.8 THERMOGRAVIMETRIC ANALYSIS (TGA)

Thermogravimetric analyses (TGA) were performed using a TA SDT Q600 instrument. The temperature was ramped from 25 to 180 °C (glucose, galactose, mannose, sucrose, maltose), to 200 °C (lactose) and to 220 °C (starch and cellulose) at a rate of 5 °C/min and kept at final temperature for 2 h using a nitrogen atmosphere.

2.2.9 INFRARED (IR) ANALYSIS

Infrared (ATR-IR) spectra were recorded using a neat material on a Bruker, Vector 33 spectrometer and on KBr pellets using a Nicolet Avatar 370 spectrometer. IR absorptions are given in wavenumbers (cm^{-1}).

2.2.10 ^1H NMR AND ^{13}C NMR

^1H and ^{13}C NMR spectra were acquired on a JEOL ECX-400 spectrometer at room temperature in D_2O , using a 5 mm probe, operating at 400 MHz and 100 MHz, respectively. The chemical shifts (δ) are reported in parts per million (ppm).

2.3 THE AIM OF THE STUDY (II)

The second part involves unraveling the composition of caramel, a complex food material, which is being consumed at levels of several millions of tons annually. The goal is to give a comprehensive view on the chemical structures of such products, derived from heating of monosaccharides (glucose, fructose, galactose, mannose) and disaccharides (sucrose, maltose, lactose). The work is focused on the characterization of the non-volatile fraction of caramel, studied only on few occasions. The searching for the components that might be responsible for a brown color of caramel is of great interest. Besides, commercial caramel products and caramel colors should be explored to find similarities between mono- and disaccharides investigated in this thesis.

The thermal decomposition products obtained from starch and cellulose model systems and then compared with the thermal degradation products in bread as a real food example are investigated.

Finally, the model systems of roasted coffee's carbohydrates are studied prior to simplify the composition of roasted coffee beans. The MS-based methodology must be evaluated for the analysis of the aforementioned food material. This involves combining the mass spectrometry with liquid chromatography techniques. Next, the complex MS data are analyzed with the exploration of several graphical interpretation techniques (van Krevelen and Kendrick).

2.4 RESULTS & DISCUSSION

2.4.1 CAMELIZATION OF MONOSACCHARIDES

This section is focused on the chemical structures of the products derived from the heating of monosaccharides: glucose (**32**), fructose (**33**), galactose (**34**) and mannose (**35**). The first step involved the optimization of the heating conditions towards caramel formation. The thermogravimetric analysis (TGA) of monosaccharides along with mass spectrometry studies at various temperatures has thus been performed. In fact, 2 h of the reaction at 180 °C for glucose (**32**), galactose (**34**) and mannose (**35**), whereas for fructose (**33**) at 140 °C revealed to be the optimum parameters. Thermogravimetric curves of all studied monosaccharides showed similar profiles with 10–12% weight loss using the aforementioned conditions, which statistically correspond to a loss of one water molecule per monosaccharide and thus completion of the reaction (example in Figure 38). In the mass spectra the signal of the starting material was reduced to around 10% of the total intensity.

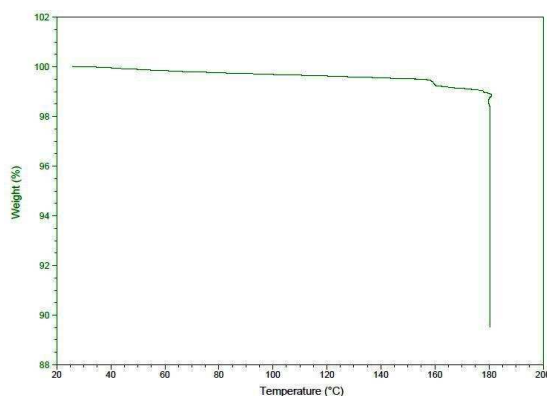


Figure 38. Thermogravimetric curve of caramelized glucose (temperature was ramped from 25 to 180 °C and kept at final temperature for 2 h)

2.4.1.1 ESI-TOF mass spectrometry

A time of flight mass analyzer (TOF-MS) with electrospray ionization (ESI) have been applied to study the composition of the obtained caramel samples. According to the study of Reemtsma and Hertkorn^[124] the resolution corresponding to the time of flight analyzer is

obviously enough to provide data for complex mixture with the components of CHO composition. The mass spectra of caramelized monosaccharides were acquired in both positive and negative ion modes. Figure 39 - Figure 42 illustrate the mass spectra of all studied caramel samples in the negative ion mode.

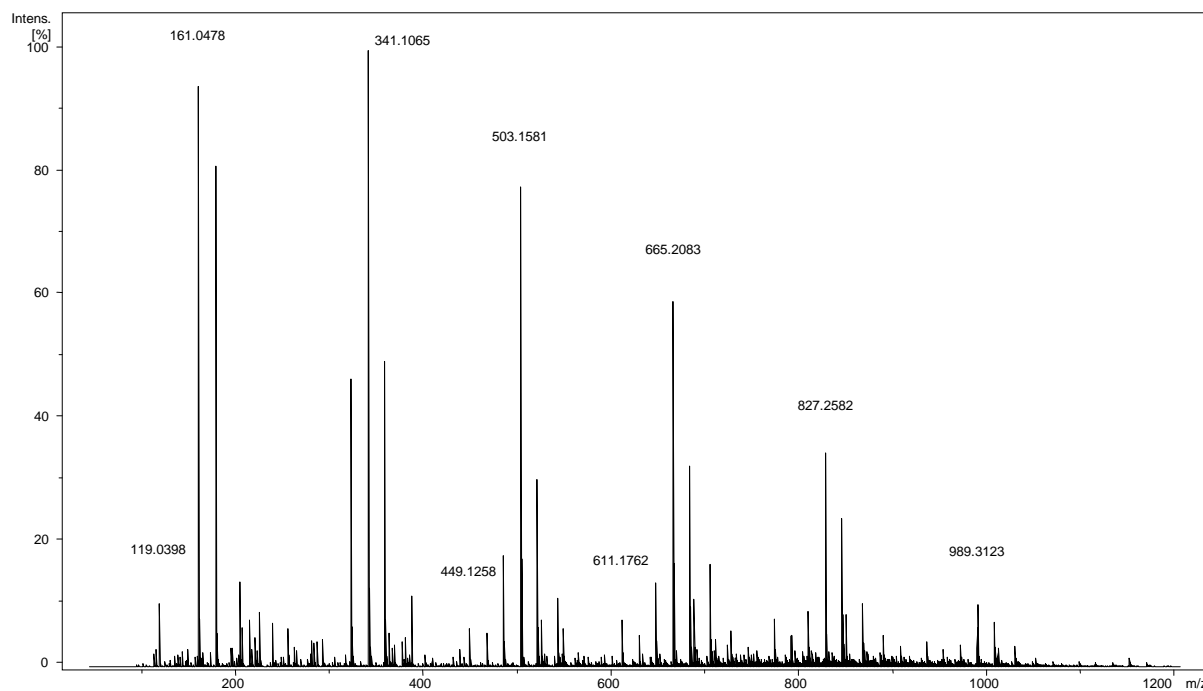


Figure 39. Mass spectrum of caramelized glucose (32) in the negative ion mode using a direct infusion into an ESI-TOF-MS instrument

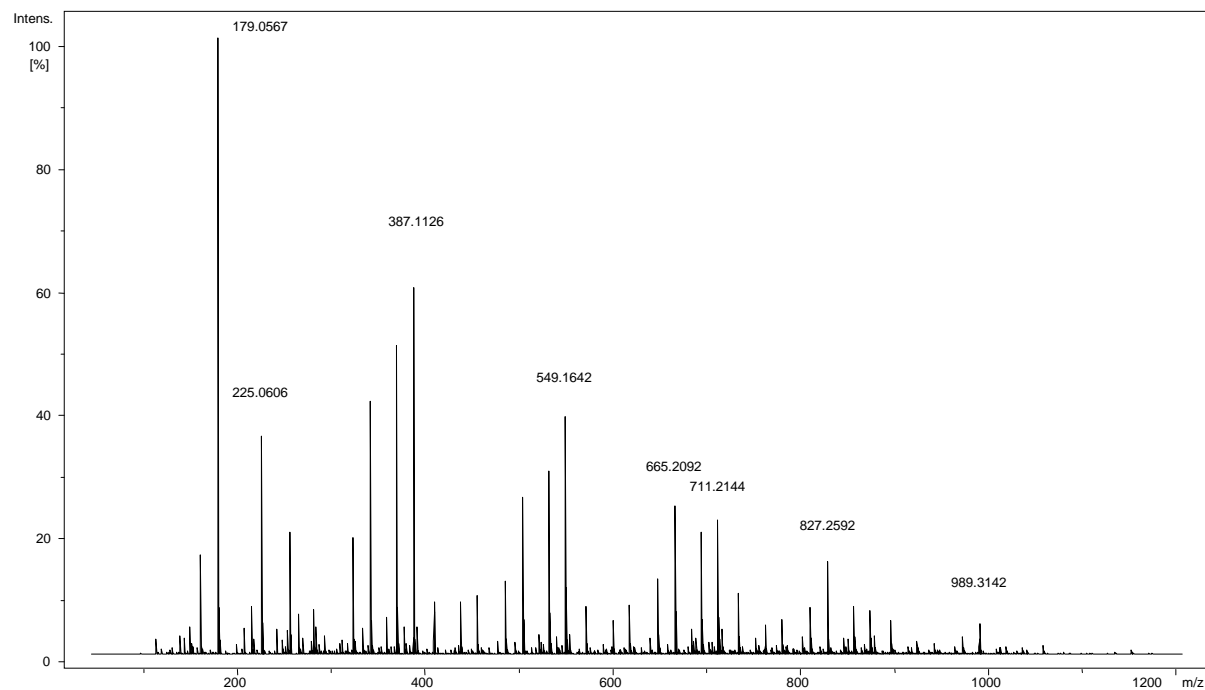


Figure 40. Mass spectrum of caramelized fructose (33) in the negative ion mode using a direct infusion into an ESI-TOF-MS instrument

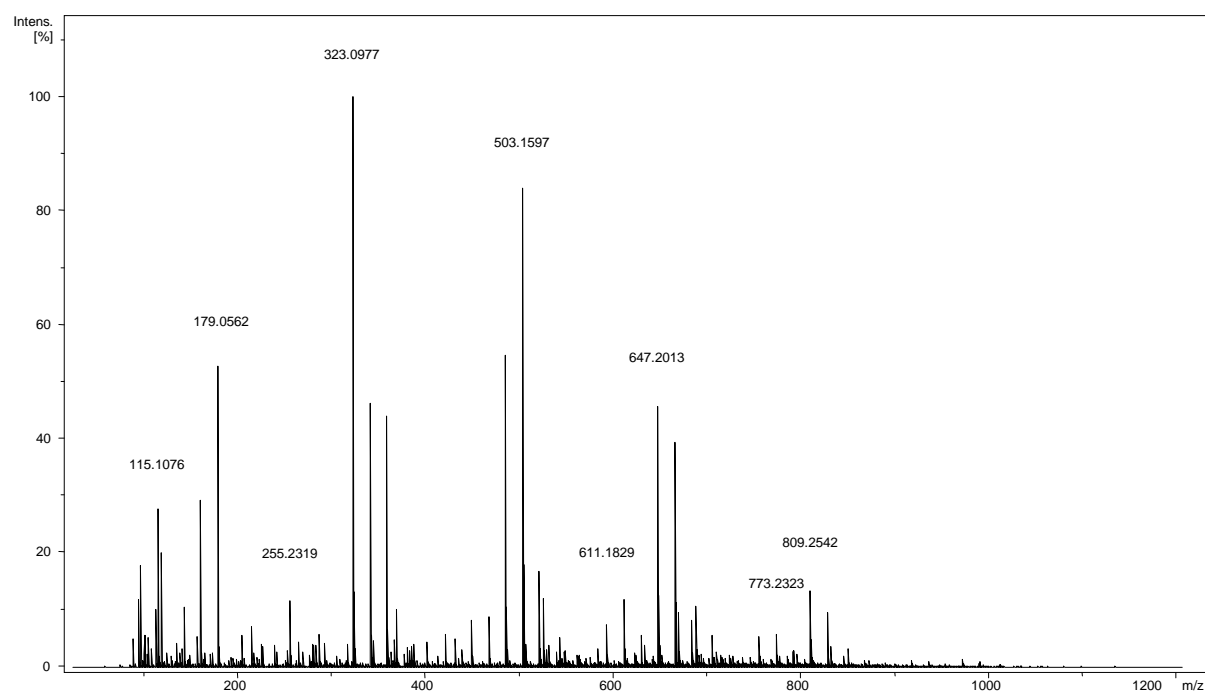


Figure 41. Mass spectrum of caramelized galactose (34) in the negative ion mode using a direct infusion into an ESI-TOF-MS instrument

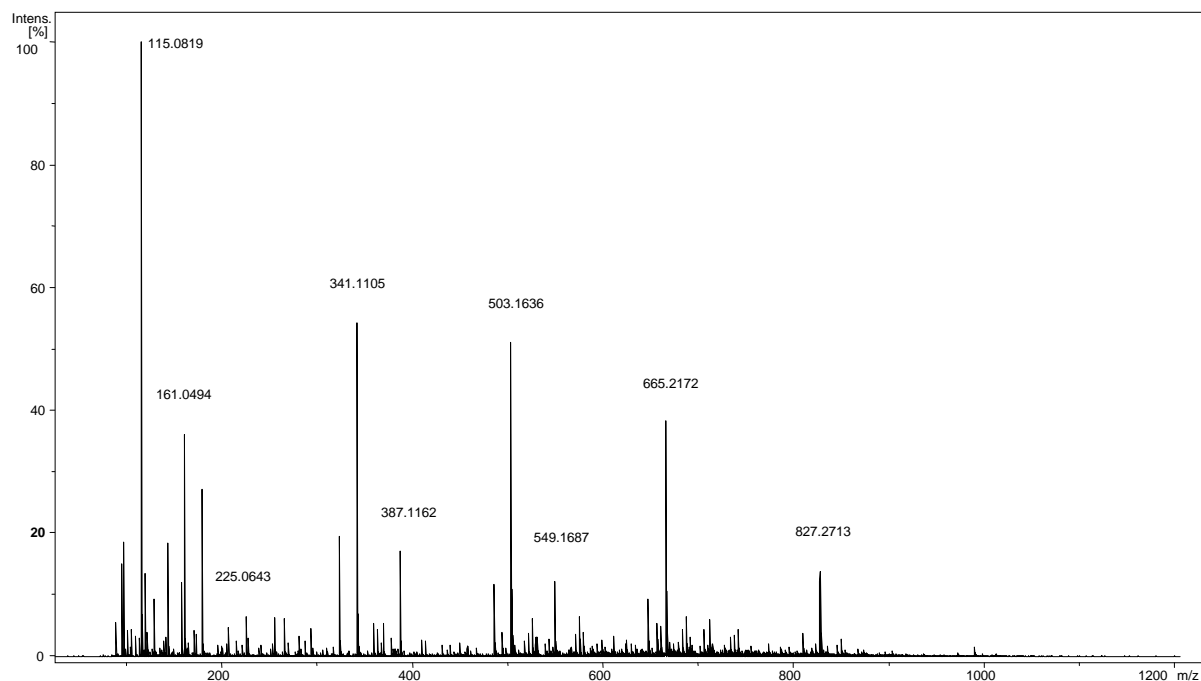


Figure 42. Mass spectrum of caramelized mannose (**35**) in the negative ion mode using a direct infusion into an ESI-TOF-MS instrument

The positive ion mass spectra were dominated by sodiated molecular ions. The spectra in a m/z range of 50–1200 contain up to several thousand signals. The number of compounds detected in a direct infusion of ESI-MS is the minimum number of compounds due to potential isomers corresponding to each ion. The molecular formula lists of compounds were generated and the assignment of the most intensive peaks for glucose is present in Table 9 (for **33**, **34** and **35**, see Table A4, Appendix)*.

* See on page 151

Table 9. High-resolution mass (MS-TOF) data for caramelized glucose in the negative ion mode

Peak Numbering	Assignment	Molecular Formula	Experimental m/z [M-H] ⁻	Theoretical m/z [M-H] ⁻	Relative Error [ppm]
1		C ₆ H ₁₂ O ₂	115.0762	115.0765	2.3
2		C ₄ H ₈ O ₄	119.0347	119.0350	2.6
3		C ₈ H ₈ O ₂	135.0452	135.0452	0.4
4		C ₈ H ₁₆ O ₂	143.1075	143.1078	2.0
5		C ₉ H ₁₈ O ₂	157.1232	157.1234	1.6
6	Glu - H ₂ O	C ₆ H ₁₀ O ₅	161.0452	161.0455	2.2
7	Glucose	C ₆ H ₁₂ O ₆	179.0563	179.0561	0.9
8		C ₇ H ₁₄ O ₈	225.0610	225.0616	2.7
9		C ₁₆ H ₃₂ O ₂	255.2320	255.2330	3.7
10		C ₁₅ H ₂₂ O ₄	265.1442	265.1445	1.1
11		C ₉ H ₁₈ O ₉	269.0875	269.0878	1.2
12		C ₁₈ H ₃₆ O ₂	283.2646	283.2643	1.3
13	(Glu) ₂ - 3×H ₂ O	C ₁₂ H ₁₆ O ₈	287.0776	287.0772	1.1
14		C ₁₇ H ₂₆ O ₄	293.1761	293.1758	1.0
15	(Glu) ₂ - 2×H ₂ O	C ₁₂ H ₁₈ O ₉	305.0869	305.0878	2.8
16	(Glu) ₂ - H ₂ O	C ₁₂ H ₂₀ O ₁₀	323.0998	323.0984	4.4
17	(Glu) ₂	C ₁₂ H ₂₂ O ₁₁	341.1076	341.1089	3.8
18	(Glu) ₂ + H ₂ O	C ₁₂ H ₂₄ O ₁₂	359.1194	359.1195	0.2
19	(Glu) ₃ - 4×H ₂ O	C ₁₈ H ₂₄ O ₁₂	431.1187	431.1195	1.7
20	(Glu) ₃ - 3×H ₂ O	C ₁₈ H ₂₆ O ₁₃	449.1308	449.1301	1.6
21	(Glu) ₃ - 2×H ₂ O	C ₁₈ H ₂₈ O ₁₄	467.1412	467.1406	1.2
22	(Glu) ₃ - H ₂ O	C ₁₈ H ₃₀ O ₁₅	485.1526	485.1512	1.2
23	(Glu) ₃	C ₁₈ H ₃₂ O ₁₆	503.1607	503.1618	2.0
24	(Glu) ₃ + H ₂ O	C ₁₈ H ₃₄ O ₁₇	521.1718	521.1723	1.0
25	(Glu) ₄ - 3×H ₂ O	C ₂₄ H ₃₆ O ₁₈	611.1853	611.1829	3.9
26	(Glu) ₄ - 2×H ₂ O	C ₂₄ H ₃₈ O ₁₉	629.1961	629.1935	4.3
27	(Glu) ₄ - H ₂ O	C ₂₄ H ₄₀ O ₂₀	647.2037	647.2040	0.5
28	(Glu) ₄	C ₂₄ H ₄₂ O ₂₁	665.2115	665.2146	4.6
29	(Glu) ₄ + H ₂ O	C ₂₄ H ₄₄ O ₂₂	683.2278	683.2251	4.0
30	(Glu) ₅ - 4×H ₂ O	C ₃₀ H ₄₄ O ₂₂	755.2242	755.2251	1.2
31	(Glu) ₅ - 3×H ₂ O	C ₃₀ H ₄₆ O ₂₃	773.2391	773.2357	4.4
32	(Glu) ₅ - 2×H ₂ O	C ₃₀ H ₄₈ O ₂₄	791.2494	791.2463	3.9
33	(Glu) ₅ - H ₂ O	C ₃₀ H ₅₀ O ₂₅	809.2565	809.2568	0.4
34	(Glu) ₅	C ₃₀ H ₅₂ O ₂₆	827.2709	827.2674	4.2
35	(Glu) ₅ + H ₂ O	C ₃₀ H ₅₄ O ₂₇	845.2821	845.2780	4.9
36	(Glu) ₆ - 3×H ₂ O	C ₃₆ H ₅₆ O ₂₈	935.2874	935.2885	1.2
37	(Glu) ₆ - 2×H ₂ O	C ₃₆ H ₅₈ O ₂₉	953.3027	953.2991	3.7
38	(Glu) ₆ - H ₂ O	C ₃₆ H ₆₀ O ₃₀	971.3109	971.3097	1.3
39	(Glu) ₆	C ₃₆ H ₆₂ O ₃₁	989.3230	989.3202	2.8

The lists of the high-resolution mass data of caramels were then subjected to further investigation. One of the areas of chemistry, which deals with complex mixtures is undoubtedly petroleum chemistry, in which some novel interpretation strategies of mass spectrometry data have been developed. The van Krevelen and Kendrick analyses were applied for the first time to caramel. These analyses have been hitherto used only two times for dietary materials, such as wine^[183] and black tea thearubigins.^[184] The van Krevelen diagrams generated from the high-resolution mass data indicating the elemental H/C and O/C ratios calculated from the molecular formulas of the experimental high-resolution MS data

and both of them were plotted in a two-dimensional graph against each other.^[20] Figure 43 represents the van Krevelen diagrams consisting of a plot of H/C vs O/C atomic ratios for caramelized **32**, **33**, **34** and **35**.

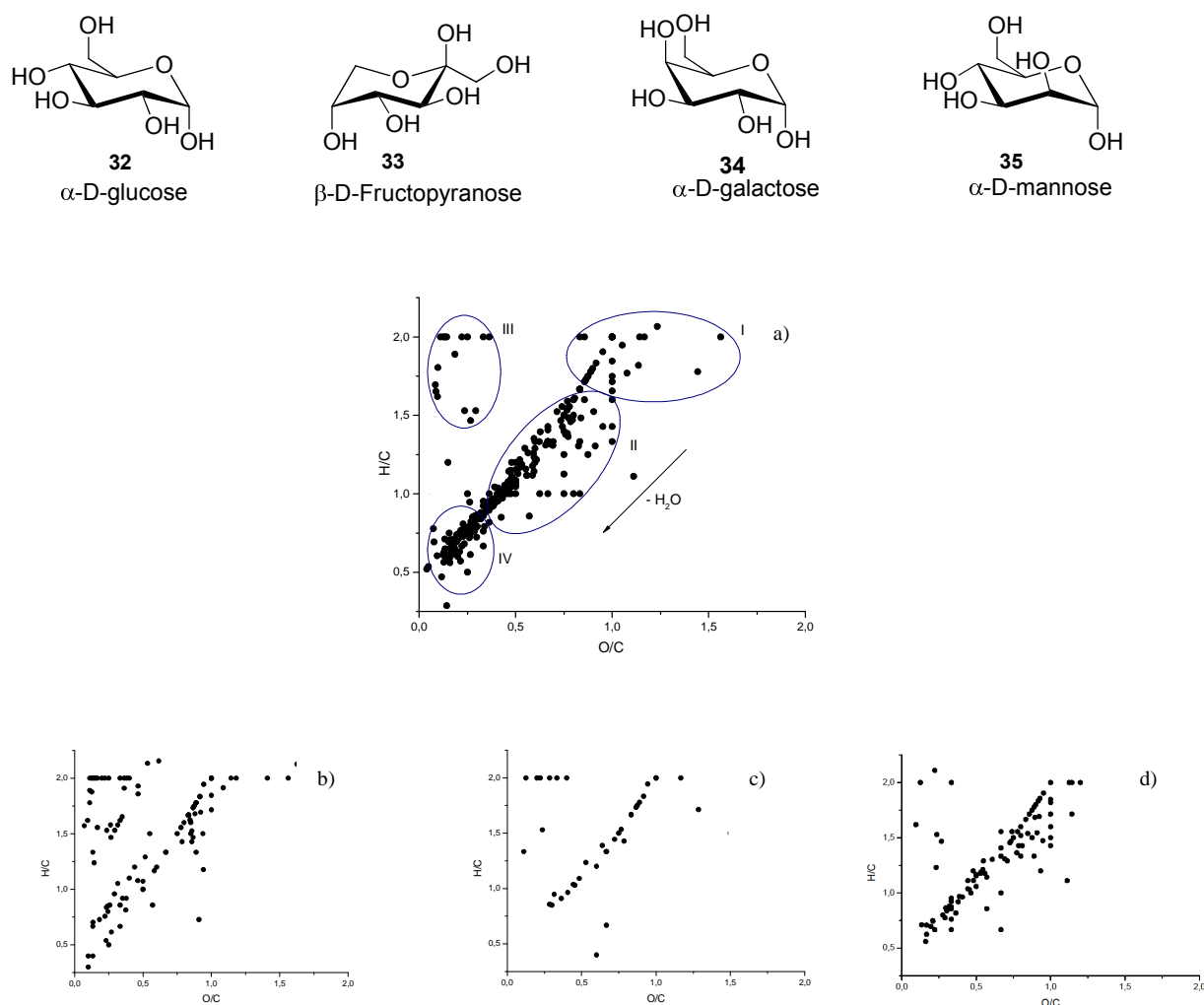


Figure 43. Two dimensional van Krevelen plots showing the O/C versus H/C ratio for caramelized: a) glucose, b) fructose, c) galactose and d) mannose in the negative ion mode in m/z range between 50–1200

This type of plot leads to two main conclusions. Firstly, certain classes of compounds can be defined by their elemental ratio boundaries, e.g. in carbohydrate H/C is ~ 2 and O/C is ~ 1 . Secondly, with the elemental ratio of the starting material known, reaction types that alter this elemental composition can be identified. The following information can be extracted from these diagrams. A significant number of points are found in the characteristic for carbohydrates area (I) of the van Krevelen plot (see plot a, Figure 43). The group of points is

present on the top right corner. Compounds with high H/C and low O/C ratios, which apparently represents compounds after reduction (III) are found in the left top corner of the plot and can be classified as lipid-like heterocycles. The next group of points on the left bottom corner with low H/C and O/C ratios suggests the formation of aromatic compounds (IV). Many points appear in the middle range of the graph like on the line with the negative slope, which comes from successive dehydration process (II). The loss of water shifts the data points towards the origin of the plot.

The second graphical representation of the MS data applied, is the Kendrick analysis. The graphs with the H₂O mass increment were prepared from the theoretical and experimental high-resolution masses derived from TOF-MS experiments for heated monosaccharides. Figure 44 shows a two-dimensional display of Kendrick mass defect *versus* nominal Kendrick mass with all peaks higher than 20 of a baseline noise for **32**, **33**, **34** and **35**.

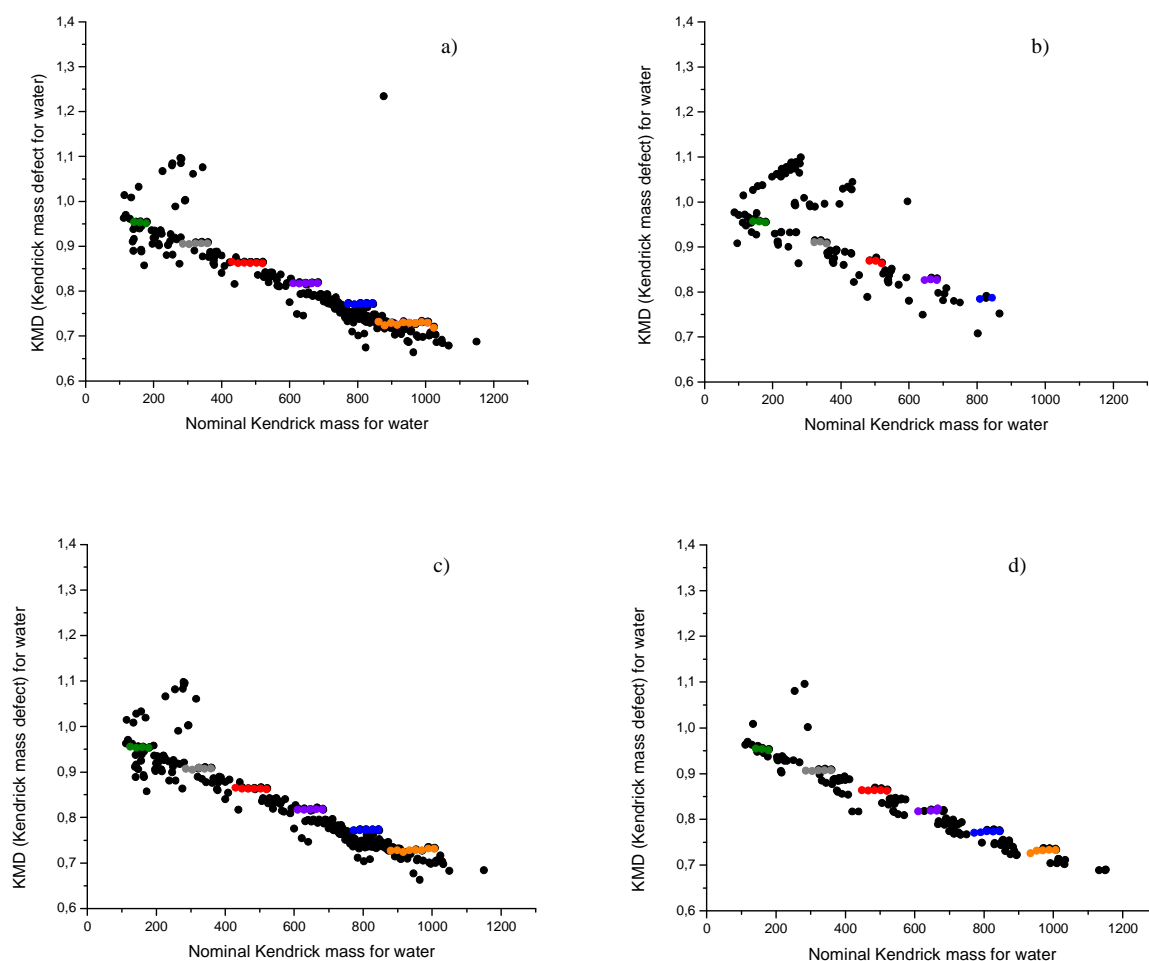


Figure 44. Two dimensional Kendrick plots for mass increment H₂O showing the distribution of the Kendrick mass defect plotted against the nominal Kendrick mass of pseudo-molecular ions for caramelized: a) **32**, b) **33**, c) **34** and d) **35** in the negative ion mode

Obviously, these diagrams suggested that several homologous series of compounds exist, which beginning from starting materials of different masses lose several molecules of water (up to eight), identified as data points on lines parallel to the x -axis on the Kendrick plot.^[6] The colored points represent starting materials of different masses losing several molecules of water (up to eight). The colors indicate the homologous series of monomers (green), dimers (gray), trimers (red), tetramers (violet), pentamers (blue) and hexamers (orange). The dehydration and hydration products of monosaccharides and their oligomers are indeed created and easily visualized.

The investigation of all the aforementioned MS spectra and graphs showed the formation of oligomeric structure of different monosaccharides with up to hexamers. The most abundant peaks belonged to dehydration products, including dehydration of monomeric carbohydrates and their oligomers demonstrating successive loss of up to eight water molecules. The presence of hydration products was found in the samples with up to two water molecules added to an oligomeric saccharide and redox disproportionation reaction products. Minor aromatic compounds were probably formed by an excessive dehydration process.

Moreover, MALDI-TOF mass spectrometry with DHB (2,5-dihydroxybenzoic acid) as a matrix showed additional oligomeric hexoses at m/z 1499.61, 1661.58 and 1805.62 corresponding to nonamers, decamers and undecamers for glucose, respectively. Coimbra *et al.* have reported a similar pattern, when studying the degradation products of coffee carbohydrates.^[185] In the following section, the chemical nature of these reaction products will be characterized by liquid chromatography coupled to tandem mass spectrometry. This approach allows an isomer separation by LC concomitant with selective ion monitoring of selected classes of compounds.

2.4.1.2 Oligomers of hexoses

Both the ESI-TOF-MS direct infusion measurements, ESI-TOF-LC-MS measurements revealed the presence of oligomers of hexoses (**36**) formed from glucose (**32'**) with a maximum number of six hexoses incorporated at m/z values of 179.1 (monosaccharide), 341.1 ($C_{12}H_{22}O_{11}$), 503.2 ($C_{18}H_{32}O_{16}$), 665.2 ($C_{24}H_{42}O_{21}$), 827.3 ($C_{30}H_{52}O_{26}$) and 989.3 ($C_{36}H_{62}O_{31}$) in the negative ion mode (Figure 45). The sodiated pseudo-molecular ions in the positive ion mode were detected at 203.1 (monosaccharide), 365.1 ($C_{12}H_{22}O_{11}$), 527.2 ($C_{18}H_{32}O_{16}$), 689.2 ($C_{24}H_{42}O_{21}$), 851.3 ($C_{30}H_{52}O_{26}$) and 913.3 ($C_{36}H_{62}O_{31}$).

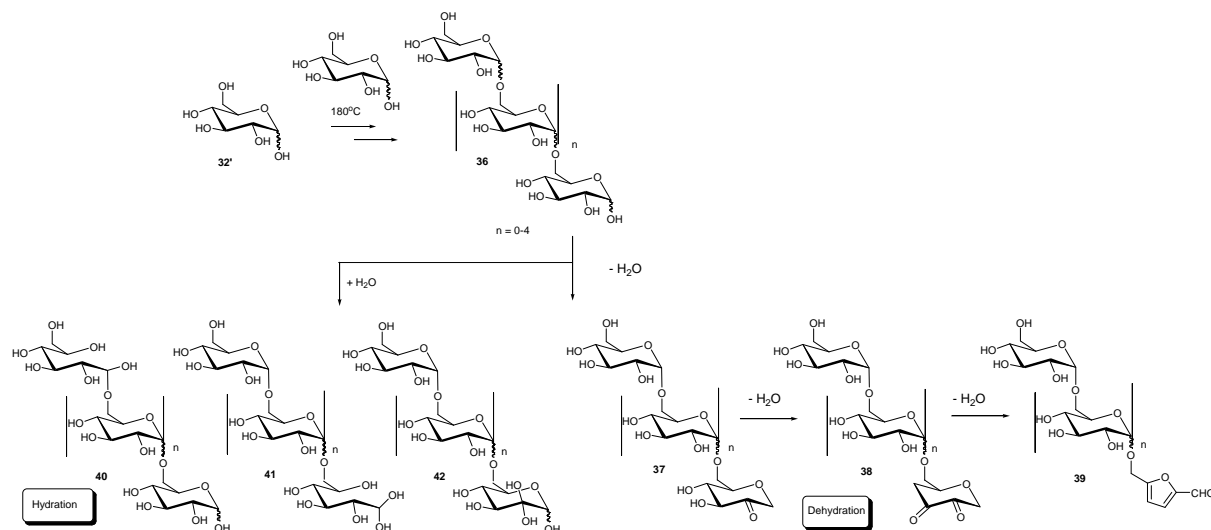


Figure 45. Structures of carbohydrate monomers and potential caramelization products (please note that regiochemistry of glycosidic linkage in **36–42**, the regiochemistry of dehydration **37–38** and the regiochemistry of hydrate **40–42** is selected randomly)

Targeted tandem-LC-MS measurements using the optimized chromatographic conditions at m/z values of 179.1, 341.1, 503.2, 665.2, 827.3 and 989.3 furnished extracted ion chromatograms (EICs) for the six m/z values that correspond to monosaccharides and oligomeric hexoses. Each EIC showed multiple chromatographic peaks; for example for the ion at m/z 341.1 corresponding to diglucose a total of eight resolved chromatographic peaks were observed, one of high, two of medium and five of low intensities, each displaying the MS^2 spectrum consistent with a dimer of glucose (Figure 46).^[186,187] Some of the MS^2 spectra were found to be identical, while others displayed subtle differences. These findings are consistent with an unselective formation of a glycosidic bond to give eight out of twenty theoretically possible regio- and stereoisomers of diglucose. An alternative epimerization process rationalizing this finding could be ruled out by control experiments. Such experiments include a comparison of the LC-MS data for caramelized glucose with that of caramelized mannose and galactose complemented by a GC-MS analysis of a caramel sample hydrolyzed by acid treatment followed by Me_3SiCl derivatization. A full set of isomeric glucose derivatives with similar tandem MS data for all ten theoretically possible caffeoyl esters of glucose, has been recently reported.^[188] Analogous multiple chromatographic peaks were observed also for trimers, tetramers, pentamers, heptamers and hexamers of monosaccharides. However with increasing molecular weight it must be assumed that the complete set of regio- and stereoisomers were not resolved chromatographically.

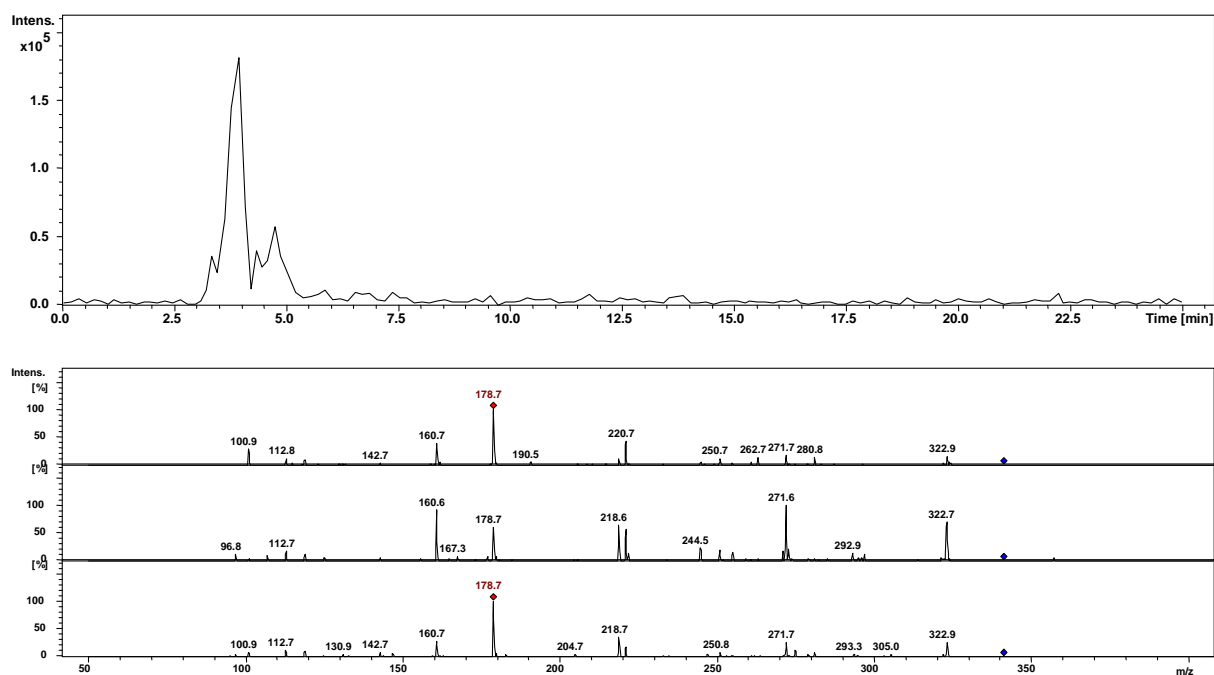


Figure 46. Extracted ion chromatogram (top) and MS² spectra (bottom) of pseudo-molecular ion at m/z 341.0 ($C_{12}H_{22}O_{11}$) for three selected chromatographic peaks of caramelized glucose in the negative ion mode

All of the monomeric and oligomeric ions of caramel samples were fragmented in the negative ion mode using a direct infusion into an ESI ion trap mass spectrometer. Fragmentations of an ion at m/z 179.0 gave the base peaks at m/z 161.0 (**34** and **35**) and 90.0 (**32** and **33**), which correspond to an anion of monosaccharide after dehydration and an anion of monosaccharide without three formaldehyde molecules, coming from the cleavage of the glycoside ring, respectively. The base peaks at m/z 179.0 are observed from dimers of **32**, **33**, **34**, formed by the glycosidic bond cleavage between two hexoses and may occur at either the reducing or non-reducing end of the molecule. Furthermore, **35** showed the base peak at m/z 323 that corresponds to a dimer without one water molecule. In particular, the dehydration process took place before the cleavage of the respective glycosidic bond. The fragment ions at m/z 221 [$4 \times CH_2O$] were relatively intense and came from the cleavage of the glycoside ring. The MS² spectra of the ion at m/z 503, a trimer of monosaccharides for all caramel samples exhibited the base peak at m/z 341, belonging to a dimer of monosaccharides formed after the glycosidic bond cleavage at the non-reducing end. Fragmentations of the ions at m/z 665, corresponding to a tetramer of monosaccharides gave in the case of **32**, **34** and **35** the base

peak at m/z 503, which indicate the glycosidic bond cleavage at the non-reducing end. In contrast to **32**, **34** and **35**, the base peak of **33** appeared at m/z 485 derived from the glycosidic bond cleavage at the reducing end.

All the MS² spectra of an ion at m/z 827 for **32**, **34** and **35** correspond to a pentamer of monosaccharides showed the base peak at m/z 665 (an anion of a tetramer). The cleavage of the glycosidic bond took place at the non-reducing end, as observed for the aforementioned tetramers. Due to the low abundance, the fragmentation process of an ion at m/z 827 for **33** did not occur at all. However, fragmentations of the ion at m/z 989, a hexamer of monosaccharides gave common fragments for all analyzed monosaccharides, while the base peak appeared at m/z 827 excluding **33** with the base peak at m/z 647. The aforementioned oligomers as well as the base peak at m/z 827 showed the particular cleavage of the external, whereas for **33** the cleavage of the internal glycosidic bond (m/z 647). The fragmentation data for oligomers of hexoses are consistent with exclusive cleavages of the glycosidic bonds on the external non-reducing part of the molecule. Only two exceptions in the case of a pentamer and a hexamer of **33** gave the main fragmentation with internal glycosidic bonds.

2.4.1.3 Dehydration products

The van Krevelen and Kendrick mass analyses suggested the presence of dehydration products including monomers of hexoses and their oligomers. Such dehydrated oligomers of caramelized **32**, **33**, **34** and **35** derived from a loss of a single water molecule are observed at m/z 323.1, 485.1, 647.2 and 809.2, respectively. In analogy to oligomers of hexoses, EICs were generated for dehydrated products and multiple peaks were found. For glucose seven dehydration products obtained from a loss of a single water molecule could be observed in extracted ion chromatograms (EICs) at m/z 161.1 in the negative ion mode. The number of signals can be interpreted as the formation of seven of the eleven theoretically possible isomers of anhydroglucose. After the water elimination from glucose at the position C1-C4 initially an enol is being formed which subsequently tautomerizes to the keto form (Figure 45)*. An evidence for the presence of such ketones is additionally determined by both IR and NMR spectroscopy analysis of the caramel products.

The observed intense peaks indicate the loss of three water molecules at m/z 287.1, 449.2, 611.2, 773.3 and 935.3 in the negative ion mode and their sodiated adducts at m/z 311.1, 473.2, 635.2, 797.3 and 959.3 in the positive ion mode. The MS² spectra for all compounds

* See on page 82

showed loss of all three waters at the same saccharide moiety with a characteristic neutral losses of 126 [C₆H₆O₃]. These data point out the formation of a hydroxymethylene furfuraldehyde moiety at the reducing end of the reaction product **39**, as suggested by Blank *et al.* in Maillard reaction of carbohydrates (Figure 45).^[189] The presence could be further substantiated by characteristic ¹H NMR (δ_H = 6.5, 7.5 and 9.8) and ¹³C NMR signals of this group (e.g. C=O at δ_C = 195) of the caramel samples.

For oligomers of glucose, dehydration products originating from a loss of a single water molecule are observed at m/z 323.1, 485.1, 647.2 and 809.2. In EICs at m/z 323.1 or 485.1 (four peaks each in EICs with one peak of high intensity) were detected. Assuming that the E₁-type water elimination in polar liquid caramel took place and the presence of furfuraldehyde moieties at the reducing end, the main peak could be assigned to a loss of water at the position C1-C2 at the reducing end (1-OH terminal glucose moiety) resulting in compound **37** (Figure 45). Alternatively the formation of deoxyglucosones followed by unselective glycosidic bond formation must be considered.^[190] This assignment of the compound **37** is convincingly supported by the MS² and MS³ spectra. For example, the main peak at m/z 485.1 of compound **43** or **44** (Glu₃-H₂O, C₁₈H₂₉O₁₅) shows a neutral loss of 102 [C₄H₆O₃] in the MS² spectrum (Figure 47). Apparently it could originate from a loss of C₄ unit at either the reducing or non-reducing end of the molecule. Dehydration at the central carbohydrate moiety can be excluded from these data. A further weak peak at m/z 341.1 in the MS² spectra corresponding to a neutral loss of 144 [C₆H₈O₄] most likely derived from dehydration at the non-reducing end. Finally, in the MS³ spectra originating from the base peak at m/z 323.1 (**45**) in MS², an intense fragment ion of 83% at m/z 221.1 corresponds to a neutral loss of 102 [C₄H₆O₃] was observed, rationalized with alternative dehydration from either the reducing end in **43** or the non-reducing terminal carbohydrate moiety in **44** (Figure 47). However, the MS³ spectra of the fragment ion obtained from a neutral loss of 102 at m/z 383.1 (**46**) shows two characteristic fragment ions at m/z 340 with a neutral loss of 43 [C₂H₃O] and m/z 265 with a neutral loss of 118 [C₄H₆O₄], which can only be explained by dehydration at the reducing moiety in a tentative structure of **46** (Figure 47).

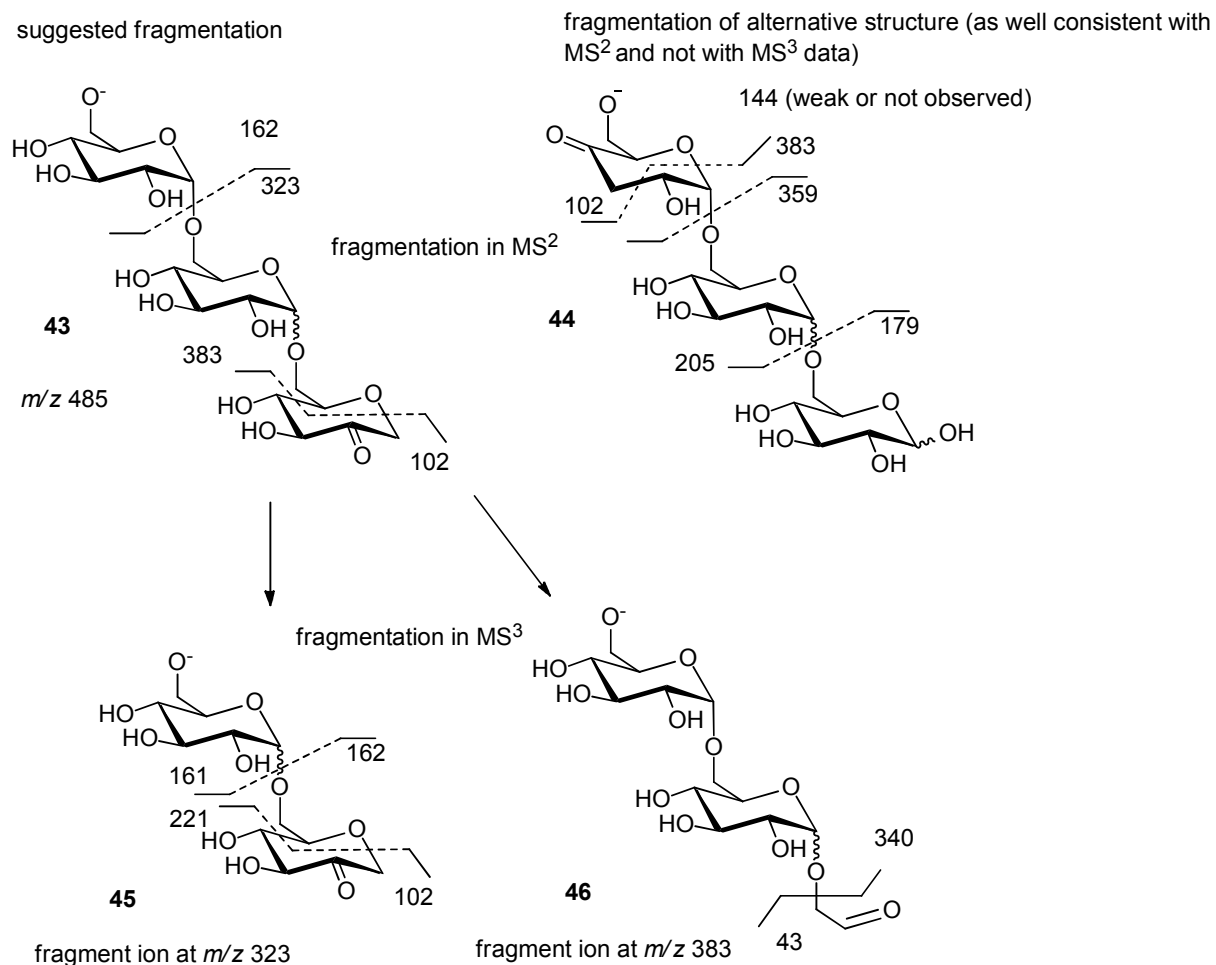


Figure 47. Suggested fragmentation mechanism at m/z 485.1 for the dehydrated ions (regiochemistry of C=O chosen randomly)

The negative ion mode data were obtained for dehydration products of caramelized monosaccharides at m/z 161.1 and further ions of dehydrated oligomers using a direct infusion into ESI ion trap mass spectrometer. The mass spectra of the fragment ion at m/z 161.1 showed the loss of 60 as the main peak in the case of **32** and **35**, which corresponds to two formaldehyde molecules and the loss of 48 as the main peak of **33** and **34**, which corresponds to one formaldehyde together with a water molecule and both derived from the cross-ring cleavage. The fragmentation of the ion at m/z 323, corresponding to its dehydrated dimer of hexoses exhibited the base peak at m/z 161 [$C_6H_9O_5$] for all caramelized monosaccharides after the glycosidic bond cleavage at the non-reducing end, whilst fragment ion at m/z 179 occurred with intensities ranging from 10–20%.

The fragmentation of the dehydrated trimers of all caramel samples at m/z 485.1 showed the base peak at m/z 323, coming from dehydrated dimers. The MS spectra of the rest dehydrated

ions at m/z 647 and 809 contain always the base peak at m/z 485 and 647 with losses of 162 [$C_6H_{10}O_5$], respectively. The further fragmentation of ions at m/z 485 gave the base peak at m/z 323 for all caramel samples. Dehydrated oligomers of caramelized **32**, **33**, **34** and **35** derived from a loss of two water molecules were observed at m/z 305.1, 467.1, 629.2 and three water molecules at m/z 287.1, 449.1, 611.2. The fragmentation of an ion at m/z 305, a dimer without two water molecule was possible only in the case of **35** with neutral losses of 16 and 66 [$CH_2O + 2 \times H_2O$]. Furthermore, the ion at m/z 287 of a dimer after losing three water molecules gave in all caramel samples neutral losses of 48 [$CH_2O + H_2O$] and 126 [$C_6H_6O_3$]. The latter peak suggests the presence of hydroxymethylfurfural supporting the elimination of all three water molecules at one saccharide moiety. The mass spectra of a trimer without two water molecules (467) showed neutral losses of 18 [H_2O], 180 [$C_6H_{12}O_6$] and 162 [$C_6H_{10}O_5$], predominantly. The base peak at m/z 287 with neutral losses of 162 for caramels except **32** (neutral loss is 18) was found for a trimer without three water molecules (m/z 449). The MS^2 spectra of **34** and **35** gave peaks with neutral losses of 126. This is consistent with the behavior of the aforementioned dehydrated dimers without three water molecules showing the presence of a hydroxymethylfurfural molecule. It also proves the elimination of three water molecules from the same hexose.

2.4.1.4 Hydration products

Next to dehydration products a series of mass spectral signals with molecular formulas corresponding to the hydration products of oligosaccharides were detected at m/z 359.2, 521.2, 683.2, 845.3 and 1007.3. The MS^2 data obtained from targeted tandem MS experiments are fully consistent with initial hydration at any of the at least two anomeric centers with a neutral loss of 180.1 Da observed from the pseudo-molecular ions at m/z 359.2, 521.2, 683.2, 845.3 and 1007.3. Hence, the hydration products were identified as open chain hemiacetal structure, such as **40** and **41** (Figure 45)*. Alternatively, a Lobry-de-Bruyn-van-Alberda-van-Ekenstein isomerization could be envisaged in which the position of the carbonyl group changes along the carbon backbone followed by water addition to ketone functionality.^[191] The tandem MS data do not allow at this stage a clear distinction between these two structural alternatives with a weak fragment ion at m/z 221 originating from a 359 precursor ion comprising the only intact hydrated fragment ion. Recent work by Köpper *et al.* suggests the possible formation of hydrate **42** (Figure 45).^[190] Interestingly, water formed in

* See on page 82

thermal dehydration does not only evaporate in caramelization but also acts as a reagent for the chemical modification of caramelization products.^[192] This represents a phenomenon observed here for the first time.

2.4.1.5 Redox disproportionation products

The van Krevelen plots revealed the presence of a series of minor compounds presumably formed in a redox reaction as “cross peaks” with the respect to the dehydration diagonal. Ions with the molecular formulas consistent with a reduction include for example $C_8H_{16}O_2$, $C_{14}H_{28}O_2$, $C_{15}H_{30}O_2$, $C_{18}H_{36}O_2$, $C_{15}H_{22}O_4$ or $C_{17}H_{24}O_4$. Using LC-tandem MS no further structural information could be obtained on these minor compounds, however similar redox disproportionations products have been suggested by Blank *et al.*, when studying the formation of furans in Maillard reactions.^[189]

2.4.1.6 Comparison of caramelized monosaccharides

Nevertheless, the mass spectra of studied monosaccharides exhibited differences in intensities of main product ions (Figure 42)*. In the spectrum of glucose, a dehydrated monomer is present as a base peak followed by oligomers up to a hexamer. In the case of galactose, mainly dehydrated products such as a dimer, tetra- and pentamer are detected. Among them, a monomer and trimer are also observed with the relatively high intensities. The MS spectrum of mannose exhibits oligomers as the predominant ions followed by dehydrated ions. The most intensive ions in the fructose's MS spectrum are its monomer along with the formic acid adducts of a dimer and trimer, accordingly. Such adducts are present in the spectra of the rest of monosaccharides, although with low intensities. Formic acid being a product of a degradation of monosaccharides, is most probably formed in higher quantities in the case of fructose that causes the formation of the formic acid adduct.

Moreover, three radar plots were prepared for a better visualization of differences between the aforementioned samples. The main axes show individual ions. The relative intensities are located from the centre of the plot to its axes and four studied monosaccharides are illustrated as colored lines (Figure 48).

* See on page 77

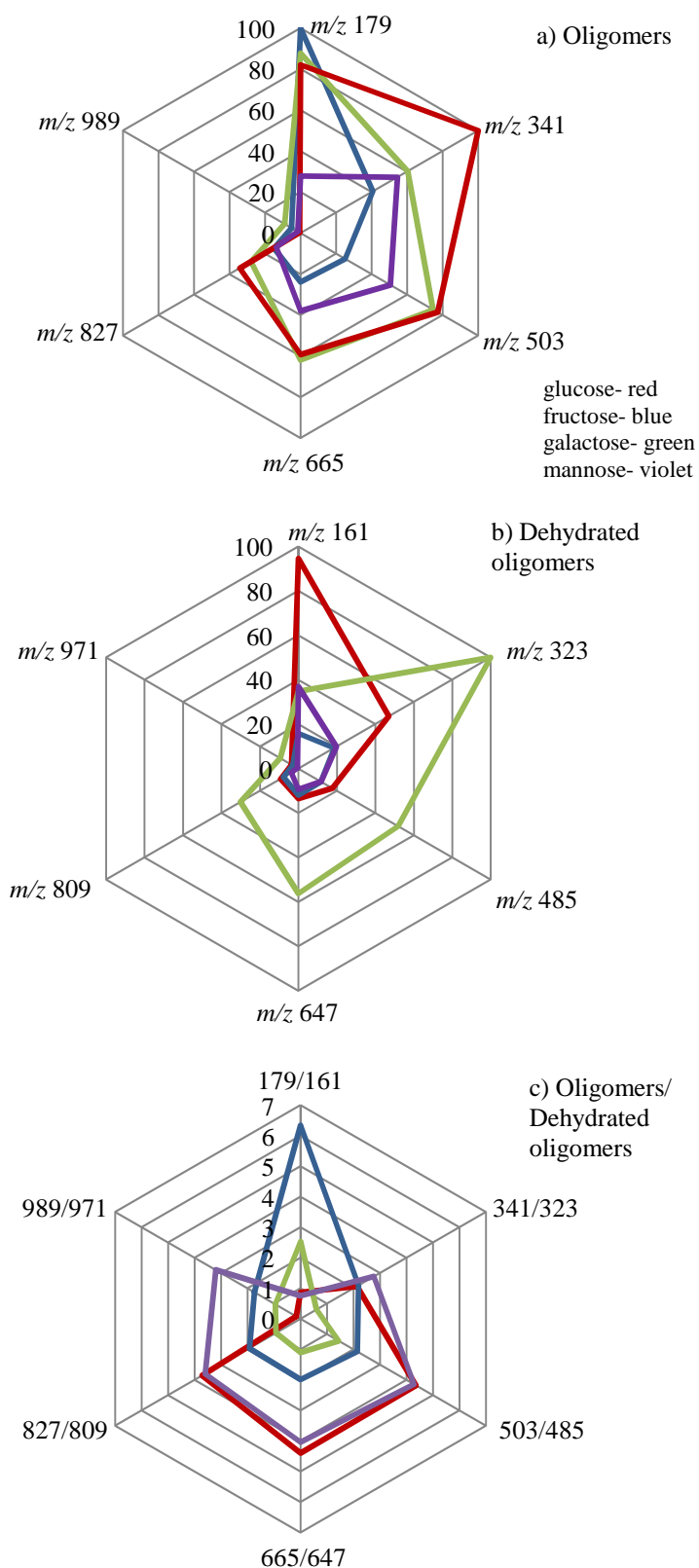


Figure 48. Radar plots of classes of ions detected in a direct infusion negative mode mass spectra of heated monosaccharides **32-35**: a) oligomeric hexoses, b) dehydrated oligomeric hexoses, c) ratio of oligomeric to dehydrated hexoses

The first chart shows differences in intensities of oligomers. The formation of oligomers occurs preferentially in the order glucose>galactose>mannose>fructose. The second plot describes dehydrated products, instead. Galactose forms dehydrated oligomers preferentially, after that glucose, mannose and fructose. On the other hand, monomeric glucose forms dehydrated ions at first. The third graph illustrates the ratios of differed intensities of oligomers to dehydrated oligomers. It is visible that fructose varies from the rest of monosaccharides in term of monomeric product with the highest ratio of 179/161, thus the lowest degree of dehydration. Galactose shows higher degree of dehydration of oligomers followed by fructose, mannose and glucose. In fact, mannose and glucose exhibit similar ratios of tetra-, penta- and hexamers to their dehydrated products. The fact that galactose preferentially formed dehydrated products might be explained by their stereochemistry. The axial *C*4-OH substituent of galactose triggers intramolecular S_N2 -type reaction producing most likely a oxygen-bridged molecule **47**, anhydro-galactose (Figure 49).^[193]

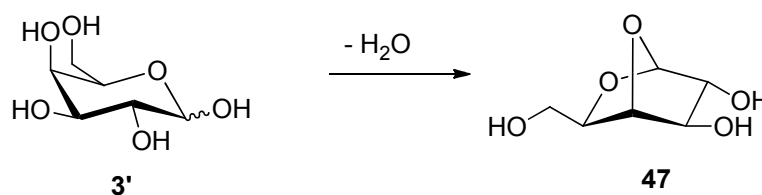


Figure 49. Formation of anhydro-galactose (**47**)

2.4.2 AROMATICS AND THE COLORED COMPOUNDS IN CARMEL

Caramel is a material of a brown color and an identity of the coloring compounds is so far unknown prompting further investigations. Caramel color produced by a base-induced heating of sugar is as well sold as food coloring under the name of E 150. The van Krevelen diagrams indicated the formation of a series of minor aromatic compounds most likely polyaromatic heterocycles falling into elemental ratio boundaries of typical aromatic dye molecules. The brown color can originate from two distinct mechanisms, either from light scattering with a λ^{-4} dependency in the absorption spectrum, which is not observed here. Alternatively brown as a “tertiary color” requires absorption at three distinct wavelengths, of which two must be complementary as shown to be the case here. The optimized chromatographic conditions using a HPLC gradient with higher organic solvent percentage, required for identification of lipophilic aromatic chromophores, which were apparent as minor products in van Krevelen plots, revealed if monitored using UV/VIS detection at 400, 450 and 500 nm a single sharp chromatographic peak at identical retention times for all three wavelengths (Figure 50).

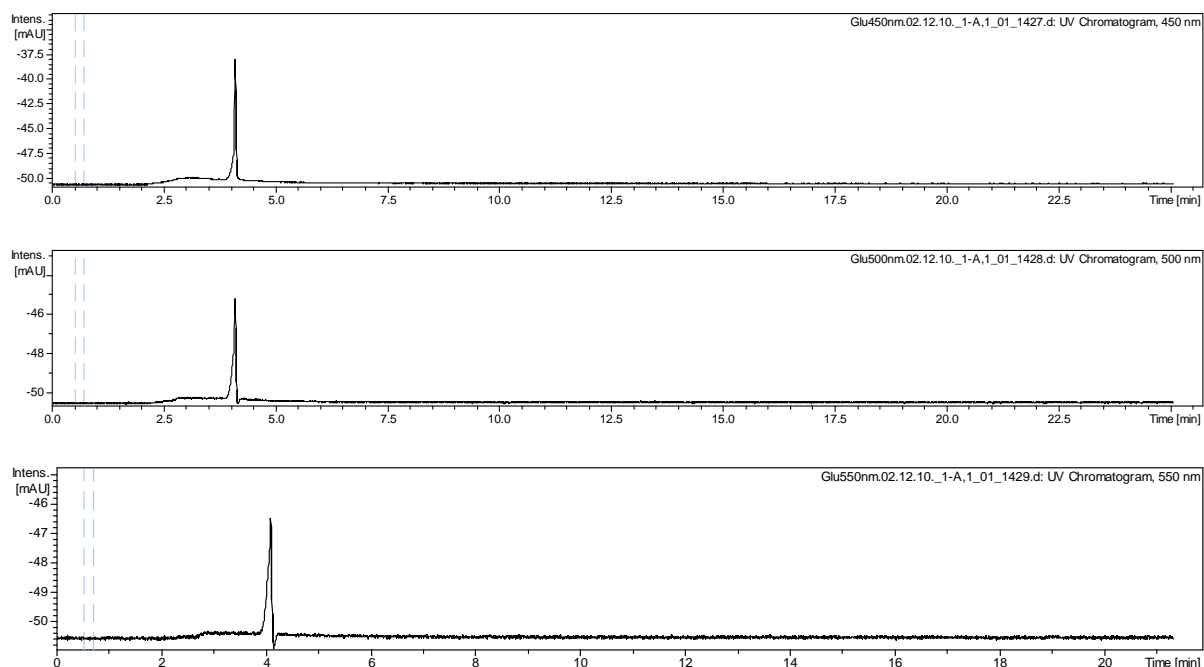


Figure 50. UV chromatograms monitored at: a) 450, b) 500, c) 550 nm of caramelized glucose in the negative ion mode

This observation suggests that caramel color arises from three distinct chromophoric molecules co-eluting or from several close eluting compounds. The mass spectra associated with the chromatographic peak in question, showed signals for around 30 co-eluting compounds (Figure 51). In order to identify caramel dyes, the van Krevelen plot was produced from the high-resolution mass data of this chromatographic peak, which suggested in the typical aromatic region a total of five compounds that would fall within the elemental ratio boundaries expected for an aromatic dye obtained from sugars upon heating with molecular formulas of $C_{24}H_{20}O_{15}$, $C_{32}H_{20}O_4$, $C_{15}H_{12}O_6$ and $C_{20}H_{10}O_4$. Similar aromatic structures have been proposed in the carbonization of glucose under high pressure in aqueous solution in the production of biofuels by Li *et al.* and Antonietti *et al.*^[194,195] Interestingly, for fructose up to four well-resolved chromatographic peaks monitored at 550 nm could be observed, indicating that the nature of the brown dyes varies significantly between different sugars (Figure 52 - Figure 53).

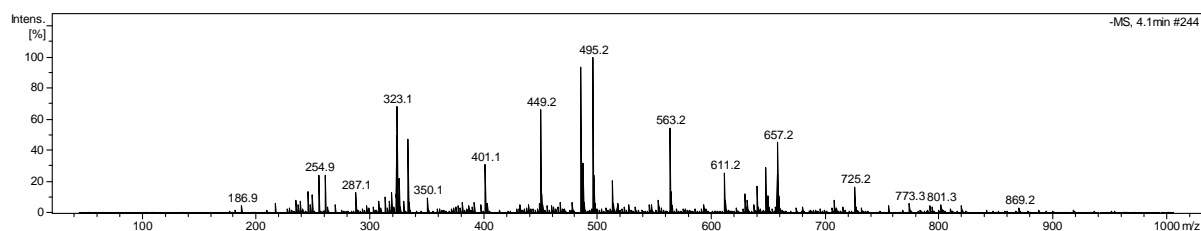


Figure 51. Mass spectrum of a chromatographic peak at retention time 4.1 min from UV at 500 nm of caramelized glucose in the negative ion mode

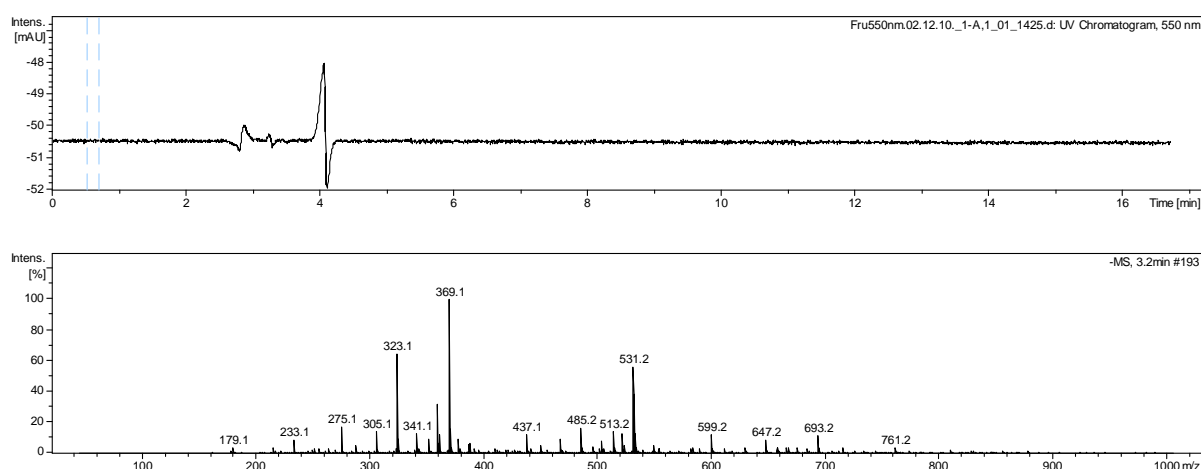


Figure 52. UV chromatogram monitored at 550 nm (top) and mass spectrum of chromatographic peak at retention time 3.2 min (bottom) of caramelized fructose in the negative ion mode

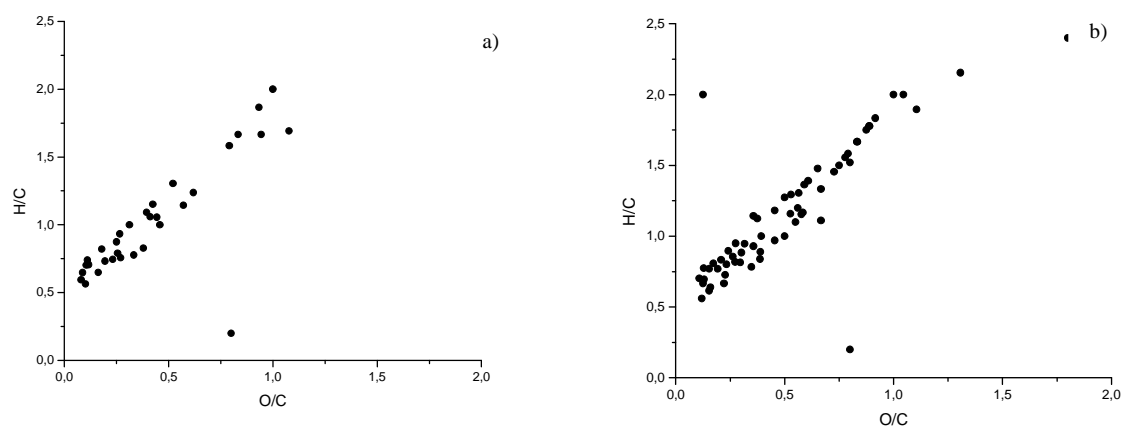


Figure 53. Two dimensional van Krevelen plots showing the O/C *versus* H/C ratio for caramelized: a) glucose from MS spectrum of a chromatographic peak from UV chromatogram monitored at 500 nm with $R_t = 4.1$ min, b) fructose from MS spectrum of a chromatographic peak from UV chromatogram monitored at 550 nm with $R_t = 3.2$

2.4.3 CARAMELIZATION OF DISACCHARIDES

Disaccharides, as being main components of many daily food products, are very important class of carbohydrates. The heating sucrose produces classical caramel used in traditional cooking, baking and as food additive for coloring of beverages or baking goods. While the heating of lactose occurs frequently in traditional baking recipes with added dairy products or the production of the Hispanic “dulce de leche”. Maltose is heated prior to traditional beer brewing. In this part, the products obtained by thermal processing from sucrose (**48**), maltose (**49**) and lactose (**50**) will be characterized. In term to find the optimized heating conditions for further analysis, the mass spectra were recorded from samples obtained at different temperatures. The studied disaccharides were thus heated from room temperature to 180 °C for sucrose and maltose, to 200 °C for lactose and kept for 2 h at the final temperature. As for monosaccharides, thermogravimetric curves showed around 10–12% weight loss, which statistically correspond to one water molecule per monosaccharide. It is worth mentioning that the heating procedure caused melting of sucrose and maltose, while lactose remained a solid.

2.4.3.1 ESI-TOF mass spectrometry

A mass spectrometric data were obtained in both negative and positive ion modes from caramelized sucrose (**48**), maltose (**49**) and lactose (**50**). Figure 54 - Figure 56 illustrate the mass spectra of all three disaccharides in the negative ion mode.

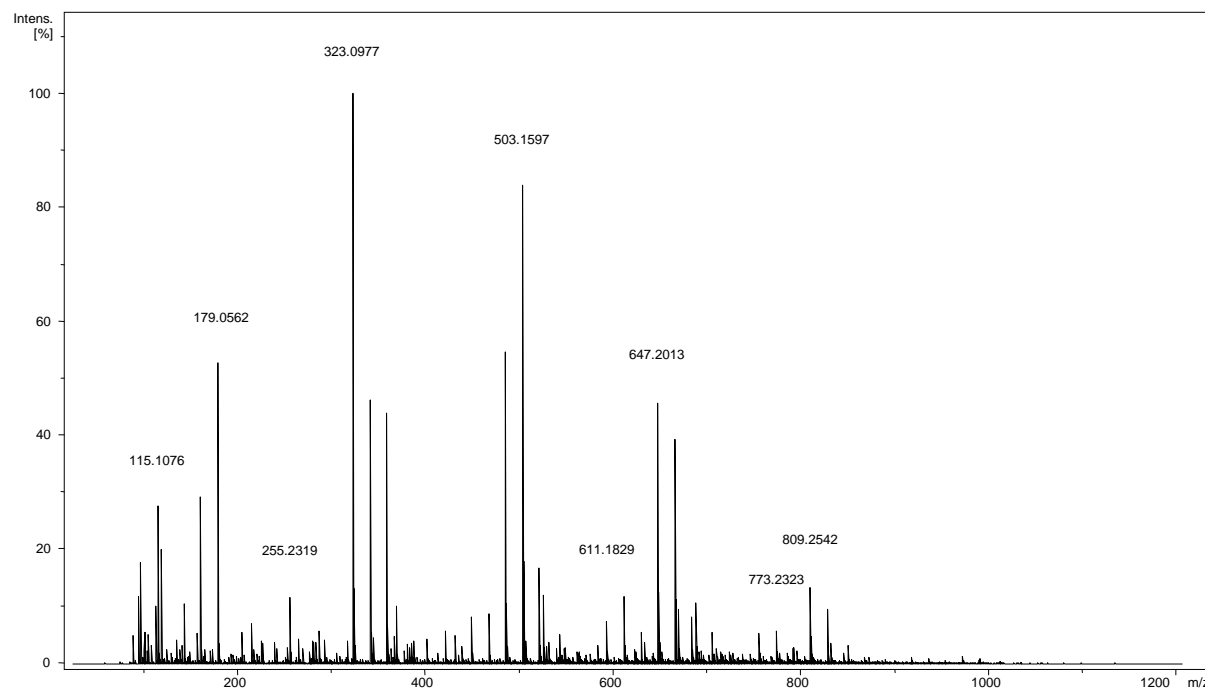


Figure 54. Mass spectrum of caramelized sucrose (**48**) in the negative ion mode using a direct infusion into an ESI-TOF-MS instrument

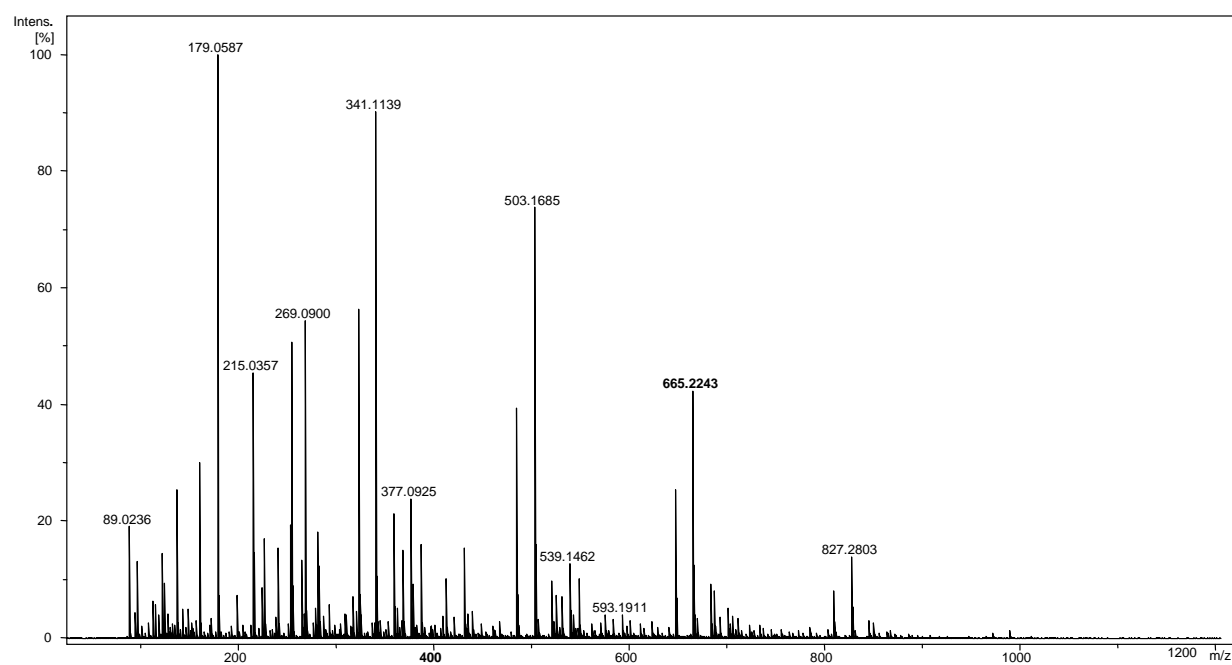


Figure 55. Mass spectrum of caramelized maltose (**49**) in the negative ion mode using a direct infusion into an ESI-TOF-MS instrument

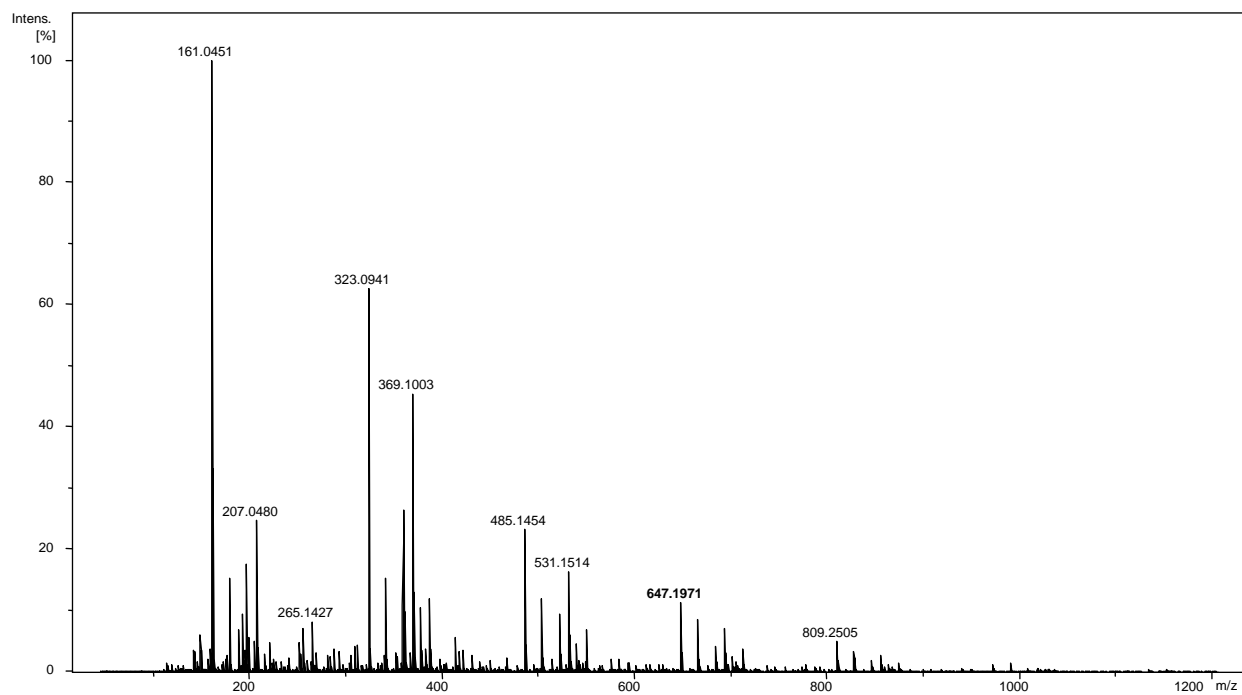


Figure 56. Mass spectrum of caramelized lactose (**50**) in the negative ion mode using a direct infusion into an ESI-TOF-MS instrument

Table 10 displays the mass/charge ratio (m/z) of the product ions, elemental composition, and average mass error for caramelized sucrose as the representative disaccharides (for the rest see Table A5, Appendix)*. The exploration of the mass spectra of caramelized disaccharides indicated mostly oligomerization, dehydration and hydration reactions of carbohydrates. Oligomers of disaccharides with up to hexamers, dehydration products of those oligomers, hydration and some redox disproportionation reaction products are observed. Furthermore, the decomposition of oligomers to monomers appeared with the formation of their dehydrated products. Subsequently, MALDI-MS technique was applied to observe a possible forming of further oligomers. The MALDI spectrum with DHB (2,5-dihydroxybenzoic acid) of caramelized sucrose was recorded yielding oligomers up to an octamer at m/z 1337.6. Hydrated and dehydrated ions have been also observed, which consequently confirm the results obtained with an electrospray ionization technique.

* See on page 154

Table 10. High-resolution mass (MS-TOF) data for caramelized sucrose in the negative ion mode

Peak Numbering	Assignment	Molecular Formula	Experimental m/z [M-H] ⁻	Theoretical m/z [M-H] ⁻	Relative Error [ppm]
1		C ₆ H ₁₂ O ₂	115.0765	115.0765	0.1
2		C ₄ H ₈ O ₄	119.0351	119.0350	1.4
3		C ₈ H ₁₆ O ₂	143.1081	143.1078	2.2
4		C ₉ H ₁₈ O ₂	157.1226	157.1234	4.9
5	Glu or Fru - H ₂ O	C ₆ H ₁₀ O ₅	161.0461	161.0455	3.5
6	Glu or Fru	C ₆ H ₁₂ O ₆	179.0562	179.0561	0.3
7		C ₁₄ H ₂₈ O ₂	227.2010	227.2017	3.0
8		C ₁₅ H ₃₀ O ₂	241.2164	241.2173	3.6
9		C ₁₆ H ₃₂ O ₂	255.2324	255.2330	2.2
10		C ₁₅ H ₂₂ O ₄	265.1448	265.1445	1.1
11		C ₁₈ H ₃₆ O ₂	283.2629	283.2643	4.8
12		C ₁₂ H ₁₆ O ₈	287.0767	287.0772	2.0
13		C ₁₇ H ₂₆ O ₄	293.1756	293.1758	0.8
14	Glu-Fru - 2×H ₂ O	C ₁₂ H ₁₈ O ₉	305.0866	305.0878	3.9
15	Glu-Fru - H ₂ O	C ₁₂ H ₂₀ O ₁₀	323.0977	323.0984	2.2
16	Glu-Fru	C ₁₂ H ₂₂ O ₁₁	341.1083	341.1089	1.7
17	Glu-Fru + H ₂ O	C ₁₂ H ₂₄ O ₁₂	359.1159	359.1195	10.0
18	3×M - 4×H ₂ O	C ₁₈ H ₂₄ O ₁₂	431.1155	431.1195	3.9
19	3×M - 3×H ₂ O	C ₁₈ H ₂₆ O ₁₃	449.1280	449.1301	4.6
20	3×M - 2×H ₂ O	C ₁₈ H ₂₈ O ₁₄	467.1391	467.1406	3.2
21	3×M - H ₂ O	C ₁₈ H ₃₀ O ₁₅	485.1494	485.1512	3.7
22	3×M	C ₁₈ H ₃₂ O ₁₆	503.1597	503.1618	4.2
23	3×M + H ₂ O	C ₁₈ H ₃₄ O ₁₇	521.1698	521.1723	4.8
24	4×M - 5×H ₂ O	C ₂₄ H ₃₂ O ₁₆	575.1613	575.1618	0.7
25	4×M - 3×H ₂ O	C ₂₄ H ₃₆ O ₁₈	611.1798	611.1829	5.0
26	4×M - 2×H ₂ O	C ₂₄ H ₃₈ O ₁₉	629.1903	629.1935	4.9
27	4×M - H ₂ O	C ₂₄ H ₄₀ O ₂₀	647.2013	647.2040	4.2
28	4×M	C ₂₄ H ₄₂ O ₂₁	665.2129	665.2146	2.6
29	4×M + H ₂ O	C ₂₄ H ₄₄ O ₂₂	683.2243	683.2251	1.2
30	5×M - 4×H ₂ O	C ₃₀ H ₄₄ O ₂₂	755.2228	755.2251	3.1
31	5×M - 3×H ₂ O	C ₃₀ H ₄₆ O ₂₃	773.2323	773.2357	4.4
32	5×M - 2×H ₂ O	C ₃₀ H ₄₈ O ₂₄	791.2478	791.2463	1.9
33	5×M - H ₂ O	C ₃₀ H ₅₀ O ₂₅	809.2536	809.2568	4.0
34	5×M	C ₃₀ H ₅₂ O ₂₆	827.2645	827.2674	3.5
35	5×M + H ₂ O	C ₃₀ H ₅₄ O ₂₇	845.2775	845.2780	0.5
36	6×M - 4×H ₂ O	C ₃₆ H ₅₄ O ₂₇	917.2748	917.2780	3.4
37	6×M - 3×H ₂ O	C ₃₆ H ₅₆ O ₂₈	935.2860	935.2885	2.7
38	6×M - 2×H ₂ O	C ₃₆ H ₅₈ O ₂₉	953.2968	953.2991	2.4
39	6×M - H ₂ O	C ₃₆ H ₆₀ O ₃₀	971.3095	971.3097	0.1
40	6×M	C ₃₆ H ₆₂ O ₃₁	989.3201	989.3202	0.1

a M designates monosaccharide, Glu glucose and Fru fructose

Similarly to monosaccharides, van Krevelen and Kendrick analyses as novel graphical mass spectrometric data interpretation strategies were applied to the complex MS data of caramelized disaccharides. These techniques visualized complex data and were used as the inspiration for further characterization of the particular groups of compounds. The van Krevelen diagrams were constructed with the atomic ratios of H/C and O/C, shown in Figure 57.

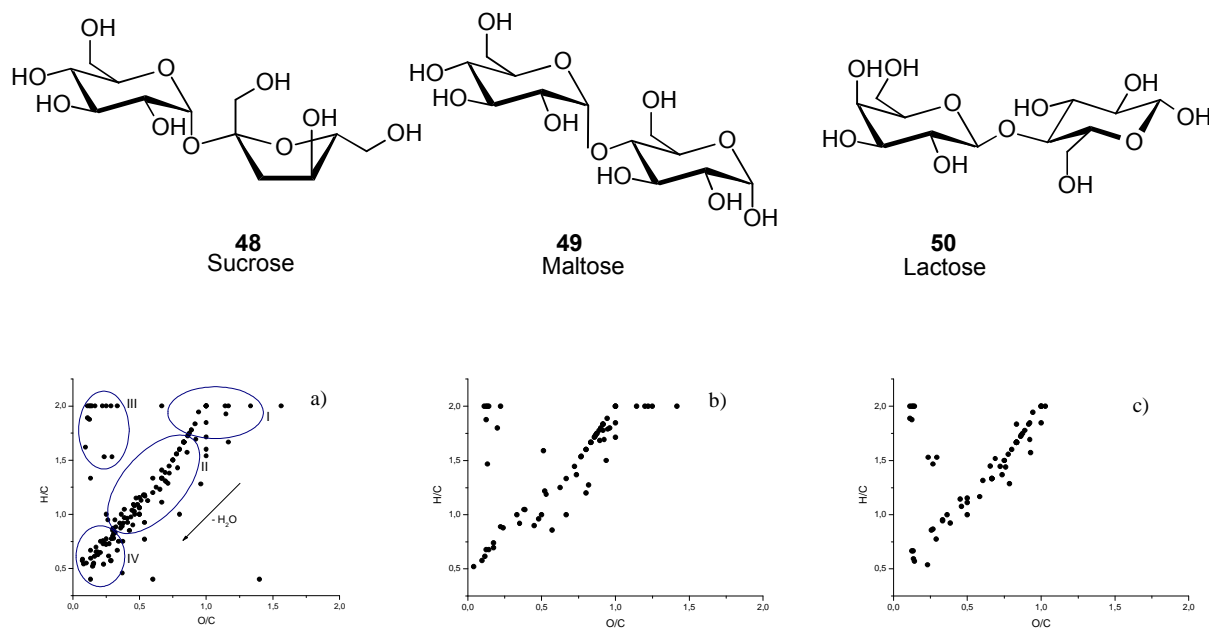


Figure 57. Two dimensional van Krevelen plots showing the O/C ratio *versus* H/C ratio for caramelized: a) sucrose, b) maltose, c) lactose in the negative ion mode in m/z range between 50–1200

The profiles of all graphs for **48**, **49** and **50** are similar and the points were grouped as in the case of studied monosaccharides' caramels. Shortly, the group (I) represents the points characteristic for carbohydrates. The points in the middle of the graphs belong to dehydrated products (II). The products of disproportionation redox reactions are present in the top left corner (III). The group of the points in the bottom left corner (IV) belongs to the products with condensed heterocyclic ring structures after successive dehydration. Both heterocyclic condensed ring structures and disproportionation products appear as minor products in the mass spectra at a concentration that does so far not allow further structural investigation by tandem MS. The second graphical technique used to study the composition of caramelized disaccharides was a Kendrick-type analysis. The Kendrick plots were created with the H_2O increment, as illustrated in Figure 58.

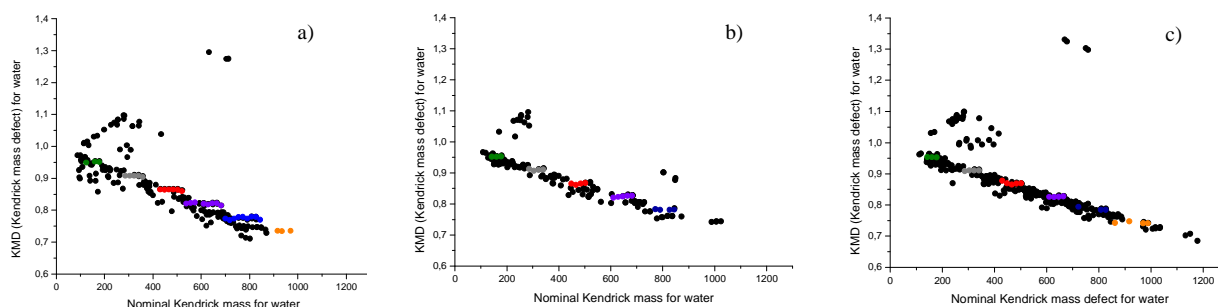


Figure 58. Two dimensional Kendrick plots for mass increment H_2O showing the distribution of the Kendrick mass defect plotted against the nominal Kendrick mass of pseudo-molecular ions for caramelized: a) **48**, b) **49**, c) **50** in the negative ion mode

The plots of caramelized disaccharides possess some homologous series of compounds. This type of graph showed the formation of oligomers with up to six monomeric hexoses of heated disaccharides. Hydrated and dehydrated ions were visualized, as well. In the following parts, the characterization of predominant products of caramelization of disaccharides will be disclosed.

2.4.3.2 Monomeric hexoses

In a direct infusion MS data for heated **48** and **49** strong peaks and for **50** a weak peak, were observed at m/z 179.1 corresponding to monomeric hexose units. LC-tandem MS experiments confirmed the monomeric hexoses as the α , β anomeric pairs for glucose (**32**) and fructose (**33'**) for **48**, the α , β anomeric pairs for glucose (**32**, **32'**) for **49'** and the α , β anomeric pairs for glucose (**32'**) and galactose (**34'**) for **50'**, respectively (Figure 59), by comparison of retention times and the MS data with authentic reference standards.

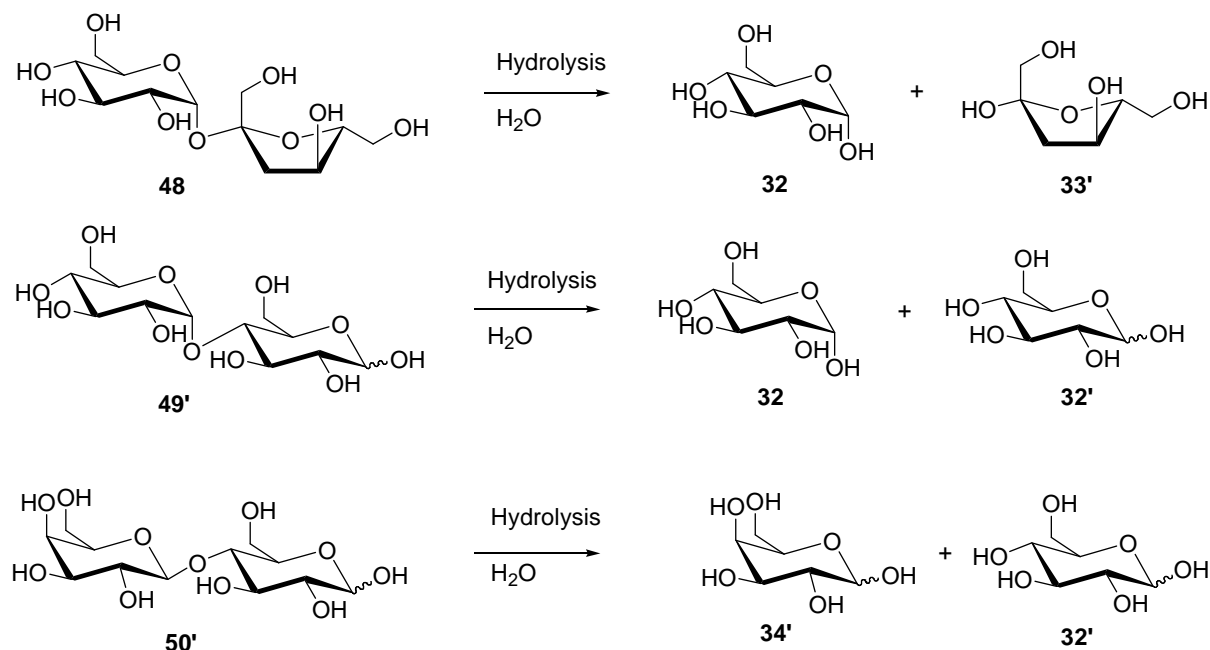


Figure 59. The formation of monomeric hexoses from disaccharides **48–50'** during heating

For example for the ion at m/z 179.1 a neutral loss of 18 as the base peak was observed for heated **48** and **50'**, and a neutral loss of 90 as the base peak for **49'**, which correspond to one water molecule and three formaldehyde molecules derived from the cross-ring cleavage, respectively. Presumably, water as the reaction product of dehydration process hydrolyses the disaccharides into their monomeric counterparts. For galactose the dehydration process led to a galactose-based ion at m/z 161.1 as favored. An epimerization was not observed for monomeric hexoses previously;^[6] however, it has been reported in quinic acid and chlorogenic acid chemistry in food processing chemistry at identical temperatures.^[188,196]

2.4.3.3 Oligomers of hexoses

The MS^{*n*} data of oligomers of hexose generated under the heating of **48**, **49** and **50** were acquired in the negative ion mode using a direct infusion into a ESI ion trap mass spectrometer. A fragmentation of precursor ions of disaccharides (C₁₂H₂₂O₁₁) at m/z 341.1 gave the main peaks at m/z 178.9 for heated sucrose, 160.9 for heated maltose and 323.0 for heated lactose. They came from the glycosidic bond cleavage between two monosacharides, which might occur on either the reducing or non-reducing end of the molecule^[197] and the removal of one water molecule. Tandem LC-MS measurements under optimized

chromatographic conditions, revealed three resolved chromatographic peaks in extracted ion chromatograms (EICs) at m/z 341 for heated **48**, one peak for heated **49** and two peaks for heated **50** (Figure 60).

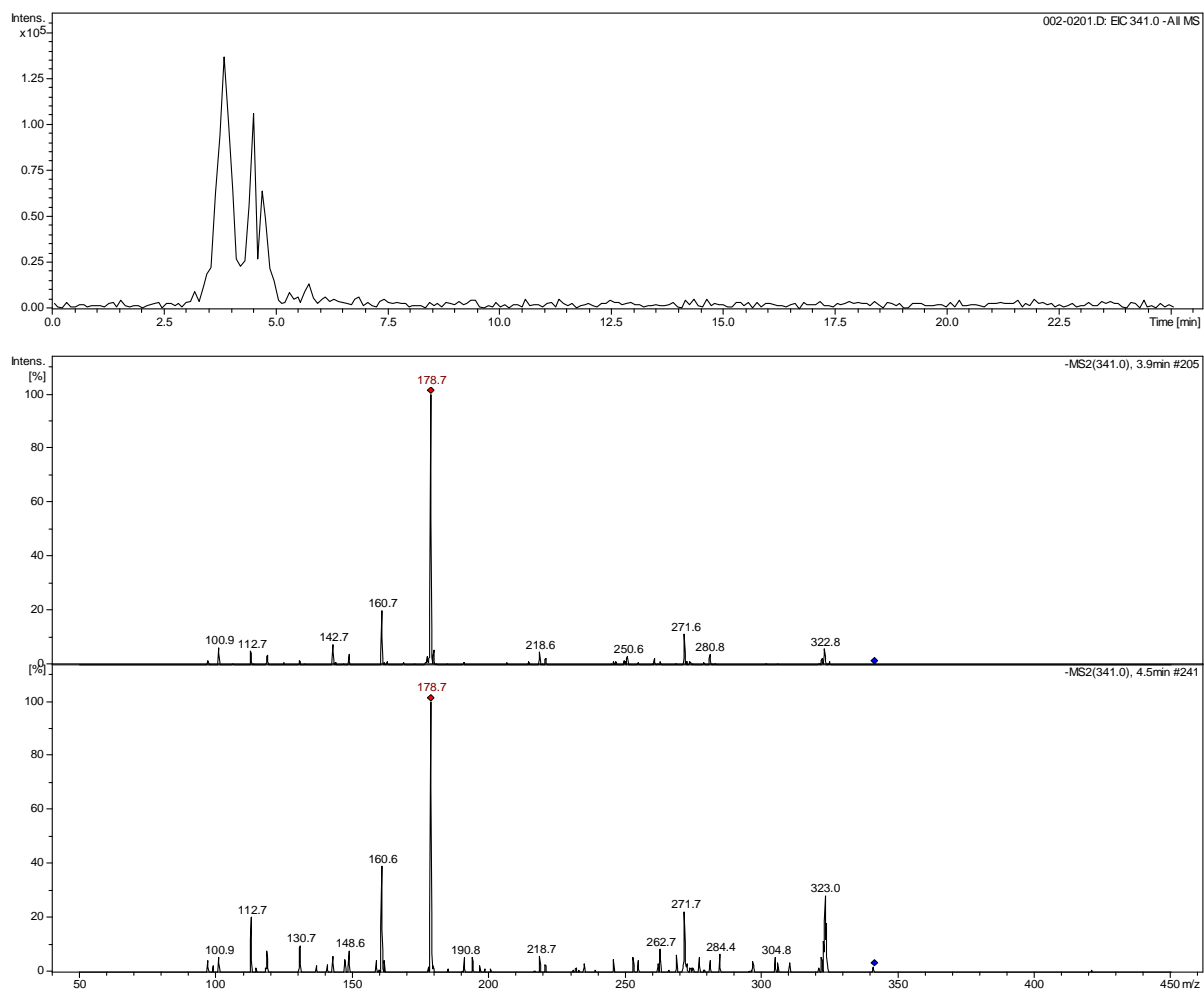


Figure 60. EIC (Extracted ion chromatogram) and MS² spectra of fragment at m/z 341.0 ($C_{12}H_{22}O_{11}$) for two chromatographic peaks of caramelized sucrose in the negative ion mode

Hence for both heated maltose and lactose the intact disaccharides are observed. For heated sucrose **48**, in contrast, hydrolysis into monomers occurred following by recombination to give a third major disaccharide, whose similarity of the MS² fragment spectra allows tentative assignment as a dimer of fructose.^[198,199] Presumably, fructose yields preferentially the more stable fructosyl cation, if compared to the glycosyl cation, serving as a glycosyl acceptor due to the increased number substituents at sp²-hybridized carbon atom.

Disaccharide ions corresponding to oligomers, containing three to six hexose units were observed at m/z 503.2, 665.2, 827.3 and 989.3 in the negative ion mode. The mass spectra of the precursor ion at m/z 503.2, trimeric hexoses showed a neutral loss of 162 as the main peak

for all studied caramel samples, arising from the glycosidic bond cleavage at the non-reducing end. Tandem LC-MS investigations revealed in the EICs at m/z of 503.2 twelve resolved chromatographic peaks for heated sucrose (**48**) (of which, only six were sufficiently strong to provide MS^n data), and four resolved chromatographic peaks for maltose and lactose, respectively. Tentative reaction products are shown in Figure 61.

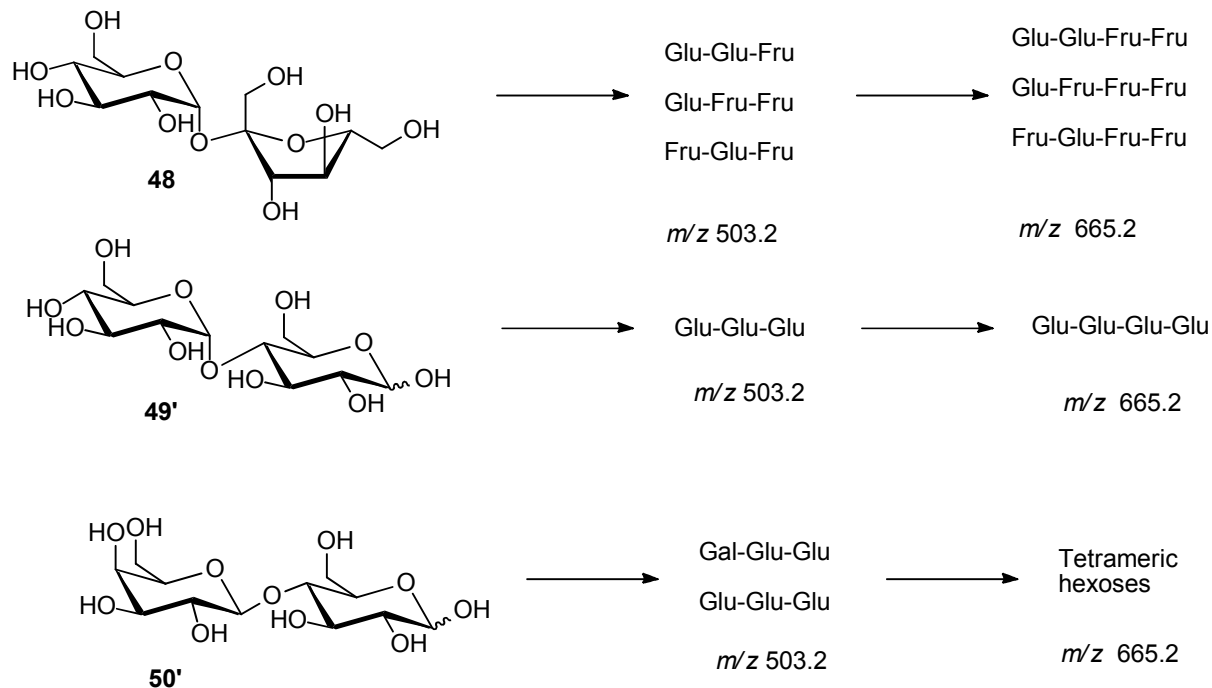


Figure 61. The formation of oligomeric saccharides from **48–50'** during heating (the regio- and stereochemistry of oligosaccharides remains open)

It must be assumed that not all isomeric compounds can be chromatographically resolved. The tandem MS fragment spectra and retention times for the four observed peaks for heated maltose (**49'**) were identical to four MS^2 spectra of caramelized glucose and have been tentatively assigned as trimers of glucose formed through non-selective glycosidic bond formation. A similar interpretation is suggested for heated lactose (**50'**). For heated sucrose (**48**) three of the compounds identified, resemble based on similarities of MS^2 fragment spectra kestose or inulin-type structures previously reported^[198-200] with a saccharide sequence of Glu-Fru-Fru, formed through non-selective glycosidic bond formation using the fructosyl cation intermediate. The other three peaks can be cautiously assigned as either Fru-Glu-Fru or Glu-Glu-Fru, for which no reference data are available (Figure 61). The detailed regio- and

stereochemistry aspects of the reaction products remain open. It must be noted that sucrose constitutes a special case among the disaccharides since the two anomeric centers are directly connected to each other, and therefore sucrose cannot act as a glycosyl acceptor directly.

The MS² spectra of the ion at m/z 665.2, a tetramer of hexoses gave the most abundant fragment at m/z 485 of (**48**, **49**) and at m/z 503 (**50**), indicating the glycosidic bond cleavage at the reducing and non-reducing end of the product ion, respectively. A neutral loss of 162 [C₆H₁₀O₅] as the main peak for all studied caramel samples was present in the MS² spectra of the ion at m/z 827.3, originating from the glycosidic bond cleavage at the non-reducing end of the product ion, as observed for the aforementioned trimers of hexoses. The MS² spectrum of m/z 989.3, a hexamer of glucose gave the base peak at m/z 827 (**48**, **50**), coming from the glycosidic bond cleavage at the reducing end, and at m/z 665.2 (**49**) from the internal glycosidic bond cleavage. Fragmentation studies of oligomeric ions of disaccharides in the negative ion mode for the studied caramel samples are consistent with glycosidic bonds cleavages at the non-reducing end rather than at reducing end.

2.4.3.4 Dehydration products

A direct infusion into ESI ion trap mass spectrometer measurements in the negative ion mode have been performed for dehydrated monomers and oligomers, which were the major products of caramelized disaccharides. Dehydrated monosaccharides were observed at m/z 161.1 and tentative product structures **51** and **47** are shown in Figure 62.

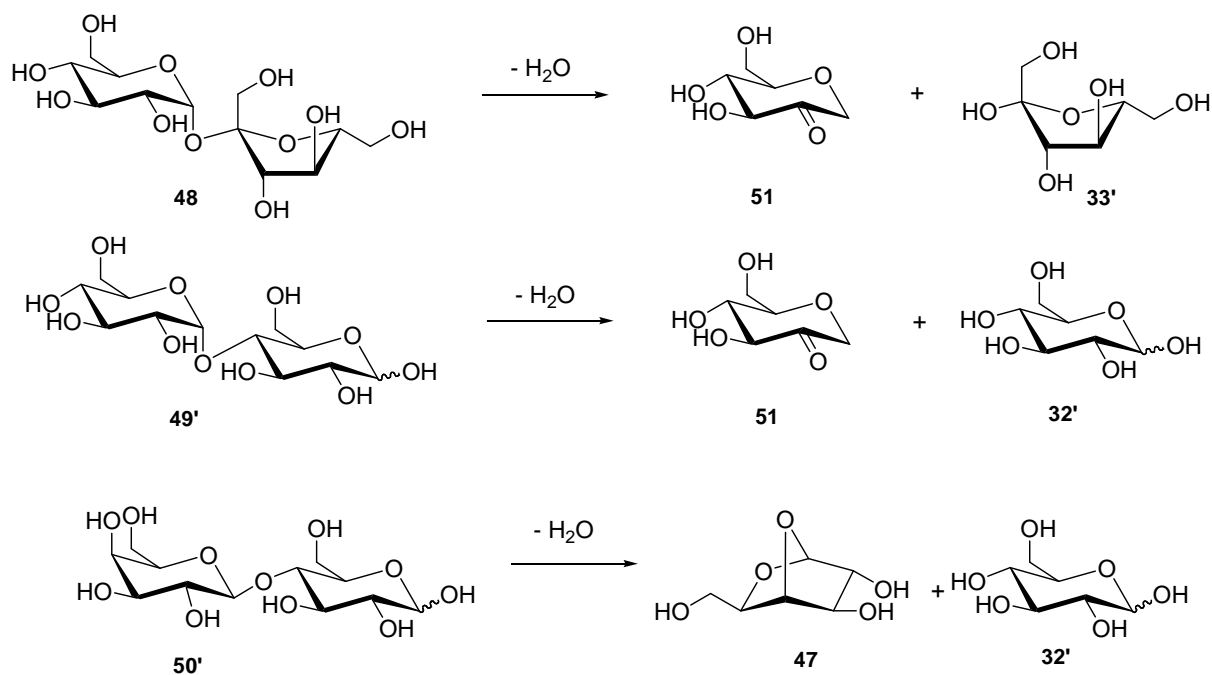


Figure 62. The formation of dehydrated hexoses from heated disaccharides **48-50'** (the regiochemistry of water elimination was chosen randomly in **51**)

Dehydrated disaccharides (C₁₂H₂₀O₁₀) were seen at m/z 323.1. The fragmentation of such precursor ions gave the fragments at m/z 160.9 (**48**, **49'**) and at m/z 178.9 (**50'**). Both of them rose from the glycosidic bond cleavage at the reducing and non-reducing ends. The elimination of water molecule from glucose at C1-C4 positions leads to an enol that tautomerizes to its carbonyl form, which is in agreement with NMR and IR spectroscopy data (Figure 63).

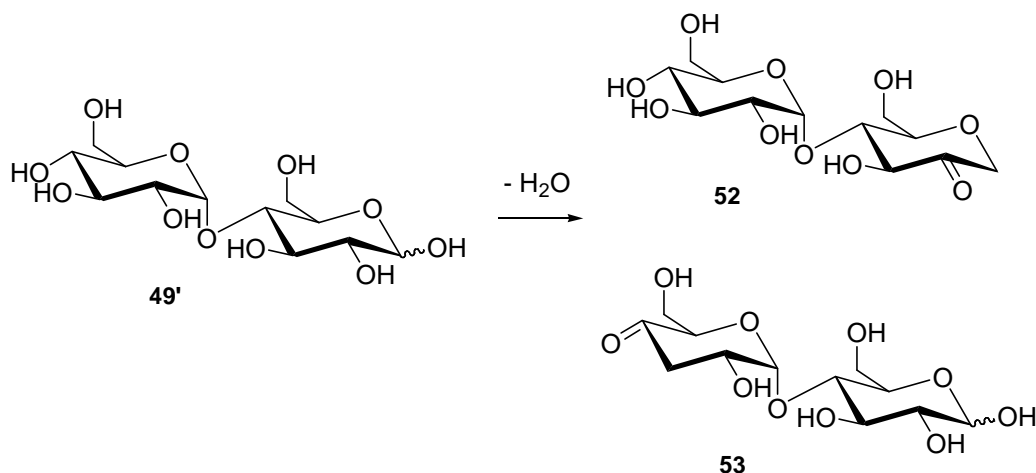


Figure 63. Dehydration products of heated maltose (**49'**) (the regiochemistry of water elimination was chosen randomly in **52**, **53**)

Moreover, monomeric hexoses undergo dehydration reactions and product ions appeared at m/z 161.1. The fragmentation data of this ion gave different main fragments for studied caramel samples, including the main fragments at m/z 113 (**48**, **50**) and 101 (**49**), arising from the cross-ring cleavage.

Dehydrated oligomers of caramel samples derived from a loss of a single water molecule were observed at m/z 485.1, 647.2, 809.2 and 971.3. The mass spectra of the fragment ion at m/z 485 showed a neutral loss of 162 [$C_6H_{10}O_5$] as the main peak for all caramel samples thus derived from the glycosidic bond cleavage. The fragmentation of monodehydrated tetramers of hexoses at m/z 647.2 gave the main fragment at m/z 485 with a neutral loss of 162 [$C_6H_{10}O_5$] for **48** and **50** arising from dehydrated dimers and at m/z 467 with a neutral loss of 180 [$C_6H_{10}O_5$] for **49**. The MS^2 spectra of the ion at m/z 809.3, its dehydrated pentamer of hexoses showed the main peak at m/z 647 and is consistent for all analyzed samples with a neutral loss of 162 [$C_6H_{10}O_5$]. The MS^3 spectra of the ion at m/z 485 gave the base peak at m/z 323 for all analyzed samples. The fragmentation of monodehydrated hexamers of hexoses at m/z 971.3 provided the main fragment at m/z 809.3 with a neutral loss of 162 [$C_6H_{10}O_5$] for heated **48** and **50** arising from dehydrated dimers. The ion at m/z 647 with a neutral loss of 324 [$C_6H_{10}O_5$] is present as a main fragment of the MS^2 spectrum of an ion at m/z 971 for **49** coming from the cleavage of the internal glycosidic bond. ESI-MS experiments with applied graphical techniques showed the formation of dehydration products with one, two and three water molecules. Didehydrated disaccharide appeared at m/z 305.1 and followed by didehydrated oligomers of hexoses at m/z 467.1, 629.2, 791.2 and 953.3, respectively. When possible, fragmentation studies in the negative ion mode were performed for the mentioned ions. Didehydrated pentamer of hexoses at m/z 791.1 of maltose gave in the MS^2 spectrum the main fragment at m/z 449 with a neutral loss of 342 [$C_{12}H_{22}O_{11}$], corresponding to the cleavage of the glycosidic bond. Dehydration reactions products with three water molecules appeared at m/z 287.1 for disaccharides and at m/z 449.1, 611.2, 773.2, 935.3 for oligomers, respectively. The MS^2 spectra of the ion at m/z 287 provided a neutral loss of 126 [$C_6H_6O_3$] as the main fragment for **48**. It could suggest the presence of hydroxymethylfurfural, supporting the elimination of all three water molecules at one saccharide moiety. The MS^2 spectra of the ion at m/z 449.1 gave product ions at m/z 323.1 for all caramelized disaccharides with a neutral loss of 126 [$C_6H_6O_3$]. This is consistent with the behavior of the aforementioned tridehydrated disaccharide showing the presence of hydroxymethylfurfural.

Targeted tandem LC-MS measurements producing EICs of the ion at m/z 323.1 revealed chromatographically resolved peaks: ten for heated sucrose (**48**), six for heated maltose (**49**) and ten for heated lactose (**50**). For maltose two compounds showed data resembling dehydration products **52** and **53**, as well as previously observed for heated glucose (Figure 63)*.^[6] Similarly multiple peaks were detected in targeted LC-tandem MS experiments in EICs at m/z 485.2 and 647.2 (up to 16 resolved peaks). Hence, it can conclude the non-selective loss of water from disaccharides generates a multitude of different carbonyl reaction products. At this point, it should be noted that such carbonyl reaction products produced during the heating of carbohydrates should be considered in Maillard-type reactions taking amino acids and peptides as electrophilic reagents.

2.4.3.5 Hydration products

Hydrated disaccharides appeared in the negative ion mode at m/z 359.2. Hydrated products of further oligomers were also formed and detected at m/z 521.2, 683.2, 845.3 and 1007.3 in the negative ion mode. The observation of such hydration products is highly unusual and could alternatively explain the formation of the non-covalent hydrated adducts. Therefore, the sample of beer containing various maltose derivatives was then investigated under identical mass spectrometrical conditions.^[201] These data revealed that hydrated oligomers are absent and should thus be considered as the genuine reaction products in the caramel formation. Tandem MS data of these ions showed a similar fragmentation behavior of hydrated ions, which involves a loss of 36 [$2 \times \text{H}_2\text{O}$], for example in the MS^2 spectrum of 359 and 521 the base peaks at m/z 323 and m/z 485 were observed, respectively. When possible, the MS^3 spectra of precursor ions 323 and 521 were recorded to obtain the main peaks with neutral losses of 162 coming from the cleavage of the glycosidic bonds. Based on recent studies by Köpper *et al.* is possible that hydrates (**42**) are formed.^[190]

2.4.3.6 Comparison of caramelized disaccharides

In the previous section, individual components formed in caramelization of disaccharides have been identified. In all three cases sucrose, lactose and maltose the same type of reaction

* See on page 105

products was observed and classified mainly as oligomers and dehydration products. However, the three different mass spectra, shown in Figure 54 - Figure 56,^{*} clearly illustrate a large variation of intensities of the individual ions pointing towards significant differences in the reaction kinetics observed in these disaccharides. Therefore, in this section those differences will be discussed.

The radar plots usually employed in a sensory analysis have been generated to graphically visualize differences in the product formation. Within the plots the individual ions are displayed on the vertices. The relative intensity presented on a scale from the center of the plot to its vertices and all three different disaccharides investigated are shown as colored lines within the plot. The first plot (Figure 64) provides the difference in intensities of various oligomeric structures. The plot clearly shows that maltose favors oligomers formation followed by sucrose, whereas lactose is most reluctant to form oligomers. The second plot demonstrates the relative intensities of various dehydrated ions. Here the opposite trend is apparent with lactose preferentially forming a monomeric dehydrated product at m/z 161. For higher molecular weight ions, sucrose is more prone to dehydration followed by maltose. The third plot shows the ratio of intensities of oligomers *versus* dehydrated parent compounds. Again for a monomeric hexose, lactose gave the highest degree of dehydration followed by sucrose and then maltose. For higher molecular weight derivatives the trend is reversed e.g., at 665/647 or 827/809 sucrose shows the highest degree of dehydration followed by maltose and lactose. The preferential formation of dehydrated monomers of lactose can be readily understood in terms of its stereochemistry. The axial 4-OH substituent in a galactose part of lactose allows an intramolecular S_N2-like reaction towards most likely a bicyclic structure **47** (Figure 49)[†]. The substitution can be classified according to Baldwin's rules as a 5-*exo*-tet cyclization and is hence favored as demonstrated previously.^[202] This fragmentation behavior has been previously proposed for galactose derivatives.^[193,203] This means that lactose readily breaks into its monosaccharide units at elevated temperatures, whereas sucrose and maltose are thermally more stable. Dehydration at the disaccharide stage is favored for sucrose, which can be rationalized by assuming that the new olefinic double bond formed in a five-membered ring furanose is favored over a double bond formed in a pyranose. A consecutive elimination of water proceeds towards the more stable aromatic furan derivative.

^{*} See on page 95

[†] See on page 90

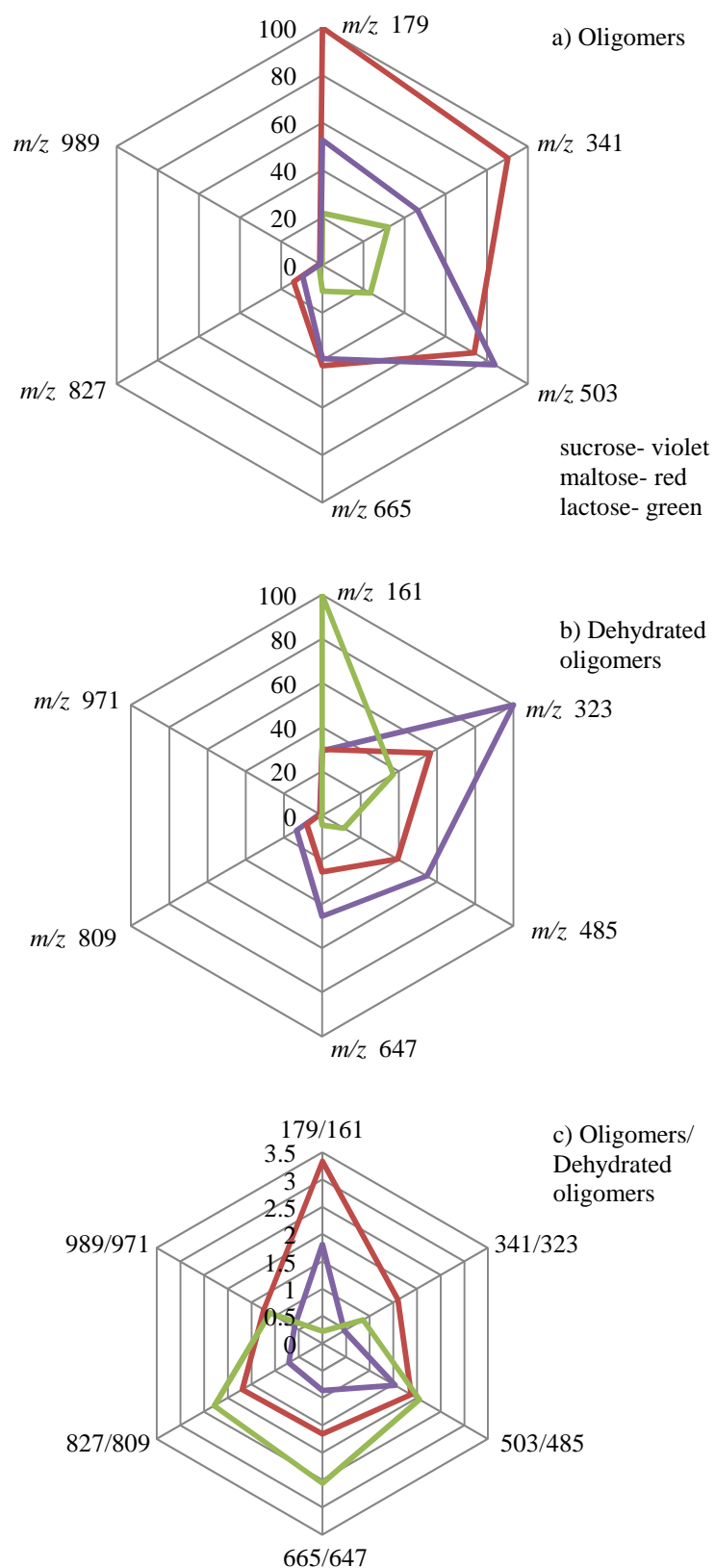


Figure 64. Radar plots of classes of ions detected in a direct infusion negative mode mass spectra of heated disaccharides **48–50**: a) oligomeric hexoses, b) dehydrated oligomeric hexoses, c) ratio of oligomeric to dehydrated hexoses

2.4.4 THERMAL TREATMENTS OF POLYSACCHARIDES AND BREAD

Carbohydrates play an important role as structural material and energy reserves.^[204] In particular, they are the most abundant biomolecules in nature present in all living systems as monosaccharides or combined as polysaccharides.^[205] Starch and cellulose are the two most common polysaccharides present in dietary plants, consisting of glucose connected *via* α -1,4- and β -1,4-glycosidic bonds, respectively.^[206] Starch is observable in various dietary plant sources (e.g., corn, potato, wheat and rice)^[207] and being the most important source of chemical energy in food as well as the predominant contributor to energy intake in a typical human diet.^[208,209] In this section the thermal decomposition of polysaccharides, namely starch and cellulose will be thus investigated.

The obtained data have been compared with those of thermally treated glucose as a benchmark, which were discussed in section 2.4.1*.^[6] The actual products of starch and cellulose thermal degradation have been investigated on two occasions by Zhang *et al.*^[210] using a solid state ^{13}C NMR spectroscopy to identify ether linkages and carbonyls formed after dehydration at 300 °C. Hakkarainen *et al.* applying a solid phase extraction followed by a GC-MS analysis^[211] have identified 138 distinct products after heating to 230 °C and only 40 after heating to 190 °C with aldehydes and ketones such as pentanal and pentanone, dicarboxylic acids and γ -butyrolactone as the main volatile products.

As previously, thermogravimetric data (TGA) for starch and cellulose were acquired and compared with glucose's. Polysaccharides were heated from ambient temperature to 220 °C and kept for 2 h at this temperature. During this time, thermogravimetric curves of glucose and polysaccharides exhibited a span of 10–12% weight loss, which statistically corresponds to one water molecule per monosaccharide moiety, yet with slightly different patterns. The gradual mass reduction was observed for polysaccharides, while for glucose the weight loss starts at higher temperature when compared to two polysaccharides[†]. An increase of temperature showed a comparable mass reduction for starch and cellulose, which gave almost identical TGA curves (Figure 65).

* See on page 74

† See Figure 38 on page 74 indicating thermogravimetric curve of caramelized glucose

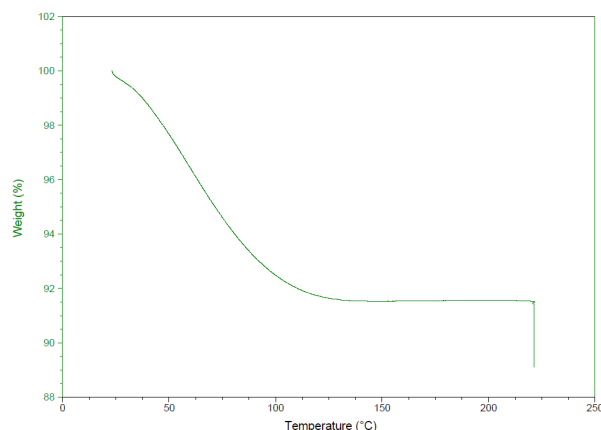


Figure 65. Thermogravimetric curve of starch

Using this information, the optimized temperature condition were chosen, based on the 10% weight loss, color formation (a visible degree of browning was observed) and recorded mass spectra of samples heated at different temperatures showing an abundance of product signals. In fact, 2 h at 220 °C for starch and cellulose turned out to be the optimized heating parameters used in further studies. The thermal degradation products were hence dissolved in water and filtered off. The weight percentage of the water-soluble fraction was 62% for starch, 23% for cellulose and 100% for glucose. It is worth noting that both polymeric cellulose and starch in the granular form display poor water solubility.

2.4.4.1 ESI-FT-ICR mass spectrometry

In the first step ESI-FT-ICR (Electrospray Fourier Transform Ion Cyclotron Resonance) mass spectra were acquired in both negative and positive ion modes for heated starch (**54**) and cellulose (**55**) (Figure 66 - Figure 68).

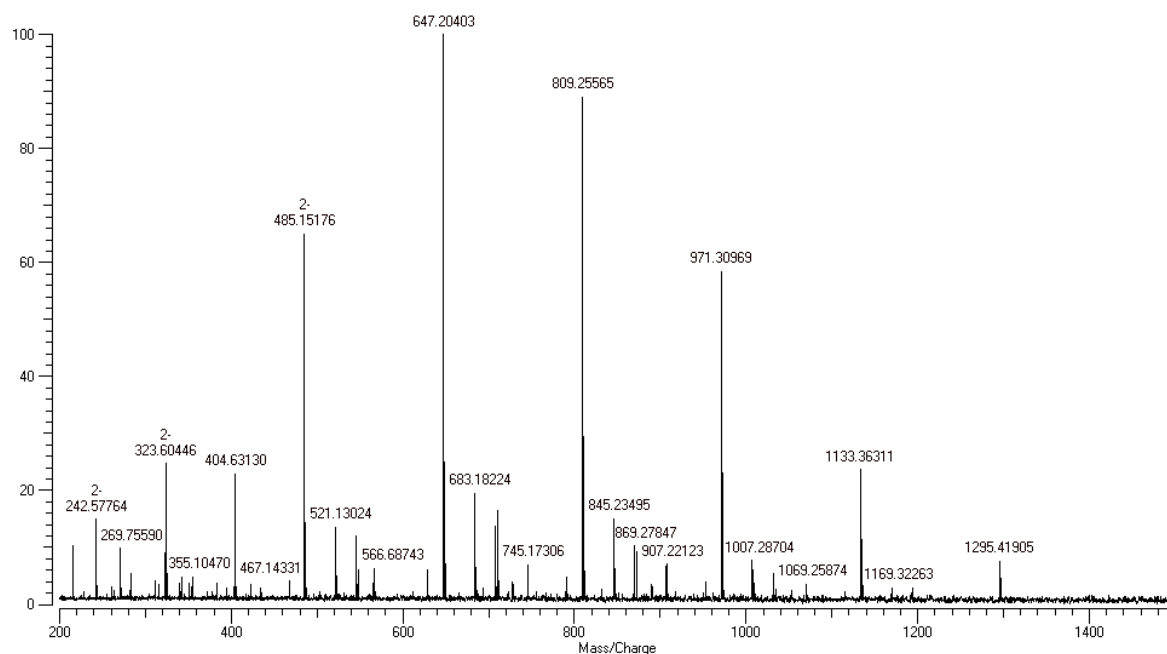


Figure 66. Mass spectrum of heated starch (54) in the negative ion mode using a direct infusion into an ESI-FT-ICR instrument

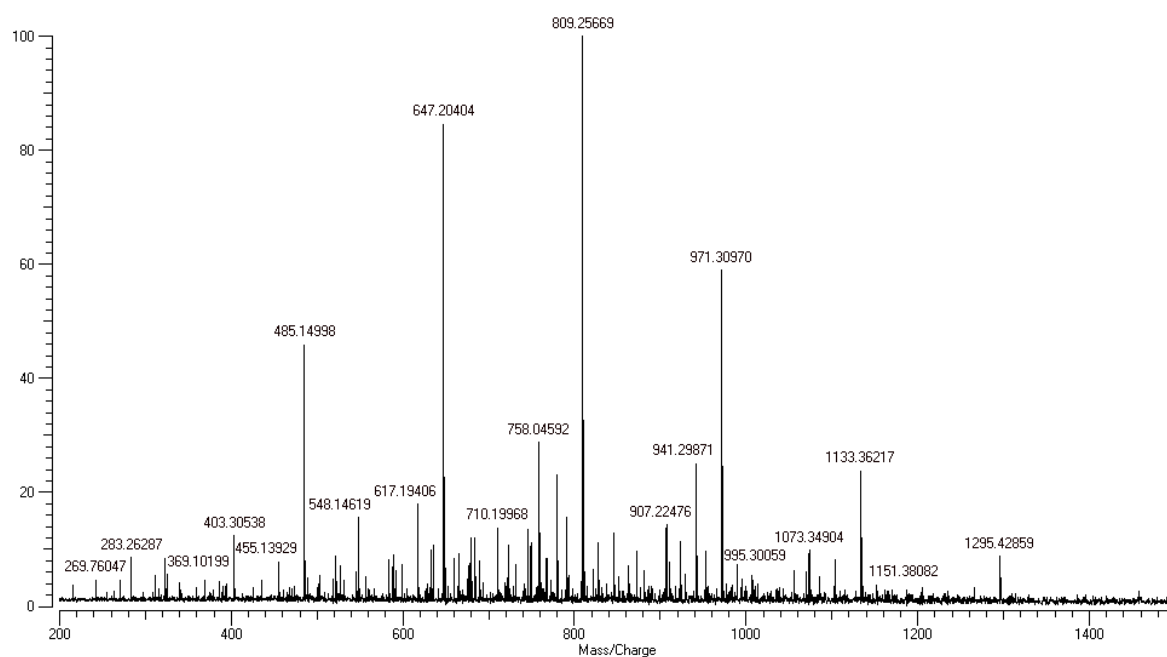


Figure 67. Mass spectrum of heated cellulose (55) in the negative ion mode using a direct infusion into an ESI-FT-ICR instrument

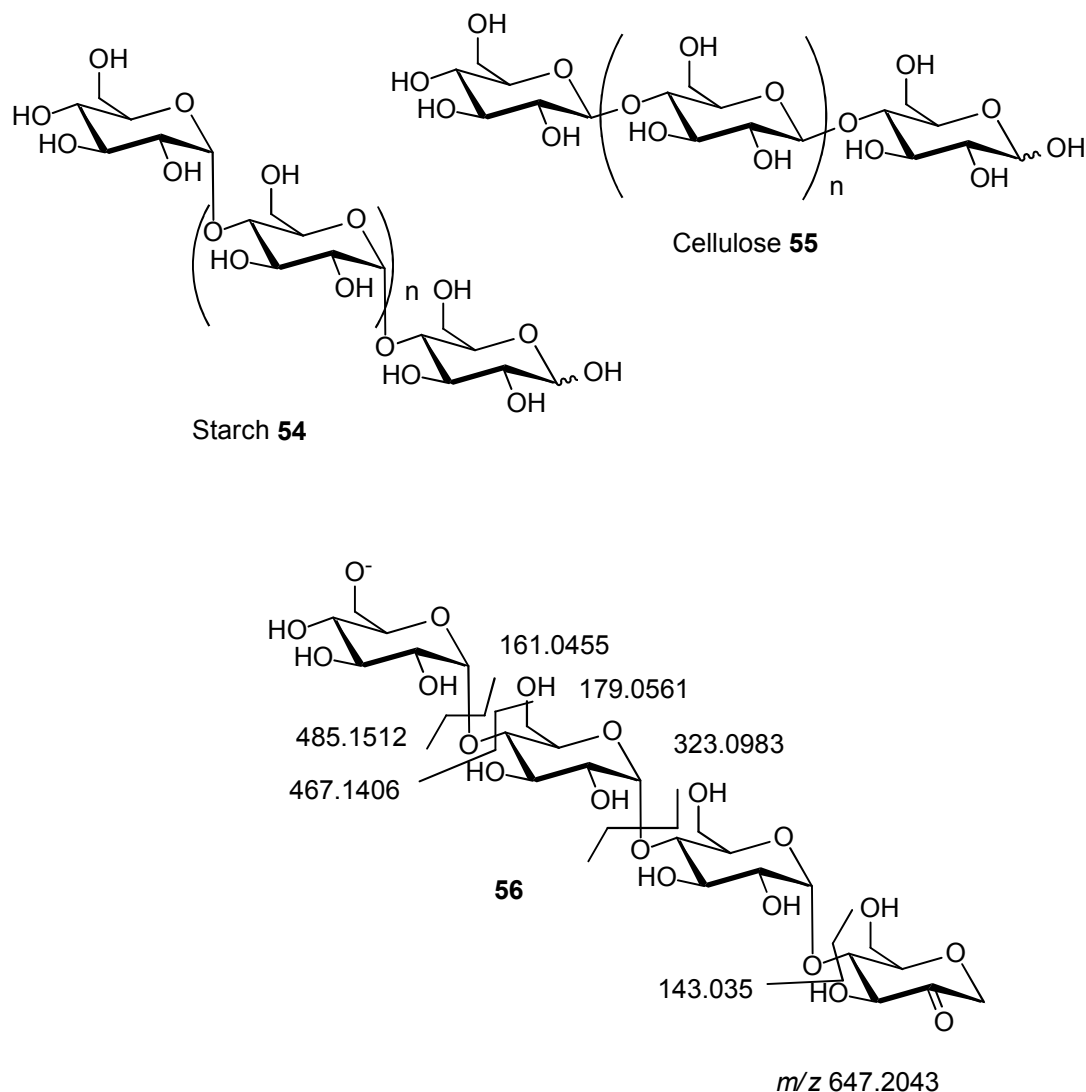


Figure 68. The chemical structures of starch, cellulose and fragmentation pattern observed for dehydrated tetramer of glucose (**56**) by IRMPD-FT-ICR-MS measurement

The positive ion mass spectra were dominated by sodiated molecular ions. Table 11 illustrates the mass/charge ratio (m/z) of the product ions, elemental composition and average mass error for heated starch as the representative saccharide in the negative ion mode. An inspection of the mass spectra showed the presence of oligomeric structures of glucose tetramer (**60**), pentamer and hexamer (**61**) at m/z 665, 827 and 989, respectively (Figure 69). Oligomers of dehydrated glucose at m/z 647, 809, 971, 1133 and 1295 dominated in the spectra. Dehydrated tetrameric (**56**) and hexameric (**58**, **59**) of glucose appeared at m/z 323 and 485 as doubly negative charged ions, respectively,. Further dehydration products arising from multiple water loss, including dehydration of monomeric carbohydrates and their oligomers demonstrated a successive loss of up to eight water molecules. Interestingly, the thermal breakdown of both

starch and cellulose leads to oligomers of glucose with a minimum number of six glucose moieties.

Table 11. High-resolution mass (ESI-FT-ICR) data for heated starch in the negative ion mode

Peak Numbering	Assignment	Molecular Formula	Experimental m/z [M-H] ⁻	Theoretical m/z [M-H] ⁻	Relative Error [ppm]
1	(Glu) ₄ – H ₂ O	C ₂₄ H ₄₀ O ₂₀	323.0998 ^b	323.0984	0.9
2	(Glu) ₆ – H ₂ O	C ₃₆ H ₆₀ O ₃₀	485.1518 ^b	485.1512	6.3
3	(Glu) ₃	C ₁₈ H ₃₂ O ₁₆	503.1597 ^a	503.1618	4.1
4	(Glu) ₄ – 3×H ₂ O	C ₂₄ H ₃₆ O ₁₈	611.1835 ^a	611.1829	1.0
5	(Glu) ₄ – 2×H ₂ O	C ₂₄ H ₃₈ O ₁₉	629.1967	629.1935	0.5
6	(Glu) ₄ – H ₂ O	C ₂₄ H ₄₀ O ₂₀	647.2036 ^a	647.2040	0.6
7	(Glu) ₅ – 2×H ₂ O	C ₃₀ H ₄₈ O ₂₄	791.2491	791.2463	0.4
8	(Glu) ₅ – H ₂ O	C ₃₀ H ₅₀ O ₂₅	809.2557	809.2568	8.6
9	(Glu) ₅	C ₃₀ H ₅₂ O ₂₆	827.2638 ^a	827.2674	4.3
10	(Glu) ₆ – 2×H ₂ O	C ₃₆ H ₅₈ O ₂₉	953.3027 ^a	953.2991	3.8
11	(Glu) ₆ – H ₂ O	C ₃₆ H ₆₀ O ₃₀	971.3097	971.3097	5.6
12	(Glu) ₆	C ₃₆ H ₆₂ O ₃₁	989.3198 ^a	989.3202	0.5
13	(Glu) ₇ – H ₂ O	C ₄₂ H ₇₀ O ₃₅	1133.3631	1133.3631	0.1
14	(Glu) ₈ – H ₂ O	C ₄₈ H ₈₀ O ₄₀	1295.4191	1295.4196	0.2

^a From TOF-MS because of mass accuracy; ^b Doubly charged ion

The smaller oligomers were not observed. Signals displaying the nominal mass of hydration products were observed to be in similarity with those of caramelized glucose. However, a close inspection of the accurate mass values in the case of starch and cellulose showed signals originating from ions with a different molecular formula and were assigned as condensed heterocyclic compounds. The mass spectra of the thermal degradation products of starch and cellulose are remarkably comparable, yet with subtle differences. In particular, the ion at m/z 683.1822 corresponding to C₃₀H₃₆O₁₈ in the negative ion mode is observed only in the spectrum of starch; whereas the ion at m/z 941.2987 (C₃₅H₅₈O₂₉; Glu₆-C₁-2H₂O) for cellulose. Both ions can be used as analytical markers indicating the presence of thermally treated starch or cellulose. In order to compare the structure and fragmentation behavior of dehydrated oligomers of glucose, an Infrared Multiple Photon Dissociation (IRMPD) experiment was carried out on a selected precursor ion at m/z 647 of a dehydrated tetramer with the empirical molecular formula C₂₄H₄₀O₂₀ (**56**) for both heated starch and cellulose.^[133]

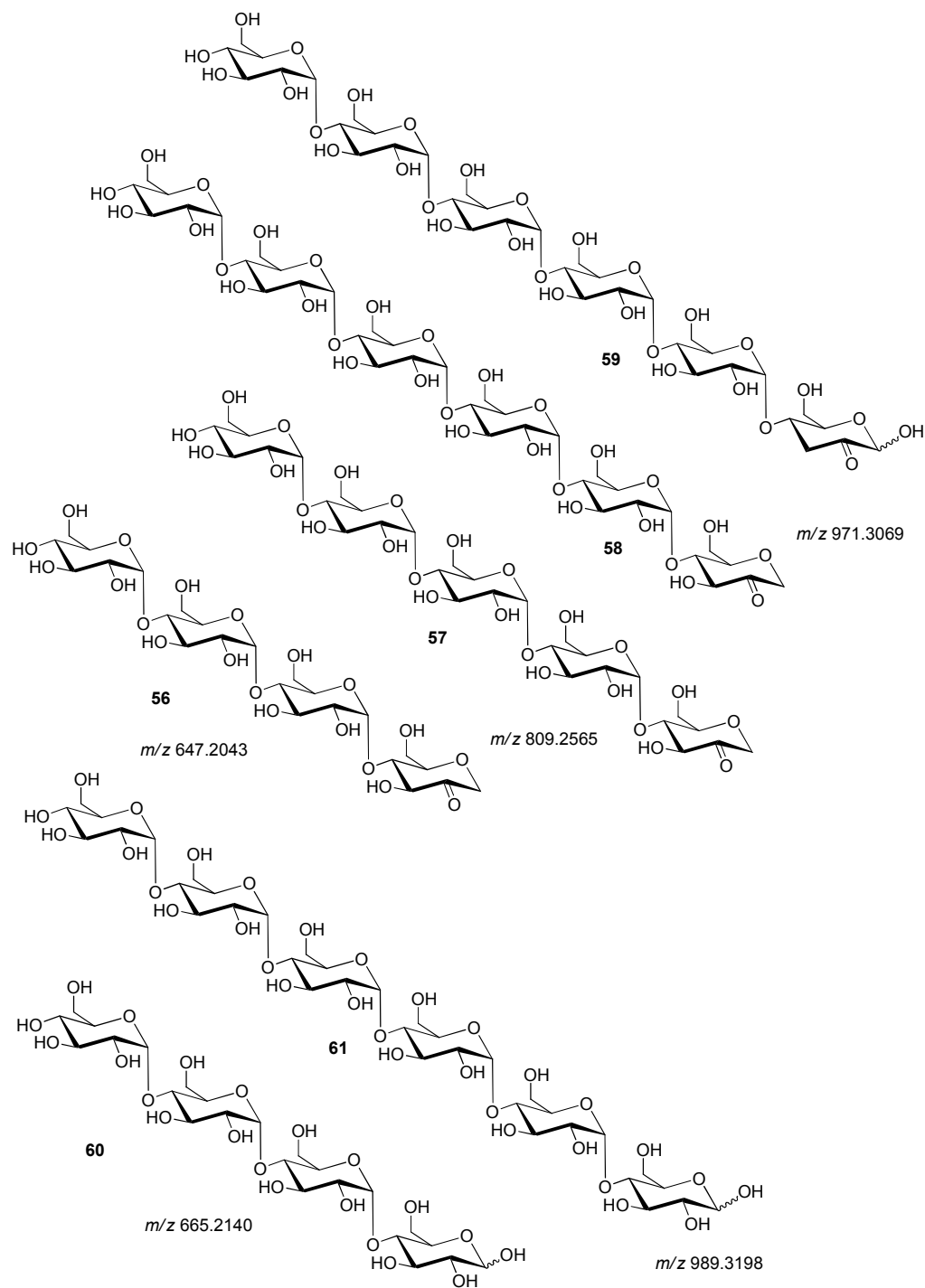


Figure 69. Structures of oligomeric and dehydrated oligomeric decomposition products **56–61** obtained from starch

The spectra are shown in Figure A1 (Appendix)*. Major fragment ions are shown as an example for starch in Figure 68.

* See on page 156

Again, the fragment ions originating from starch and cellulose are remarkably similar displaying the following subtle differences. The unique fragment ions for starch are present at m/z 467.1405, which correspond to its didehydrated trimer with molecular formula of $C_{18}H_{28}O_{14}$ and ions at m/z 383.1170 ($C_{14}H_{24}O_{12}$) and 221.0665 ($C_8H_{13}O_7$), both originating from cross-ring cleavages. The unique peaks for cellulose, on the other hand, are present at m/z 394.7669 and 254.8556. The intensity of the fragment ion at m/z 179 varied for cellulose (30%) and starch (50%). Reinhold *et al.* have demonstrated that α -glycosidic linkages in fragmentation processes are more labile when comparing with β -glycosidic linkages observed in cellulose, which is in agreement with these observations.^[212]

Novel mass spectrometric data interpretation strategies, such as van Krevelen and Kendrick plot analyses have been applied to visualize the complex data of heated polysaccharides; to give a general overview on all products of heated carbohydrates and the use as an inspiration for the further characterization of groups of compounds. Herein such methods were explored for the first time to heated polysaccharides. A general chemical reaction like dehydration, reduction or oxidation involves changes in the atomic ratios of O/C and H/C and consequently some classes of compounds can be characterized by a defined location on the graph. For instance, carbohydrates have typical atomic ratios ($H/C \sim 2$ and $O/C \sim 1$).^[124] The van Krevelen plots generated from the experimental high-resolution MS data for heated **54** and **55**, shown in Figure 70, have been annotated according to the class of products formed in the thermal decomposition reactions.

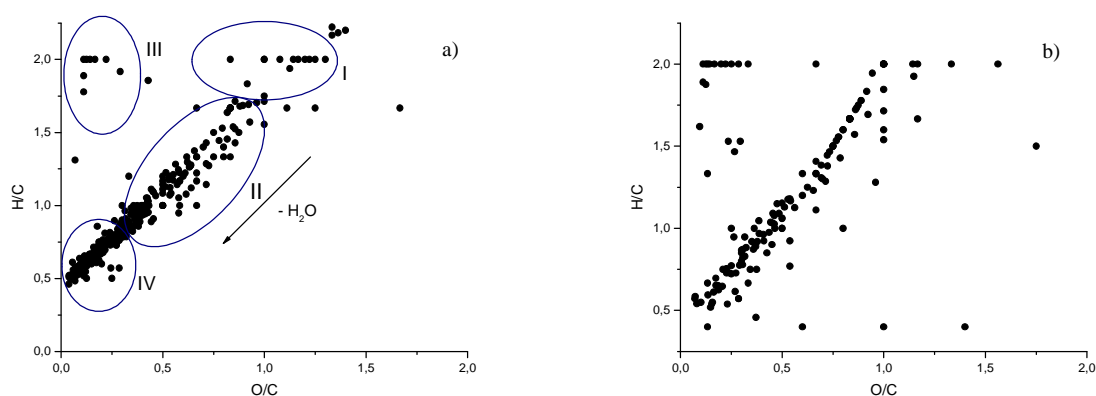


Figure 70. Two dimensional van Krevelen plots showing the O/C ratio *versus* H/C ratio for heated: a) starch and b) cellulose in the negative ion mode in m/z range between 50–1200

In general, the profile of all graphs is similar with the predominant visible trend of dehydration process for the group of points in the middle of the graph (II) and the group of points of carbohydrates in the top right corner (I) (Figure 70 a)). The group of points is present in the top left corner (III) with a significant deficiency in O among the molecules, probably due to the formation of disproportional redox reaction products. The next group of points in the bottom left corner (IV) with a significant deficiency in H indicates the presumably the presence of condensed heterocyclic ring structures. The second graphical technique applied to study the composition of heated polysaccharides is the Kendrick plot. It allows identification of homologous series of compounds, differing by a predefined mass increment. Here, the Kendrick plots are constructed using the values of Kendrick mass defect *versus* nominal Kendrick mass with a water mass increment (Figure 71). To afford Kendrick mass, IUPAC mass of a compound is multiplied by 0.999413399, originating from 18/18.010565 for water molecule. Nominal Kendrick mass (NKM) is defined as the Kendrick mass rounded to the nearest integer, while Kendrick mass defect (KMD) is defined as the difference between the exact Kendrick mass and nominal Kendrick mass (NKM).^[21]

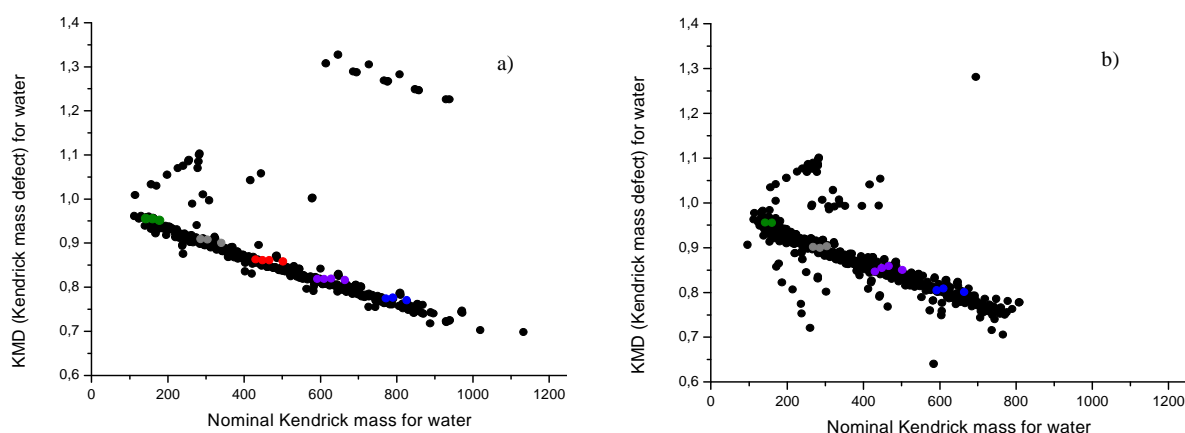


Figure 71. Two dimensional Kendrick plots for mass increment H_2O showing the distribution of the Kendrick mass defect plotted against the nominal Kendrick mass of pseudo-molecular ions for: a) starch and b) cellulose in the negative ion mode

If compounds belong to the same homologous series they would have an identical Kendrick mass defect and lie on the horizontal lines in the graphs. The graphs for all heated samples showed the presence of homologous series of the compounds with an increment of water molecule indicating the presence of oligomers with up to six monomeric glucoses in the case

of heated glucose and up to five glucoses in the case of heated polysaccharides showing consecutive loss of up to eight water units. Different colors have been used to represent the groups of polymers and green color represents monomers, grey dimers, red trimers, violet tetramers and blue pentamers. Two novel high-resolution mass data interpretation techniques gave the whole range of products and reactions during the heating procedure of polysaccharides. The further investigation was focused on the characterization of predominant products of the thermal treatment of studied carbohydrates. Tandem mass spectrometry and tandem MS coupled to liquid chromatography data for heated polysaccharides were acquired, analyzed and compared to data of their monomeric glucose to allow further structure elucidation combined with separation of isomeric products in the chromatographic dimension.^[14]

2.4.4.2 Oligomers of glucose

The MSⁿ data of monomeric glucose and their oligomers under heating of **54**, **55** and **32** has been acquired in the negative ion mode using a direct infusion into a ESI ion trap mass spectrometer. The mass spectra of the fragment ion at m/z 179.0, monomers of glucose in the negative ion mode showed a neutral loss of 18 as the main peak of **54** and **55**, and a loss of 90 as the main peak of **32**, which correspond to a water molecule and three formaldehyde molecules derived from the cross-ring cleavage, respectively. Pentamers and hexamers (**61**) of glucose appeared at m/z 827 and 989, respectively. The fragmentation of a tetrameric ion at m/z 341 (note it is the dimeric ion for **32** gave different main peaks for all studied samples). The base fragment at m/z 179.0 detected for **32**, is formed by the glycosidic bond cleavage between two monosaccharides and may occur at either the reducing or non-reducing end. Whereas the main peak at m/z 323 present for **54** and **55** corresponds to a dimer without one water molecule. The MS² spectra of the ion at m/z 503 showed the main fragment at m/z 341 for glucose and 485 for starch and cellulose, derived from the glycosidic bond cleavage at the non-reducing end and dehydration of the precursor ion, respectively. The MS² fragmentation of the ion at m/z 665, a tetramer of glucose gave predominant ions at m/z 503 for glucose and at m/z 647 for starch indicated the cleavage of the glycosidic bond at the non-reducing end and dehydration, respectively. The fragmentation of a tetrameric ion of cellulose was not possible due to the low intensity. The MS² spectra of the ion at m/z 827 exhibited the main fragment at m/z 809 for starch and cellulose with a neutral loss of 18 [H₂O]. While the base

peak at m/z 665, attributed to a pentamer of glucose, is present in the MS^2 spectrum of heated glucose and came from the glycosidic bond cleavage at the non-reducing end, as observed for the aforementioned tetramers. The MS^2 spectra of m/z 989, a hexamer of glucose provided a base peak at m/z 827 originated from the glycosidic bond cleavage at the non-reducing end for glucose and at m/z 971 for starch and cellulose. The predominant fragmentation pathway for glucose's oligomers of heated glucose involves cleavages of glycosidic bonds at the non-reducing end of molecules. The fragmentation data of oligomers of glucose for studied polysaccharides are consistent with dehydration in the product ions. ESI-LC-MS experiments were carried out using the optimized chromatographic conditions for all heated carbohydrates. The extracted ion chromatograms (EICs) were generated for all oligomers of glucose detecting different numbers of chromatographic peaks. As an example, the EIC of the ion at m/z 665 of tetrameric glucose gave one chromatographic peak for heated cellulose (Figure 72).

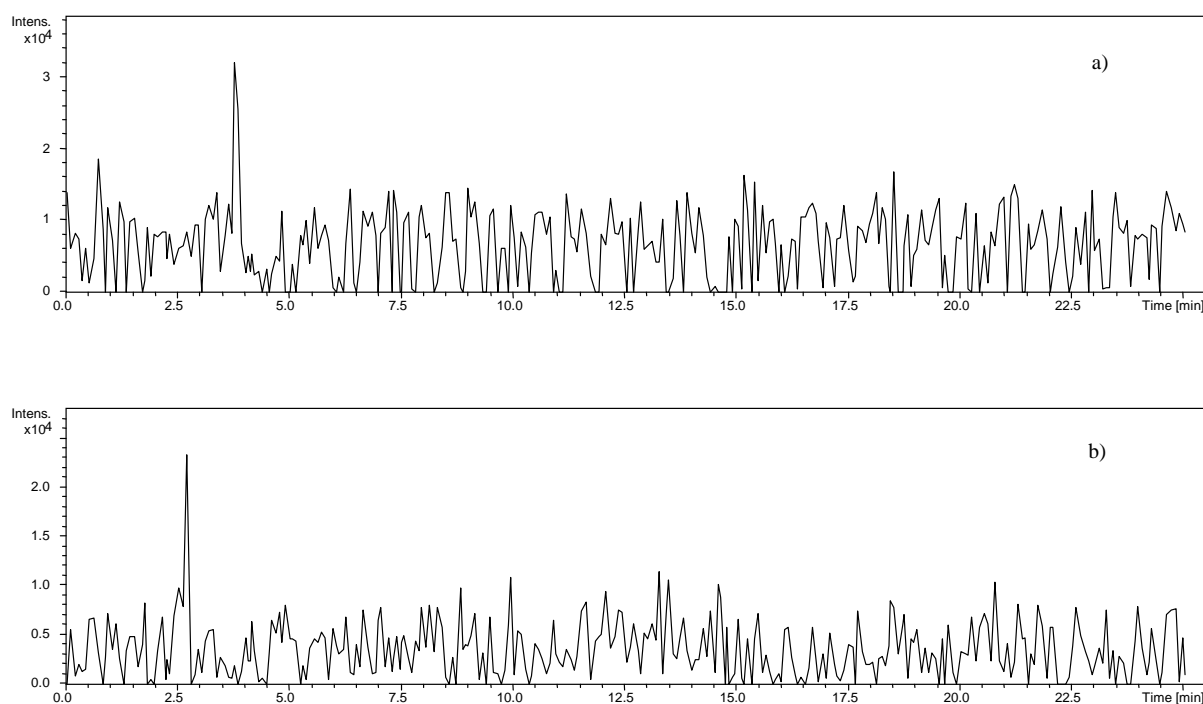


Figure 72. EICs from LC/MS experiments of pseudo-molecular ions at m/z : a) 665.0 ($C_{24}H_{42}O_{21}$) and b) 647.0 ($C_{24}H_{40}O_{20}$) of heated cellulose in negative ion mode

The presence of one single chromatographic peak suggested that chemoselective single site cleavages of the glycosidic bonds occur in starch and cellulose as opposed to glycosidic bond breaking to form monomeric glucose followed by reassembling through *de novo* glycosidic

bond formation as observed for caramelized glucose. Multiple chromatographic peaks were seen for a tetramer of heated glucose indicating a non-selective formation of numerous isomers.

2.4.4.3 Dehydration products

Dehydrated oligomers of glucose with dehydrated glucose were the predominant products of thermal treatment of studied carbohydrates and all were visualized and assigned using the van Krevelen and Kendrick mass analyses. Dehydrated oligomers of heated samples derived from a loss of a single water molecule were observed at m/z 323.1, 485.1, 647.2 and 809.2 with a dehydrated monomer of glucose at m/z 161.1 for glucose and at m/z 647.2, 809.2 971.3, 1133.4 and 1295.4 for heated starch and cellulose. When water molecule is eliminated from glucose at C1-C4 positions an enol is formed, which tautomerizes to its carbonyl form (**63**) (Figure 73). The NMR and IR data analyses of all heated samples support the presence of such a carbonyl group.

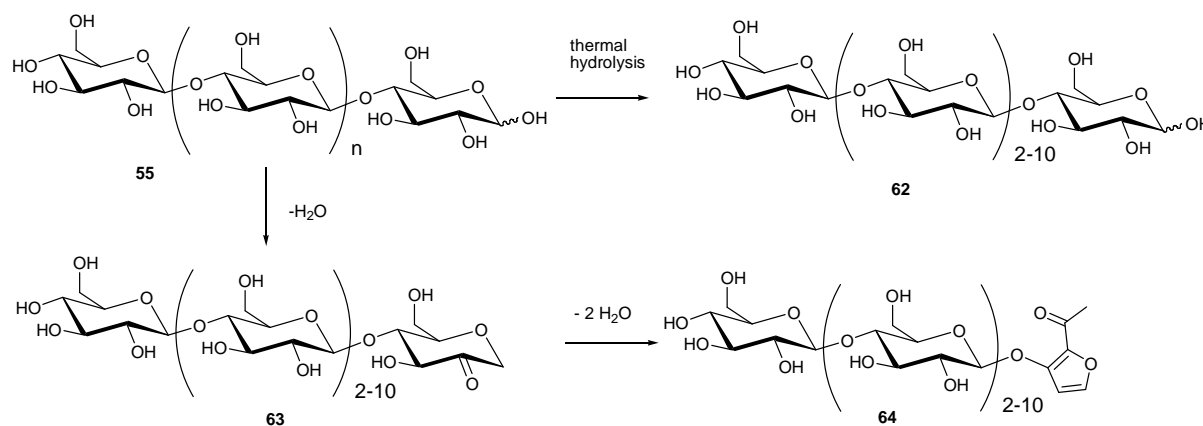


Figure 73. Reaction mechanism illustrating thermal decomposition of cellulose

The fragmentation of monodehydrated trimers at m/z 485 furnished the main fragment at m/z 323 with a neutral loss of 162 [$\text{C}_6\text{H}_{10}\text{O}_5$] for all analyzed samples. The MS^2 spectra of the ion at m/z 647 monodehydrated tetramer of glucose showed the main peak at m/z 485 and is consistent for all analyzed samples with a neutral loss of 162 [$\text{C}_6\text{H}_{10}\text{O}_5$]. In comparison to the previously discussed IRMPD data of this precursor ion, the collision-induced dissociation (CID) obtained herein reveals a smaller number of fragment ions, as expected. The

fragmentation of a monodehydrated pentamer at m/z 809 gave the main peaks at m/z 647 for all studied saccharides excluding the cleavage of the glycosidic bond at the internal part of the molecule. Dehydration reaction products with two or more water molecules were observed for studied oligomers of glucose of heated polysaccharides and glucose itself. Didehydrated ions of a dimer, trimer and tetramer appeared at m/z 305.1, 467.1 629.2 and 791.2 in the negative ion mode. The MS^2 spectra of an ion at m/z 467 exhibited for all studied samples the main fragment with a neutral loss of 18 [H_2O], although the MS^2 data are not discussed in detail. Tridehydrated oligomers of glucoses appeared at m/z 287.1, 449.1 and 611.2. The MS^2 spectra of the ion at m/z 287, a dimer after losing three water molecules gave neutral losses of 126 [$C_6H_6O_3$] as the main fragments for **55** and **32**, which support the elimination of all three water molecules from one saccharide moiety. The main fragment ion for 287 of heated glucose appeared at m/z 238.7, while the ion with a neutral loss of 126 was present with the 20% intensity. The MS^2 data of tridehydrated tetramer at m/z 611 was only recorded for heated glucose and gave the ion at m/z 449 as the base peak. The ion of its tridehydrated pentamer at m/z 773 gave the main ion at m/z 611 for glucose and at m/z 755 for starch and cellulose, which derived from the glycosidic bond cleavage at the non-reducing end and dehydration, respectively.

The EIC of the ion at m/z 647 of its dehydrated tetramer of glucose gave one chromatographic peak in the case of heated cellulose (Figure 72)*. This confirmed the extensive cleavage of the glycosidic bonds.

2.4.4.4 Comparison of heated polysaccharides

In order to visualize differences in ions observed in heated starch, cellulose and glucose radar plots were then created to show the intensities of various ions on the apices of the plot with all three different samples given as lines of different colors (Figure 74). The first graph illustrates the differences in intensities of monomeric and oligomeric ions. The formation of oligomers in the case of glucose appeared with similar manner as the degradation of polysaccharides. Cellulose degrades preferentially, when comparing to starch. The second chart shows differences in intensities of dehydrated products. The formation of dehydrated oligomers occurs in order starch>cellulose>glucose. On the other hand, monomeric glucose forms dehydrated products at first, then starch and cellulose in the similar manner.

* See on page 119

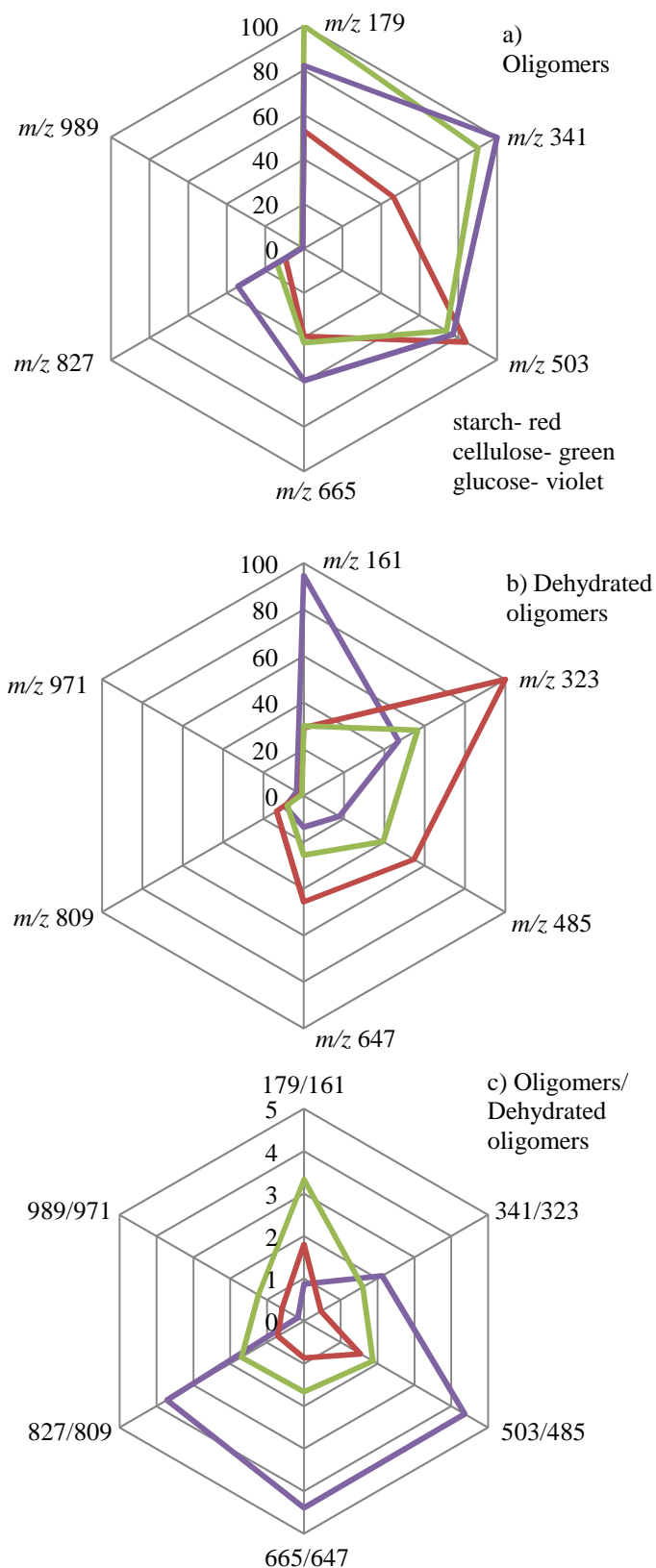


Figure 74. Radar plots of classes of ions detected in a direct infusion negative mode mass spectra of heated polysaccharides **54**, **55** and glucose **32**: a) oligomeric hexoses, b) dehydrated oligomeric hexoses, c) ratio of oligomeric to dehydrated hexoses

Finally, the third plot describes the ratios of intensities of oligomers to dehydrated oligomers. Glucose differs from polysaccharides with lower degree of dehydration and is followed by cellulose and starch.

2.4.4.5 MALDI-MS analysis of thermally treated glucose and polysaccharides

MALDI-MS analysis with 2,5-dihydroxybenzoic acid (DHB) as a matrix was performed for heated polysaccharides and glucose (Figure 75).

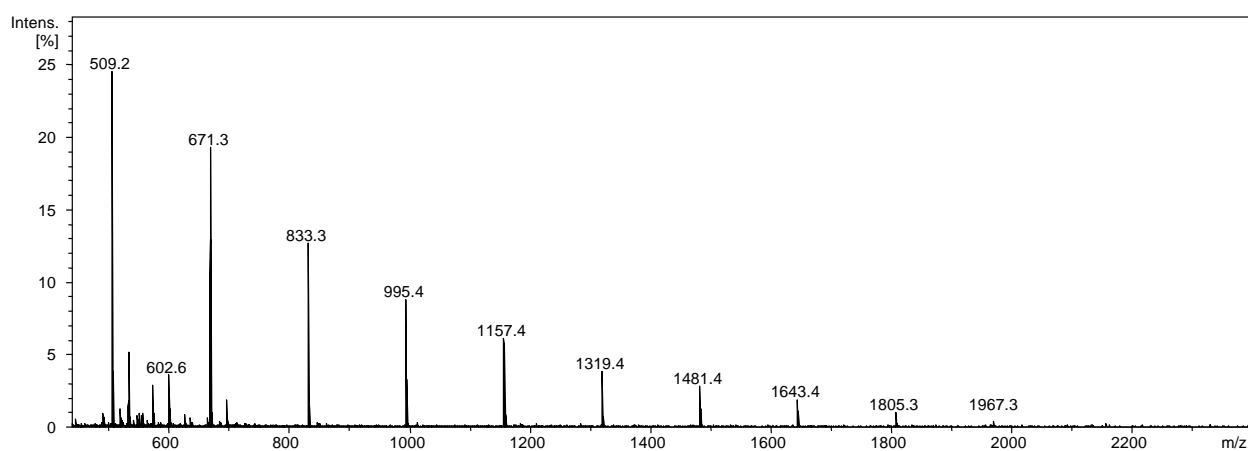


Figure 75. Mass spectrum of heated starch in the positive ion mode using a MALDI-TOF-MS instrument

In addition to the mass spectra recorded with ESI technique, high molecular weight oligosaccharides were observed up to undecamers in the case of glucose and dodecamers for starch and cellulose (Figure 69 and Figure 73)*. Ions at m/z 527, 689, 851, 1013, 1175, 1337, 1499, 1661 and 1823 were detected in the positive ion mode attributed to sodiated adducts of oligomeric glucoses up to undecamers. The MALDI-MS spectra of heated starch and cellulose showed the presence of the most intense ions at m/z 347, 509, 671, 833, 995, 1157, 1319, 1481, 1643, 1805 and 1967, which correspond to dehydrated sodiated adducts of oligomers up to dodecamers. The observation of ions with increased m/z ratios indicates the utility of MALDI-MS to cover an extended mass range in carbohydrate analysis. Yost *et al.* have observed similar products in intact wood tissues.^[213] The MALDI-MS data eventually

* See pages 115 and 120

confirmed the polymerization process of glucose, depolymerization of polysaccharides and the formation of dehydrated derivatives of all saccharides achieved by ESI-MS. Moreover, the MS² spectra of oligomers and dehydrated oligomeric ions of heated samples were recorded. The tandem MALDI-MS/MS data confirmed the identity of the ion structures observed in a MALDI-MS, when compared to those from ESI-MS.

2.4.4.6 Analysis of polysaccharide thermal degradation products in bread

Baked bread is one of the mankind's oldest foods. Polysaccharides are the main components of bread, where the white bread contains 42.5% of starch and 1.5% of cellulose.^[214] In order to provide insights into the chemistry involved in bread baking and relate the findings to the model systems studied above, the carbohydrate fraction of baked bread were investigated.

Using a simple extraction procedure of wheat based bread heated in the toaster followed by an ESI-TOF-MS experiment resulted in extremely complex spectra not enable to further interpretation. The use of MALDI-TOF-MS, however, provided spectra dominated by signals corresponding to oligomeric carbohydrates. It is worth noting that such ions appeared as sodiated and sometimes sodiated and protonated ions in the positive ion mode (example in Figure 76).

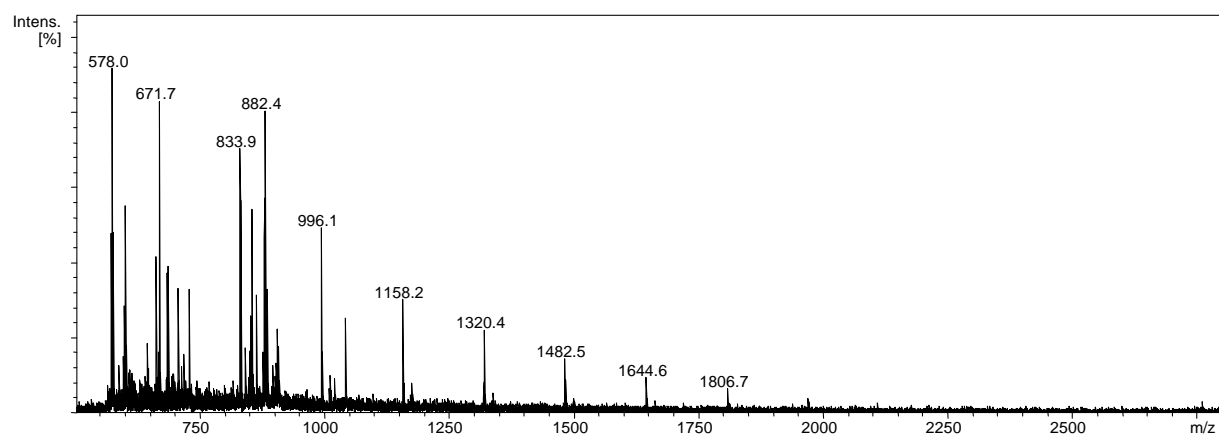


Figure 76. Mass spectrum of baked bread in the positive ion mode using a MALDI-TOF-MS instrument

Table 12 illustrates the fragment ions of three oligomeric glucoses and dehydrated oligomeric glucoses.

Table 12. MALDI-MS/MS data for the bread sample in the positive ion mode (presented ions are sodiated adducts)

<i>m/z</i>	Assignment	MS ²
		<i>m/z</i> (Intensity)
527.0	(Glu) ₃	85.2 (1%); 103.2 (5%); 123.9 (1%); 182.7 (9%); 201.8 (1%); 345.4 (4%); 363.4 (11%); 380.7 (1%); 465.4 (3%)
689.0	(Glu) ₄	74.6 (2%); 331.8 (10%); 346.3 (2%); 354.2 (4%); 364.4 (3%); 508.4 (3%); 526.4 (6%)
1175.0	(Glu) ₇	74.5 (19%); 346.8 (13%); 508.8 (18%); 526.8 (8%); 670.9 (16%); 688.9 (11%); 832.8 (7%); 850.9 (8%); 1013.2 (14%)
1157.0	(Glu) ₇ – H ₂ O	70.0 (2%); 347.0 (9%); 509.1 (21%); 671.3 (22%); 833.4 (15%); 851.4 (2%); 995.7 (11%)
1319.0	(Glu) ₈ – H ₂ O	104.0 (22%); 347.1 (40%); 509.2 (60%); 671.3 (60%); 833.4 (34%); 995.6 (22%); 1157.6 (19%)
1643.0	(Glu) ₁₀ – H ₂ O	74.1 (33%); 346.7 (26%); 508.6 (40%); 670.6 (41%); 832.7 (34%); 994.8 (22%); 1156.8 (14%); 1318.7 (14%); 1480.7 (18%)

Similar to the starch model system, ions corresponding to dehydrated oligomers were observed indicating that the identical thermal degradation processes in the model systems did take place, as well, in bread baking. The main fragmentation pattern involves cleavages of the glycosidic bonds, which additionally prove the identity of the compounds present in bread.

2.4.5 CARAMELIC PRODUCTS AND CARAMEL COLORS ANALYSIS

The analyses of model caramels were followed by the study of commercial caramellic products and caramel colors. Commercial caramellic products such as the Werther's Original[®] candies, fudge candies (Krowka[®]), bar (Caramac[®], Nestle) and caramel syrup were analyzed by high-resolution mass spectrometry. The MS spectrum of one product is shown in Figure 77. The data have been compared with the previously analyzed caramel samples. A number of peaks in the case of commercial products is lower than for model caramels. The mass formulas of most of the compounds have been assigned. Mainly monomeric carbohydrates with dehydrated ions and oligomeric products with their dehydrated and hydrated derivatives can be found.

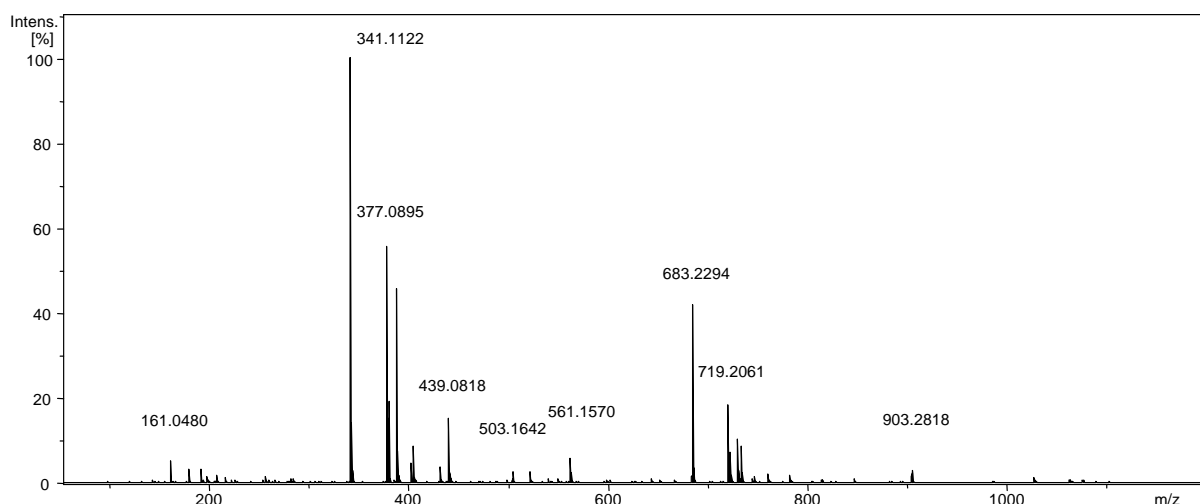


Figure 77. Mass spectrum of a candy fudge (Krowka[®]) in the negative ion mode using a direct infusion into an ESI-TOF-MS instrument

Furthermore, four types of caramel colors, such as E 150a (plane), E 150b (caustic sulphite), E 150c (ammonia) and E 150d (sulphite ammonia) have been analyzed by high-resolution mass spectrometry. The spectra recorded in the negative ion mode are shown in Figure 78 - Figure 81.

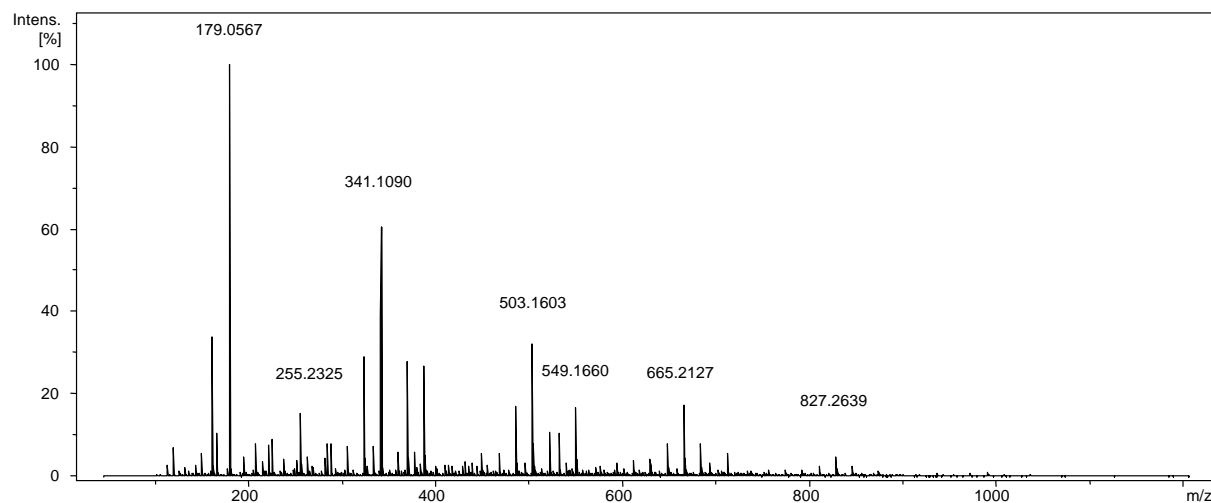


Figure 78. Mass spectrum of a caramel color E 150a in the negative ion mode using a direct infusion into an ESI-TOF-MS instrument

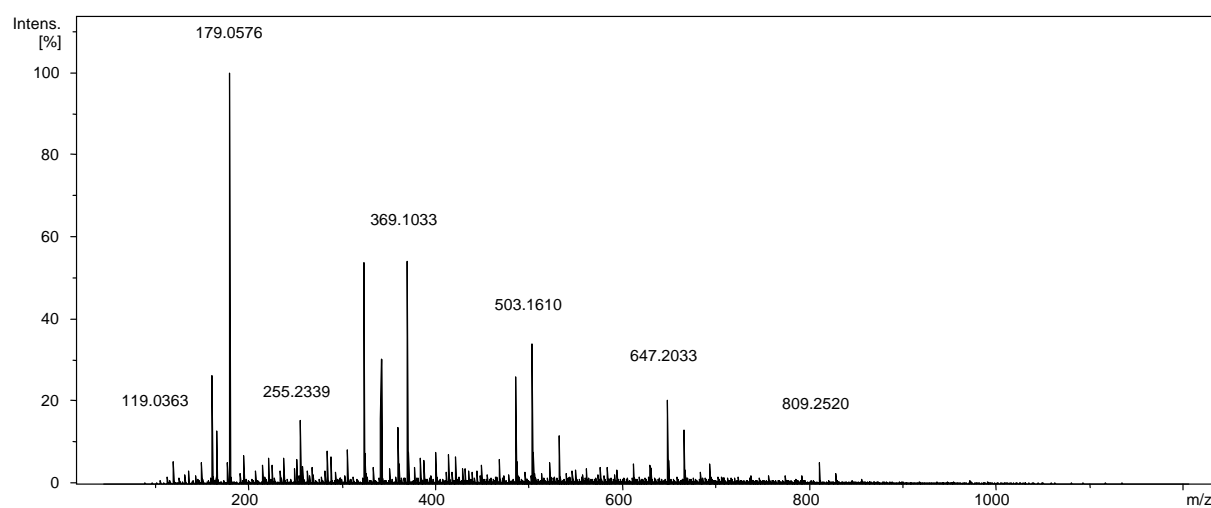


Figure 79. Mass spectrum of a caramel color E 150b in the negative ion mode using a direct infusion into an ESI-TOF-MS instrument

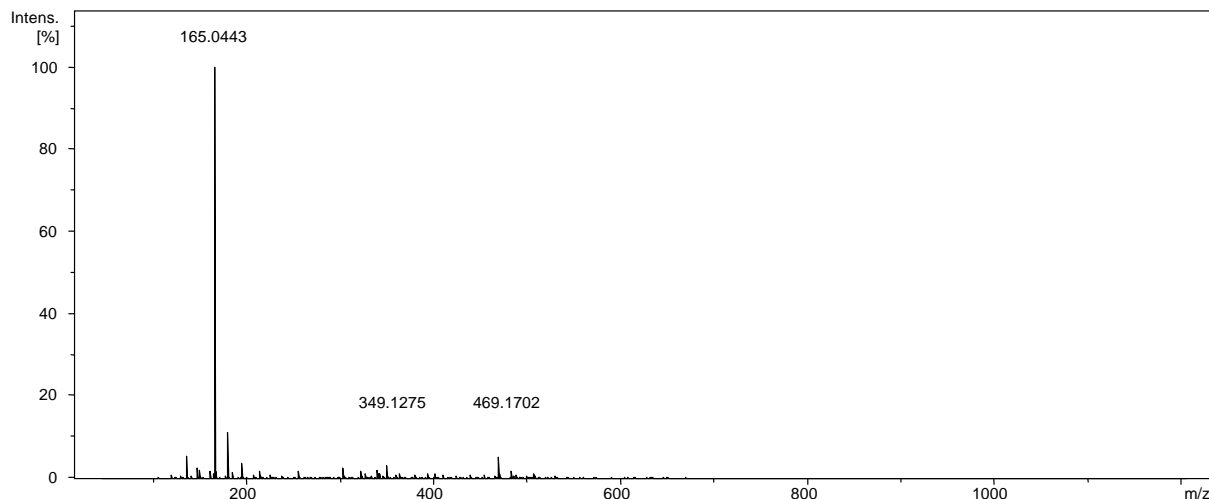


Figure 80. Mass spectrum of a caramel color E 150c in the negative ion mode using a direct infusion into an ESI-TOF-MS instrument

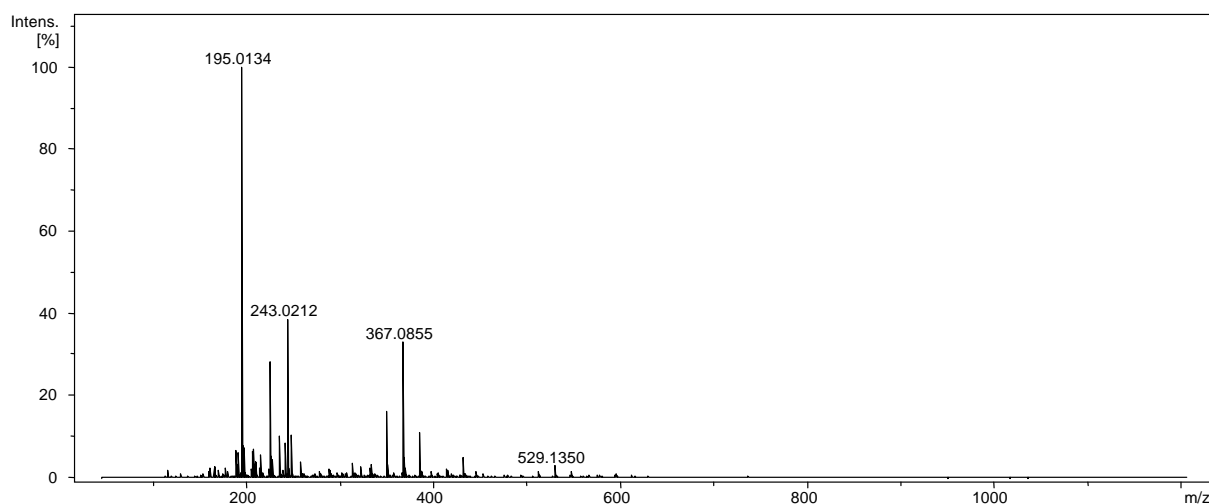


Figure 81. Mass spectrum of a caramel color E 150d in the negative ion mode using a direct infusion into an ESI-TOF-MS instrument

The data were compared with previously investigated monosaccharides. All the components from the caramelized glucose have been found in the mass spectra of plane and sulphite caramel and only few of them in the last two. The MS spectra of caramel color E 150a and E 150b are certainly similar to the MS spectrum of caramelized glucose with oligomeric hexamers and their dehydrated products as main ions (Table 13). The MS spectra of caramel color E 150c and E 150d significantly varied from others. They exhibit less complexity with few high intensities ions. An introduction of nitrogen atom into the molecules causes the

increased number of possible formula's suggestions. The identity of compounds could be resolved by the FT-ICR MS study in the future work. The presence of 4-methylimidazole (4-MEI) in caramel has received worldwide attention, because of its possible toxicity. The acceptable limit of 4-MEI is 200 ppm based on a caramel color with an intensity of 20 000 EBC units 111 according to the World Health Organization.^[215] The next nitrogen-containing compound, such as acrylamide is being considered as a probable human carcinogen.^[216] The MS spectra of analyzed caramel colors were screened for the presence of such compounds but none of them were detected.

Table 13. High-resolution mass (MS-TOF) data for a caramel color E 150a in the negative ion mode

Peak Numbering	Assignment	Molecular Formula	Experimental m/z [M-H] ⁻	Theoretical m/z [M-H] ⁻	Relative Error [ppm]
1		C ₄ H ₈ O ₄	119.0353	119.0350	2.8
2	Glu - 2×H ₂ O	C ₆ H ₈ O ₄	143.0352	143.0352	1.6
3	Glu - H ₂ O	C ₆ H ₁₀ O ₅	161.0460	161.0455	3.0
4	Glucose	C ₆ H ₁₂ O ₆	179.0568	179.0561	3.7
5		C ₆ H ₁₂ O ₇	195.0508	195.0510	1.1
6		C ₇ H ₁₄ O ₈	225.0624	225.0616	3.6
7		C ₁₆ H ₃₂ O ₂	255.2326	255.2330	1.5
8		C ₁₈ H ₃₆ O ₂	283.2646	283.2643	1.1
9	(Glu) ₂ - 3×H ₂ O	C ₁₂ H ₁₆ O ₈	287.0773	287.0772	0.1
10	(Glu) ₂ - 2×H ₂ O	C ₁₂ H ₁₈ O ₉	305.0873	305.0878	1.7
11	(Glu) ₂ - H ₂ O	C ₁₂ H ₂₀ O ₁₀	323.0982	323.0984	0.5
12	(Glu) ₂	C ₁₂ H ₂₂ O ₁₁	341.1091	341.1089	0.6
13	(Glu) ₃ - 3×H ₂ O	C ₁₈ H ₂₆ O ₁₃	449.1280	449.1301	4.7
14	(Glu) ₃ - H ₂ O	C ₁₈ H ₃₀ O ₁₅	485.1490	485.1512	4.5
15	(Glu) ₃	C ₁₈ H ₃₂ O ₁₆	503.1605	503.1618	2.5
16	(Glu) ₄ - 3×H ₂ O	C ₂₄ H ₃₆ O ₁₈	611.1800	611.1829	4.7
17	(Glu) ₄ - 2×H ₂ O	C ₂₄ H ₃₈ O ₁₉	629.1926	629.1935	1.4
18	(Glu) ₄ - H ₂ O	C ₂₄ H ₄₀ O ₂₀	647.2009	647.2040	4.7
19	(Glu) ₄	C ₂₄ H ₄₂ O ₂₁	665.2127	665.2146	2.8
20	(Glu) ₄ + H ₂ O	C ₂₄ H ₄₄ O ₂₂	683.2227	683.2251	3.6
21	(Glu) ₅ - 3×H ₂ O	C ₃₀ H ₄₆ O ₂₃	773.2325	773.2357	4.2
22	(Glu) ₅ - 2×H ₂ O	C ₃₀ H ₄₈ O ₂₄	791.2491	791.2463	3.6
23	(Glu) ₅ - H ₂ O	C ₃₀ H ₅₀ O ₂₅	809.2565	809.2568	0.2
24	(Glu) ₅	C ₃₀ H ₅₂ O ₂₆	827.2662	827.2674	1.5
25	(Glu) ₆ - 3×H ₂ O	C ₃₆ H ₅₆ O ₂₈	935.2854	935.2885	3.4
26	(Glu) ₆ - H ₂ O	C ₃₆ H ₆₀ O ₃₀	971.3063	971.3097	3.4
27	(Glu) ₆	C ₃₆ H ₆₂ O ₃₁	989.3229	989.3202	2.7

2.4.6 ROASTING PROCEDURE OF COFFEE CARBOHYDRATES

Coffee is being the third most consumed beverage followed by water and black tea with an annual production of around 8 Mt and average daily consumption of 2.3 billion cups a day.^[217] Coffee is produced from the seeds of cherries of *caffea Arabica* or *caffea contifera* (known as Robusta coffee) and referred to as green coffee beans.^[218] To obtain beverage green coffee beans are roasted at temperatures ranging from 180 to 250 °C within 5–30 minutes. The roasting process of green coffee beans leads to formation of characteristic aroma and dark color. A composition of roasted coffee beans it is not well understood. Carbohydrates being of 50% composition of coffee beans play an important role during the roasting procedure and melanoidins formation. The fraction of coffee beans' carbohydrates includes monosaccharides, disaccharides and polysaccharides among them galactomannan, arabinogalactan and cellulose.^[219-221] Hydrolysis of coffee carbohydrates gives following percentage from a total dry weight base: 22% mannose, 4% arabinose, 7% glucose, 11% galactose and 7% fructose.^[3] Carbohydrates profile remains similar for both coffee species, except sucrose, which concentration is almost doubled in Arabica coffee. Due to the fact that 50% of a dry mass of coffee beans belongs to carbohydrates, they play an important part in the composition of roasted coffee.

The model system of carbohydrates of Robusta and Arabica coffee has been prepared, heated for 1 h at 180 °C and subsequently analyzed by high-resolution mass spectrometry (ESI-TOF-MS). The mass spectra of heated carbohydrates of Arabica and Robusta coffee are shown in Figure 82 - Figure 83. The molecular formulas of 10 the most intensive ions of Arabica coffee carbohydrates composition as an example are listed in Table 14.

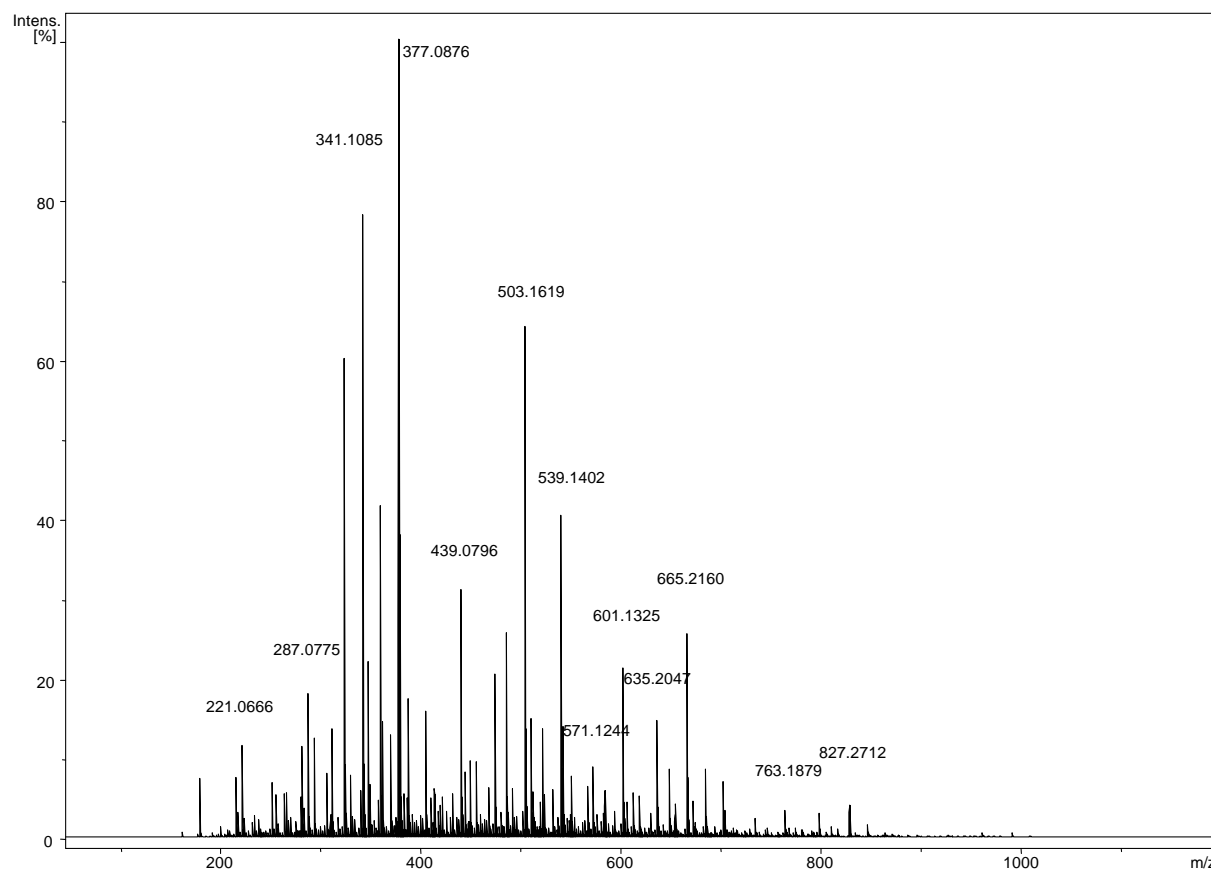


Figure 82. Mass spectrum of Arabica coffee' carbohydrates in the negative ion mode using a direct infusion into an ESI-TOF-MS

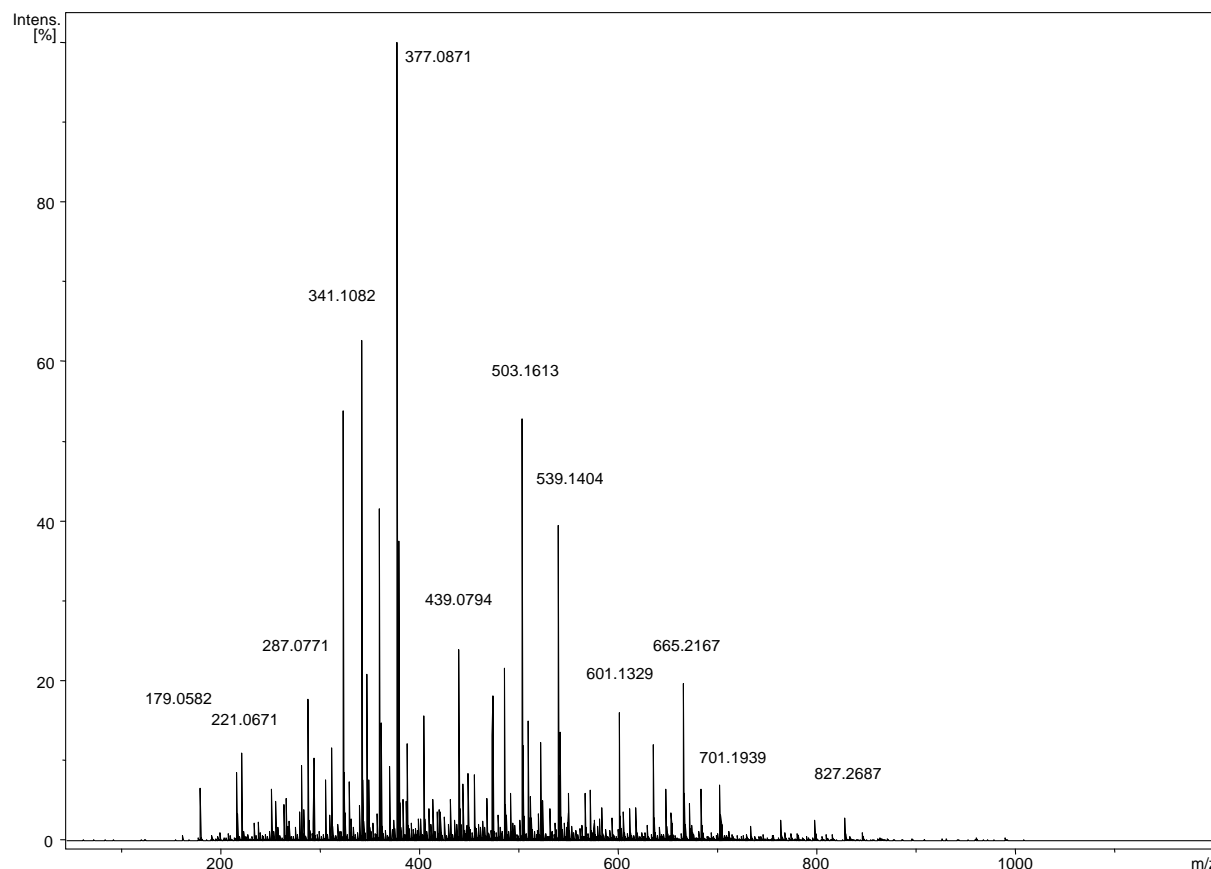


Figure 83. Mass spectrum of Robusta coffee' carbohydrates in the negative ion mode using a direct infusion into an ESI-TOF-MS

Table 14. High-resolution mass (MS-TOF) data for Arabica coffee' carbohydrates in the negative ion mode

Peak Numbering	Assignment	Molecular Formula	Experimental m/z $[M-H]^-$	Theoretical m/z $[M-H]^-$	Relative Error [ppm]
1		$C_{18}H_{17}O_9$	377.0876	377.0878	1.8
2	$(Hex)_3 - H_2O$	$C_{18}H_{30}O_{15}$	341.1085	341.1089	1.4
3	$(Hex)_3$	$C_{18}H_{32}O_{16}$	503.1620	503.1618	0.8
7	$(Hex)_2 - H_2O$	$C_{12}H_{20}O_{10}$	323.0945	323.0984	11.9
5		$C_{11}H_{20}O_{13}$	359.0807	359.0831	6.6
6		$C_{24}H_{28}O_{14}$	539.1402	539.1406	0.7
7		$C_{26}H_{16}O_7$	439.0795	439.0823	6.4
8		$C_{32}H_{22}O_5$	485.1425	485.1359	6.3
9	$(Hex)_2$	$C_{24}H_{42}O_{21}$	665.2160	665.2146	2.2
10		$C_{17}H_{16}O_8$	347.0769	347.0772	1.0

Moreover, the high-resolution mass data have been obtained previously for roasted coffee beans samples and compared here with the model mixtures of coffee carbohydrates. The investigation of the mass spectra revealed the presence of some of the components found

previously in roasted coffee bean and caramel samples. Additionally, chemometric techniques, such as the Kendrick and van Krevelen diagrams have been generated from the high-resolution mass data of heated coffee carbohydrates and a whole composition of roasted coffee beans and then compared. The van Krevelen and Kendrick diagrams for Arabica and Robusta coffee's carbohydrates are present in Figure 84 and Figure 85, respectively.

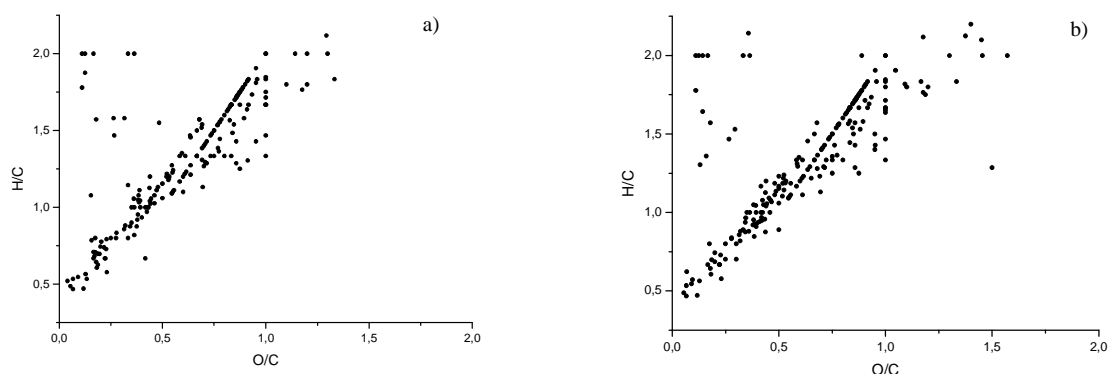


Figure 84. Two dimensional van Krevelen plots showing the O/C ratio *versus* H/C ratio for: a) Arabica and b) Robusta coffee's carbohydrates in the negative ion mode in m/z range between 50–1200

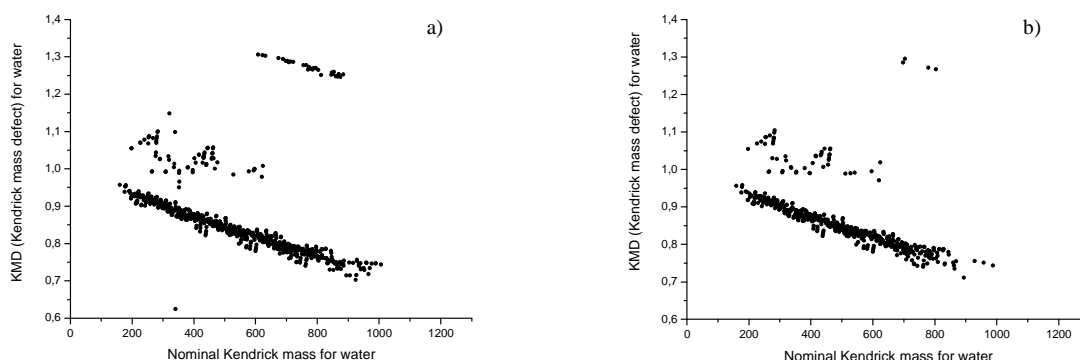


Figure 85. Two dimensional Kendrick plots for mass increment H_2O showing the distribution of the Kendrick mass defect plotted against the nominal Kendrick mass of pseudo-molecular ions for: a) Arabica and b) Robusta coffee's carbohydrates in the negative ion mode

The overlapping of these graphs with Kendrick and van Krevelen diagrams of roasted coffee beans showed the presence of similar points. The composition of roasted coffee could be simplified by a comparison with the fraction of carbohydrates consisted in roasted coffee.

2.5 CONCLUSION

The components formed in caramelization have been characterized using a conceptually novel mass spectrometry approach applied for the first time to thermally processed food. High-resolution and tandem mass spectrometry together with recently novel data interpretation strategies have been employed. High-resolution mass spectrometry provided the molecular formula lists of all components formed in the reactions. The process of examination have been continued using graphical interpretation tools, such as van Krevelen and Kendrick analyses to give a rough picture about structural trends. Targeted tandem LC-MS and direct infusion tandem MS experiments have confirmed the structures and gave a comprehensive illustration on the chemical composition of caramel. It has been shown that caramel, a challenging and enigmatic material formed from a single pure chemical substance, is thermally transformed into several thousand reaction products, displaying an astonishing level of the chemical diversity. The study showed that these compounds are formed by a small number of unselective and chemoselective reactions. The caramelization products of monosaccharides and disaccharides including oligomers with up to six carbohydrate units were formed *via* unselective glycosidic bond formation, dehydration products of oligomers losing up to eight water molecules, containing products of initial dehydration at the reducing end sugar leading to hydroxyfurfural derivatives, hydration products of sugar oligomers and disproportionation products. In the case of disaccharides, next to oligomers of hexoses created with up to eight carbohydrate units, monomeric hexoses have been generated with their dehydrated products, as well. The regio- and stereochemistry aspects of the caramelization products remain unresolved. Progress in understanding of tandem MS data might resolve many issues in regio- and stereochemical assignments in the future. In general, such aspects can be addressed using tandem mass spectrometry, however, it has not yet been established in the field of carbohydrate chemistry. The molecular formulas for some colored aromatic products that might be responsible for a brown color of caramel have been suggested. In addition, an advanced mass spectrometric study has illustrated the composition of heated polysaccharides. The obtained data for common polysaccharides, such as starch and cellulose have been compared with their monomeric glucose. During thermal treatments of polysaccharides the degraded oligomers of glucoses were found with up to five carbohydrate

units. In the case of starch and cellulose, dehydration products of oligomers were formed predominantly.

The analyses of polysaccharides were followed by the characterization of toast bread confirming the majority of their components. The composition of caramel colors E 150a and E 150b are similar to the previously studied mono- and disaccharides. Whereas, E 150c and E 150d due to the ammonium compounds present during their formation revealed to have different mass spectrometric data.

This work shows a comprehensive view of the chemical composition of one of the mankind's oldest and most popular dietary materials by using innovative analytical strategies for complex mixture analysis. Therefore, the work provided better understanding of the heating procedure of carbohydrates as the renewable sources that could efficiently contribute to a renewable energy production.

Besides, the study of model roasted coffee carbohydrates' fraction contributes to understand the composition of coffee, one of the main consumable beverages.

REFERENCES

1. Panda, S.; Andersson, J.; Schrader, W. Mass-spectrometric analysis of complex volatile and nonvolatile crude oil components: a challenge. *Anal. Bioanal. Chem.* **2007**, *389*, 1329-1339.
2. Menet, M.-C.; Sang, S.; Yang, C. S.; Ho, C.-T.; Rosen, R. T. Analysis of theaflavins and thearubigins from black tea extract by MALDI-TOF mass spectrometry. *J. Agric. Food. Chem.* **2004**, *52*, 2455-2461.
3. Jaiswal, R.; Matei, M. F.; Golon, A.; Witt, M.; Kuhnert, N. Understanding the fate of chlorogenic acids in coffee roasting using mass spectrometry based targeted and non-targeted analytical strategies. *Food Funct.* **2012**, *3*, 976-984.
4. Mortensen, A. Analysis of a complex mixture of carotenes from oil palm (*Elaeis guineensis*) fruit extract. *Food Res. Int.* **2005**, *38*, 847-853.
5. Frauendorfer, F.; Schieberle, P. Identification of the key aroma compounds in cocoa powder based on molecular sensory correlations. *J. Agric. Food. Chem.* **2006**, *54*, 5521-5529.
6. Golon, A.; Kuhnert, N. Unraveling the chemical composition of caramel. *J. Agric. Food. Chem.* **2012**, *60*, 3266-3274.
7. Rice, G. E.; Teuschler, L. K.; Bull, R. J.; Simmons, J. E.; Feder, P. I. Evaluating the similarity of complex drinking-water disinfection by-product mixtures: overview of the issues. *J. Toxicol. Environ. Health A.* **2009**, *72*, 429-436.
8. Dallüge, J.; van Stee, L. L. P.; Xu, X.; Williams, J.; Beens, J.; Vreuls, R. J. J.; Brinkman, U. A. T. Unravelling the composition of very complex samples by comprehensive gas chromatography coupled to time-of-flight mass spectrometry: cigarette smoke. *J. Chromatogr. A* **2002**, *974*, 169-184.
9. Hayter, J. R.; Robertson, D. H. L.; Gaskell, S. J.; Beynon, R. J. Proteome analysis of intact proteins in complex mixtures. *Mol. Cell. Proteomics* **2003**, *2*, 85-95.
10. Fay, R. M.; Feron, V. J. Complex mixtures: hazard identification and risk assessment. *Food Chem. Toxicol.* **1996**, *34*, 1175-1176.
11. Martin, F. L. Complex mixtures that may contain mutagenic and/or genotoxic components: a need to assess *in vivo* target-site effects associated with *in vitro*-positives. *Chemosphere* **2007**, *69*, 841-848.
12. Lee, S.; Li, Z.; Valentine, S. J.; Zucker, S. M.; Webber, N.; Reilly, J. P.; Clemmer, D. E. Extracted fragment ion mobility distributions: a new method for complex mixture analysis. *Int. J. Mass Spectrom.* **2012**, *309*, 154-160.
13. Williams, J. D.; Burinsky, D. J. Mass spectrometric analysis of complex mixtures then and now: the impact of linking liquid chromatography and mass spectrometry. *Int. J. Mass Spectrom.* **2001**, *212*, 111-133.
14. Kuhnert, N.; Clifford, M. N.; Muller, A. Oxidative cascade reactions yielding polyhydroxy-theaflavins and theacitrins in the formation of black tea thearubigins: evidence by tandem LC-MS. *Food Funct.* **2010**, *1*, 180-199.
15. Kendrick, E. A mass scale based on $\text{CH}_2 = 14.0000$ for high resolution mass spectrometry of organic compounds. *Anal. Chem.* **1963**, *35*, 2146-2154.
16. Hughey, C. A.; Hendrickson, C. L.; Rodgers, R. P.; Marshall, A. G.; Qian, K. Kendrick mass defect spectrum: a compact visual analysis for ultrahigh-resolution broadband mass spectra. *Anal. Chem.* **2001**, *73*, 4676-4681.

17. Hughey, C. A.; Rodgers, R. P.; Marshall, A. G. Resolution of 11 000 compositionally distinct components in a single electrospray ionization Fourier transform ion cyclotron resonance mass spectrum of crude oil. *Anal. Chem.* **2002**, *74*, 4145-4149.
18. Koch, B. P.; Dittmar, T.; Witt, M.; Kattner, G. Fundamentals of molecular formula assignment to ultrahigh resolution mass data of natural organic matter. *Anal. Chem.* **2007**, *79*, 1758-1763.
19. Stenson, A. C.; Marshall, A. G.; Cooper, W. T. Exact masses and chemical formulas of individual Suwannee River fulvic acids from ultrahigh resolution electrospray ionization Fourier transform ion cyclotron resonance mass spectra. *Anal. Chem.* **2003**, *75*, 1275-1284.
20. Kim, S.; Kramer, R. W.; Hatcher, P. G. Graphical method for analysis of ultrahigh-resolution broadband mass spectra of natural organic matter, the van Krevelen diagram. *Anal. Chem.* **2003**, *75*, 5336-5344.
21. Wu, Z.; Rodgers, R. P.; Marshall, A. G. Two- and three-dimensional van Krevelen diagrams: a graphical analysis complementary to the Kendrick mass plot for sorting elemental compositions of complex organic mixtures based on ultrahigh-resolution broadband Fourier transform ion cyclotron resonance mass measurements. *Anal. Chem.* **2004**, *76*, 2511-2516.
22. Marshall, A. G.; Rodgers, R. P. Petroleomics: chemistry of the underworld. *Proc. Nat. Acad. Sci. USA* **2008**, *105*, 18090-18095.
23. Kim, S.; Stanford, L. A.; Rodgers, R. P.; Marshall, A. G.; Walters, C. C.; Qian, K.; Wenger, L. M.; Mankiewicz, P. Microbial alteration of the acidic and neutral polar NSO compounds revealed by Fourier transform ion cyclotron resonance mass spectrometry. *Org. Geochem.* **2005**, *36*, 1117-1134.
24. Kuhnert, N. Unraveling the structure of the black tea thearubigins. *Arch. Biochem. Biophys.* **2010**, *501*, 37-51.
25. Gough, M. A.; Rowland, S. J. Characterization of unresolved complex mixtures of hydrocarbons in petroleum. *Nature* **1990**, *344*, 648-650.
26. Booth, A. M.; Sutton, P. A.; Lewis, C. A.; Lewis, A. C.; Scarlett, A.; Chau, W.; Widdows, J.; Rowland, S. J. Unresolved complex mixtures of aromatic hydrocarbons: thousands of overlooked persistent, bioaccumulative, and toxic contaminants in mussels. *Environ. Sci. Technol.* **2006**, *41*, 457-464.
27. Booth, A. M.; Scarlett, A. G.; Lewis, C. A.; Belt, S. T.; Rowland, S. J. Unresolved complex mixtures (UCMs) of aromatic hydrocarbons: branched alkyl indanes and branched alkyl tetralins are present in UCMs and accumulated by and toxic to, the mussel *Mytilus edulis*. *Environ. Sci. Technol.* **2008**, *42*, 8122-8126.
28. Blumer, M.; Souza, G.; Sass, J. Hydrocarbon pollution of edible shellfish by an oil spill. *Mar. Biol.* **1970**, *5*, 195-202.
29. Frysinger, G. S.; Gaines, R. B.; Xu, L.; Reddy, C. M. Resolving the unresolved complex mixture in petroleum-contaminated sediments. *Environ. Sci. Technol.* **2003**, *37*, 1653-1662.
30. Killops, S. D.; Al-Juboori, M. A. H. A. Characterisation of the unresolved complex mixture (UCM) in the gas chromatograms of biodegraded petroleums. *Org. Geochem.* **1990**, *15*, 147-160.
31. Peter Mason, R. A comparison of fluorescence and GC for the determination of petroleum hydrocarbons in mussels. *Mar. Pollut. Bull.* **1987**, *18*, 528-533.
32. Zafiriou, O. C. Petroleum hydrocarbons in Narragansett Bay: II. Chemical and isotopic analysis. *Estuarine Coastal Mar. Sci.* **1973**, *1*, 81-87.
33. Rodgers, R. P.; Blumer, E. N.; Freitas, M. A.; Marshall, A. G. Jet fuel chemical composition, weathering, and identification as a contaminant at a remediation site, determined by Fourier transform ion cyclotron resonance mass spectrometry. *Anal. Chem.* **1999**, *71*, 5171-5176.

34. Lundanes, E.; Greibrokk, T. Separation of fuels, heavy fractions, and crude oils into compound classes. *J. High Res. Chromatog.* **1994**, *17*, 197-202.
35. Wang, Z.; Fingas, M. Developments in the analysis of petroleum hydrocarbons in oils, petroleum products and oil-spill-related environmental samples by gas chromatography. *J. Chromatogr. A* **1997**, *774*, 51-78.
36. Boehm, P. D.; Douglas, G. S.; Burns, W. A.; Mankiewicz, P. J.; Page, D. S.; Bence, A. E. Application of petroleum hydrocarbon chemical fingerprinting and allocation techniques after the Exxon Valdez oil spill. *Mar. Pollut. Bull.* **1997**, *34*, 599-613.
37. Tran, T. C.; Logan, G. A.; Grosjean, E.; Ryan, D.; Marriott, P. J. Use of comprehensive two-dimensional gas chromatography/time-of-flight mass spectrometry for the characterization of biodegradation and unresolved complex mixtures in petroleum. *Geochim. Cosmochim. Ac.* **2010**, *74*, 6468-6484.
38. Chen, G.; White, P. A. The mutagenic hazards of aquatic sediments. *Mutat. Res.* **2004**, *567*, 151-225.
39. Donkin, P.; Smith, E. L.; Rowland, S. J. Toxic effects of unresolved complex mixtures of aromatic hydrocarbons accumulated by mussels, *Mytilus edulis*, from contaminated field sites. *Environ. Sci. Technol.* **2003**, *37*, 4825-4830.
40. Rowland, S.; Donkin, P.; Smith, E.; Wraige, E. Aromatic hydrocarbon “humps” in the marine environment: unrecognized toxins? *Environ. Sci. Technol.* **2001**, *35*, 2640-2644.
41. Scarlett, A.; Galloway, T.; Rowland, S. Chronic toxicity of unresolved complex mixtures (UCM) of hydrocarbons in marine sediments. *J. Soil. Sediment.* **2007**, *7*, 200-206.
42. Thomas, K. V.; Donkin, P.; Rowland, S. J. Toxicity enhancement of an aliphatic petrogenic unresolved complex mixture (UCM) by chemical oxidation. *Water Res.* **1995**, *29*, 379-382.
43. Atlas, R. M. Microbial degradation of petroleum hydrocarbons: an environmental perspective. *Microbiol. Rev.* **1981**, *45*, 180-209.
44. Li, L.; Cunningham, C. J.; Pas, V.; Philp, J. C.; Barry, D. A.; Anderson, P. Field trial of a new aeration system for enhancing biodegradation in a biopile. *Waste Manage.* **2004**, *24*, 127-137.
45. Liu, C. W.; Chang, W. N.; Liu, H. S. Bioremediation of *n*-alkanes and the formation of bioflocules by *Rhodococcus erythropolis* NTU-1 under various saline conditions and sea water. *Biochem. Eng. J.* **2009**, *45*, 69-75.
46. Mao, D.; Lookman, R.; Van De Weghe, H.; Van Look, D.; Vanermen, G.; De Brucker, N.; Diels, L. Detailed analysis of petroleum hydrocarbon attenuation in biopiles by high-performance liquid chromatography followed by comprehensive two-dimensional gas chromatography. *J. Chromatogr. A* **2009**, *1216*, 1524-1527.
47. Penet, S.; Vendeuvre, C.; Bertoncini, F.; Marchal, R.; Monot, F. Characterisation of biodegradation capacities of environmental microflorae for diesel oil by comprehensive two-dimensional gas chromatography. *Biodegradation* **2006**, *17*, 577-585.
48. Morselli, L.; Santini, A.; Passarini, F.; Vassura, I. Automotive shredder residue (ASR) characterization for a valuable management. *Waste Manage.* **2010**, *30*, 2228-2234.
49. Forton, O. T.; Harder, M. K.; Moles, N. R. Value from shredder waste: ongoing limitations in the UK. *Resour. Conserv. Recy.* **2006**, *46*, 104-113.
50. Nourreddine, M. Recycling of auto shredder residue. *J. Hazard. Mater.* **2007**, *139*, 481-490.
51. Zorpas, A. A.; Inglezakis, V. J. Automotive industry challenges in meeting EU 2015 environmental standard. *Technol. Soc.* **2012**, *34*, 55-83.

52. LAGA, Bestimmung des Gehaltes an Kohlenwasserstoffen in Abfällen-Untersuchungs und Kurzbezeichnung: KW/04. Mitteilung der Länderarbeitsgemeinschaft Abfall. In 2004.
53. Abu-Elgheit, M. A. Oil spill source identification by infrared, gas chromatographic, and trace metal analyses. *Environ. Int.* **1982**, 7, 305-308.
54. Delft, R. J.; Doveren, A. S. M. J.; Snijders, A. G. The determination of petroleum hydrocarbons in soil using a miniaturized extraction method and gas chromatography. *Fresen. J. Anal. Chem.* **1994**, 350, 638-641.
55. Saari, E.; Perämäki, P.; Jalonen, J. Evaluating the impact of GC operating settings on GC-FID performance for total petroleum hydrocarbon (TPH) determination. *Microchem. J.* **2010**, 94, 73-78.
56. Anastassiades, M.; Maštovská, K.; Lehotay, S. J. Evaluation of analyte protectants to improve gas chromatographic analysis of pesticides. *J. Chromatogr. A* **2003**, 1015, 163-184.
57. Qiu, X.; Zhu, T.; Li, J.; Pan, H.; Li, Q.; Miao, G.; Gong, J. Organochlorine pesticides in the air around the Taihu Lake, China. *Environ. Sci. Technol.* **2004**, 38, 1368-1374.
58. Čajka, T.; Hajšlová, J. Gas chromatography-high-resolution time-of-flight mass spectrometry in pesticide residue analysis: advantages and limitations. *J. Chromatogr. A* **2004**, 1058, 251-261.
59. Bailey, R. Injectors for capillary gas chromatography and their application to environmental analysis. *J. Environ. Monitor.* **2005**, 7, 1054-1058.
60. Buser, H.-R.; Haglund, P.; Müller, M. D.; Poiger, T.; Rappe, C. Discrimination and thermal degradation of toxaphene compounds in capillary gas chromatography when using split/splitless and on-column injection. *Chemosphere* **2000**, 41, 473-479.
61. Zrostlíková, J.; Hajšlová, J.; Godula, M.; Maštovská, K. Performance of programmed temperature vaporizer, pulsed splitless and on-column injection techniques in analysis of pesticide residues in plant matrices. *J. Chromatogr. A* **2001**, 937, 73-86.
62. Brossa, L.; Marcé, R. M.; Borrull, F.; Pocurull, E. Application of on-line solid-phase extraction-gas chromatography-mass spectrometry to the determination of endocrine disruptors in water samples. *J. Chromatogr. A* **2002**, 963, 287-294.
63. Kristenson, E. M.; Angioi, S.; Vreuls, R. J. J.; Gennaro, M. C.; Brinkman, U. A. T. Miniaturised pressurised liquid extraction of chloroanilines from soil with subsequent analysis by large-volume injection-gas chromatography-mass spectrometry. *J. Chromatogr. A* **2004**, 1058, 243-249.
64. Slobodník, J.; Ramalho, S.; van Baar, B. L. M.; Louter, A. J. H.; Brinkman, U. A. T. Determination of microcontaminants in sediments by on-line solid-phase extraction-gas chromatography-mass spectrometry. *Chemosphere* **2000**, 41, 1469-1478.
65. Kristenson, E. M.; Kamminga, D. A.; Catalina, M. I.; Espiga, C.; Vreuls, R. J. J.; Brinkman, U. A. T. Role of the retaining precolumn in large-volume on-column injections of volatiles to gas chromatography. *J. Chromatogr. A* **2002**, 975, 95-104.
66. Hankemeier, T.; Kok, S. J.; Vreuls, R. J. J.; Brinkman, U. A. T. Optimization of large-volume on-column injection conditions in gas chromatography by monitoring the actual carrier gas flow. *J. Chromatogr. A* **1999**, 841, 75-94.
67. Arrebola, F. J.; Martínez Vidal, J. L.; Mateu-Sánchez, M.; Álvarez-Castellón, F. J. Determination of 81 multiclass pesticides in fresh foodstuffs by a single injection analysis using gas chromatography-chemical ionization and electron ionization tandem mass spectrometry. *Anal. Chim. Acta* **2003**, 484, 167-180.
68. Kochman, M.; Gordin, A.; Goldschlag, P.; Lehotay, S. J.; Amirav, A. Fast, high-sensitivity, multipesticide analysis of complex mixtures with supersonic gas chromatography-mass spectrometry. *J. Chromatogr. A* **2002**, 974, 185-212.

69. Vermeulen, A.; Welvaert, K.; Vercammen, J. Evaluation of a dedicated gas chromatography-mass spectrometry method for the analysis of phenols in water. *J. Chromatogr. A* **2005**, *1071*, 41-46.
70. Lin, W.-C.; Chen, H.-C.; Ding, W.-H. Determination of pharmaceutical residues in waters by solid-phase extraction and large-volume on-line derivatization with gas chromatography-mass spectrometry. *J. Chromatogr. A* **2005**, *1065*, 279-285.
71. Saari, E.; Perämäki, P.; Jalonen, J. Effect of sample matrix on the determination of total petroleum hydrocarbons (TPH) in soil by gas chromatography-flame ionization detection. *Microchem. J.* **2007**, *87*, 113-118.
72. Becker, R.; Buge, H.-G.; Bremser, W.; Nehls, I. Mineral oil content in sediments and soils: comparability, traceability and a certified reference material for quality assurance. *Anal. Bioanal. Chem.* **2006**, *385*, 645-651.
73. Becker, R.; Koch, M.; Wachholz, S.; Win, T. Quantification of total petrol hydrocarbons (TPH) in soil by IR-spectrometry and gas chromatography-conclusions from three proficiency testing rounds. *Accred. Qual. Assur.* **2002**, *7*, 286-289.
74. Ventura, G. T.; Kenig, F.; Reddy, C. M.; Frysinger, G. S.; Nelson, R. K.; Mooy, B. V.; Gaines, R. B. Analysis of unresolved complex mixtures of hydrocarbons extracted from Late Archean sediments by comprehensive two-dimensional gas chromatography (GC×GC). *Org. Geochem.* **2008**, *39*, 846-867.
75. Skoczyńska, E.; Korytár, P.; Boer, J. D. Maximizing chromatographic information from environmental extracts by GC×GC-TOF-MS. *Environ. Sci. Technol.* **2008**, *42*, 6611-6618.
76. Reddy, C. M.; Eglinton, T. I.; Hounshell, A.; White, H. K.; Xu, L.; Gaines, R. B.; Frysinger, G. S. The West Falmouth oil spill after thirty years: the persistence of petroleum hydrocarbons in marsh sediments. *Environ. Sci. Technol.* **2002**, *36*, 4754-4760.
77. Frysinger, G. S.; Gaines, R. B. Separation and identification of petroleum biomarkers by comprehensive two-dimensional gas chromatography. *J. Sep. Sci.* **2001**, *24*, 87-96.
78. Nelson, R. K.; Kile, B. M.; Plata, D. L.; Sylva, S. P.; Xu, L.; Reddy, C. M.; Gaines, R. B.; Frysinger, G. S.; Reichenbach, S. E. Tracking the weathering of an oil spill with comprehensive two-dimensional gas chromatography. *Environ. Foren.* **2006**, *7*, 33-44.
79. Liu, Z.; Phillips, J. B. Comprehensive two-dimensional gas chromatography using an on-column thermal modulator interface. *J. Chromatogr. Sci.* **1991**, *29*, 227-231.
80. Mao, D.; Lookman, R.; Weghe, H. V. D.; Weltens, R.; Vanermen, G.; Brucker, N. D.; Diels, L. Estimation of ecotoxicity of petroleum hydrocarbon mixtures in soil based on HPLC-GC×GC analysis. *Chemosphere* **2009**, *77*, 1508-1513.
81. Silverstein, R. M.; Webster, F. X.; Kiemle, D. J. Spectrometric Identification of Organic Compounds; John Wiley & Sons: Danvers, MA, 2005, 1-550.
82. Ludányi, K.; Dallos, A.; Kühn, Z.; Vékey, K. Mass spectrometry of very large saturated hydrocarbons. *J. Mass Spectrom.* **1999**, *34*, 264-267.
83. Field, F. H. Chemical ionization mass spectrometry. VIII. Alkenes and alkynes. *J. Am. Chem. Soc.* **1968**, *90*, 5649-5656.
84. Zhan, D.; Fenn, J. B. Electrospray mass spectrometry of fossil fuels. *Int. J. Mass Spectrom.* **2000**, *194*, 197-208.
85. Kim, S.; Rodgers, R. P.; Blakney, G. T.; Hendrickson, C. L.; Marshall, A. G. Automated electrospray ionization FT-ICR mass spectrometry for petroleum analysis. *J. Am. Soc. Mass. Spectrom.* **2009**, *20*, 263-268.

86. Zhou, X.; Shi, Q.; Zhang, Y.; Zhao, S.; Zhang, R.; Chung, K. H.; Xu, C. Analysis of saturated hydrocarbons by redox reaction with negative-ion electrospray Fourier transform ion cyclotron resonance mass spectrometry. *Anal. Chem.* **2012**, *84*, 3192-3199.
87. Millan, M.; Behrouzi, M.; Karaca, F.; Morgan, T. J.; Herod, A. A.; Kandiyoti, R. Characterising high mass materials in heavy oil fractions by size exclusion chromatography and MALDI-mass spectrometry. *Catal. Today* **2005**, *109*, 154-161.
88. Schmidt, C. E.; Sprecher, R. F.; Batts, B. D. Low-voltage, high-resolution mass spectrometric methods for fuel analysis: application to coal distillates. *Anal. Chem.* **1987**, *59*, 2027-2033.
89. Robb, D. B.; Covey, T. R.; Bruins, A. P. Atmospheric pressure photoionization: an ionization method for liquid chromatography-mass spectrometry. *Anal. Chem.* **2000**, *72*, 3653-3659.
90. Bell, S. E.; Ewing, R. G.; Eiceman, G. A.; Karpas, Z. Atmospheric pressure chemical ionization of alkanes, alkenes, and cycloalkanes. *J. Am. Soc. Mass. Spectrom.* **1994**, *5*, 177-185.
91. Borsdorf, H.; Nazarov, E.; Eiceman, G. Atmospheric pressure chemical ionization studies of non-polar isomeric hydrocarbons using ion mobility spectrometry and mass spectrometry with different ionization techniques. *J. Am. Soc. Mass. Spectrom.* **2002**, *13*, 1078-1087.
92. Qian, K.; Dechert, G. J. Recent advances in petroleum characterization by GC field ionization time-of-flight high-resolution mass spectrometry. *Anal. Chem.* **2002**, *74*, 3977-3983.
93. Mitschke, S.; Welthagen, W.; Zimmermann, R. Comprehensive gas chromatography-time-of-flight mass spectrometry using soft and selective photoionization techniques. *Anal. Chem.* **2006**, *78*, 6364-6375.
94. Allgood, C.; Ma, Y. C.; Munson, B. Quantitation using benzene in gas chromatography/chemical ionization mass spectrometry. *Anal. Chem.* **1991**, *63*, 721-725.
95. Dzidic, I.; Petersen, H. A.; Wadsworth, P. A.; Hart, H. V. Townsend discharge nitric oxide chemical ionization gas chromatography/mass spectrometry for hydrocarbon analysis of the middle distillates. *Anal. Chem.* **1992**, *64*, 2227-2232.
96. Isaacman, G.; Wilson, K. R.; Chan, A. W. H.; Worton, D. R.; Kimmel, J. R.; Nah, T.; Hohaus, T.; Gonin, M.; Kroll, J. H.; Worsnop, D. R.; Goldstein, A. H. Improved resolution of hydrocarbon structures and constitutional isomers in complex mixtures using gas chromatography-vacuum ultraviolet-mass spectrometry. *Anal. Chem.* **2012**, *84*, 2335-2342.
97. Kim, Y. H.; Kim, S. Improved abundance sensitivity of molecular ions in positive-ion APCI MS analysis of petroleum in toluene. *J. Am. Soc. Mass. Spectrom.* **2010**, *21*, 386-392.
98. Holmes, J. C.; Morrell, F. A. Oscillographic mass spectrometric monitoring of gas chromatography. *Appl. Spectrosc.* **1957**, *11*, 86-87.
99. Field, F. H.; Hastings, S. H. Determination of unsaturated hydrocarbons by low voltage mass spectrometry. *Anal. Chem.* **1956**, *28*, 1248-1255.
100. Lumpkin, H. E.; Aczel, T. Low-voltage sensitivities of aromatic hydrocarbons. *Anal. Chem.* **1964**, *36*, 181-184.
101. Clegg, H.; Horsfield, B.; Stasiuk, L.; Fowler, M.; Vliex, M. Geochemical characterisation of organic matter in Keg River Formation (Elk point group, Middle Devonian), La Crete Basin, Western Canada. *Org. Geochem.* **1997**, *26*, 627-643.
102. Poster, D.; Schantz, M.; Sander, L.; Wise, S. Analysis of polycyclic aromatic hydrocarbons (PAHs) in environmental samples: a critical review of gas chromatographic (GC) methods. *Anal. Bioanal. Chem.* **2006**, *386*, 859-881.

103. Carroll, D. I.; Dzidic, I.; Stillwell, R. N.; Haegele, K. D.; Horning, E. C. Atmospheric pressure ionization mass spectrometry. Corona discharge ion source for use in a liquid chromatograph-mass spectrometer-computer analytical system. *Anal. Chem.* **1975**, *47*, 2369-2373.
104. Kim, Y.; Kim, S. Improved abundance sensitivity of molecular ions in positive-ion APCI MS analysis of petroleum in toluene. *J. Am. Soc. Mass. Spectrom.* **2010**, *21*, 386-392.
105. Roussis, S. G.; Fedora, J. W. Quantitative determination of polar and ionic compounds in petroleum fractions by atmospheric pressure chemical ionization and electrospray ionization mass spectrometry. *Rapid Commun. Mass Spectrom.* **2002**, *16*, 1295-1303.
106. Hsu, C. S.; Dechert, G. J.; Robbins, W. K.; Fukuda, E. K. Naphthenic acids in crude oils characterized by mass spectrometry. *Energy Fuels* **1999**, *14*, 217-223.
107. Marotta, E.; Paradisi, C. A mass spectrometry study of alkanes in air plasma at atmospheric pressure. *J. Am. Soc. Mass. Spectrom.* **2009**, *20*, 697-707.
108. Karasek, F. W.; Tatone, O. S.; Denney, D. W. Plasma chromatography of the *n*-alkyl halides. *J. Chromatogr. A* **1973**, *87*, 137-145.
109. Karasek, F. W.; Denney, D. W.; DeDecker, E. H. Plasma chromatography of normal alkanes and its relation to chemical ionization mass spectrometry. *Anal. Chem.* **1974**, *46*, 970-973.
110. Herrera, L.; Grossert, J.; Ramaley, L. Quantitative aspects of and ionization mechanisms in positive-ion atmospheric pressure chemical ionization mass spectrometry. *J. Am. Soc. Mass. Spectrom.* **2008**, *19*, 1926-1941.
111. Borsdorf, H.; Schelhorn, H.; Flachowsky, J.; Döring, H.-R.; Stach, J. Corona discharge ion mobility spectrometry of aliphatic and aromatic hydrocarbons. *Anal. Chim. Acta* **2000**, *403*, 235-242.
112. Kolakowski, B. M.; Grossert, J. S.; Ramaley, L. Studies on the positive-ion mass spectra from atmospheric pressure chemical ionization of gases and solvents used in liquid chromatography and direct liquid injection. *J. Am. Soc. Mass. Spectrom.* **2004**, *15*, 311-324.
113. Gao, J.; Owen, B.; Borton, D.; Jin, Z.; Kenttämää, H. HPLC/APCI mass spectrometry of saturated and unsaturated hydrocarbons by using hydrocarbon solvents as the APCI reagent and HPLC mobile phase. *J. Am. Soc. Mass. Spectrom.* **2012**, *23*, 816-822.
114. Mitchum, R. K.; Moler, G. F.; Korfmacher, W. A. Combined capillary gas chromatography/atmospheric pressure negative chemical ionization/mass spectrometry for the determination of 2,3,7,8-tetrachlorodibenzo-p-dioxin in tissue. *Anal. Chem.* **1980**, *52*, 2278-2282.
115. Korfmacher, W. A.; Mitchum, R. K.; Hileman, F. D.; Mazer, T. Analysis of 2,3,7,8-tetrachlorodibenzofuran by fused silica GC combined with atmospheric pressure ionization MS. *Chemosphere* **1983**, *12*, 1243-1249.
116. Korfmacher, W. A.; Rushing, L. G.; Arey, J.; Zielinska, B.; Pitts, J. N. Identification of mononitropyrenes and mononitrofluoranthenes in air particulate matter via fused silica gas chromatography combined with negative ion atmospheric pressure ionization mass spectrometry. *J. High Res. Chromatog.* **1987**, *10*, 641-646.
117. Kinouchi, T.; Miranda, A. T. L.; Rushing, L. G.; Beland, F. A.; Korfmacher, W. A. Detection of 2-aminofluorene at femtogram levels via high resolution gas chromatography combined with negative ion atmospheric pressure ionization mass spectrometry. *J. High Res. Chromatog.* **1990**, *13*, 281-284.
118. Korfmacher, W. A.; Rushing, L. G.; Siitonen, P. H.; Branscomb, C. J.; Holder, C. L. Confirmation of heptachlor epoxide and octachlor epoxide in milk via fused silica gas chromatography/negative ion chemical ionization mass spectrometry. *J. High Res. Chromatog.* **1987**, *10*, 332-336.
119. Carrasco-Pancorbo, A.; Nevedomskaya, E.; Arthen-Engeland, T.; Zey, T.; Zurek, G.; Baessmann, C.; Deelder, A. M.; Mayboroda, O. A. Gas chromatography/atmospheric pressure chemical ionization-time of flight

mass spectrometry: analytical validation and applicability to metabolic profiling. *Anal. Chem.* **2009**, *81*, 10071-10079.

120. Bristow, T.; Harrison, M.; Sims, M. The application of gas chromatography/atmospheric pressure chemical ionisation time-of-flight mass spectrometry to impurity identification in pharmaceutical development. *Rapid Commun. Mass Spectrom.* **2010**, *24*, 1673-1681.

121. García-Villalba, R.; Pacchiarotta, T.; Carrasco-Pancorbo, A.; Segura-Carretero, A.; Fernández-Gutiérrez, A.; Deelder, A. M.; Mayboroda, O. A. Gas chromatography-atmospheric pressure chemical ionization-time of flight mass spectrometry for profiling of phenolic compounds in extra virgin olive oil. *J. Chromatogr. A* **2011**, *1218*, 959-971.

122. Hourani, N.; Kuhnert, N. Development of a novel direct-infusion atmospheric pressure chemical ionization mass spectrometry method for the analysis of heavy hydrocarbons in light shredder waste. *Anal. Methods* **2012**, *4*, 730-735.

123. Green, J. M. Peer reviewed: a practical guide to analytical method validation. *Anal. Chem.* **1996**, *68*, 305A-309A.

124. Hertkorn, N.; Frommberger, M.; Witt, M.; Koch, B. P.; Schmitt-Kopplin, P.; Perdue, E. M. Natural organic matter and the event horizon of mass spectrometry. *Anal. Chem.* **2008**, *80*, 8908-8919.

125. Marshall, A. G.; Rodgers, R. P. Petroleomics: the next grand challenge for chemical analysis. *Acc. Chem. Res.* **2003**, *37*, 53-59.

126. Jinno, D.; Gupta, A. K.; Yoshikawa, K. Thermal decomposition characteristics of critical components in solid wastes. *Environ. Eng. Sci.* **2004**, *21*, 65-72.

127. Davidson, A. *The Oxford Companion to Food*, 3rd ed.; Oxford University Press: Oxford, U.K., 2008.

128. Lee, G. C.; Lee, C. Y. Inhibitory effect of caramelisation products on enzymic browning. *Food Chem.* **1997**, *60*, 231-235.

129. Cotton, R. H.; Rebers, P. A.; Maudru, J. E.; Rorabaugh, G. The Role of Sugar in the Food Industry. In *Use of Sugars and Other Carbohydrates in the Food Industry*; American Chemical Society: Washington, DC, 1955; *12*, 3-20.

130. Kroh, L. W. Caramelisation in food and beverages. *Food Chem.* **1994**, *51*, 373-379.

131. Pons, I.; Garrault, C.; Jaubert, J.-N.; Morel, J.; Fenyo, J.-C. Analysis of aromatic caramel. *Food Chem.* **1991**, *39*, 311-320.

132. Fogliano, V.; Morales, F. J. Estimation of dietary intake of melanoidins from coffee and bread. *Food Funct.* **2011**, *2*, 117-123.

133. Golon, A.; González, F. J.; Dávalos, J. Z.; Kuhnert, N. Investigating the thermal decomposition of starch and cellulose in model systems and toasted bread using domino tandem mass spectrometry. *J. Agric. Food. Chem.* **2012**, *61*, 674-684.

134. Lee, J. W.; Thomas, L. C.; Schmidt, S. J. Effects of heating conditions on the glass transition parameters of amorphous sucrose produced by melt-quenching. *J. Agric. Food. Chem.* **2011**, *59*, 3311-3319.

135. Lee, J. W.; Thomas, L. C.; Jerrell, J.; Feng, H.; Cadwallader, K. R.; Schmidt, S. J. Investigation of thermal decomposition as the kinetic process that causes the loss of crystalline structure in sucrose using a chemical analysis approach (Part II). *J. Agric. Food. Chem.* **2010**, *59*, 702-712.

136. Hurkman, W. J.; Wood, D. F. High temperature during grain fill alters the morphology of protein and starch deposits in the starchy endosperm cells of developing wheat (*Triticum aestivum* L.) grain. *J. Agric. Food. Chem.* **2011**, *59*, 4938-4946.

137. Klemm, D.; Heublein, B.; Fink, H.-P.; Bohn, A. Cellulose: fascinating biopolymer and sustainable raw material. *Angew. Chem. Int. Edit.* **2005**, *44*, 3358-3393.
138. Walter, R. H.; Fagerson, I. S. Volatile compounds from- heated glucose. *J. Food Sci.* **1968**, *33*, 294-297.
139. Luning, P. A.; de Rijk, T.; Wichers, H. J.; Roozen, J. P. Gas chromatography, mass spectrometry, and sniffing port analyses of volatile compounds of Fresh Bell Peppers (*Capsicum annuum*) at different ripening stages. *J. Agric. Food. Chem.* **1994**, *42*, 977-983.
140. Blank, I.; Fay, L. B. Formation of 4-Hydroxy-2,5-dimethyl-3(2*H*)-furanone and 4-Hydroxy-2(or 5)-ethyl-5(or 2)-methyl-3(2*H*)-furanone through Maillard reaction based on pentose sugars. *J. Agric. Food. Chem.* **1996**, *44*, 531-536.
141. Homoki-Farkas, P.; Örsi, F.; Kroh, L. W. Methylglyoxal determination from different carbohydrates during heat processing. *Food Chem.* **1997**, *59*, 157-163.
142. Sugisawa, H. The thermal degradation of sugars. II. The volatile decomposition products of glucose caramel. *J. Food Sci.* **1966**, *31*, 381-385.
143. Ruiz-Matute, A. I.; Weiss, M.; Sammataro, D.; Finely, J.; Sanz, M. L. Carbohydrate composition of high-fructose corn syrups (HFCS) used for bee feeding: effect on honey composition. *J. Agric. Food. Chem.* **2010**, *58*, 7317-7322.
144. Murkovic, M.; Pichler, N. Analysis of 5-hydroxymethylfurfural in coffee, dried fruits and urine. *Mol. Nutr. Food Res.* **2006**, *50*, 842-846.
145. Ramírez-Jiménez, A.; García-Villanova, B.; Guerra-Hernández, E. Hydroxymethylfurfural and methylfurfural content of selected bakery products. *Food Res. Int.* **2000**, *33*, 833-838.
146. Arribas-Lorenzo, G.; Morales, F. J. Estimation of dietary intake of 5-hydroxymethylfurfural and related substances from coffee to Spanish population. *Food Chem, Toxicol.* **2010**, *48*, 644-649.
147. Román-Leshkov, Y.; Chheda, J. N.; Dumesic, J. A. Phase modifiers promote efficient production of hydroxymethylfurfural from fructose. *Science* **2006**, *312*, 1933-1937.
148. Smuda, M.; Glomb, M. A. Novel insights into the Maillard catalyzed degradation of maltose. *J. Agric. Food. Chem.* **2011**, *59*, 13254-13264.
149. Smuda, M.; Voigt, M.; Glomb, M. A. Degradation of 1-deoxy-d-erythro-hexo-2,3-diulose in the presence of lysine leads to formation of carboxylic acid amides. *J. Agric. Food. Chem.* **2010**, *58*, 6458-6464.
150. Ratsimba, V.; Fernández, J. M. G.; Defaye, J.; Nigay, H.; Voilley, A. Qualitative and quantitative evaluation of mono- and disaccharides in d-fructose, d-glucose and sucrose caramels by gas-liquid chromatography-mass spectrometry: di-D-fructose dianhydrides as tracers of caramel authenticity. *J. Chromatogr. A* **1999**, *844*, 283-293.
151. Kitaoka, S.; Suzuki, K. Caramels and caramelization Part I. The nature of caramelan. *Agric. Biol. Chem.* **1967**, *31*, 753-755.
152. Tomasik, P.; Pałasiński, M.; Wiejak, S. The thermal decomposition of carbohydrates. Part I. The decomposition of mono-, di-, and oligo-saccharides. In *Advances in Carbohydrate Chemistry and Biochemistry*, 1989; *47*, 203-278.
153. Idri, I.; Havet, J.-L.; Garcia Fernandez, J. M.; Ferroud, C.; Porte, C. Microwave-assisted synthesis of prebiotic di-D-fructose dianhydride-enriched caramels. *Food Chem.* **2012**, *134*, 1527-1532.
154. Defaye, J.; Gadelle, A.; Pedersen, C. The behaviour of d-fructose and inulin towards anhydrous hydrogen fluoride. *Carbohydr. Res.* **1985**, *136*, 53-65.

155. Defaye, J.; García Fernández, J. M. Selective protonic activation of isomeric glycosylfructoses with pyridinium poly(hydrogen fluoride) and synthesis of spirodioxanyl oligosaccharides. *Carbohydr. Res.* **1992**, *237*, 223-247.
156. Defaye, J.; García Fernández, J. M. Synthesis of dispirodioxanyl pseudo-oligosaccharides by selective protonic activation of isomeric glycosylfructoses in anhydrous hydrogen fluoride. *Carbohydr. Res.* **1994**, *251*, 1-15.
157. Defaye, J.; García Fernández, J. M. Protonic reactivity of sucrose in anhydrous hydrogen fluoride. *Carbohydr. Res.* **1994**, *251*, 17-31.
158. Tschiersky, H.; Baltes, W. Untersuchungen an Caramel Curiepunkt-Pyrolyse von Caramelzuckersirupen und andere strukturspezifische Untersuchungen. *Z. Lebensm. Unters. Forsch.* **1989**, *189*, 132-137.
159. Defaye, J.; García Fernández, J. M. Protonic and thermal activation of sucrose and the oligosaccharide composition of caramel. *Carbohydr. Res.* **1994**, *256*, C1-C4.
160. Manley-Harris, M.; Richards, G. N. Di-D-fructose dianhydrides and related oligomers from thermal treatments of inulin and sucrose. *Carbohydr. Res.* **1996**, *287*, 183-202.
161. Christian, T. J.; Manley-Harris, M.; Field, R. J.; Parker, B. A. Kinetics of formation of di-D-fructose dianhydrides during thermal treatment of inulin. *J. Agric. Food. Chem.* **2000**, *48*, 1823-1837.
162. Mellet, C.; Fernández, J. Difuctose dianhydrides (DFAs) and DFA-enriched products as functional foods. In *Carbohydrates in Sustainable Development I*. 2010; 294, 49-77.
163. Suárez-Pereira, E.; Rubio, E. M.; Pilard, S.; Ortiz Mellet, C.; García Fernández, J. M. Di-D-fructose dianhydride-enriched products by acid ion-exchange resin-promoted caramelization of d-fructose: chemical analyses. *J. Agric. Food. Chem.* **2009**, *58*, 1777-1787.
164. Hoffmann, E.; Stroobant, V. Mass Spectrometry: Principles and Applications; John Wiley & Sons: Chichester, U.K., 2007.
165. Han, J.-Y. Structural characteristics of arabinoxylan in barley, malt, and beer. *Food Chem.* **2000**, *70*, 131-138.
166. Ruiz-Matute, A. I.; Hernández-Hernández, O.; Rodríguez-Sánchez, S.; Sanz, M. L.; Martínez-Castro, I. Derivatization of carbohydrates for GC and GC-MS analyses. *J. Chromatogr. B* **2011**, *879*, 1226-1240.
167. Peter-Katalinic, J. Analysis of glycoconjugates by fast atom bombardment mass spectrometry and related MS techniques. *Mass Spectrom. Rev.* **1994**, *13*, 77-98.
168. Mauri, P.; Minoggio, M.; Simonetti, P.; Gardana, C.; Pietta, P. Analysis of saccharides in beer samples by flow injection with electrospray mass spectrometry. *Rapid Commun. Mass Spectrom.* **2002**, *16*, 743-748.
169. Verardo, G.; Duse, I.; Callea, A. Analysis of underivatized oligosaccharides by liquid chromatography/electrospray ionization tandem mass spectrometry with post-column addition of formic acid. *Rapid Commun. Mass Spectrom.* **2009**, *23*, 1607-1618.
170. Mulroney, B.; Traeger, J. C.; Stone, B. A. Determination of both linkage position and anomeric configuration in underivatized glucopyranosyl disaccharides by electrospray mass spectrometry. *J. Mass Spectrom.* **1995**, *30*, 1277-1283.
171. Harvey, D. J.; Naven, T. J. P.; Küster, B.; Bateman, R. H.; Green, M. R.; Critchley, G. Comparison of fragmentation modes for the structural determination of complex oligosaccharides ionized by matrix-assisted laser desorption/ionization mass spectrometry. *Rapid Commun. Mass Spectrom.* **1995**, *9*, 1556-1561.
172. Hao, C.; Ma, X.; Fang, S.; Liu, Z.; Liu, S.; Song, F.; Liu, J. Positive- and negative-ion matrix-assisted laser desorption/ionization mass spectrometry of saccharides. *Rapid Commun. Mass Spectrom.* **1998**, *12*, 345-348.

173. Unterrieser, I.; Cuers, J.; Voiges, K.; Enebro, J.; Mischnick, P. Quantitative aspects in electrospray ionization ion trap and matrix-assisted laser desorption/ionization time-of-flight mass spectrometry of malto-oligosaccharides. *Rapid Commun. Mass Spectrom.* **2011**, *25*, 2201-2208.
174. Xue, J.; Song, L.; Khaja, S. D.; Locke, R. D.; West, C. M.; Laine, R. A.; Matta, K. L. Determination of linkage position and anomeric configuration in Hex-Fuc disaccharides using electrospray ionization tandem mass spectrometry. *Rapid Commun. Mass Spectrom.* **2004**, *18*, 1947-1955.
175. Zhu, X.; Sato, T. The distinction of underivatized monosaccharides using electrospray ionization ion trap mass spectrometry. *Rapid Commun. Mass Spectrom.* **2007**, *21*, 191-198.
176. Domon, B.; Costello, C. E. A systematic nomenclature for carbohydrate fragmentations in FAB-MS/MS spectra of glycoconjugates. *Glycoconjugate J.* **1988**, *5*, 397-409.
177. Cancilla, M. T.; Penn, S. G.; Lebrilla, C. B. Alkaline degradation of oligosaccharides coupled with matrix-assisted laser desorption/ionization Fourier transform mass spectrometry: a method for sequencing oligosaccharides. *Anal. Chem.* **1998**, *70*, 663-672.
178. Socaciu, C. Food Colorants: Chemical and Functional Properties; Taylor & Francis group: Boca Raton, FL, 2008.
179. Wissgott, U.; Bortlik, K. Prospects for new natural food colorants. *Trends Food Sci. Tech.* **1996**, *7*, 298-302.
180. Chappel, C. I.; Howell, J. C. Caramel colours- a historical introduction. *Food Chem. Toxicol.* **1992**, *30*, 351-357.
181. Myers, D. V.; Howell, J. C. Characterization and specifications of caramel colours: an overview. *Food Chem, Toxicol.* **1992**, *30*, 359-363.
182. Houben, G. F.; Penninks, A. H. Immunotoxicity of the colour additive Caramel Colour III. A review on complicated issues in the safety evaluation of a food additive. *Toxicology* **1994**, *91*, 289-302.
183. Gougeon, R. D.; Lucio, M.; Frommberger, M.; Peyron, D.; Chassagne, D.; Alexandre, H.; Feuillat, F.; Voilley, A.; Cayot, P.; Gebefügi, I.; Hertkorn, N.; Schmitt-Kopplin, P. The chemodiversity of wines can reveal a metabo-geography expression of cooperage oak wood. *Proc. Natl. Acad. Sci. USA* **2009**, *106*, 9174-9179.
184. Kuhnert, N.; Drynan, J. W.; Obuchowicz, J.; Clifford, M. N.; Witt, M. Mass spectrometric characterization of black tea thearubigins leading to an oxidative cascade hypothesis for thearubigin formation. *Rapid Commun. Mass Spectrom.* **2010**, *24*, 3387-3404.
185. Moreira, A. S. P.; Coimbra, M. A.; Nunes, F. M.; Simões, J.; Domingues, M. R. M. Evaluation of the effect of roasting on the structure of coffee galactomannans using model oligosaccharides. *J. Agric. Food. Chem.* **2011**, *59*, 10078-10087.
186. Novotny, M. V.; Mechref, Y. New hyphenated methodologies in high-sensitivity glycoprotein analysis. *J. Sep. Sci.* **2005**, *28*, 1956-1968.
187. Tang, H.; Mechref, Y.; Novotny, M. V. Automated interpretation of MS/MS spectra of oligosaccharides. *Bioinformatics* **2005**, *21*, i431-i439.
188. Jaiswal, R.; Sovdat, T.; Vivan, F.; Kuhnert, N. Profiling and characterization by LC-MSⁿ of the chlorogenic acids and hydroxycinnamoylshikimate esters in maté (*Ilex paraguariensis*). *J. Agric. Food. Chem.* **2010**, *58*, 5471-5484.
189. Limacher, A.; Kerler, J.; Davidek, T.; Schmalzried, F.; Blank, I. Formation of furan and methylfuran by Maillard-type reactions in model systems and food. *J. Agric. Food. Chem.* **2008**, *56*, 3639-3647.

190. Freimund, S.; Huwig, A.; Giffhorn, F.; Köpper, S. Rare keto-aldoses from enzymatic oxidation: substrates and oxidation products of pyranose 2-oxidase. *Chem. Eur. J.* **1998**, *4*, 2442-2455.
191. Milijkovic, M. Carbohydrates: Synthesis, Mechanisms and Stereoelectronic Effects; Springer: London, U.K., 2010.
192. Jiang, B.; Liu, Y.; Bhandari, B.; Zhou, W. Impact of caramelization on the glass transition temperature of several caramelized sugars. Part I: chemical analyses. *J. Agric. Food. Chem.* **2008**, *56*, 5138-5147.
193. Hernández-Hernández, O.; Calvillo, I.; Lebrón-Aguilar, R.; Moreno, F. J.; Sanz, M. L. Hydrophilic interaction liquid chromatography coupled to mass spectrometry for the characterization of prebiotic galactooligosaccharides. *J. Chromatogr. A* **2012**, *1220*, 57-67.
194. Sun, X.; Li, Y. Colloidal carbon spheres and their core/shell structures with noble-metal nanoparticles. *Angew. Chem. Int. Edit.* **2004**, *43*, 597-601.
195. Titirici, M.-M.; Antonietti, M.; Baccile, N. Hydrothermal carbon from biomass: a comparison of the local structure from poly- to monosaccharides and pentoses/hexoses. *Green Chem.* **2008**, *10*, 1204-1212.
196. Jaiswal, R.; Dickman, M. H.; Kuhnert, N. First diastereoselective synthesis of methyl caffeoyl- and feruloyl-muco-quinates. *Org. Biomol. Chem.* **2012**, *10*, 5266-5277.
197. March, R. E.; Stadey, C. J. A tandem mass spectrometric study of saccharides at high mass resolution. *Rapid Commun. Mass Spectrom.* **2005**, *19*, 805-812.
198. Seipert, R. R.; Barboza, M.; Ninonuevo, M. R.; LoCascio, R. G.; Mills, D. A.; Freeman, S. L.; German, J. B.; Lebrilla, C. B. Analysis and quantitation of fructooligosaccharides using matrix-assisted laser desorption/ionization Fourier transform ion cyclotron resonance mass spectrometry. *Anal. Chem.* **2007**, *80*, 159-165.
199. Visnapuu, T.; Zamfir, A. D.; Mosoarca, C.; Stanescu, M. D.; Alamäe, T. Fully automated chip-based negative mode nano-electrospray mass spectrometry of fructooligosaccharides produced by heterologously expressed levansucrase from *Pseudomonas syringae* pv. tomato DC3000. *Rapid Commun. Mass Spectrom.* **2009**, *23*, 1337-1346.
200. Manley-Harris, M.; Richards, G. N. Formation of trisaccharides (kestoses) by pyrolysis of sucrose. *Carbohydr. Res.* **1991**, *219*, 101-113.
201. Clowers, B. H.; Dodds, E. D.; Seipert, R. R.; Lebrilla, C. B. Dual polarity accurate mass calibration for electrospray ionization and matrix-assisted laser desorption/ionization mass spectrometry using maltooligosaccharides. *Anal. Biochem.* **2008**, *381*, 205-213.
202. Eames, J.; Kuhnert, N.; Sansbury, F. H.; Warren, S. Kinetic and thermodynamic control in the synthesis of tetrahydro-pyrans and -furans from 1,4-diols by stereospecific phenylsulfanyl (PhS) migration: competition between exo and endo transition states and between [1,2] and [1,4]sulfanyl participation. *Synlett* **1999**, 1211-1214.
203. Cuyckens, F.; Shahat, A. A.; Pieters, L.; Claeys, M. Direct stereochemical assignment of hexose and pentose residues in flavonoid O-glycosides by fast atom bombardment and electrospray ionization mass spectrometry. *J. Mass Spectrom.* **2002**, *37*, 1272-1279.
204. Hernández-Hernández, O.; Ruiz-Aceituno, L.; Sanz, M. a. L.; Martínez-Castro, I. Determination of free inositols and other low molecular weight carbohydrates in vegetables. *J. Agric. Food. Chem.* **2011**, *59*, 2451-2455.
205. Simões, J.; Domingues, P.; Reis, A.; Nunes, F. M.; Coimbra, M. A.; Domingues, M. R. M. Identification of anomeric configuration of underivatized reducing glucopyranosyl-glucose disaccharides by tandem mass spectrometry and multivariate analysis. *Anal. Chem.* **2007**, *79*, 5896-5905.

206. Deguchi, S.; Tsujii, K.; Horikoshi, K. Cooking cellulose in hot and compressed water. *Chem. Commun.* **2006**, 3293-3295.
207. Siljeström, M.; Björck, I.; Westerlund, E. Transglycosidation reactions following heat treatment of starch-effects on enzymic digestibility. *Starch - Stärke* **1989**, *41*, 95-100.
208. Pizzoferrato, L.; Paci, M.; Rotilio, G. Structural modification and bioavailability of starch components as related to the extent of Maillard reaction: an enzymatic degradation and a solid-state ^{13}C CPMAS NMR study. *J. Agric. Food. Chem.* **1998**, *46*, 438-441.
209. Abdel-Aal, E.-S. M.; Rabalski, I. Effect of baking on nutritional properties of starch in organic spelt whole grain products. *Food Chem.* **2008**, *111*, 150-156.
210. Zhang, X.; Golding, J.; Burgar, I. Thermal decomposition chemistry of starch studied by ^{13}C high-resolution solid-state NMR spectroscopy. *Polymer* **2002**, *43*, 5791-5796.
211. Hakkarainen, M.; Albertsson, A.-C.; Karlsson, S. Solid-phase extraction and subsequent gas chromatography-mass spectrometry analysis for identification of complex mixtures of degradation products in starch-based polymers. *J. Chromatogr. A* **1996**, *741*, 251-263.
212. Ashline, D.; Singh, S.; Hanneman, A.; Reinhold, V. Congruent strategies for carbohydrate sequencing: mining structural details by MS^n . *Anal. Chem.* **2005**, *77*, 6250-6262.
213. Lunsford, K. A.; Peter, G. F.; Yost, R. A. Direct matrix-assisted laser desorption/ionization mass spectrometric imaging of cellulose and hemicellulose in Populus tissue. *Anal. Chem.* **2011**, *83*, 6722-6730.
214. Carpenter, T. M. Composition of some common foods with respect to the carbohydrate content. *J. Nutr.* **1940**, *19*, 415-422.
215. Kvasnička, F. Determination of 4-methylimidazole in caramel color by capillary isotachopheresis. *Electrophoresis* **1989**, *10*, 801-802.
216. Friedman, M. Chemistry, biochemistry, and safety of acrylamide. *J. Agric. Food. Chem.* **2003**, *51*, 4504-4526.
217. Bekedam, E. K.; Loots, M. J.; Schols, H. A.; Van Boekel, M. A. J. S.; Smit, G. Roasting effects on formation mechanisms of coffee brew melanoidins. *J. Agric. Food. Chem.* **2008**, *56*, 7138-7145.
218. Alves, R. C.; Casal, S.; Alves, M. R.; Oliveira, M. B. Discrimination between arabica and robusta coffee species on the basis of their tocopherol profiles. *Food Chem.* **2009**, *114*, 295-299.
219. Nunes, F. M.; Coimbra, M. A. Chemical characterization of the high molecular weight material extracted with hot water from green and roasted arabica coffee. *J. Agric. Food. Chem.* **2001**, *49*, 1773-1782.
220. Nunes, F. M.; Coimbra, M. A. Melanoidins from coffee infusions, fractionation, chemical characterization, and effect of the degree of roast. *J. Agric. Food. Chem.* **2007**, *55*, 3967-3977.
221. Díaz-Rubio, M. E.; Saura-Calixto, F. Dietary fiber in brewed coffee. *J. Agric. Food. Chem.* **2007**, *55*, 1999-2003.

APPENDIX

Table A1. Repeatability of a retention time for the light shredder waste fraction (intraday)

Compound	Rt 1[min]	Rt 2[min]	Rt [min]	Rt[min]	Rt 5[min]	Mean	SD ^a	RSD[%] ^b
C ₂₀ H ₄₂	12.96	12.97	12.97	12.97	12.97	12.9658	0.001166	0.00899
C ₂₁ H ₄₄	13.61	13.61	13.61	13.61	13.61	13.6076	0.000800	0.00588
C ₂₂ H ₄₆	14.22	14.22	14.22	14.22	14.22	14.2196	0.001020	0.00717
C ₂₃ H ₄₈	14.81	14.81	14.81	14.81	14.81	14.8068	0.000748	0.00505
C ₂₄ H ₅₀	15.37	15.37	15.37	15.37	15.37	15.3710	0.001095	0.00713
C ₂₅ H ₅₂	15.91	15.91	15.91	15.92	15.91	15.9140	0.000632	0.00397
C ₂₆ H ₅₄	16.44	16.44	16.44	16.44	16.44	16.4372	0.000748	0.00455
C ₂₇ H ₅₆	16.94	16.94	16.94	16.94	16.94	16.9418	0.000400	0.00236
C ₂₈ H ₅₈	17.45	17.45	17.45	17.45	17.46	17.4538	0.000748	0.00429
C ₂₉ H ₆₀	18.02	18.02	18.02	18.02	18.02	18.0220	0.001265	0.00702
C ₃₀ H ₆₂	18.67	18.67	18.67	18.67	18.67	18.6682	0.000748	0.00401
C ₃₁ H ₆₄	19.41	19.41	19.41	19.42	19.42	19.4148	0.001470	0.00757
C ₃₂ H ₆₆	20.29	20.29	20.29	20.29	20.29	20.2916	0.001356	0.00669
C ₃₃ H ₆₈	21.33	21.34	21.34	21.34	21.34	21.3362	0.003816	0.01788
C ₃₄ H ₇₀	22.59	22.58	22.59	22.59	22.59	22.5878	0.004792	0.02121
C ₃₅ H ₇₂	24.09	24.09	24.08	24.09	24.10	24.0886	0.007255	0.03012
C ₃₆ H ₇₄	25.90	25.90	25.91	25.90	25.91	25.9024	0.004271	0.01649
C ₃₇ H ₇₆	28.11	28.11	28.11	28.09	28.12	28.1066	0.010171	0.03619
C ₃₈ H ₇₈	30.78	30.78	30.79	30.78	30.78	30.7816	0.004317	0.01403
C ₃₉ H ₈₀	34.03	34.01	34.03	34.06	34.02	34.0286	0.015628	0.04593
C ₄₀ H ₈₂	37.99	37.98	37.99	37.99	38.00	37.9910	0.006663	0.01754

^a Standard deviation; ^b Relative standard deviation

Table A2. Repeatability of a peak area for the light shredder waste fraction (intraday)

Compound	P. area 1	P. area 2	P. area 3	P. area 4	P. area 5	Mean	SD ^a	RSD[%] ^b
C ₂₀ H ₄₂	114998.2	110423.7	120212.0	109298.3	102603.4	111507.1	5887.130	5.3
C ₂₁ H ₄₄	120397.8	129131.6	114440.5	107900.1	108576.9	116089.4	7935.773	6.8
C ₂₂ H ₄₆	87666.4	122798.3	122454.2	109836.0	107175.0	109986.0	12850.680	11.7
C ₂₃ H ₄₈	134293.3	135572.8	132808.3	136247.0	127102.0	133204.7	3269.514	2.5
C ₂₄ H ₅₀	164901.5	182722.0	199137.3	163984.5	171916.6	176532.4	13140.210	7.4
C ₂₅ H ₅₂	131472.1	156396.4	168354.1	147690.2	157691.6	152320.9	12317.740	8.1
C ₂₆ H ₅₄	274324.3	267218.8	265266.2	184329.4	236085.9	245444.9	33237.630	13.6
C ₂₇ H ₅₆	257219.9	250582.6	381709.7	329257.8	341059.0	311965.8	50546.320	16.2
C ₂₈ H ₅₈	186817.3	185830.7	212441.1	188674.4	193246.0	193401.9	9854.387	5.1
C ₂₉ H ₆₀	176805.6	187587.0	134266.0	158311.3	168534.2	165100.8	18173.070	11.0
C ₃₀ H ₆₂	203100.7	193954.4	205420.9	177626.2	200055.4	196031.5	9973.922	5.1
C ₃₁ H ₆₄	121514.0	126289.0	102386.8	117492.7	115343.8	116605.3	8030.118	6.9
C ₃₂ H ₆₆	133329.4	144691.3	124914.3	136556.7	111994.2	130297.2	11131.410	8.5
C ₃₃ H ₆₈	83498.9	86791.4	84838.0	119267.3	79197.0	90718.52	14490.710	16.0
C ₃₄ H ₇₀	144540.7	145483.4	153532.6	124829.6	128473.6	139372.0	10907.280	7.8
C ₃₅ H ₇₂	128229.4	128377.1	114871.4	115780.4	126777.0	122807.1	6140.622	5.0
C ₃₆ H ₇₄	89548.4	93973.6	83176.3	66723.0	104755.2	87635.3	12602.630	14.4
C ₃₇ H ₇₆	77720.4	78221.8	68232.6	78470.8	88518.3	78232.8	6420.511	8.2
C ₃₈ H ₇₈	69643.0	80020.8	68232.6	57515.8	72214.1	69525.3	7256.696	10.4
C ₃₉ H ₈₀	69297.9	58511.1	56483.9	49239.0	85980.6	63902.5	12772.420	20.0
C ₄₀ H ₈₂	68527.2	53106.6	58075.9	40593.7	71510.0	58362.7	11132.070	19.1
Total	2837846.0	2917684.0	2971255.0	2719624.0	2898810.0			

^a Standard deviation; ^b Relative standard deviation**Table A3** High-resolution mass (GC-APCI-TOF-MS) data for PAHs (polyaromatic hydrocarbons) in the light shredder waste fraction in the positive ion mode

Peak Numbering	Assignment	Molecular Formula	Experimental m/z [M-H] ⁺	Theoretical m/z [M-H] ⁺	Error [ppm]
1	Naphthalene	C ₁₀ H ₁₀	129.0700	129.0699	-0.9
2	Acenaphthylene	C ₁₂ H ₁₀	153.0701	153.0699	-1.6
3	Acenaphthene	C ₁₂ H ₁₂	155.0855	155.0855	-0.3
4	Fluorene	C ₁₃ H ₁₂	167.0856	167.0855	-0.7
5	Phenanthrene	C ₁₄ H ₁₂	179.0858	179.0855	-1.6
6	Anthracene	C ₁₄ H ₁₂	179.0858	179.0855	-1.6
7	Fluoroanthene	C ₁₆ H ₁₂	203.0857	203.0855	-0.6
8	Pyrene	C ₁₆ H ₁₂	203.0855	203.0855	0.3
9	benzo[a]anthracene	C ₁₈ H ₁₄	229.1010	229.1012	0.9
10	chrysene	C ₁₈ H ₁₄	229.1010	229.1012	0.9
11	benzo[b]fluoroanthene	C ₂₀ H ₁₄	253.1037	253.1012	-10.1
12	benzo[k]fluoroanthene	C ₂₀ H ₁₄	253.1006	253.1012	2.5
13	benzo[a]pyrene	C ₂₀ H ₁₄	253.1033	253.1012	-8.6

Table A4 High-resolution mass (MS-TOF) data for caramelized: a) fructose, b) galactose and c) mannose in the negative ion mode

a)

Peak Numbering	Assignment	Molecular Formula	Experimental m/z [M-H] ⁻	Theoretical m/z [M-H] ⁻	Relative Error [ppm]
1		C ₉ H ₁₈ O ₂	157.1236	157.1234	1.5
2	Fru - H ₂ O	C ₆ H ₁₀ O ₅	161.0457	161.0455	0.7
3	Fru	C ₆ H ₁₂ O ₆	179.0561	179.0561	0.0
4		C ₇ H ₁₄ O ₈	225.0608	225.0616	3.7
5		C ₁₄ H ₂₈ O ₂	227.2018	227.2017	0.7
6		C ₁₅ H ₃₀ O ₂	241.2181	241.2173	3.3
7		C ₁₆ H ₃₂ O ₂	255.2341	255.2330	4.6
8		C ₁₈ H ₃₆ O ₂	283.2653	283.2643	3.8
9		C ₁₂ H ₁₆ O ₈	287.0765	287.0772	2.8
10		C ₁₇ H ₂₆ O ₄	293.1760	293.1758	0.7
11	(Fru) ₂ - 2×H ₂ O	C ₁₂ H ₁₈ O ₉	305.0891	305.0878	4.3
12	(Fru) ₂ - H ₂ O	C ₁₂ H ₂₀ O ₁₀	323.0977	323.0984	2.0
13	(Fru) ₂	C ₁₂ H ₂₂ O ₁₁	341.1083	341.1089	1.9
14	(Fru) ₂ + H ₂ O	C ₁₂ H ₂₄ O ₁₂	359.1189	359.1195	1.7
15		C ₁₃ H ₂₄ O ₁₃	387.1150	387.1144	1.5
16		C ₂₂ H ₄₄ O ₈	435.2970	435.2963	1.5
17	(Fru) ₃ - 3×H ₂ O	C ₁₈ H ₂₆ O ₁₃	449.1305	449.1301	0.9
18	(Fru) ₃ - 2×H ₂ O	C ₁₈ H ₂₈ O ₁₄	467.1408	467.1406	0.4
19	(Fru) ₃ - H ₂ O	C ₁₈ H ₃₀ O ₁₅	485.1518	485.1512	1.3
20	(Fru) ₃	C ₁₈ H ₃₂ O ₁₆	503.1628	503.1618	2.0
21	(Fru) ₃ + H ₂ O	C ₁₈ H ₃₄ O ₁₇	521.1710	521.1723	2.5
22	(Fru) ₄ - 3×H ₂ O	C ₂₄ H ₃₆ O ₁₈	611.1846	611.1829	2.9
23	(Fru) ₄ - 2×H ₂ O	C ₂₄ H ₃₈ O ₁₉	629.1920	629.1935	1.4
24	(Fru) ₄ - H ₂ O	C ₂₄ H ₄₀ O ₂₀	647.2027	647.2040	2.0
25	(Fru) ₄	C ₂₄ H ₄₂ O ₂₁	665.2134	665.2146	1.8
26	(Fru) ₄ + H ₂ O	C ₂₄ H ₄₄ O ₂₂	683.2268	683.2251	2.4
27	(Fru) ₅ - 3×H ₂ O	C ₃₀ H ₄₆ O ₂₃	773.2334	773.2357	2.9
28	(Fru) ₅ - 2×H ₂ O	C ₃₀ H ₄₈ O ₂₄	791.2431	791.2463	4.0
29	(Fru) ₅ - H ₂ O	C ₃₀ H ₅₀ O ₂₅	809.2545	809.2568	2.9
30	(Fru) ₅	C ₃₀ H ₅₂ O ₂₆	827.2701	827.2674	3.2
31	(Fru) ₅ + H ₂ O	C ₃₀ H ₅₄ O ₂₇	845.2815	845.2780	4.2
32	(Fru) ₆ - H ₂ O	C ₃₆ H ₆₀ O ₃₀	971.3119	971.3097	2.3
33	(Fru) ₆	C ₃₆ H ₆₂ O ₃₁	989.3173	989.3202	2.9

b)

Peak Numbering	Assignment	Molecular Formula	Experimental m/z [M-H] ⁻	Theoretical m/z [M-H] ⁻	Relative Error [ppm]
1		C ₆ H ₁₂ O ₂	115.0767	115.0765	2.1
2		C ₇ H ₆ O ₂	121.0294	121.0295	0.7
3		C ₄ H ₈ O ₄	119.0349	119.0350	0.7
4		C ₇ H ₁₄ O ₂	129.0925	129.0921	3.0
5		C ₈ H ₁₆ O ₂	143.1084	143.1078	4.9
6		C ₉ H ₁₈ O ₂	157.1236	157.1234	1.0
7	Gal - H ₂ O	C ₆ H ₁₀ O ₅	161.0461	161.0455	3.7
8	Galactose	C ₆ H ₁₂ O ₆	179.0564	179.0561	1.4
9		C ₇ H ₁₄ O ₈	225.0608	225.0616	3.6
10		C ₁₆ H ₃₂ O ₂	255.2324	255.2330	2.0
11		C ₁₅ H ₂₂ O ₄	265.1452	265.1445	2.5
12		C ₉ H ₁₈ O ₉	269.0869	269.0878	3.5
13		C ₁₈ H ₃₆ O ₂	283.2629	283.2643	4.6
14	(Gal) ₂ - 3×H ₂ O	C ₁₂ H ₁₆ O ₈	287.0769	287.0772	1.2
15		C ₁₇ H ₂₆ O ₄	293.1758	293.1758	0.1
16	(Gal) ₂ - 2×H ₂ O	C ₁₂ H ₁₈ O ₉	305.0863	305.0878	4.9
17	(Gal) ₂ - H ₂ O	C ₁₂ H ₂₀ O ₁₀	323.0985	323.0984	0.3
18	(Gal) ₂	C ₁₂ H ₂₂ O ₁₁	341.1094	341.1089	1.3
19	(Gal) ₂ + H ₂ O	C ₁₂ H ₂₄ O ₁₂	359.1183	359.1195	3.2
20	(Gal) ₃ - 4×H ₂ O	C ₁₈ H ₂₄ O ₁₂	431.1211	431.1195	3.8
21	(Gal) ₃ - 3×H ₂ O	C ₁₈ H ₂₆ O ₁₃	449.1281	449.1301	4.4
22	(Gal) ₃ - 2×H ₂ O	C ₁₈ H ₂₈ O ₁₄	467.1401	467.1406	1.2
23	(Gal) ₃ - H ₂ O	C ₁₈ H ₃₀ O ₁₅	485.1500	485.1512	2.4
24	(Gal) ₃	C ₁₈ H ₃₂ O ₁₆	503.1606	503.1618	2.3
25	(Gal) ₃ + H ₂ O	C ₁₈ H ₃₄ O ₁₇	521.1729	521.1723	1.1
26	(Gal) ₄ - 3×H ₂ O	C ₂₄ H ₃₆ O ₁₈	611.1805	611.1829	3.9
27	(Gal) ₄ - 2×H ₂ O	C ₂₄ H ₃₈ O ₁₉	629.1907	629.1935	4.4
28	(Gal) ₄ - H ₂ O	C ₂₄ H ₄₀ O ₂₀	647.2021	647.2040	3.0
29	(Gal) ₄	C ₂₄ H ₄₂ O ₂₁	665.2135	665.2146	1.6
30	(Gal) ₄ + H ₂ O	C ₂₄ H ₄₄ O ₂₂	683.2222	683.2251	4.3
31	(Gal) ₅ - 5×H ₂ O	C ₃₀ H ₄₂ O ₂₁	737.2156	737.2146	1.4
32	(Gal) ₅ - 4×H ₂ O	C ₃₀ H ₄₄ O ₂₂	755.2227	755.2251	3.2
33	(Gal) ₅ - 3×H ₂ O	C ₃₀ H ₄₆ O ₂₃	773.2324	773.2357	4.2
34	(Gal) ₅ - 2×H ₂ O	C ₃₀ H ₄₈ O ₂₄	791.2425	791.2463	4.7
35	(Gal) ₅ - H ₂ O	C ₃₀ H ₅₀ O ₂₅	809.2538	809.2568	3.4
36	(Gal) ₅	C ₃₀ H ₅₂ O ₂₆	827.2671	827.2674	0.3
37	(Gal) ₅ + H ₂ O	C ₃₀ H ₅₄ O ₂₇	845.2752	845.2780	3.0
38	(Gal) ₆ - 3×H ₂ O	C ₃₆ H ₅₆ O ₂₈	935.2877	935.2885	0.9
39	(Gal) ₆ - 2×H ₂ O	C ₃₆ H ₅₈ O ₂₉	953.3013	953.2991	2.3
40	(Gal) ₆ - H ₂ O	C ₃₆ H ₆₀ O ₃₀	971.3096	971.3097	0.0
41	(Gal) ₆	C ₃₆ H ₆₂ O ₃₁	989.3187	989.3202	1.5
42	(Gal) ₆ + H ₂ O	C ₃₆ H ₆₄ O ₃₂	1007.3352	1007.3308	4.3

c)

Peak Numbering	Assignment	Molecular Formula	Experimental m/z [M-H] ⁻	Theoretical m/z [M-H] ⁻	Relative Error [ppm]
1		C ₃ H ₆ O ₃	89.0241	89.0244	3.9
2		C ₆ H ₁₂ O ₂	115.0764	115.0765	0.1
3		C ₇ H ₆ O ₂	121.0298	121.0295	2.3
4		C ₄ H ₈ O ₄	119.0344	119.0350	5.0
5		C ₇ H ₁₄ O ₂	129.0917	129.0921	2.8
6		C ₈ H ₁₆ O ₂	143.1079	143.1078	0.7
7		C ₉ H ₁₈ O ₂	157.1228	157.1234	3.6
8	Man - H ₂ O	C ₆ H ₁₀ O ₅	161.0463	161.0455	4.7
9	Mannose	C ₆ H ₁₂ O ₆	179.0565	179.0561	1.9
10		C ₇ H ₁₄ O ₈	225.0610	225.0616	2.5
11		C ₁₆ H ₃₂ O ₂	255.2320	255.2330	3.6
12		C ₁₅ H ₂₂ O ₄	265.1448	265.1445	0.9
13		C ₉ H ₁₈ O ₉	269.0879	269.0878	0.4
14		C ₁₈ H ₃₆ O ₂	283.2634	283.2643	3.1
15	(Man) ₂ - 3×H ₂ O	C ₁₂ H ₁₆ O ₈	287.0759	287.0772	4.8
16		C ₁₇ H ₂₆ O ₄	293.1764	293.1758	1.9
17	(Man) ₂ - 2×H ₂ O	C ₁₂ H ₁₈ O ₉	305.0873	305.0878	1.7
18	(Man) ₂ - H ₂ O	C ₁₂ H ₂₀ O ₁₀	323.0971	323.0984	3.9
19	(Man) ₂	C ₁₂ H ₂₂ O ₁₁	341.1094	341.1089	1.5
20	(Man) ₂ + H ₂ O	C ₁₂ H ₂₄ O ₁₂	359.1180	359.1195	4.1
21	(Man) ₃ - 4×H ₂ O	C ₁₈ H ₂₄ O ₁₂	431.1217	431.1195	5.0
22	(Man) ₃ - 3×H ₂ O	C ₁₈ H ₂₆ O ₁₃	449.1286	449.1301	3.2
23	(Man) ₃ - 2×H ₂ O	C ₁₈ H ₂₈ O ₁₄	467.1411	467.1406	0.9
24	(Man) ₃ - H ₂ O	C ₁₈ H ₃₀ O ₁₅	485.1494	485.1512	3.6
25	(Man) ₃	C ₁₈ H ₃₂ O ₁₆	503.1617	503.1618	0.0
26	(Man) ₃ + H ₂ O	C ₁₈ H ₃₄ O ₁₇	521.1699	521.1723	4.7
27	(Man) ₄ - 3×H ₂ O	C ₂₄ H ₃₆ O ₁₈	611.1818	611.1829	1.7
28	(Man) ₄ - 2×H ₂ O	C ₂₄ H ₃₈ O ₁₉	629.1909	629.1935	4.0
29	(Man) ₄ - H ₂ O	C ₂₄ H ₄₀ O ₂₀	647.2033	647.2040	1.1
30	(Man) ₄	C ₂₄ H ₄₂ O ₂₁	665.2172	665.2146	4.0
31	(Man) ₄ + H ₂ O	C ₂₄ H ₄₄ O ₂₂	683.2238	683.2251	2.0
32	(Man) ₅ - 5×H ₂ O	C ₃₀ H ₄₂ O ₂₁	737.2122	737.2146	3.2
33	(Man) ₅ - 4×H ₂ O	C ₃₀ H ₄₄ O ₂₂	755.2225	755.2251	3.5
34	(Man) ₅ - 3×H ₂ O	C ₃₀ H ₄₆ O ₂₃	773.2340	773.2357	2.1
35	(Man) ₅ - 2×H ₂ O	C ₃₀ H ₄₈ O ₂₄	791.2436	791.2463	3.4
36	(Man) ₅ - H ₂ O	C ₃₀ H ₅₀ O ₂₅	809.2580	809.2568	1.5
37	(Man) ₅	C ₃₀ H ₅₂ O ₂₆	827.2653	827.2674	2.5
38	(Man) ₅ + H ₂ O	C ₃₀ H ₅₄ O ₂₇	845.2753	845.2780	3.1
39	(Man) ₆ - 3×H ₂ O	C ₃₆ H ₅₆ O ₂₈	935.2862	935.2885	2.5
40	(Man) ₆ - 2×H ₂ O	C ₃₆ H ₅₈ O ₂₉	953.2975	953.2991	1.7
41	(Man) ₆ - H ₂ O	C ₃₆ H ₆₀ O ₃₀	971.3061	971.3097	3.6
42	(Man) ₆	C ₃₆ H ₆₂ O ₃₁	989.3177	989.3202	2.5
43	(Man) ₆ + H ₂ O	C ₃₆ H ₆₄ O ₃₂	1007.3277	1007.3308	3.0

Table A5 High-resolution mass (MS-TOF) data for caramelized: a) maltose, b) lactose in the negative ion mode

a)

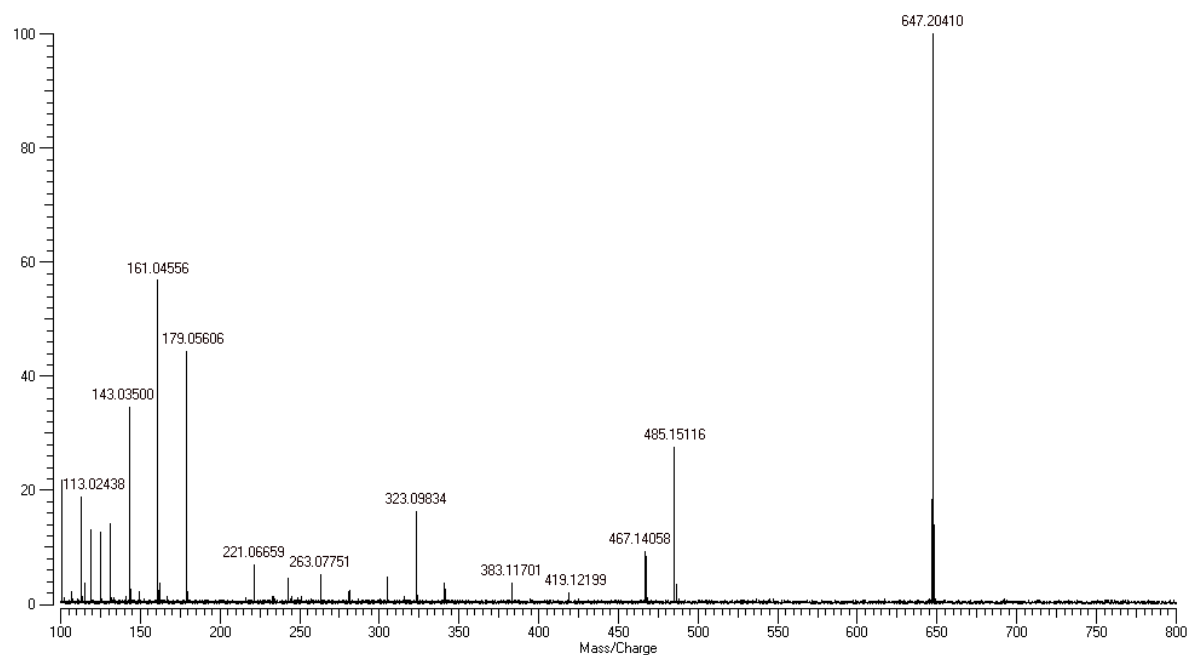
Peak Numbering	Assignment	Molecular Formula	Experimental m/z [M-H] ⁻	Theoretical m/z [M-H] ⁻	Relative Error [ppm]
1		C ₄ H ₈ O ₄	119.0350	119.0350	0.3
2	Glu - H ₂ O	C ₆ H ₁₀ O ₅	161.0462	161.0455	3.9
3	Glu	C ₆ H ₁₂ O ₆	179.0567	179.0561	3.4
4		C ₁₄ H ₂₈ O ₂	227.2011	227.2017	2.5
5		C ₁₆ H ₃₂ O ₂	255.2319	255.2330	4.3
6		C ₁₅ H ₂₂ O ₄	265.1440	265.1445	2.0
7		C ₁₈ H ₃₆ O ₂	283.2634	283.2643	3.1
8		C ₁₂ H ₁₆ O ₈	287.0796	287.0772	8.1
9		C ₁₇ H ₂₆ O ₄	293.1763	293.1758	1.6
10	Glu-Glu - 2×H ₂ O	C ₁₂ H ₁₈ O ₉	305.0874	305.0878	1.2
11	Glu-Glu - H ₂ O	C ₁₂ H ₂₀ O ₁₀	323.0992	323.0984	2.5
12	Glu-Glu	C ₁₂ H ₂₂ O ₁₁	341.1105	341.1089	4.7
13	Glu-Glu + H ₂ O	C ₁₂ H ₂₄ O ₁₂	359.1159	359.1195	10.0
14	3×M - 3×H ₂ O	C ₁₈ H ₂₆ O ₁₃	449.1290	449.1301	2.4
15	3×M - 2×H ₂ O	C ₁₈ H ₂₈ O ₁₄	467.1401	467.1406	1.2
16	3×M - H ₂ O	C ₁₈ H ₃₀ O ₁₅	485.1504	485.1512	1.7
17	3×M	C ₁₈ H ₃₂ O ₁₆	503.1625	503.1618	1.4
18	3×M + H ₂ O	C ₁₈ H ₃₄ O ₁₇	521.1721	521.1723	0.4
19	4×M - 5×H ₂ O	C ₂₄ H ₃₂ O ₁₆	575.1619	575.1618	0.2
20	4×M - 3×H ₂ O	C ₂₄ H ₃₆ O ₁₈	611.1827	611.1829	0.3
21	4×M - 2×H ₂ O	C ₂₄ H ₃₈ O ₁₉	629.1919	629.1935	2.5
22	4×M - H ₂ O	C ₂₄ H ₄₀ O ₂₀	647.2038	647.2040	0.8
23	4×M	C ₂₄ H ₄₂ O ₂₁	665.2169	665.2146	3.5
24	4×M + H ₂ O	C ₂₄ H ₄₄ O ₂₂	683.2274	683.2251	3.4
25	5×M - 4×H ₂ O	C ₃₀ H ₄₄ O ₂₂	755.2253	755.2251	0.2
26	5×M - 3×H ₂ O	C ₃₀ H ₄₆ O ₂₃	773.2370	773.2357	1.7
27	5×M - 2×H ₂ O	C ₃₀ H ₄₈ O ₂₄	791.2451	791.2463	1.4
28	5×M - H ₂ O	C ₃₀ H ₅₀ O ₂₅	809.2603	809.2568	4.3
29	5×M	C ₃₀ H ₅₂ O ₂₆	827.2664	827.2674	1.2
30	5×M + H ₂ O	C ₃₀ H ₅₄ O ₂₇	845.2774	845.2780	0.6
31	6×M - 3×H ₂ O	C ₃₆ H ₅₆ O ₂₈	935.2894	935.2885	0.9
32	6×M - 2×H ₂ O	C ₃₆ H ₅₈ O ₂₉	953.3013	953.2991	2.3
33	6×M - H ₂ O	C ₃₆ H ₆₀ O ₃₀	971.3077	971.3097	2.0
34	6×M	C ₃₆ H ₆₂ O ₃₁	989.3228	989.3202	2.6
35	6×M + H ₂ O	C ₃₆ H ₆₄ O ₃₂	1007.3343	1007.3308	3.5

a M designates monosaccharide, Glu glucose

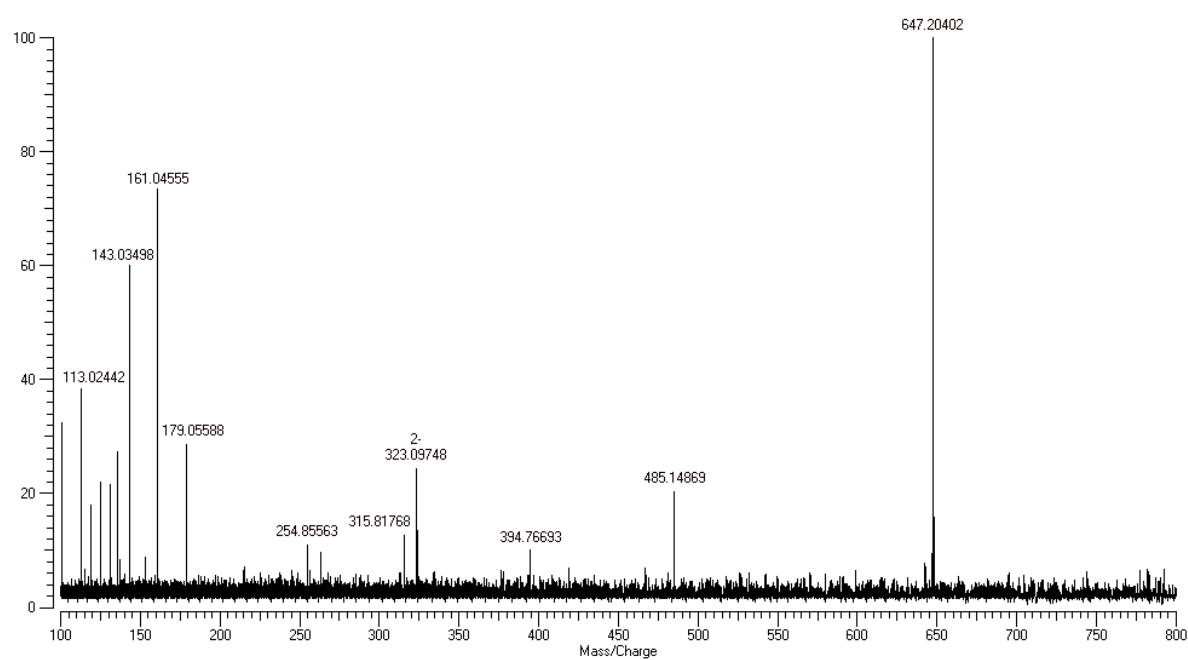
b)

Peak Numbering	Assignment	Molecular Formula	Experimental m/z [M-H] ⁻	Theoretical m/z [M-H] ⁻	Relative Error [ppm]
1		C ₅ H ₆ O ₃	113.0243	113.0244	1.0
2		C ₆ H ₁₂ O ₂	115.0765	115.0765	0.4
3		C ₄ H ₈ O ₄	119.0349	119.0350	0.7
4		C ₆ H ₈ O ₄	143.0348	143.0350	1.2
5		C ₉ H ₁₈ O ₂	157.1235	157.1234	0.6
6	Glu or Gal - H ₂ O	C ₆ H ₁₀ O ₅	161.0459	161.0455	2.1
7	Glu or Gal	C ₆ H ₁₂ O ₆	179.0568	179.0561	3.9
8		C ₁₄ H ₂₈ O ₂	227.2010	227.2017	2.8
9		C ₁₅ H ₃₀ O ₂	241.2169	241.2173	1.8
10		C ₁₆ H ₃₂ O ₂	255.2328	255.2330	0.6
11		C ₁₈ H ₃₆ O ₂	283.2640	283.2643	0.9
12		C ₁₂ H ₁₆ O ₈	287.0766	287.0772	2.2
13		C ₁₇ H ₂₆ O ₄	293.1752	293.1758	2.1
14	Glu-Gal - 2×H ₂ O	C ₁₂ H ₁₈ O ₉	305.0891	305.0878	4.4
15	Glu-Gal - H ₂ O	C ₁₂ H ₂₀ O ₁₀	323.0974	323.0984	3.1
16	Glu-Gal	C ₁₂ H ₂₂ O ₁₁	341.1082	341.1089	2.3
17	Glu-Gal + H ₂ O	C ₁₂ H ₂₄ O ₁₂	359.1159	359.1195	10.0
18	3×M - 3×H ₂ O	C ₁₈ H ₂₆ O ₁₃	449.1303	449.1301	0.6
19	3×M - 2×H ₂ O	C ₁₈ H ₂₈ O ₁₄	467.1396	467.1406	2.1
20	3×M - H ₂ O	C ₁₈ H ₃₀ O ₁₅	485.1505	485.1512	1.4
21	3×M	C ₁₈ H ₃₂ O ₁₆	503.1612	503.1618	1.2
22	3×M + H ₂ O	C ₁₈ H ₃₄ O ₁₇	521.1697	521.1723	5.0
23	4×M - 3×H ₂ O	C ₂₄ H ₃₆ O ₁₈	611.1849	611.1829	3.3
24	4×M - 2×H ₂ O	C ₂₄ H ₃₈ O ₁₉	629.1937	629.1935	0.3
25	4×M - H ₂ O	C ₂₄ H ₄₀ O ₂₀	647.2034	647.2040	0.9
26	4×M	C ₂₄ H ₄₂ O ₂₁	665.2142	665.2146	0.9
27	4×M + H ₂ O	C ₂₄ H ₄₄ O ₂₂	683.2233	683.2251	2.7
28	5×M - 4×H ₂ O	C ₃₀ H ₄₄ O ₂₂	755.2282	755.2251	4.1
29	5×M - 3×H ₂ O	C ₃₀ H ₄₆ O ₂₃	773.2347	773.2357	1.3
30	5×M - 2×H ₂ O	C ₃₀ H ₄₈ O ₂₄	791.2481	791.2463	2.3
31	5×M - H ₂ O	C ₃₀ H ₅₀ O ₂₅	809.2564	809.2568	0.5
32	5×M	C ₃₀ H ₅₂ O ₂₆	827.2675	827.2674	0.2
33	5×M + H ₂ O	C ₃₀ H ₅₄ O ₂₇	845.2799	845.2780	1.9
34	6×M - 4×H ₂ O	C ₃₆ H ₅₄ O ₂₇	917.2751	917.2780	3.1
35	6×M - 3×H ₂ O	C ₃₆ H ₅₆ O ₂₈	935.2918	935.2885	3.5
36	6×M - 2×H ₂ O	C ₃₆ H ₅₈ O ₂₉	953.2984	953.2991	0.7
37	6×M - H ₂ O	C ₃₆ H ₆₀ O ₃₀	971.3118	971.3097	2.2
38	6×M	C ₃₆ H ₆₂ O ₃₁	989.3216	989.3202	1.4

a M designates monosaccharide, Glu glucose and Gal galactose



a)



b)

Figure A1 MS^2 spectra of the dehydrated oligomers of glucose in an Infrared multiple photon dissociation (IRMPD) experiment on a selected ion at m/z 647 of: a) starch and b) cellulose

CURRICULUM VITAE

PERSONAL INFORMATION

Name: Agnieszka Golon
Date of Birth: 20.04.1985
Nationality: Polish
E-mail: gonon.agnieszka@googlemail.com
Marital status: single



ACADEMIC EDUCATION

October 2012 – present
Jacobs University Bremen
Postdoctoral Fellow

October 2009 – November 2012
Jacobs University Bremen

School of Engineering and Science, Doctoral study, Subject of the graduate's thesis: Characterization of complex mixtures of the light shredder waste fraction and caramelization processes by mass spectrometry (Prof. Dr. Nikolai Kuhnert)

March 2008 – August 2008
University in Bremen

Lifelong Learning Programme/Socrates, Department Chemistry, Subject of research project: Synthesis of different derivatives of nitrogen containing bisphosphonates; Oxidation of perfluorinated alcohol (Prof. Dr. Gerd-Volker Röschenhaler)

2007 – 2009

Pedagogical course, specialization chemistry, Faculty of Chemistry, Adam Mickiewicz University, Poznan, Poland

October 2006 – June 2009

Adam Mickiewicz University in Poznań

Department Biology, Faculty of Biotechnology, Bachelor study, Subject of the graduate's thesis: Mutation of DNA induced by products of lipid peroxidation and repair these damages (Prof. Dr. Artur Jarmołowski)

October 2004 – June 2009

Adam Mickiewicz University in Poznań

Department Chemistry, Division of Bioorganic and Organic Chemistry, Master study (with highest credits) Subject of the graduate's thesis: Studies of reactivity of malondialdehyde and methyloglyoxal towards aminoacids (Prof. Dr. Henryk Koroniak)

September 2000 – June 2004

High School in Koło

EXPERIENCE AND CAREER HISTORY

April 2009

European Chemistry Thematic Network (ECTN) Annual Conference in Poznań,

Volunteering work in the organizing committee

August 2007

GlaxoSmithKline in Poznań, Professional practices in the Quality Control Department

August 2006

Lab-Med S.C. Koło, Professional practices

2005 – 2006

Phumica, Poznań, Promotional Agency, hostess

ACHIEVEMENTS

September 2009

GlaxoSmithKline Residential Chemistry Training Programme, selected as one of the 30 chemists from whole of UK and Poland to attend this training programme

2006, 2007, 2009

Scientific scholarship, Adam Mickiewicz University in Poznań

Publications:

1. Golon, A.; Kuhnert, N. Unraveling the chemical composition of caramel. *J. Agric. Food Chem.* **2012**, *60* (12), 3266-3274.
2. Golon, A.; Kuhnert, N. Mass spectrometric investigation of the chemical composition of caramel formed upon heating of disaccharides. *J. Food Sci. Eng.* Accepted.
3. Golon, A.; Gonzalez, F. J.; Davalos, J. Z.; Kuhnert, N. Investigating the thermal decomposition of starch and cellulose in model systems and bread baking using domino tandem mass spectrometry. *J. Agric. Food Chem.* **2013**, *61*, 674-684.
4. Kuhnert, N.; Golon, A. Untersuchung von Karamel durch Domino Tandem Massen spektrometrie. *Deut. Lebensm-Rundsch.* **2012**, *23*, 345-349.
5. Jaiswal, R.; Matei, M. F.; Golon, A.; Witt, M.; Kuhnert, N. Understanding the fate of chlorogenic acids in coffee roasting using mass spectrometry based targeted and non-targeted analytical strategies. *Food Funct.* **2012**, *3*, 976-984.
6. Kuhnert, N.; Dairpoosh, F.; Jaiswal, R.; Matei, M. F.; Desphande, S.; Golon, A.; Nour, H. F.; Karaköse, H.; Hourani, N. Hill coefficients of dietary polyphenolic enzyme inhibitors can beneficial health effects of dietary polyphenols be explained by allosteric enzyme denaturing? *J. Chem. Biol.* **2011**, *4*, 109-116.
7. Golon, A.; Kuhnert, N. Characterization of "caramel-type" thermal decomposition products of selected monosaccharides including fructose, mannose, galactose, arabinose and ribose by advanced electrospray ionization mass spectrometry. *Food Funct.* Accepted.
8. Golon, A.; Tellström, V., Kuhnert, N. Characterization of heavy hydrocarbons in the light shredder waste fraction by gas chromatography/mass spectrometry. In preparation
9. Nour, H.; Golon, A.; Islam, T.; Fernández-Lahore, M.; Kuhnert N. Synthesis, self-assembly and ESI-MS complexation studies of novel chiral bis-N-substituted-hydrazinecarboxamide receptors. *Tetrahedron*. In preparation
10. Nour, H.; Golon, A.; Kuhnert, N. Synthesis of novel chiral tetra-(hydrazinecarboxamide) cyclophane macrocycles. *Eur. J. Org. Chem.* In Preparation
11. Nour, H.; Golon, A.; Le Gresley, A.; Kuhnert, N. Novel synthesis of enantiomerically pure dioxaspiro[4.5]decane tetra-carbohydrazide cyclophane macrocycles. *Chem. Eur. J.* Submitted.

Paper 1 was marked as the most read article of *Journal of Agricultural and Food Chemistry* in April, paper highlighted by ACS association and was featured in several press releases.

Poster presentations:

Polish-American Symposium on Chemical Biology

Lodz, Poland, September 13-14, 2009

Donata Pluskota-Karwatka, Agnieszka Golon

"Studies on the reactivity of malonaldehyde and methylglyoxal towards 2'-deoxyadenosine and N^α - acetyllysine"

GDCh Wissenschaftsforum Chemie 2011

Bremen, Germany, September 4-7, 2011,

A.Golon, N. Kuhnert

"Unraveling the chemical composition of caramel"

5th International Symposium on Recent Advances in Food Analysis

Prague, Czech Republic, November 1-4, 2011,

A.Golon, N. Kuhnert

"Unraveling the chemical composition of caramel"

Joint Conference of Polish Mass Spectrometry Society and German Mass Spectrometry Society

Poznań, Poland, March 4-7, 2012,

A.Golon, N. Kuhnert

"Mass spectrometric analysis of caramelization products derived from disaccharides"

Oral presentations:

Molife Retreat

Seefeld, Germany, Mai 19-21, 2011,

A.Golon, N. Kuhnert

"Chemical characterization of caramel"

ADDITIONAL INFORMATION

Languages Polish (mother tongue), English fluent in speaking and writing, German upper intermediate

Computer literacy MS Word, MS Excel, MS Power Point, Chem Draw, SciFinder, Origin, Bruker software, Mac OS X

Skills Driving Licence category B, since 2002

Hobbies:

- swimming
- traveling

REFERENCES

References available upon request:

Professor Nikolai Kuhnert, Jacobs University, School of Engineering and Science, Campus Ring 1, 28759, Bremen, Germany (n.kuhnert@jacobs-university.de)

Professor Henryk Koroniak, Adam Mickiewicz University, Department of Chemistry, Umultowska 89b, 61-614 Poznań, Poland (koroniak@amu.edu.pl)

Professor Gerd-Volker Röschenhaler, Jacobs University Bremen, School of Engineering and Science, Campus Ring 1, 28759, Bremen, Germany (g.roeschenthaler@jacobs-university.de)